Università degli Studi di Napoli Federico II
Facoltà di Ingegneria

Corso di Dottorato in Ingegneria dei Materiali e delle Strutture

CICLO XXVI   ING-IND/22

MULTICOMPONENT BIOMIMETIC SYSTEMS FOR BONE AND OSTEOCHONDRAL DEFECTS

COORDINATORE
Ch.mo Prof. Giuseppe Mensitieri

                                                CANDIDATA
TUTOR   **Daniela Giugliano**
Ch.mo Prof. Luigi Ambrosio

CO-TUTOR
Dr. Maria Grazia Raucci

Index

2.3   CELLULOSE-BASED HYDROGELS CROSSLINKED BY CITRIC ACID

3.2 GELATIN/HYDROXYAPATITE 3D MULTICOMPONENT SYSTEMS

Chapter 2 *INJECTABLE MODIFIED HYDROXYAPATITE GEL FOR BONE DEFECT*

2.1 STRONTIUM-SUBSTITUTED HYDROXYAPATITE CEMENT

2.2 BIOACTIVE HYDROXYAPATITE-GRAPHENE OXIDE INJECTABLE MATERIAL

2.3   CELLULOSE-BASED HYDROGELS CROSSLINKED BY CITRIC ACID

Chapter 3   POROUS SCAFFOLD FOR OSTEOCHONDRAL DEFECT

3.1   BIOMINERALIZED GELATIN SCAFFOLD

3.2 GELATIN/HYDROXYAPATITE 3D MULTICOMPONENT SYSTEMS

3.2   GELATIN/HYDROXYAPATITE 3D MULTICOMPONENT SYSTEMS

Abstract

T*he extracellular matrix of bone has been described as a composite material made constituted by collagen type I fibrils mineralized with nanocrystals of hydroxyapatite. Approximately 70% of bone by weight is composed of calcium salts, with hydroxyapatite $Ca_{10}(PO_4)_6(OH)_2$ as the primary mineral constituent. Bone formation occurs in two phases: matrix synthesis followed by extracellular mineralization. An impaired balance of bone resorption and formation by osteoclasts and osteoblasts, respectively, induces osteoporosis. Other bone defects can be caused by tumor removal, fractures (especially in the hip, wrist, knee and spine) or congenital defects. A more complex substrate is represented by osteochondral tissue, where defects penetrate the subchondral bone.*

To mimic natural structure, we propose different approaches to repair bone and osteochondral defects and to promote a potential bone healing filler.

In general, injectable materials (cements/natural polymer) hold great promise in tissue engineering applications due to the ability of these systems to conform to complex bone shapes, contours, and defects with less invasive surgery. The target is the osteogenic differentiation induced by bioactive component (natural polymers and/or modified hydroxyapatite) of the injectable systems. In this work, we proposed the following bone filler materials:

1. *Strontium-substituted hydroxyapatite cement (to contrast bone resorpsion).*
2. *Bioactive hydroxyapatite - graphene oxide (to support high viability and osteogenic differentiation of hMSC cells).*
3. *Modified-cellulose hydrogels crosslinked by citric acid (to increase hydrophilicity and roughness surface in order to stimulate osteogenic differentiation of hMSC).*

Osteocondral region has two distinct tissues (bone and cartilage) with different properties: to mimic its structure, we realized two different gelatin scaffolds biomineralized by HA. The use of a 3D scaffold depends on the necessity to provide a shape control, while the biological signals are induced by HA presence, realized by bulk sol-gel transition, and surface biomimetic treatment, as reported in the two type of scaffolds realized:

1. *Gelatin scaffold crosslinked by EDC solution, and biomineralized by modified Kokubo treatment (to increase osteogenic proliferation and differentiation);*

2. *Gelatin/hydroxyapatite scaffold realized by in situ sol-gel synthesis and crosslinked by EDC solution (where the biological signals occur into the scaffold as a gradient and crystalline degree is modulated by gelatin/hydroxyapatite ratio).*

The results are confirming the feasibility of the proposed systems a potential substitutes/scaffolds for both bone an osteochondral tissue regeneration.

INTRODUCTION

Cartilage and bone injuries occur due to several reasons including degenerative, surgical, and traumatic processes, which significantly compromise quality of life and for this reason, they have long presented a challenge to physicians. Currently, millions of patients are suffering from bone and cartilage defects. One approach is the regenerative medicine, a thriving new area of multidisciplinary research that has the potential to revolutionize the treatment of disease and damaged tissue. The ability to develop materials that can interface with tissues structurally, mechanically and biofunctionally is important to the success of regenerative strategies [1]. Bone and cartilage are highly organized tissues that assemble from the nano- to macro-scales to produce complex structural networks (Figure 1). Cartilage is an avascular tissue with a disperse cell population, and has a limited capacity for self-renewal [2]. Even small chondral defects may necessitate surgical intervention and would benefit from the development of new materials that fill the damaged area and integrate with the surrounding tissue, preventing further degeneration and consequent osteoarthritis. By contrast, bone is a highly vascular tissue, and remodels rapidly to heal traumatic fractures [3]. There is, however, a driving need to develop scaffolds or injectable systems that guide bone regeneration across defects that are too large to heal naturally. For both cartilage and bone tissues, it is advantageous to find two different strategies that direct tissue regeneration:

- versatile, implantable, biocompatible scaffold;
- non invasive injectable systems, as a bone filler.

Successful design of scaffold and injectable materials requires an intimate understanding of molecular interactions that occur within tissues, between cells and the extracellular matrix (ECM). Both must provide space and a supportive environment for development, while avoiding hostile immune response, and degrade slowly to allow for tissue in-growth. In this project, we explore recent approaches that combine varying degrees of synthetic, natural and biomimetic materials and different fabrication techniques to construct highly tailored environments for bone and osteochondral regeneration.

The molecular interplay within tissues leans heavily towards weak interactions — hydrogen bonding, electrostatics, and the effects of solvation forces, such as hydrophobicity. These lower energy molecular couplings are responsive and adaptive, enabling rapid assembly and

disassembly, protein conformation changes and structural remodelling. The self-assembly of collagen, a major ECM protein found in bone and cartilage, is strongly dependent on hydrophobic interactions within the physiological environment, and takes place over multiple steps from the expression of pro-collagen proteins to their assembly into triple-helical fibres [4]. Weak forces complement the dynamic nature of tissue, for example, the shock absorbing nature of cartilage is provided in part by the movement of water from a network of hydrophilic proteoglycan molecular chains. Likewise, bone is strengthened by the nucleation of hydroxyapatite into the nanodimensional gaps between collagen molecules. Secondary to assembly, stronger covalent bonding, termed covalent capture [5], also occurs throughout tissues, to reinforce structures. For example, the enzymatic crosslinking of lysine leads to the stabilization of proteins, such as collagen and elastin. In addition to a structural role, the ECM that surrounds bone and cartilage presents cells with instructive cues needed to maintain cell phenotype and behaviour [6].

Many strategies for guiding tissue regeneration involve the incorporation of varying degrees of biological context into implantable scaffolds to create biomimetic environments.

One way to mimic this context is to create scaffolds from natural biopolymers such as fibrin, collagen and hyaluronic acid, which incorporate many of the cues needed by cells. However, non-autologous materials carry the risk of disease transmission and immunological rejection, and are associated with challenges pertaining to material quality, harvesting, and processing. In light of this, many researchers are investigating the development of biofunctional synthetic polymers as alternative scaffold materials.

Biomineralisation in bone is another form of natural self-assembly, where the nucleation and alignment of hydroxyapatite crystals onto bundles of collagen fibres results in a composite material resistant to high compressive loads. Although the mechanisms of this protein-mediated mineralisation are not fully understood, it is known that acidic phosphoproteins play a significant role in the control over non-specific nucleation by sequestering calcium ions from the physiological environment [5,7].
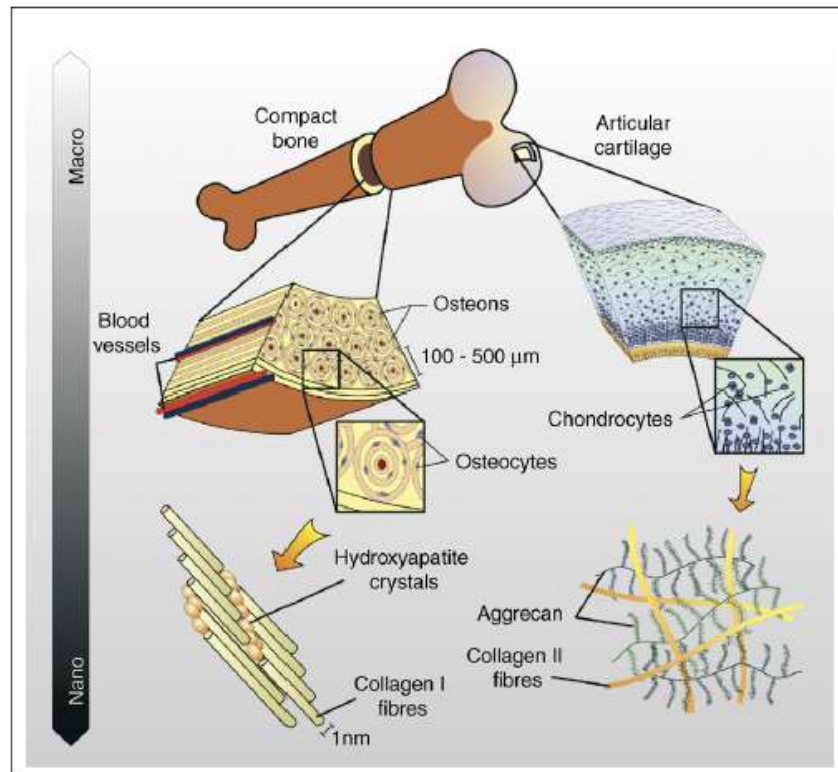
Fig. 1: complex structural networks [19].

Aim

In the bone defects, there are often three-dimensional complex shapes. Presently, the strategies to address bone defects include the use of autogeneous grafts and flaps, allograft or xenograft bone, non-degradable bone cement, metals and ceramics. The use of autogenous bone grafts and bone flap is considered the standard in management of bony defects but has limited source of graft material, especially in children. The allograft and xenograft are good substitutes of autogenous bone graft, however, there are potentials of transferring pathogens and difficulties of shaping into the desired form. Most of synthetic implants are not biodegradable and may result in stress shielding in the surrounding bone or fatigue failure of the implant. Therefore, the search for improved materials and surgical strategies for repairing skeletal defects continues [8-11].

The approaches of tissue engineering have the potential to evolve the present clinical strategies. They attempt to create tissue replacements by providing a scaffold with the proper size and predetermined shape for tissue development and permitting cells from the surrounding tissue to migrate into the matrixes [10,12,13].

In 1893, Barth [11,14] first introduced the concept of "scaffolding" as a porous matrix or an implant in which cells can infiltrate and regenerate the local tissue. In the last two decades, this concept has been extended to indicate natural and synthetic substrates that can temporarily support cells and direct their fate towards cell-material interactions and the release of biological factors [11,14].

The scaffolds are often three-dimensional porous polymeric matrices, which provides a space with the proper size and shape for tissue regeneration [4,12]. The surface of the polymers (natural or synthetic) would also ideally promote cell attachment, as many cells are anchorage dependent for survival. More concerns in truly clinical need, are to engineer structural tissues with supporting vascular network. Under these circumstances, the reconstructions with tissue engineering techniques require different strategies that establish an extensive, patent vascular network within the engineered bone [9,13].

The evolution consists on the development of novel scaffold materials, compatible with the cell guidance concept and resulting from contemporary advances in the fields of materials science and molecular biology [15].

The aim is to realize a scaffold with these properties and an increased biological and biochemical signals. However these porous structures have been produced in several ways, both by using conventional fabrication methods and more advanced methods.

In the other hand, it is possible to consider an injectable gel like support to cells growth and drug delivery base.

A gel is defined as a three-dimensional network swollen by a solvent. Usually, the solvent is the major component of the gel system. Gels can be classified into two categories based on the way the network is connected: chemical gels formed by covalent bonds and physical gels formed by secondary forces [16]. Some of physical gels are heat reversible and these are called thermoreversible gels [17].

The mechanisms that may be involved in the in situ gel formation are the following: gelation in response to temperature or pH change, ionic cross-linking, solvent exchange or crystallization, and simply thickening upon removal of the injection shear [18].

Anyway collagen and hydroxyapatite, are the two major components of bone tissue and they have been used as the bone substitute materials in orthopedic, oral-maxillo-facial and plastic surgery. The collagen fibers can serve as the scaffold for cell growth and tissue repair, and the hydroxyapatite (HA) is biocompatible and osteoconductive for bone regeneration [3,9,13].

While most of the collagen matrices are prepared in a slab form, spherical gel beads of collagen and hydroxyapatite are more versatile in biomedical applications [10].

The aim of this work, is realized two different systems for the bone and osteochondral defect respectively.

To obtain the optimization of this result, we study different systems:

1. ***Injectable modified gel for bone defect:***

    a) *Injectable modified-hydroxyapatite:* Sr substituted nano-hydroxyapatite (Sr-HA) was synthesized to simulate bone crystal with Sr incorporation. Based on pilot studies, Sr-HA with different Sr concentrations were synthesized. The purpose of this study was to examine the effects of Sr incorporation on chemical composition, crystal size, crystallinity and lattice structure, growth of biocompatibility and cell adhesion and proliferation, of Sr-HA nanocrystallite.

    b) *Bioactive hydroxyapatite - Graphene oxide hybrid injectable material*: HA-GO hybrid material was prepared by sol-gel technology using different GO concentration. Throw physico-chemical, morphological and biological analysis, was evaluated the hybridization of HA nanoparticles in GO sheet and the cell proliferation.

    c) *Modified Cellulose-based hydrogels*: natural polymer was crosslinked with a innovative treatment by citric acid. The study evaluated the possibility to increase the hydrophilicity and roughness surface of modified-cellulose hydrogels. Injectable modified-cellulose gels have potentially a good effect on the cell attachment, cell proliferation and osteoblastic differentiation.

2. ***Porous scaffold for osteocondral defect:***

    a) *Three-dimensional (3D) porous gelatin scaffolds* fabricated by freeze-drying followed by biomimetic method in order to obtain a superficial mineralization. This work shows the hydroxyapatite coating and the effect of crosslinking time on the scaffold.

b) *Gelatin/hydroxyapatite 3D multicomponent systems* were prepared by sol-gel and freeze-drying technologies. The aim is obtain an HA gradient in a scaffold structure how the osteogenic differentiation growth with the gradient meanwhile the chondrocyte ones decrease. Physico-Chemical-characterization (FTIR-XRD) and morphological analysis (SEM) were performed to evaluate the composition, the chemical interaction among the phases and the presence of hydroxyapatite gradient.

References

[1] Griffith LG, Naughton G. Tissue engineering: current challenges and expanding opportunities. Science 2002;295:1009-14.

[2] Poole AR, Kojima T, Yasuda T, Mwale F, Kobayashi M, Laverty S. Composition and structure of articular cartilage: a template for tissue repair. Clin Orthop Relat Res 2001;391:S26-S33.

[3] Hing KA. Bone repair in the twenty-first century: biology, chemistry or engineering. Philos. Transact. A Math Phys Eng Sci 2004;362:2821-50.

[4] Prockop DJ, Kivirikko KI. Collagens: molecular biology, diseases, and potentials for therapy. Annu Rev Biochem 1995;64:403-34.

[5] He G, Dahl T, Veis A, George A. Nucleation of apatite crystals in vitro by self-assembled dentin matrix protein 1. Nat Mater 2003;2:552-8.

[6] Stevens MM, George JH. Exploring and engineering the cell surface interface. Science 2005;310:1135-8.

[7] Bonzani IC, George JH, Stevens MM. Novel materials for bone and cartilage regeneration. Current Opinion in Chemical Biology. 2006;10:568–75.

[8] Langer R, Vacanti JP. Tissue engineering. Science 1993; 260: 920-6.

[9] Gloria A, Russo T, De Santis R, Ambrosio L. 3D fiber deposition technique to make multifunctional and tailor-made scaffolds for tissue engineering applications. J Appl Biomat Biomech 2009;7:141-52.

[10] Chang SH, Hsu YM, Wang YJ, Tsao YP, Tung KY, Wang TY. Fabrication of pre-determined shape of bone segment with collagen-hydroxyapatite scaffold and autogenous platelet-rich plasma. J Mater Sci Mater Med 2009;20:23-31.

[11] Barth A. Ueber histologische befunde nach knochenimplantationen. Arch Klein Chir 1893;46:409-11.

[12] Guarino V, Causa F and Ambrosio L. Bioactive scaffolds for bone and ligament tissue. Expert Rev Med Dev 2007;4:405–18

[13] Arrington ED, Smith WJ, Chambers HG, Bucknell AL, Davino NA. Complications of iliac crest bone graft harvesting. Clin Orthop Relat Res 1996;329:300–9.-

[14] Vacanti JP, Morse MA, Saltzman WM, Domb AJ, Perez-Atayde A, Langer R. Selective cell transplantation using bioabsorbable artificial polymers as matrices. J Pediatr Surg 1988;23:3-9.

[15] Nair LS, Laurencin CT. Polymers as biomaterials for tissue engineering and controlled drug delivery. Adv Biochem Eng Biotechnol 2006;102:47-90.

[16]   Higgs PG, Ball RC. Some ideas concerning the elasticity of biopolymer networks.Macromolecules. 1989;22:2432–2437.

[17] Guenet JM. (1992). Thermoreversible gelation of polymer and biopolymers, New York: Academic Pree.

[18] Gutowska A, Jeong B and Jasionowski M. Injectable Gels for Tissue Engineering. The anatomical record 2001;263:342–349

[19] M.M. Stevens, J.H. George. Exploring and engineering the cell surface interface. Science2005;310:1135–8.

CHAPTER 1

SYSTEMS FOR BONE AND OSTEOCHONDRAL DEFECTS

*C*onnective tissue is one of the four traditionally classified types of biological tissue. There are many different kinds of connective tissue. In general, they serve functions of structure and support, often connecting two other types of tissue to each other and usually derives from the mesoderm, the middle of three layers in an animal embryo. The characteristics of connective tissue are largely derived from the extracellular matrix, non-living material that surrounds and supports the living cells. The older classification of connective tissue had two subtypes: proper, which covered fibrous tissue; and specialized, which included bone, blood, cartilage, adipose (fat) tissue, and reticular tissue. A wider classification can be made considering the proper connective tissue, such as bone and cartilage to support function, and blood as a fluid connective tissue.
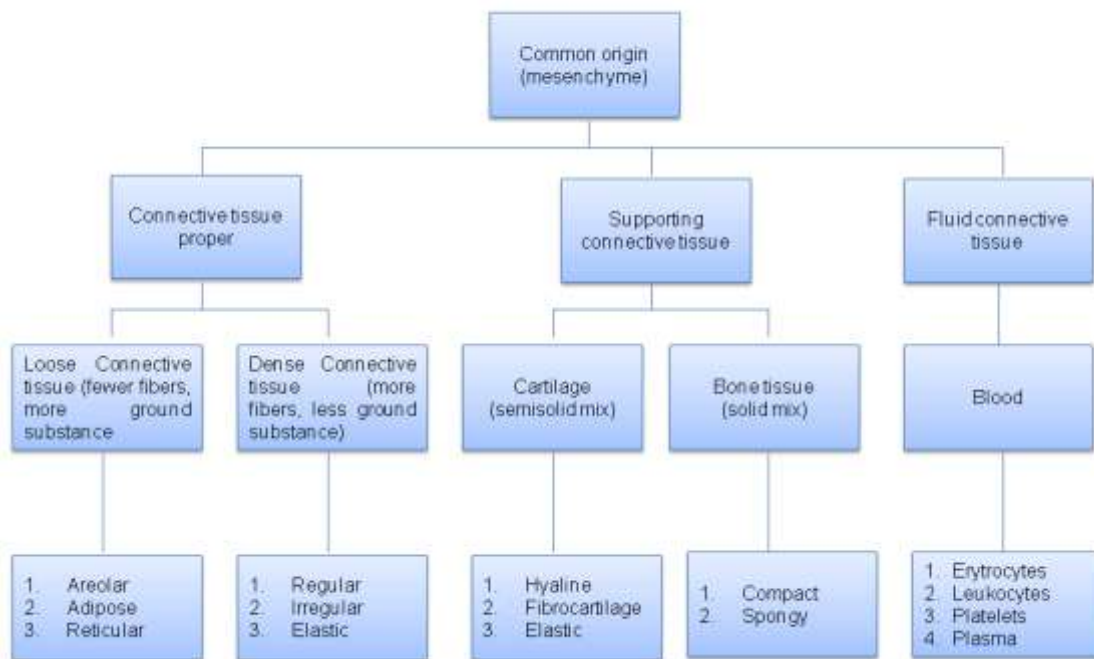
Fig. 1: Connective tissue. Classification.

As reported, our target is realized a biointeractive systems able to regenerate a complex environment. In this chapter, we propose an overview on bone and cartilage tissues, in order to correlate the natural structures with synthetic systems proposed.

1.1   Bone

Bones are the main constituent of the skeleton and differs from the soft tissue (i.e. cartilage, ligaments and tendons) in rigidity and hardness. Bones are important to the body both biomechanically and metabolically. The skeletal tissue performs three main functions for the life of any vertebrate; support, protection and homeostasis of calcium. In fact the rigidity and hardness of bone enable the skeleton to maintain the shape of the body and support it, to transmit muscular forces from one part of the body to another during movement, to protect the soft tissues of the cranial, thoracic and pelvic cavities, to supply the framework for the bone marrow. The mineral content of bone serves as a reservoir for ions, particularly calcium, and also contributes to the regulation of extracellular fluid composition, mainly ionized calcium ion concentration.

Fig. 2: Anterior view of a human adult male skeleton.

1.1.1 Bone composition

Bone matrix is composed of approximately 28% by weight of organic matter, from 60% of inorganic substance and the remaining 12% of water (38.4% in volume organic matter, 37.7% mineral and 23.9% water) [1]. The mineral is largely impure hydroxyapatite, $Ca_{10}(PO_4)_6(OH)_2$,

containing carbonate, citrate, fluoride and strontium. The organic matrix consists of 90% collagen and about 10% noncollagenous proteins. From a mechanical point of view, the bone matrix is comparable to a composite material: the organic matrix is responsible to give toughness to the bone, while the inorganic matrix has the function to stiffen and strengthen the bone [2].

1.1.2 Cortical and Trabecular bone

Bones are composed in general of two basic structures, i.e. cortical and trabecular, or cancellous, bone (figure 3) [2]. Cortical bone is solid compact bone, containing microscopic channels. Approximately 80% of the skeletal mass in the adult skeleton is cortical bone. However, due to the different structures, Ftrabecular bone fill the bigger volume. Cortical bone forms the outer wall of all bones, being largely responsible for the supportive and protective function of the skeleton. The remaining 20% of the bone mass is cancellous bone, a lattice of plates and rods having typical mean thicknesses ranging from 50 μm to 300 μm known as trabecula, found in the inner parts of the skeleton.
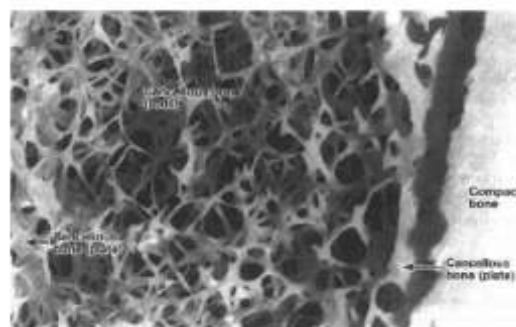
Fig. 3: Photograph of a section of a tibia showing trabecular (cancellous) and cortical (compact) bone.

Cortical Bone

Adult cortical bone is composed of 3- to 7-μm-thick unit layers (called lamellae) which contain collagen fibres that run parallel to each other [2]. In histological preparations, under polarized light, the lamellae appear as alternating light and dark levels, which is the result of differing orientations of collagen fibers within adjacent lamellae (figure 4). The main structural unit of cortical bone is given by the osteon or Haversian system (figures 4,5). A typical osteon is a cylinder about 200 μm in diameter, consisting of a central canal (Haversian canal) surrounded by about 20-30 concentric lamellae. The external surface of every bone is surrounded by several layers of lamellae, called circumferential lamellae.

13
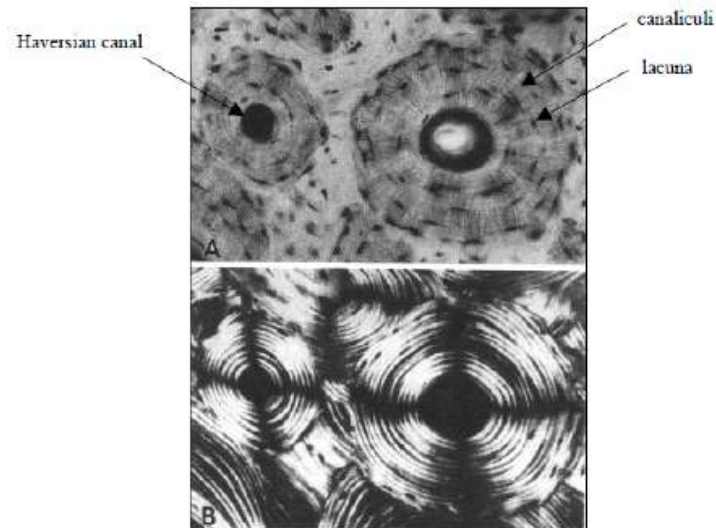
Fig. 4: (A) Histological cross-section of cortical bone, showing osteon with its Haversian canals, lacunae and capillar canaliculi. (B) Same cross-section in polarized light, which shows the osteons composed of numerous concentric lamellae

Within the Haversian canals run blood and lymphatics vessels, and nerves. The outer border of each osteon is surrounded by a cement line, which is a 1- to 2-µm-thick layer of mineralized matrix, deficient in collagen fibers. Throughout the bone, small cavities (lacunae) containing entrapped bone cells (osteocytes) are found.
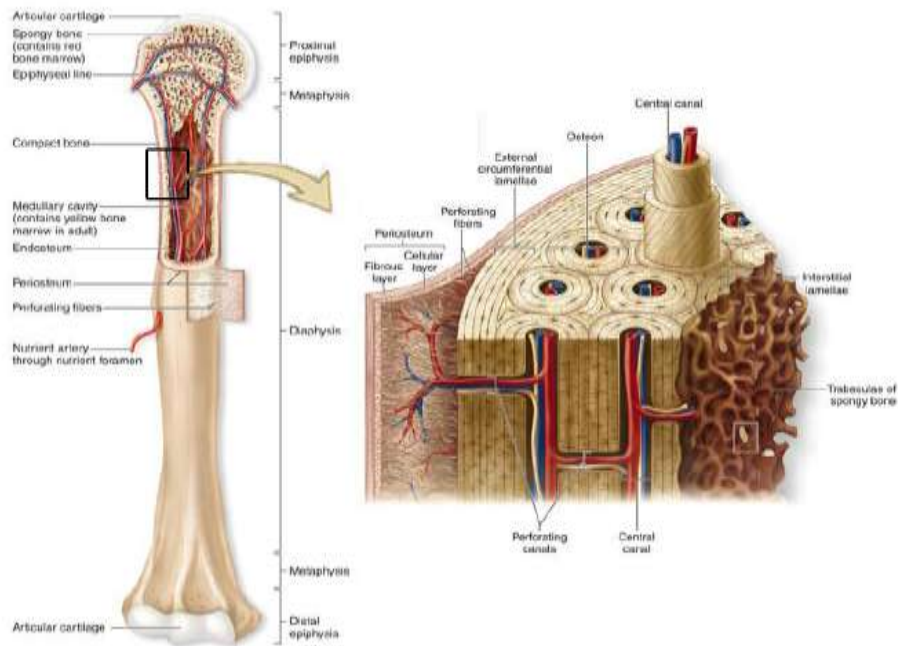
Fig. 5: Representation of a long bone with a detailed schematic representation of cortical bone and periosteum.

Trabecular Bone

The trabecular bone has not Havers systems, but consists of an array of interconnected beams (trabecule), of a thickness less than 0.2 mm and variable in shape (figure 6). Each trabecula is constituted by a packages of parallel lamellae. Usually a package of lamellae is up to 1 mm long and 50-60 microns in section. According to the site of analysis is possible to find trabecular bone with different characteristics, within different anatomical sites. This leads to great differences in bone density. Moreover the orientation of the trabecular structure is tightly bonded to the anatomical site and its mechanical role. In fact the correlation between the trabecular orientation and the load direction was already showed in literature [3,4]; trabecular structure result to be mainly oriented along the primary load direction. However load direction depends by the motion, therefore trabecular structure can became very complex. In order to classify structure that can be very different, and to obtain some quantitative information, some models were developed [5].
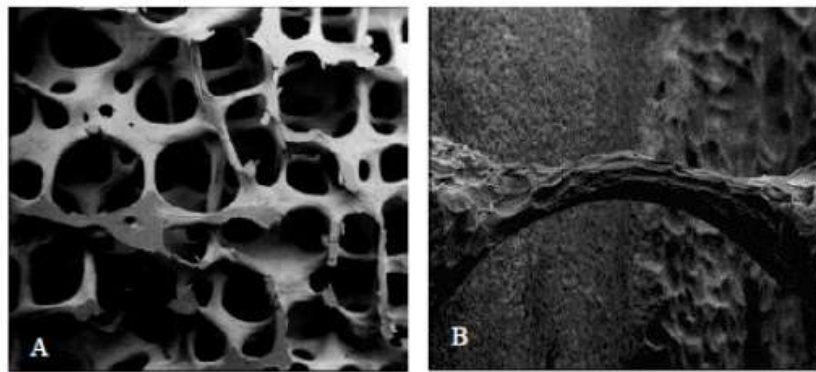
Fig. 6: (A) vertical section of trabecular bone from lumbar vertebra. (B) single trabecula leaving from the endosteal wall.

The trabecular bone is compliant and less strong than cortical bone, generally because of its discontinuous structure. Consequently it gives a smaller contribute to the rigidity of the bone. Moreover can show greater variability in mechanical behaviour than cortical bone, due to its greater structural irregularity. However we must not underestimate his role:

• It stiffens the structure connecting the outer shell of cortical bone;

• It supports the layer of the cortex and distributes the loads in the case of lateral impacts;

• It supports the articular cartilage and act as shock-absorber during loads;

• It transfers and distributes the load to the surrounding cortical bone;

• It protects the cave bones from phenomena of instability (buckling).

1.1.3 Bone development and turnover

In normal conditions, bone is characterized by a balanced coexistence of resorptive and appositional processes. The main characters of these processes are the bone cells. Even if they represent a not influential part of the whole skeletal weight they are responsible for all the processes of bone resoption, formation, modeling and remodeling. It is still not clear what really drive them behaviour, however the scientific community agrees to the hypothesis that the development of a particular structure, during remodelling process, can be a reaction to mechanical loads.

1.1.4 Bone cells

The major cellular elements of bone can be grouped in [2,6]:

• osteoblasts

• bone-lining cells

• osteocytes

• osteoclasts

Osteoblasts

Osteoblasts are bone-forming cells that synthesize and secrete unmineralized bone matrix (the osteoid). They seem to participate in the calcification and resorption of bone and to regulate the flux of calcium and phosphate in and out of bone. Osteoblasts (figure 7) occur as a layer of contiguous cells which in their active state are cuboidal (15 to 30 μm thick). Bone formation occurs in two stages: matrix formation followed by mineralization, denoted by deposition of crystals of hydroxyapatite.

Their life cycle can be summarized as follows [2,6,7]: the birth from a progenitor cell; the differentiation from stem cells to osteoblasts and participation in elaborating matrix and calcifying units; either returning to the pre-osteoblast pool, transform into bone-lining cell and burial as osteocytes, or death.

The development of osteoblasts and osteoclasts are inseparably linked on a molecular basis. Both are derived from precursor cells originating in bone marrow with osteoblasts from multipotent mesenchymal stem cells, while osteoclasts from hemaiopoietic cells of the monocyte/macrophage lineage), and osteoblast differerentiation is a prerequisite for osteoclast development [2].
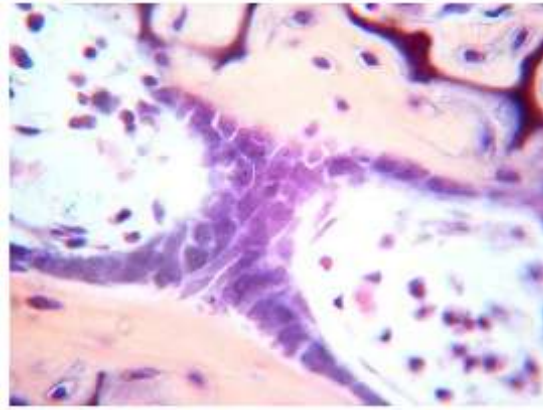
Fig. 7: Histological picture of osteoblasts.

Bone-lining cells

Bone-lining cells are believed to be derived from osteoblasts that have become inactive, or osteoblast precursors that have ceased activity or differentiated and flattened out on bone surfaces. Bone-lining cells occupy the majority of the adult bone surface. They serve as an ion barrier separating fluids percolating through the osteocyte and lacunar canalicular system from the interstitial fluids. Bone lining cells are also involved in osteoclastic bone resorption, by digesting the surface osteoid and subsequently allow the osteoclast access to mineralized tissue. Furthermore, it has been postulated that the 3D-networks of bone-lining cells and osteocytes are able to sense the shape of the bone, together with its reaction to stress and strain, and to transmit these sensations as signals to the bone surface for new bone formation/resorption.

Osteocytes

During bone formation, some osteoblasts are left behind in the newly formed osteoid as osteocytes when the bone formation moves on. The osteoblasts embedded in lacunae differentiate into osteocytes. In mature bone osteocytes are the most abundant cell type. They are found to be about ten times more than osteoblasts in normal human bone. Mature osteocytes posses a cell body that has the shape of an ellipsoid, with the longest axis (25 μm) parallel to the surrounding bone lamella. The osteocytes are thought to be the cells best placed to sense the magnitude and distribution of strains. They are thought both to respond to changes in mechanical strain and to respond to fluid flow to transduce information to surface cells, via the canalicular processes and the communicating gap junctions. Osteocytes play a key role in homeostatic, morphogenetic and restructuring process of bone mass that constitute the regulation of mineral and architecture [2].

Osteoclasts

Osteoclasts are bone-resorbing cells, which contain one to more than 50 nuclei and range in diameter from 20 to over 100 μm. Their role is to resorb bone, by solubilizing both the mineral and the organic component of the matrix. The signals for the selection of sites to be resorbed are unknown. Biphoshponates, calcitonin and estrogen are commonly used to inhibit resorption. These are believed to act by inhibiting the formation and activity of osteoclats and promoting osteoclasts apoptosis.
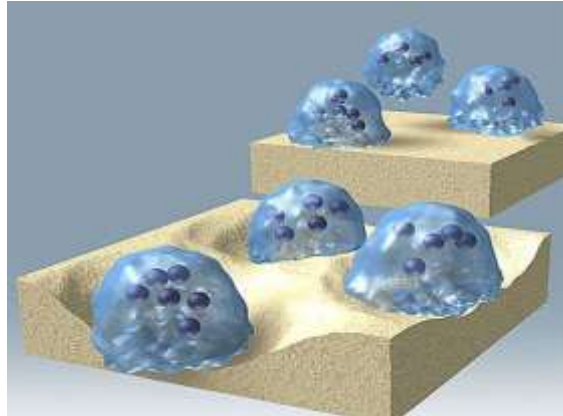
Fig. 8: osteoclasts with more 50 nuclei.

1.1.5 Bone resorption

The actual mechanism for the activation of osteoclast bone resorption is still unclear. Osteoclasts begin to erode the bone while coming in contact with the surface of bone. During this activity osteoclasts form cavities (Howship's lacunae) in cancellous bone, and cutting cones or resorption cavities in cortical bone. The resorption process occurs in two steps, which occur essentially simultaneosly: dissolution of mineral and enzymic digestion of organic macromolecules.
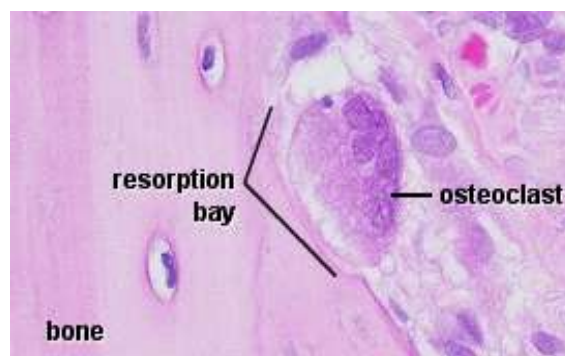
Fig. 9: Image representative of bone resorption.

1.1.6 Bone formation

Bone formation occurs in two phases: matrix synthesis followed by extracellular mineralization. The osteoblasts begin to deposit a layer of bone matrix, referred to as the osteoid seam. After about 5 to 10 days, the osteoid seam reaches a level of approximately 70% of its mineralization. The complete mineralization takes about 3 to 6 months in both cortical and trabecular bone. Bone formation is a complex process regulated by hormones (e.g. Parathyroid hormones) and growth factors (e.g. Transforming Growth Factor). The building of bone as a functional organ is an important process, as bone constantly enlarges, renews and develops itself in time. In the same time it adapts itself to support protection, mechanical needs and numerous metabolic and hematopoietic activities [8-10]. In this thesis, the normal growing of long bones will be addressed only briefly. It is just mentioned that this growth follows a cartilaginous model, involving the growth through the epiphyseal plates, the metaphyseal spongiosa growth, and the circumferential growth of the bone shaft. Modeling and remodeling process, play an important role both for normal bone growth as also for the adaptation processes that occur in pathological modification of bone (e.g. osteoporosis).

1.1.7 Modeling

In general, growth and modelling are linked together [2]. Modeling allows the development of normal architecture during growth, controlling the shape, size, strength and anatomy of bones and joints. It increases the outside cortex and marrow cavity diameters, gives shape to the ends of long bones, drifts trabeculae and cortices, enlarges the cranial vault and changes the cranial curvature. During normal growth, periostal bone is added faster by formation drifts than endosteal bone is removed by resorption drifts. This process is regulated so that the cylindrical shaft markedly expands in diameter, whereas the thickness of the wall and the marrow cavity slowly increase. Modeling controls also the modulation of the bone architecture and mass when the mechanical condition changes [11]. For example, bone surfaces can be moved to respond to mechanical requirements. A coordinate action of bone resorption and formation of one side of the periosteal and endosteal surfaces can move the entire shaft to the right or left, allowing some bones to grow eccentrically [12].

1.1.8 Remodeling

Remodelling can be defined as a process that produces and maintains bone that is biomechanically and metabolically competent [2]. At infancy, the immature (woven) bone at the metaphysis is structurally inferior to mature bone. In adult bone, the quality (e.g. mechanical properties) of bone deteriorates with time. Thus, as many other tissues, bone must replace or renew itself. This replacement of immature and old bone occurs by a process called remodeling, which is a sequence of resorption followed by formation of new lamellar bone [11]. The remodeling characterizes the whole life of bones. For normal rates of periodic bone replacement (bone turnover), cancellous bone has a mean age of 1 to 4 years, while cortical bone about 20 years. The remodeling has both positive and negative effects on bone quality on the tissue level. It allows to remove microdamage, replace dead and hyper-mineralized bone, adapt the microarchitecture to local stresses. But remodeling may also perforate or remove trabeculae, increase cortical bone porosity, decrease cortical width and possibly reduce bone strength.
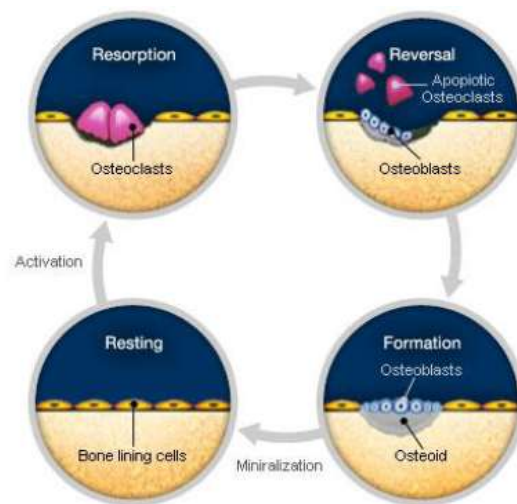
Fig. 10: Four phases of bone remodelling process.

The group of bone cells that carries out one quantum of bone turnover, osteoclast, osteoblast and their progenitors, is called a bone remodeling unit (BRU). The life cycle of a unit can be summarized in the following stages: resting, activation, resorption, reversal (coupling), formation, mineralization and back to resting.

Resting: About 80% of the cancellous and cortical bone surfaces (periosteal and endosteal) and about 95% of the intracortical bone surfaces in large adult animals (including humans) are inactive

with respect to bone remodeling stage, at any given time. These inactive surfaces are covered by bone-lining cells and a thin endosteal membrane.

Activation: As activation is defined the conversion of the quiescent bone surface to resorption activity. Which factor initiates this process is unknown. However, activation is believed to occur partly in response to local structural or biomechanical stimuli. The remodeling cycle necessitates the recruitment of osteoclasts and the mean for them to access the bone surface.

Resorption: Osteoclasts begin to erode bone, forming cavities.

Reversal: The 1- to 2- week interval between completion of resorption and the beginning of bone formation is called reversal.

Formation and mineralization: Bone formation occurs, through matrix synthesis followed by extracellular mineralization. Bone turnover depends both on the surface-restricted activation frequency and on the surface-to-volume ratio. The activation frequency is the inverse of the time interval between consecutive cycles of remodeling at the same site. The surface to- volume ratio of cancellous bone is about 5- to 10 times bigger than in cortical bone. There are studies showing that remodeling does differ in different parts of the skeleton and also in different parts of a given bone at any moment. Possible reasons are that where micro-damage occurs, BRU-based remodeling increases to try to repair it. Usually, such regions are highly loaded sites, like the epiphyseal spongiosa [2,13]. Another reason could be, that during growth parts of the skeleton accumulated more bone than actually needed for mechanical usage, which will increase remodeling-dependent bone loss [2,9]. In the adult bone the bone remodeling provides a mechanism for the skeleton to adapt to its mechanical environment, due to inactivity or to hypervigorous activity. These phenomena are grouped together as biomechanical-driven remodeling. Conversely, it is sustained that there exist genetically driven remodeling or stochastic remodeling that prevents fatigue damage. This hypothesis is highly disputed [2,13,14].
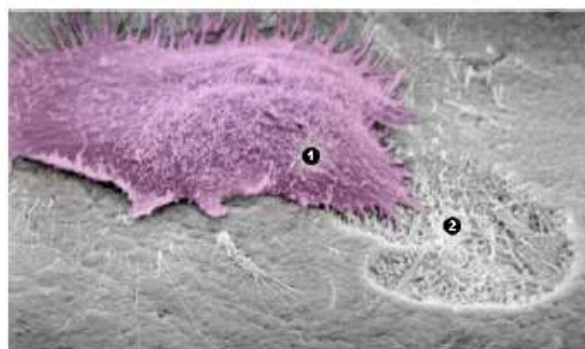
Fig. 11: In the picture are represented 1. Osteoclast. 2. Bone surface resorbed by osteolclast.

1.1.9 Mechanical properties of bone

The intimate blend of hard inorganic and resilient organic components results in excellent mechanical properties. For example, compact bone specimens have been found to have tensile strength in the range of 700 to 1400 kg/cm^2, and compressive strength in the range of 1400 to 2100 kg/cm^2. These values are within the same magnitude as for aluminum or mild steel, but bone is much lighter. The great strength of bone exists principally along its axis and hence roughly parallel both to the collagen fiber axis and to the long axis of mineral crystals. Although apparently stiff, bones exhibit a considerable degree of elasticity, which is important in the skeleton's ability to withstand impact. Estimates of modulus of elasticity of bone samples are of the order of 420 to 700 kg/cm^2, values very much less than steel, for example, indicating much greater elasticity of bone [15].

1.2 Cartilage tissue

Cartilage is a connective tissue with special support functions. The cartilage is a particular tissue of mesenchymal origin characterized by a cellular component surrounded by an extracellular matrix that gives texture to fabric.

According to the composition and texture of the amorphous component and the fibers contained in it is possible to distinguish the cartilaginous tissue in three types:

- Elastic cartilage
- Fibrous cartilage
- Hyaline cartilage

The elastic cartilage has a structure similar to hyaline. The difference between the two is due to the fact that the elastic cartilage is characterized by a lower amount of intercellular substance and large amounts of elastic fibers associated with collagen II fibers, which give greater flexibility and elasticity. These fibers form a three-dimensional network and are thicker and abundant in the central portion than in the peripheric areas.

Hyaline cartilage (from the greek hyalos, glass) is characterized by an amorphous component and a rich proteoglycans rich in fibrillar collagen II. Due to its intracellular component, the high presence of water, the surface smooth and the synovial fluid, the cartilage allows the joint to withstand pressure from various directions and to make joint movement without friction.

The three zones (Elastic cartilage - Fibrous cartilage - Hyaline cartilage) contain different collagen organization have different amounts of proteoglycans. Infact the superficial or tangential zone contains the highest collagen content, about 85% by dry weight. In addition, the collagen fibrils are oriented parallel to the joint surface, indicating that the purpose of this zone may be primarily to resist shear stresses. The amount of collagen decreases in each zone moving closer to the tidemark, dropping to 68% in the middle zone. Moreover collagen changes its configuration from a central area of a cartilage layer to a more peripheral area. The structure of the collagen network is thought to be related to the mechanical stability of the tissue [16].

(A) (B) (C)

(D)
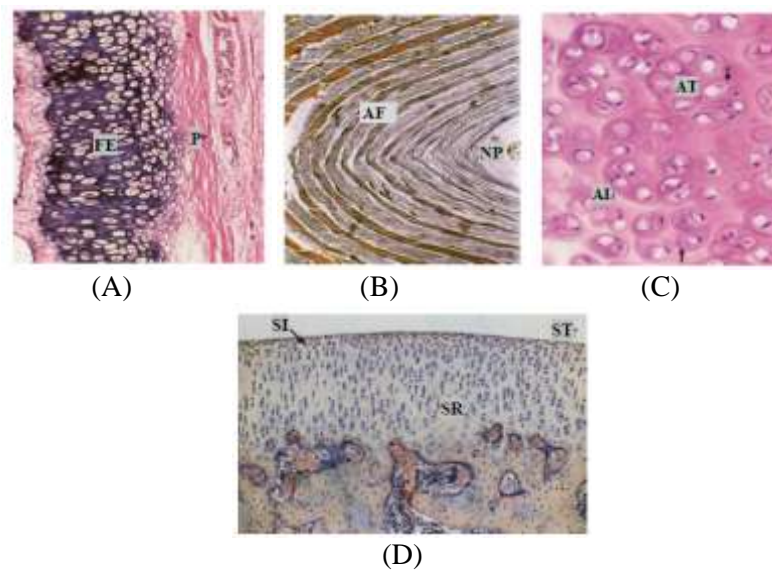
Fig. 12: A) cartilage, P = perichondrium, FE = elastic fibers; B) Cross section of disk inervertebrale, AF = fibrous ring, NP = nucleus pulposus; C) hyaline cartilage, AI = inter-territorial areas, AT = geographical areas, arrow = proteoglycan; D) articular cartilage, ST = tangential layer, IS = intermediate, SR = radial artery.

The surface layer of cartilage is like the wall of a pressure vessel that is designed to withstand the swelling pressure in the tissue; the collagen fibers are oriented to achieve an optimal tangential stiffness of the tissue. Chondrocytes have different shapes and different volumetric concentrations in the different layers of articular cartilage. A given chondrocyte shape produces different effects on the global material properties, depending on the structure of the collagen fiber network. The shape and volumetric concentration of chondrocytes in articular cartilage appear to be related to the mechanical stability of the matrix [16].

(A)   (B)
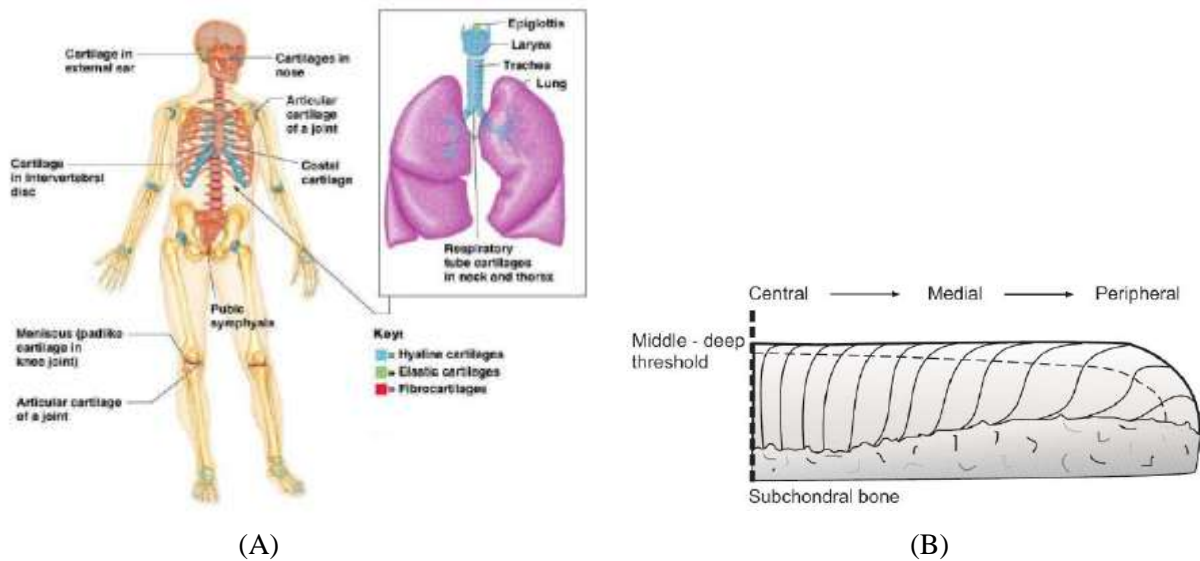
Fig. 13: (A) Cartilage types in the body. (B) Schematic representation of a normal collagen architecture from central area to peropheal area. Additional laminae are visible depending on the location in the joint.

1.2.1 Chondrocytes

Chondrocytes are quiescent cells derived from chondroblasts, was secreting. Is contained in lacunae of the extracellular matrix such capsules basophils. Their morphology and distribution is a function of the level of depth within the cartilage. In the intermediate zone appear rounded, enclosed in capsules and isolated, moving towards the perichondrium are increasingly flattened with major axis parallel to the surface and aggregated. These groupings are made for those groups isogenic cell mitosis and are characterized by three to five cells per capsule. Moreover, since the matrix is jerky, while separating the cells completely go away.

1.2.2 Extracellular matrix

The extracellular matrix consists of an amorphous component or ground substance, a fibrillar component (fibrous proteins) and high amount of interstitial fluid (mainly water) that makes the matrix well hydrated. It consists of several channels that allow diffusion of nutrients, oxygen and metabolic products. Can be divided into three main areas:

- Territorial, around the capsule basophil, characterized by an abundance of proteoglycans;

- Inter-territorial, characterized by a smaller number of rich proteoglycans and collagen;

- Pericellulare capsule, surrounds and protects the chondrocyte lacunae of mechanical stress.

1.2.3 Collagen components configuration

Collagen is the most abundant protein in the human organism. It is primarily responsible for the tensile behaviour of soft connective tissues, and in particular, tendons and ligaments. Collagen is characterised by a strongly hierarchical organization: small tropocollagen molecules link together to form fibrils, which in turn give rise to fibres and fibre bundles. The primary structure of the tropocollagen molecule consists of an uninterrupted sequence of about 300 Glycine-X-Y triplets, where X and Y are frequently represented by proline. During post-translational modification, hydroxylation, oxidation and glycosylation processes of amino acid residues usually occur [17]. The triplets organize themselves into a right-handed α-helix secondary structure and the conformational arrangement is defined by a left-handed helix tertiary structure. The quaternary super-structure of the tropocollagen molecule is obtained by linking three helixes by hydrogen bonds (figure 14). The molecule is approximately 300 nm in length and 1.5 nm in diameter [17]. Tropocollagen molecules are highly reactive and undergo spontaneous fibrillogenesis. For collagen types I, II, III, V and XI, tropocollagen molecules link together by inter-molecular covalent bonds to form fibrils (Figure 2.30), that are characterised by diameter and length ranging between 20 to over 280 nm [18] and 5 μm to over 1 mm respectively [19]. Possible sites of cleavage by chemomechanical caries removal reagents by degradation of glycine or hydroxyproline are indicated by red arrows. b, triple helix. Sites of cleavage by degradation of intra-molecular cross links are shown by red arrows. c, tropocollagen molecules link together to form fibrils and inter-molecular cross links are shown by arrows in the following figure.
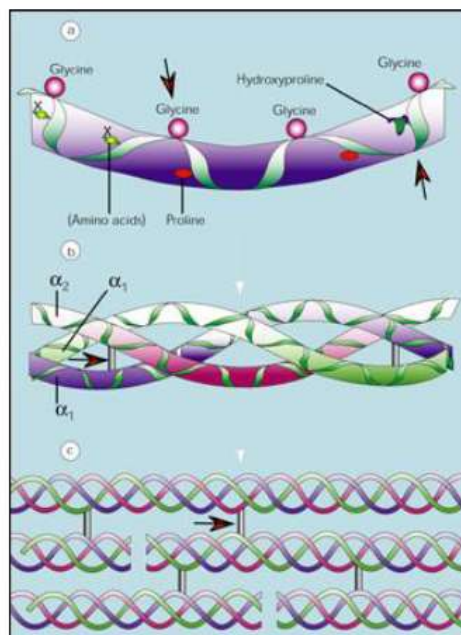
Fig. 14: Schematic representation of polypeptide chain.

1.2.4 Elastic components

Elastic fibers are a fibrous proteins found in large amounts in tissues and constist of two components: an amorphous central region containing elastin suttounded by a sheath of 14nm tubular microfibrils. The amino acid composition of elastin resembles that of collagen in that elstin is rich in glycine (Gly) and proline (Pro). Differences include greater quantities of valine (Val) and alanine (Ala) along with small amounts of hydroxyproline and no hidroxylysine.
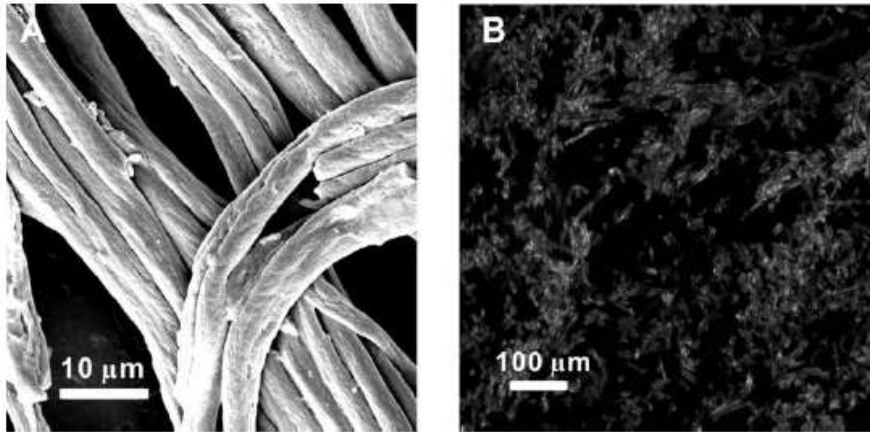
Fig. 15: (A) SEM image of elastic fibers with diameters in the range of 3 to 5 μm. (B) Fluorescence microscope image of immunostained fibrillin-microfibrils in elastic fibers.

Elastin contains two unsual amino acid, desmosine and isodemsmosine, formed by covalent reactions among 4 lysine (Lys) residues. These are organized in two repetitive sequences: Val-Pro-Gly-Val-Gly and Gly-Val-Gly-Val-Gly. Desmosine and isodesmosine need to be synthesized by a particular enzyme, lysyl oxidase, that contains copper. Elastin molecules are joined together by covalent bonds to generate an extensive cross-linked network. Because each elastin molecule in the network can expand and contracts as a random coil, the entire network can stretch and recoil lije a rubber. The effectively cross-links elastin and is thought to account for the rubberlike qualities of this protein. Through this structure and its numerous links, elastic fibers are capable of stretching to one and one-half times their length, yield easily to very small traction forces but return to their original shape when these forces are relaxed.
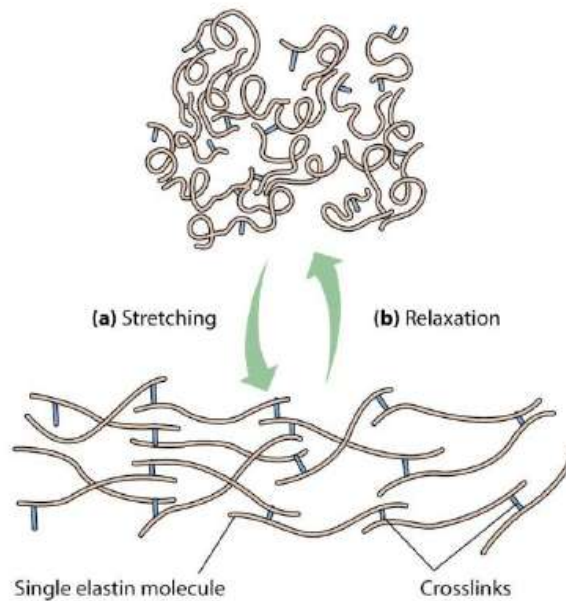
Fig. 16: Schematic explanation of stretching and relaxation of elastin molecules.

1.2.5 Ground substance

The amorphous intercellular ground substance is colorness, transparent and homogeneous. It fills the space between cells and fibers of the connective tissue. The ground substance is a viscous gel mainly composed of an electrolytic water solution and highly negatively charged proteoglycans (PGs). The water solution behaves as a pore fluid within the solid skeleton of the extracellular matrix and dissolved ionic species are mainly sodium Na^+ cations and chloride Cl^- anions. Proteoglycans are long molecular structures, developing along an axis made of hyaluronic acid (figure 17). On that axis are laterally attached other proteins (aggregans) structured around their own axis. Along this axis are attached in turn threads of amino-acids, called glycosaminoglycans (GAGs). The basic structure of GAGs is made by disaccharide units containing a uronic acid and an amino-glycan. The uronic acid displays a negatively charged carboxyl COO^- and the amino-glycan displays at least one sulphate SO_3^-. The two main GAGs that compose proteoglycans are chondroitin-sulphate with valence -2 and keratin-sulphate with valence -1. Because of the high water content of ground substance, proteoglycans are hydrated and electroneutrality is ensured by sodium cations [20].
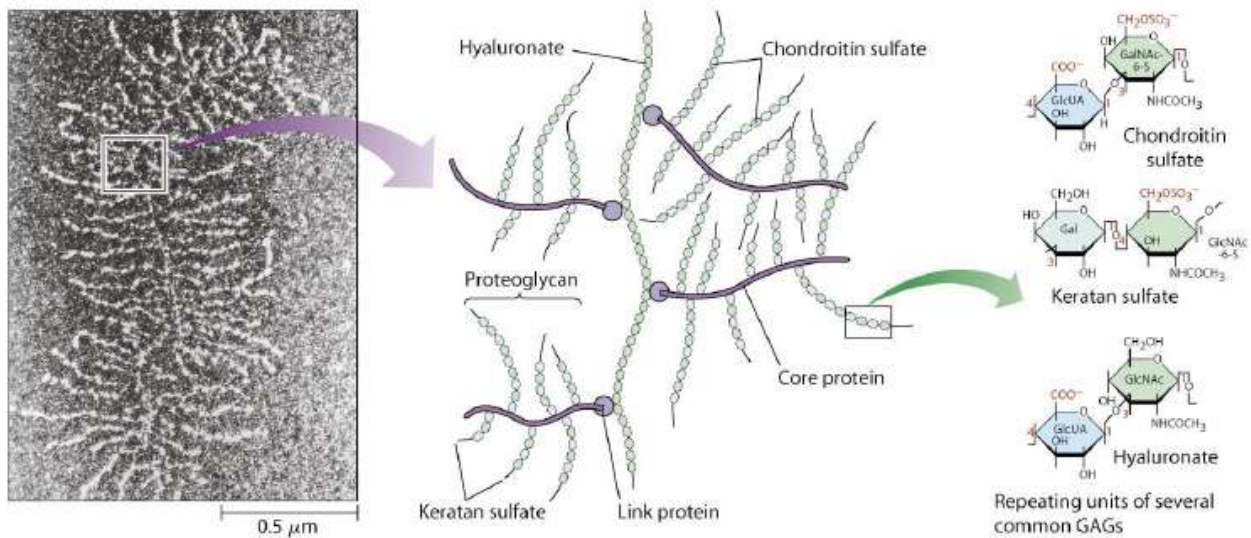
Fig. 17: SEM micrograph and schematic representation of proteoglycans structure.

The compressive properties of cartilage are partly provided by the proteoglycans that resist compression because GAGs repulse each other due to their negative charges (figure 18A). The presence of cations Na^+ shields the negative charges of the PG, and the mutual repulsive forces decrease with increasing sodium concentration [20]. Shielding results in decreasing macroscopic compressive moduli when the salt content increases (figure 18B) [21].
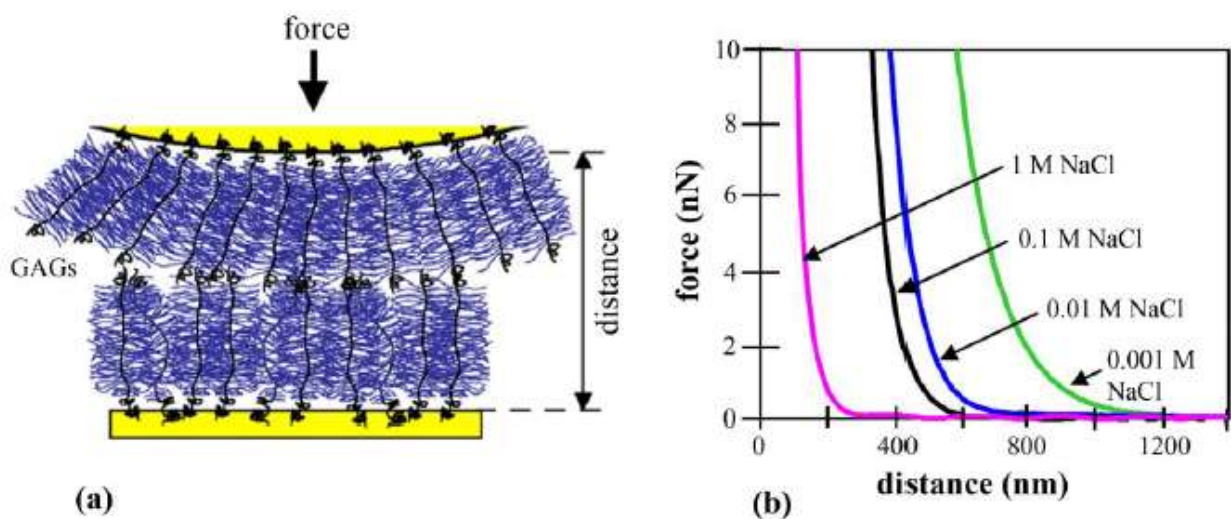
Fig. 18: Compressive mechanical behaviour of glycosamminoglycans in NaCl solutions. (A) Schematic representation of the experimental setup and (B) experimental results for different concentrations of NaCl [21].

1.3 Materials and methods

1.3.1 Technology

Tissue engineering strategies rely on the use of cells, bioactive factors, and scaffolds or combinations thereof. The scaffold serves the purpose of a delivery vehicle, a space-filling and structurally supportive agent, and can be designed to be biointeractive, i.e. to guide tissue regeneration. The coordinated regeneration of multiple tissues in the complex osteocondral and bone environment requires a deep understanding of their physiology and remodeling characteristics. Complex tissues must be engineered with the structural and functional characteristics of native tissue in a process that is not only biocompatible but also interactive and integrative with neighboring tissues simultaneously. Another challenge lies in that one type of tissue can be found in various structures that serve different functions and have therefore different properties. In our case, for example, the structures found in the bone and/or osteocondral region have very distinct characteristics. A specifically tailored approach may be required to regenerate a weight-bearing, dense, and bilaminar cartilage, and a quite different approach required to create a compact and mineralized bone. The extracellular matrix of bone has been described as a composite material composed of collagen type I fibrils mineralized with nanocrystals of hydroxyapatite [22]. Approximately 70% of bone by weight is composed of calcium salts, with hydroxyapatite $(Ca_{10}(PO_4)_6(OH)_2$ as the primary mineral constituent [23]. Moreover, the inorganic mineral component provides the mechanical strength of the matrix [24]. Desirable bone tissue engineering constructs are osteoconductive and osteoinductive. Review articles on bone tissue engineering considerations have been extensively published [25-30]. Our group have been proposing: a) natural biomaterials in conjunction with growth factors and/or cellular delivery to regenerate bone and cartilage; b) injectable systems modified to improve the matrix properties.

In general materials of natural, synthetic, semi-synthetic and hybrid origins have been proposed and tested as supports for tissue regeneration [31,32]. Synthetic and natural inorganic ceramic materials, such as hydroxyapatite and tricalcium phosphate, have been considered as candidates for injectable materials and biological active signals on scaffold surface or composition, for bone tissue engineering. These ceramics resemble the natural inorganic component of bone and possess osteoconductive properties [33].

Combining the literature whit our target, in the case (a) we propose a strategy employs the use of a scaffolds (natural polymer such as gelatin) and bioactive factors (hydroxyapatite crystalline); in the other case (b) the use of injectable biomaterial (hydroxyapatite or cellulose) bone filler.

To realize these systems, we propose two consolidate technologies: sol-gel technique for the hydroxyapatite formation, and liophylization due to obtain a gelatin or gelatin hybrid system porous scaffold.

SOL-GEL technique

The sol–gel process is a wet chemical method that needs an high pH value and not too high sintering temperature. This method offers a molecular mixing of the calcium and phosphorus which is capable of improving the chemical homogeneity. Moreover, the high reactivity of the sol–gel powders allows a reduction of the processing temperature and of any degradation phenomena during sintering. Many reported sol–gel processes require a strict pH control, vigorous agitation and a long time for hydrolysis. Here we will report a simple sol–gel method that does require controlling pH values, slowly stirring and short time for hydrolysis of phosphates [34].

Freeze-drying

Porous scaffolds have been manufactured using a freeze-drying, or lyophilization, technique [35,36]. Using this technique, a gelatin solution is solidified (frozen) to promote growing ice crystals, forming a continuous, interpenetrating network of ice. Sublimation of the ice crystals leads to formation of a highly porous sponge. The final pore structure depends on the underlying freezing processes during fabrication. The rapid, uncontrolled quench freezing process typically used in fabricating porous scaffolds via freeze-drying results in space- and time variable heat transfer through the suspension, leading to non-uniform nucleation and growth of ice crystals and, ultimately, scaffold heterogeneity. In localized regions of poor contact between the pan in which the suspension is frozen and the freeze-dryer shelf, there is a lower rate of ice-crystal nucleation than in neighboring regions, giving increased variation in pore size; due to poor heat conduction and the increased temperature of the suspension at these points, these areas have been termed 'hot spots'. So, concentration of the polymer solution and freezing conditions used determine the pore size and orientation of formed matrices, as the porous structure depends on the crystallization of water into ice in the homogeneous polymer solution. After frozen, the samples were lyophilized for a several hours: the water sublimation create the porous structure.

1.3.2 Materials

Natural polymers

✓ *Gelatin*

Collagens are the major structural proteins of most connective tissues as skin, bone and tendons, where they provide structural integrity to the tissues. The peculiarity of the amino acid sequence accounts for the characteristic coiled coil structure of the collagen molecule, where three distinct polypeptide chains, each of which is coiled into a left-handed helix, are thrown into a right-handed superhelix stabilized through interchain hydrogen bonds and covalent crosslinks. Thermal denaturation or physical and chemical degradation of collagen involves the breaking of the triplehelix structure into random coils to give gelatin. The present wide interest in gelatin is mainly due to its biodegradability [37].

Gelatin is a naturally occurring biopolymer derived from collagen, which is the major structural protein in the connective tissue of animal bone and skin [38].

As a protein-based biomaterial, gelatin is biodegradable and has no antigenicity under physiological conditions. Thus, it is an indispensable ingredient in modern pharmaceuticals. Tabata *et al.* [39] have explored gelatin hydrogels as a delivery system to achieve the controlled release of biologically active growth factors. When electrostatically complexed with a positively or negatively charged gelatin, an oppositely charged protein can be modified to increase its stability, targeting, and sustained release, leading to enhanced therapeutic efficacy. Gelatin exhibits very high bio-absorptivity when placed in vivo. In general, biocompatibility is governed mainly by the interface between foreign materials and host living cells/tissues. The intrinsic nature of the material including chemical composition, molecular weight, charge, and hydrophilicity may have an impact on the biocompatibility.

Gelatin is obtained by thermal, physical or chemical degradation of collagen which involves the breaking of the triple-helix structure. The result is a biodegradable, biocompatible and nonimmunogenic product, suitable for medical applications [40,42].

The collagen molecule consists of three polypeptide chains, alpha chains, that spontaneously coil together, zipper fashion, to form a right-handed helix [43,44]. The strands are held together primarily by hydrogen bonds between adjacent –COO and –NH groups, but also by covalent bonds [45]. The conversion of collagen to gelatin occurs through one of two processes: an acid process (gelatin type A) or an alkaline process (gelatin type B). The collagen to gelatin transformation

generally produces a mixture of single alpha (MW = 80,000 to 125,000), double alpha (also known as beta, MW = 160,000 to 250, 000), and triple alpha (also known as gamma, MW = 240,000 to 375,000) stranded gelatin [46]. All the molecular species resulting from the processing of collagen to gelatin are considered to be gelatin provided that the molecular weight exceeds an arbitrary minimum of approximately 30,000 [47].

It is important to know by which of these two processes the gelatin was made, since the two types differ in properties: different viscosity, gel strength (Bloom index) and different isotonic point. Infact, the network structure and the physical properties of the gelatin gels are mainly conditioned by the source and the conditions of extraction of the gelatin.

The processing of collagen can produce two types of gelatin with different isoelectric points (pI). The alkaline process, through hydrolysis of the asparagine to aspartic acid and glutamine to glutamic acid, yields a gelatin (Type B) with a high density of carboxyl groups, which makes the gelatin negatively charged with an isoelectric point of 4.5-5.2 [38,46]. The acid process, which is less invasive, produces little change in the isoelectric nature of collagen. As a result, the isoelectric point of the gelatin (Type A) that is obtained will remain similar to that of collagen, between 7-9. Gelatin swells least at its isoelectric point and it swells more in solutions of pH above and below its pI [48]. In general, gelatin extracted at lower temperature is stiffer, and exhibit greater value of the Bloom index, which is a measure of the stiffness of the hydrogel [38].

It has been reported that the increase in Bloom index of the gelatin leads to a remarkable improvement in the mechanical properties and a significant reduction in water-absorbing capacity of the membranes [38]. In addition, the Bloom strength strongly affects the atomistic structure of gelatin and therefore its biomedical applications including tissue engineering and drug delivery. Furthermore, the mechanical properties of drawn gelatin films have been related to the denaturation level of the protein, that is the triple-helix content, evaluated through differential scanning calorimetry [37].
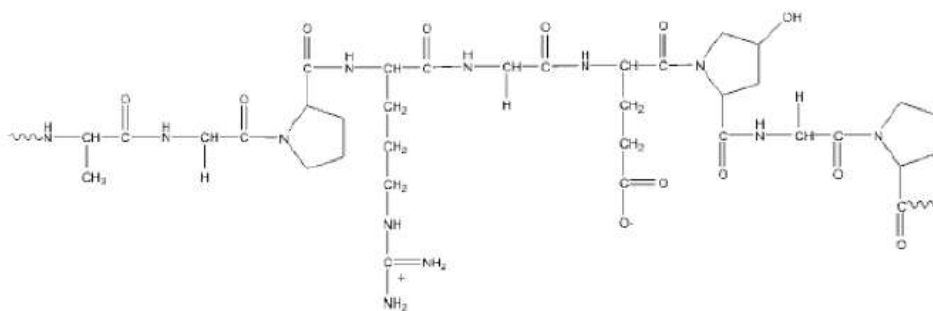
Fig. 19: Gelatin structural unit.

Alanina	11.3
Arginina*	9.0
Acido aspartico	6.7
Acido glutammico	11.6
Glicina	27,2
Istidina*	0,7
Prolina	15,2
Idrossiprolina	13,3
Idrossilisina	0,8
Isoleucina*	1,6
Leucina*	3,5
Lisina*	4,4
Metionina*	0,6
Fenilalanina*	2,5
Serina	3,7
Treonina*	2,4
Triptofano*	0,0
Tirosina	0,2
Valina*	2,8

Table1: amminoacids (g) for 100g of gelatin.

Chemical structure. Regarding the chemical structure of gelatin, being it a protein, it contains 18 different amino acids (AA) linked together in sequence to form polypeptide chains of about 1000 AA for chain, known as primary structure (Table 1). The most frequent amino acid sequences are: - (Gly-X-Pro) n-and - (Gly-X-Hypro) n [37]. The most frequent amino acid sequences are: - (Gly-X-Pro $_n$- and -(Gly-X-Hypro)$_n$. As reported in the table 1 glycine, proline and lysine are present in the extremely high concentration. In general, regardless of the type of extraction, gelatin obtained is a heterogeneous mixture of single or multi-stranded polypeptides, each with extended left-handed proline helix conformations and containing between 50 – 1000 amino acids.

Serine, theronine, aspartic acid, and glutamic acid are predominate at the N-terminal in alkali processed gelatin and alanine in the acid processed gelatin [49]. At the C-terminal, glycine, glutamic acid, and aspartic acid are the predominate amino acids [49]. Amino Acids are linked together by peptide bonds, covalent bonds between the carbon atom of an AA carboxyl group (COOH) and the nitrogen atom of another AA amino group (NH_2). Amino acids are characterised by the presence in their structure of simultaneously basic (NH_2) and acid (COOH) groups, bound to an α carbon atom in an hydrocarbon chain.

A key feature of collagen is its "isoelectric point", or pI, that is represented by the medium's pH value at which the protein's positive and negative charges balance each other; in other words, the protein is in a state of great reactive inertia.

At pI value, collagen presents a great chemical and physical inertia, characterized by:

• Low tendency to react;

• Low viscosity;

• Minimal swelling.

Thanks to the large number of functional side groups it contains, gelatin readily undergoes chemical cross-linking, which is very important for its possible use as a biomaterial. In fact, as collagen based biomaterials are rapidly degraded in vivo, their structure must be reinforced so that they will not significantly alter in the body for the required period. Since gelatin is soluble in aqueous solution, gelatin materials for long-term biomedical applications must be submitted to crosslinking, which improves both the thermal and the mechanical stability of the biopolymer [38].

Crosslinking. Depending on what degradable properties are desired, different cross-linking treatments, including chemical and physical methods, can be used to prolong the absorption of the gelatin. Physical cross-linking methods include drying, heating or exposure to gamma or ultraviolet radiation. The primary advantage of physical methods is that they do not cause potential harm. However, the limitation of such methods is that obtaining the desired amount of cross-linking is difficult . In chemical cross-linking methods, cross-linkers are used to bond functional groups of amino acids [50-53]. Because gelatin itself is nontoxic, it is important that the crosslinking agents also are nontoxic to the cells that will attach to the scaffold. However, many chemical cross-linking agents are cytotoxic as a result of the residual unreacted cross-linking agent or the degradation products that result from hydrolytic or enzymatic degradation [51,52,54].

According to the cytotoxic study, Sisson and colleagues compared the most commonly agent for crosslinking gelatin: glyceraldehydes, glutaraldehyde and genipin. Glutaraldehyde is the most commonly used agent for crosslinking collagen and gelatin. It is inexpensive, soluble in aqueous solution and has a rapid reaction rate due to the many available amine groups in proteins [55]. Glutaraldehyde reacts to form crosslinks in two different ways. First, the aldehyde group can react with the amine group of lysine, hydroxlysine, or arginine in the collagen polypeptide and form a Schiff base [55]. Second, two adjacent aldehydes can undergo aldol condensation [55]. Glutaraldehyde has, however, been shown to be cytotoxic at high concentrations. The residual unreacted glutaraldehyde, cross-linked collagen and gelatin, and the products from the hydrolytic degradation of the cross-linked collagen are cytotoxic [56]. Cytotoxicity can be reduced by using low concentrations of glutaraldehyde for crosslinking and thoroughly washing the scaffolds before use in tissue engineering applications. D,L-Glyceraldehyde has been used to cross-link gelatin and

is nontoxic. Furthermore, glyceraldehyde is a natural product of a metabolic process. Studies suggest that gelatin crosslinked with glyceraldehyde is well tolerated in vivo. However, the mechanism of the cross-linking reaction between glyceraldehydes and amine groups remains widely debated and the subject of continued discussion [56].

In the present study we propose the gelatin scaffold realized by freezing-dried, cross-linked with 1-ethyl-3-(3-dimethylaminopropyl) carbodiimide (EDC) was proposed.

EDC reaction. The mechanism of crosslinking with carbodiimide involves the formation of an *O*-acylisourea derivative between carbodiimide and the carboxylic acid groups of glutamic and aspartic acid residues in gelatin molecules, followed by a nucleophilic substitution with an amino group, most often -NH$_2$ of a lysine residue [57]. No spacer is introduced for this amide-bond-type crosslinking [58].
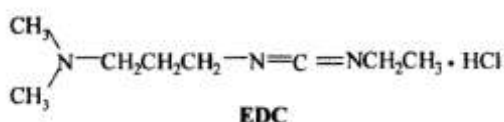
Fig. 20: 1-ethyl-3-(3-dimethylaminopropyl) carbodiimide (EDC) structure.

However, Nakajima and Ikada [59] reported that amide formation from carboxyl and amino groups in aqueous media in the presence of carbodiimide required the formation of carboxylic anhydride as an intermediate. Hence, carbodiimide may couple carboxylic acid and amino groups that are located within 1.0 nm of one another [60]. Therefore, carbodiimide may form intramolecular crosslinks within a gelatin molecule or short-range intermolecular crosslinks between two adjacent gelatin molecules as long as the crosslinked carboxylic acid and amino groups are less than 1.0 nm apart. The free-amino-group contents of the EDC-crosslinked gelatin hydrogels declined significantly within 30 min of crosslinking and stayed at their minimal values subsequently [61]. This indicated that the crosslinking of a gelatin hydrogel with carbodiimide was essentially completed within 30 min after the initiation of crosslinking. It has been reported that carbodiimide crosslinking is a rapid reaction [58,62].

As Hsing-Wen Sung et *al.* [61] have reported, the reduction in the free-amino-group content for the carbodiimide-crosslinked gelatin was approximately 33%. This was because carbodiimide could basically form intramolecular and short-range intermolecular crosslinks within collagen based

materials, and each crosslinking produced with carbodiimide simply consumed one free amino group [61].

Gelation. Gelatin has the ability to immobilize liquid and undergo gelation. Gelation is a disorder to order transition usually induced by cooling and is always reversible. Gelation begins with conformational changes which result in partial unfolding of gelatin within the solution, exposing the interior reactive region of the gelatin. As the gelatin is cooled, the unfolded proteins create a network throughout the system through intermolecular contacts or covalent bonds. The network is then stabilized by secondary forces rather than by covalent bonds and the intermolecular attractions are negligible [63]. As the molecular network develops, additional gelatin molecules become attracted through electrostatic interactions. This ultimately leads to a more rigid structure and thickening of the gel. The maturation process involves two processes: an increasing order and stiffening of the network and general thickening of the whole network. As the gel continues to cool, additional parts of the gelatin chain become more ordered and stable due to the growth of existing links and formation of new links (both physical and chemical bonds) [63]. The decrease in temperature causes the water molecules to be less mobile, the hydrogen bonds remain intact, ultimately rendering the chains immobile. The ability of the chains to continue to re-organize is lost. A slow cooling rate produces a strong, stable network.
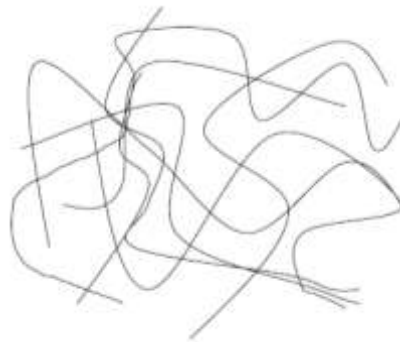
Fig. 21: Fishnet structure of gelatin with strong points separated by flexible strands.

Russo [64] morphologically classified gelatin as a fishnet gel (figure 21) in which cross-links, whether reversible or covalent, provide 'strong points' of the structure (formation of crystallites) and are separated by flexible strands which provide elasticity. The strong points within the gelatin strands are due to intermolecular cross-linking (interstrand) that can occur between arginine-lysine or arginine-arginine within the same strand. Amino acid residues from two neighboring strands may

also interact and form intramolecular (intrastrand) cross-linked strands that provide strength to the gelatin.

Swelling phenomena. Two physical processes occur when a gelatin matrix is exposed to water. The first phase is the transition to a rubbery state as water penetrates the gelatin matrix and mobilizes the entangled strands [65]. The second phase is the continual swelling of the rubbery network as more water is absorbed. The rate of water absorption will be governed by pH of the environment, gelatin isoelectric point (pI), moisture content, particle size, presence of dissolved salts, and the extent of cross-linking. The pH and the isoelectric point are important because when the pH of the environment and the isoelectric point are equal there is a net neutral charge on the gelatin. At this point, there is minimal absorption and swelling. Extensive swelling is seen when the pH deviates from the pI range. The extent of cross-linking is an essential characteristic of the delivery system due to its ability to reduce polymer chain mobility, increase glass transition temperature and decrease molecular diffusivity.

Factors that influence the swelling:

a) **Effect of Bloom strength**

The gel strength is one of important criteria which determine the quality of gelatin as required by manufacturers and users. It indicates the hardness, stiffness, firmness and compressibility of the gel at a particular temperature and concentration. It is associated with the contents of proline and hydroxyproline in gelatin and molecular weight [66]. In general, a high molecular weight gelatin gives a high Bloom value [67].

Haixia Ren et *al*. [68], supposed that it is difficult to develop a firm network formation for low molecular weight protein chain, so as to hydrogel cannot be formed. The Bloom strength has a significant influence on the swelling behavior of hydrogel: in fact lower swelling ratio was observed at higher Bloom strength. This is most likely due to a higher molecular weight gelatin chain, which are able to interact with one another and are prone to form a more compact network, and hence a lower water holding capacity.
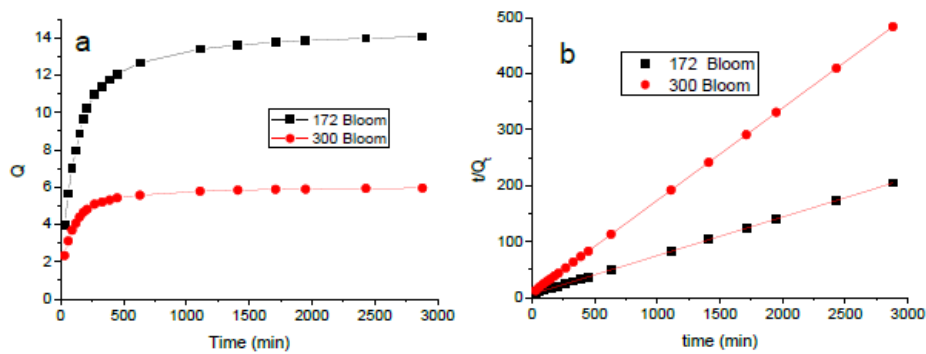
Fig. 22: The swelling ratio Q (a) and t/Qt (b) of gelatin-based hydrogels obtained with different Bloom strength gelatins versus the swelling time [68].

b)   Effect of temperature

The equilibrium swelling and swelling ratio is significantly different over the temperature range of [25 – 50]°C. It is known that the ratio increases with increasing the temperature. Moreover, the swelling rate is not significantly affected when the temperature exceeds 30°C. On the other hand, the swelling at lower temperature (25°C to 30°C) shows a much lower swelling rate. The observed results can be explained by the fact that when the temperature increases from lower to 30°C, the water sorption capacity increases significantly due to an increased segmental mobility of hydrogel chains. Several studies [69,70] have investigated that gelatin gel involves formation of triple helical sequences connected in an essentially random fashion by peptide sequences in disordered conformation. The gelatin chains in hydrogel revert partially to the tropocollagenic triple helix, from disordered to rather ordered status, depending on temperature, concentration and rate of cooling. This phenomenon occurs usually at around 28°C, where the coil to helix transition is observed. And when a crosslinker was introduced the resulting gelatin hydrogel is composed of both chemical and physical cross-links. The result is that parts of either three chains or two chains in a physical ''hair-pin'' bond type [71] are stabilized mainly through hydrogen bonds, forming thus a basic physical network coupled to the covalent one (figure 23, left). As temperature increased to 30°C, the hydrogen bonds within tropocollagenic triple helix break (figure 23, right), and a majority of triple helix disappear. Therefore, the hydrogel chains become more mobile and the swelling of hydrogel is increased. However, on increasing the temperature from 30°C to 50°C, the hydrogel chains must have acquired complete relaxation, so that with a further increase in temperature, they do not loosen and, as a consequence, no appreciable change in swelling behavior could be observed at a higher temperature.
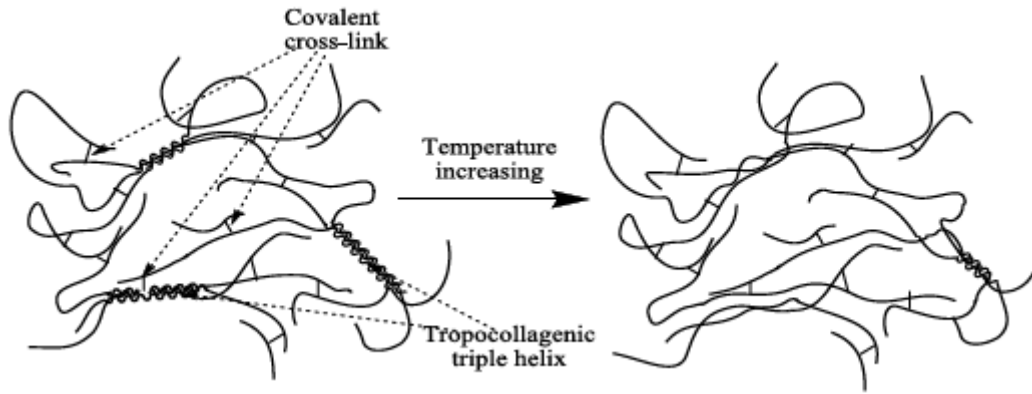
Fig. 23: Scheme illustrating a gelatin hydrogel network [68].
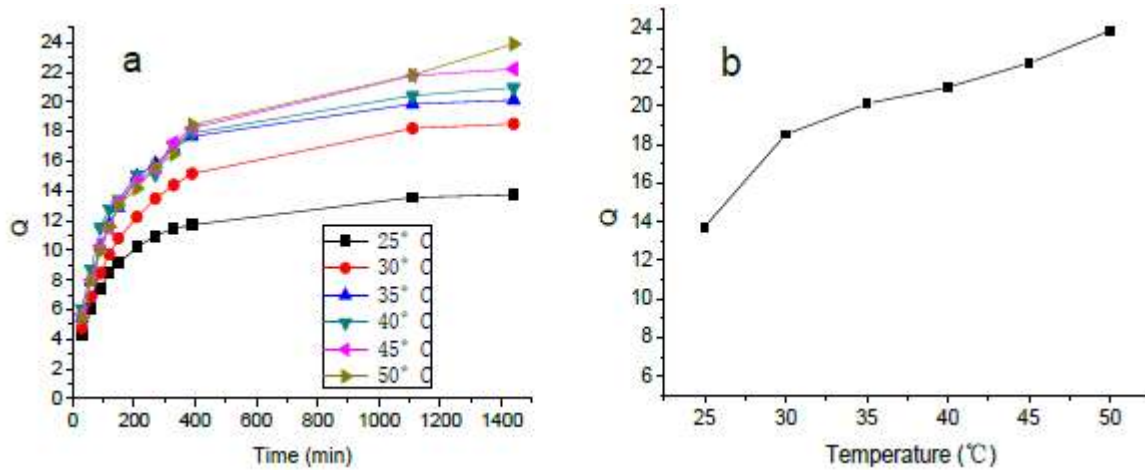
Fig. 24: The effect of temperature on the weight equilibrium swelling ratio in distilled water. (A): Swelling behavior of hydrogels at different temperature. (B): Viability of swelling ratio immerging in distilled water for 24h at different temperature [68].

c)   Effect of pH

Ionic hydrogels exhibit swelling changes at a wide range of pH values. Since the swelling capacity of all "ionic" hydrogels is appreciably decreased by addition of counter ions to the swelling medium [72] , without any buffer solutions.

Haixia Ren et *al*. [68], have used a series solutions with acidic and basic pH values, prepared by dilution of NaOH (pH 12.0) and HCl (pH 1.0) solutions to achieve pH>6.0 and pH < 6.0, respectively.

Figure 25 (A) shows the effect of pH on the swelling ratio of hydrogel. The results clearly indicate that the hydrogel exhibits extensive swelling in the swelling medium of pH<2 and pH>8, whereas the hydrogel demonstrates low degree of swelling in the medium between pH 3 to pH 7.

In general, a polyampholytic gelatin hydrogel crosslinked presents a network that contains positive and negative ionizing groups. In acidic medium, gelatin acts as base and takes up H^+ ions from the medium forming $-NH_3^+$ and $-COOH$ and proteins become positively charged. In alkaline medium, protein acts as an acid gives H^+, forming $-COO^-$ and $-NH_2$ groups and proteins become negatively charged. In an acidic environment, the swelling is controlled mainly by the $-NH_3^+$, in basic medium by COO^-, and between pH 3.0 and 7.0 by $-NH_3^+$ and COO^-. In figure 25 (A), we can observe that in basic medium the swelling is higher; this behavior is due to the presence of the hydrophilic functional groups (mainly COO^-) in the gelatin structure. Moreover, the gelatin hydrogels begin hydrolyze in a pH close to 11.0, giving up carboxy groups, which also result in increasing of swelling ratio. The swelling datum of pH 12 was not present in figure 25 (A) because the hydrolysis degree of hydrogel sample was too severe to measure the swelling ratio accurately.

d)   Effect of salts

The swelling ratio is mainly related to the characteristics of the external solution, such as charge number, ionic strength and polymer nature, i.e. network elasticity, presence of hydrophilic functional groups, and extent of crosslinking density [73].

Same study have demonstrated that the electrolyte effect has been observed by adding univalents salts to the external solution in the concentration range 0.05M to 0.5 M and the results are depicted in figure 25 (B). It could be noted that the swelling ratio of the hydrogel increased in the concentration range investigated. This situation between the swollen hydrogel and the surrounding aqueous phase is usually described as a Donnan equilibrium where the biopolymer network acts as its own membrane [74,75] thus preventing the diffusion of the attached ionizing groups toward aqueous phase. Therefore, the osmotic pressure resulting from the mobile ion concentration difference between the gel and aqueous phase increased in a certain range of NaCl concentration, and consequently, the swelling ratio increased. A similar type of increase has also been reported by Baker [76] and Bajpai [77] in ampholytic and non-ionic acrylamide based hydrogels. The effect of cation type (cations with different radius and charge) on swelling behavior is shown in figure 25. From these data, a distinct effect on swelling ratio could be found for trivalent cations ($FeCl_3$, $CrCl_3$) comparing to monovalent (NaCl) and divalent ($CaCl_2$). Electrostatic screening effect and ionic crosslinking are the main explanations for the intense loss of swelling [73]. The electrostatic

screening effect of salt can weaken the electrostatic interaction and de-swell hydrogel through causing a non-perfect anion-anion electrostatic repulsion. As for ionic crosslinking, it is well known that gelatin hydrogels consisting of carboxylic groups can chelate with multivalent cations, such as Cr^{3+}, and Fe^{3+} ions, which leads to network contraction and decreases porosity of the gel network, therefore, results in the deswelling of hydrogels. It could be noted from figure 26 that $CaCl_2$ affect the swelling behavior of hydrogel non significantly, and the swelling ratio was slightly higher than that in distilled water. Moreover, the swelling ratio increases when NaCl concentration range is from 0.05M to 0.5 M. Therefore, the effect of the ionic crosslinking acts as more effective factor against swelling rather than the electrostatic screening effect of the cation [68].

(A) (B)
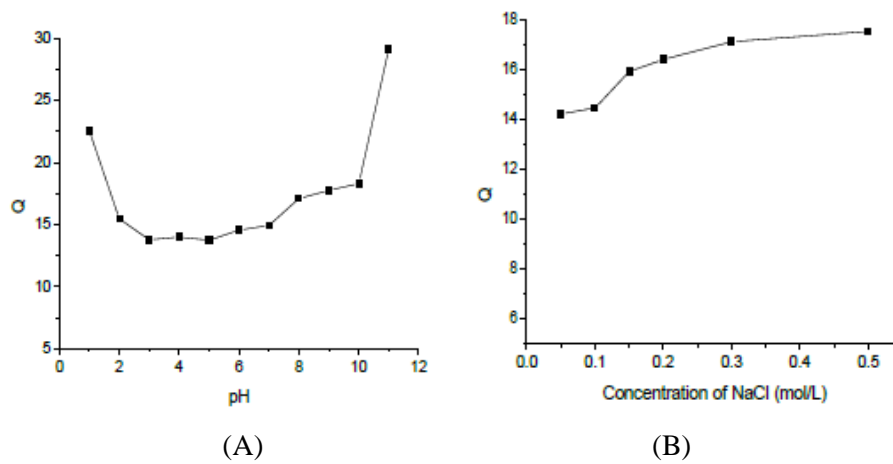
Fig. 25: (A) Effect of pH of solutions on swelling capacity of the hydrogel at 25°C for 12h [68]; (B) The swelling ratio of the hydrogel in NaCl solution with the concentration range 0.05M to 0.5M 25°C for 12h.
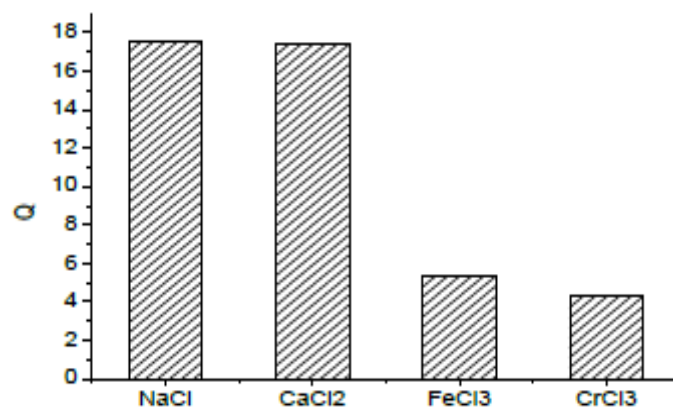
Fig. 26: Swelling capacity of hydrogel in different chloride salt solutions at 25°C for 12h [68].

Dissolution. The dissolution of a polymer into water involves two transport processes, solvent diffusion and chain disentanglement [78]. The dissolution of an uncross-linked, amorphous, glassy polymer occurs when a solvent diffuses into the polymer forming a gel-like layer. This layer is formed due to the increased mobility of the polymer strands and is contiguous to the solvent-polymer front. After an induction time (dissolution is not immediate upon polymer exposure to water), the polymer dissolves [78].

Semicrystalline polymers, such as cross-linked gelatin, undergo a slightly different dissolution process. Semicrystalline polymers contain both amorphous and crystalline sections spread throughout the polymer. An additional step, unfolding of the crystalline regions, must take place in order for the polymer to dissolve when exposed to a solvent. The penetration of solvent into the amorphous sections is fast and extensive because of their lower density, producing high initial swelling rates and leading to high equilibrium uptakes [79]. Crystalline regions are more tightly ordered with a higher density resulting in a limited and slower penetration of the solvent. The equilibrium swelling of the crystalline sections is considerably less extensive than that of the amorphous regions because the regular arrangement of the polymer chains in the crystallites results in greater lateral interchain attraction and greater elastic forces resisting expansion and swelling [79]. The final step in the dissolution process is chain disentanglement in which the polymer structure falls apart and dissolves.

The dissolution of polymer and non-polymer materials differs in two ways. Polymers require an induction time before starting to dissolve, while non-polymeric materials can dissolve instantaneously [78]. The external mass transfer resistance through a liquid layer adjacent to the solid-liquid interface (diffusion layer and its thickness) generally controls non-polymeric material dissolution. Polymer dissolution can be controlled either by the disentanglement of the polymer chains or by diffusion of the chains through a boundary layer adjacent to the solvent-polymer interface [78]. These processes contribute to the induction time prior to the polymer dissolution.

Type of chemical bond importance for polymer degradation. It is mainly the type of bond within the polymer backbone that determines the rate of hydrolysis [80]. Several classifications for ranking the reactivity exist which are either based on hydrolysis kinetics data for polymers [81,82] or are extrapolated from low-molecular weight compounds containing the same functional group [83]. Reactivities can change tremendously upon catalysis [84,85] or by altering the chemical neighborhood of the functional group [86] through steric and electronic effects in is demonstrated that steric effects decrees the degradation, because the voluminous group hinders the attack of

water. Polymer erosion is far more complex than degradation, because it depends on many other processes, such as degradation, swelling, the dissolution and diffusion of oligomers and monomers, and morphological changes. Although degradation is the most important process of erosion, depending on the type of polymer, other parameters may also become critical in controlling erosion behavior. The knowledge of the erosion mechanism is, therefore, most important for the successful application of a degradable polymer. In tissue engineering, surface properties or porosity determine the performance of implantable scaffolds [87]. For example, in drug delivery, swelling and porosity are critical to the release behaviour of drugs". As with degradation, many different indicators of erosion have been proposed, such as molecular weight loss, sample weight loss and changing geometry.

Degradation and erosion phenomena. All degradable polymers share the property of eroding upon degradation. Degradation and erosion are the decisive performance parameters of a device made of such materials. To classify degradable polymers a distinction is made between surface [or heterogeneous) and bulk (or homogeneous) eroding materials [88], which is illustrated in figure 27. During an application, surface eroding polymers lose material from the surface only. They get smaller but keep their original geometric shape. For bulk eroding polymers, degradation and erosion are not confined to the surface of the device. Therefore, the size of a device will remain constant for a considerable portion of time during its application [89].
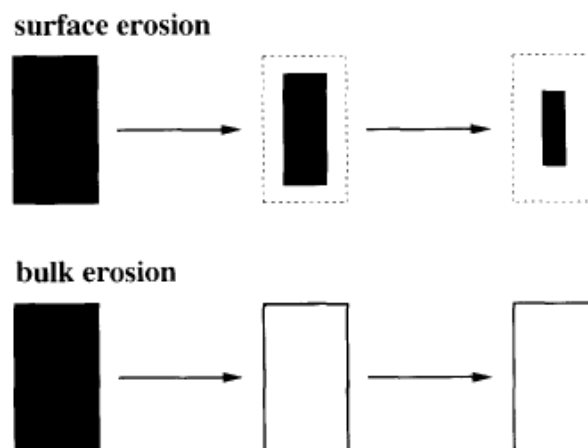
Fig. 27: Schematic illustration of surface erosion and bulk erosion [90].

The first morphological changes during erosion are confined to the polymer surface. With proceeding erosion, polymers change to more porous structures [90].

As already mentioned, the degradation rate depends strongly on pH. Through the chain scission, polymers are transformed into oligomers and monomers, which have different functional groups than the polymer [90].

✓ *Cellulose*

Cellulose is the world's most abundant natural, renewable and biodegradable polymer. It is produced by various species in nature, both plants and other organisms. It has versatile properties such as hydrophilicity, chirality, biodegradability, biocompatibility etc. Similarly to other polysaccharides, cellulose has a long background in medical applications, essentially due to its lack of toxicity (monomer residues are part of metabolites found in the human body), water solubility or high swelling ability, and stability to temperature and pH variations. The biocompatibility of unmodified and derivative cellulose is well documented.

Chemical properties. The structure of cellulose can be described as a carbohydrate polymer with repeating D-glucose units which are covalently linked through $\beta(1{\rightarrow}4)$-glycosidic bonds. The most stable conformation about the $\beta(1{\rightarrow}4)$ linkage involves alternating 180° flips of every second glucose unit, so that the repeating unit of cellulose is rather a cellobiose molecule than a glucose unit.
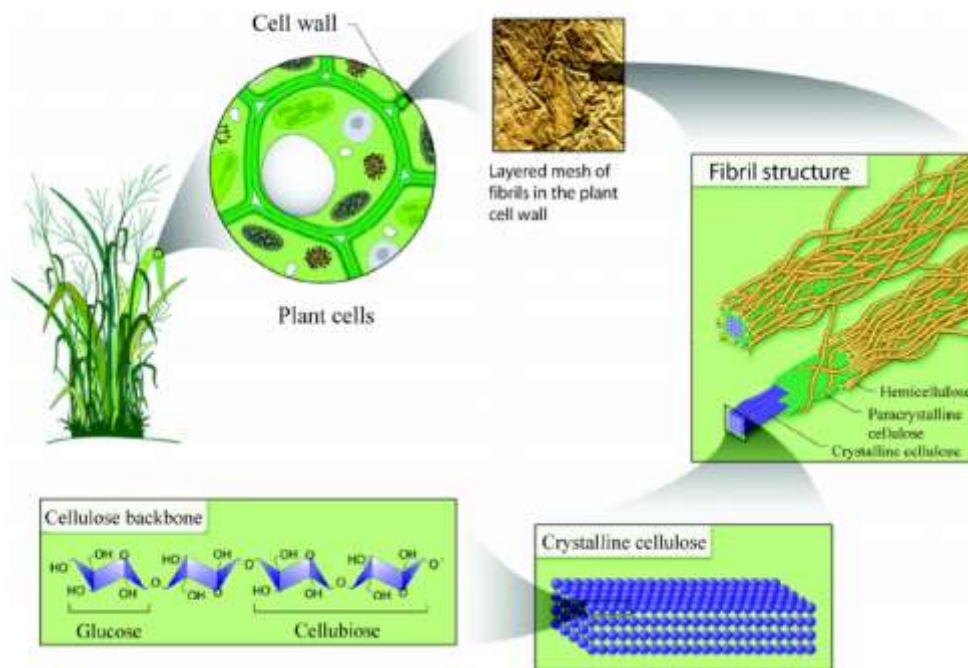
Fig. 28: The cell wall hierarchy, from a single cellulose polymer to the cellulose fibre composite.

Thus, cellulose is a polymer with multiple hydroxyl groups which form hydrogen bonds with oxygen atoms on the same or an adjacent chain, holding the chains firmly alongside each other. In other words, the cellulose molecules form long, straight chains which are strengthened by intramolecular hydrogen bonds and van der Waals interaction, which pack together to form crystalline structures. Cousins and Brown Jr. [91] also showed that the hydrophobic groups contributed to the crystal stability by calculating the inter- and intramolecular energy for cellulose forms.

Due to its supra-molecular structure, the solid state of cellulose reveals as both crystalline (high order) and amorphous (low order). The crystalline structure of native cellulose appears as cellulose I, presenting in two polymorphs: triclinic (Iα) and monoclinic (Iβ) which appear alongside each other. Iα and Iβ are two crystalline allomorphs phases of native cellulose (cellulose I) [92]. The main difference between the two crystalline phases is the relative position of the chains to each other. This difference brings a staggered conformation to the cellulose chains in the Iβ phase, stabilising the structure like bricks in a wall. Allomorph Iα can irreversibly be transformed into Iβ by annealing (slightly heating), thus Iβ is the most stable phase.

Corresponding to the inter- and intra- molecular hydrogen bonds, cellulose may occur in other crystal structures, e.g. cellulose II, III and IV. By treatment with aqueous sodium hydroxide (mercerization) or by dissolution of the cellulose followed by precipitation, cellulose II which has an antiparallel orientation, in contrast to native cellulose parallel chains (figure 29) can be formed. The conversion cannot be reversed, indicating that cellulose II is more stable. Cellulose III and IV can be produced by treatment with various chemicals and in combination of heating and pressure [93- 94].
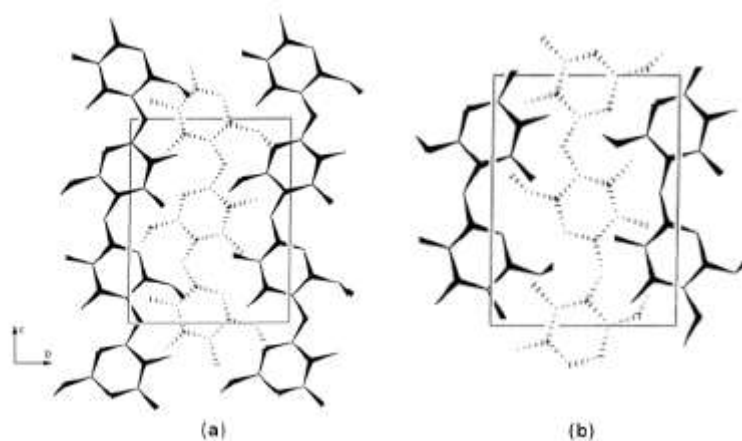
Fig. 29: Projection of a two-chain model of cellulose I and II. (a) cellulose I: parallel orientation; (b) cellulose II: anti-parallel orientation [93].

The properties and numerous applications of cellulose depends highly on its chain length and its fiber morphology. The chain length, i.e the number of glucose units, varies with the origins and the chemical treatment of the raw materials. The chain length for a cellulose from wood pulp is between 300 and 1700 units; cotton and other plant fibers have the values ranging from 800 to 10,000 units; bacterial cellulose are observed to have similar range as cotton and other plant fibers. The number of the repeating units of the regenerated cellulose varies depending on the dissolution/regeneration process, Klemm *et al.*[94] reviewed that it is about 250-500. Powdery cellulose can be produced from partial chain degradation, yielding chain length of 150-300 units, e.g microcrystalline cellulose.

Cellulose is insoluble in water and in most conventional organic solvents. Most of the literatures agree on that the insolubility of cellulose is due to the hydrogen bonding between cellulose and the solvent. However, Lindman *et al.* [95] has another explanation on that, which is that the amphiphilic property of the cellulose draws strong attention to the hydrophobic interactions which may result in low aqueous solubility. Yamane *et al.* [96] also reported the hydrophobic nature of cellulose from a structural point of view.

Cellulose derivatives. This work is focused on the preparation of new environmentally friendly hydrogels derived from cellulose and hence originating from renewable resources and characterized by biodegradable properties. Two cellulose derivatives, sodium carboxymethylcellulose (CMCNa) and hydroxyethylcellulose (HEC), were used for superabsorbent hydrogel preparation. CMCNa and HEC are crosslinked hydrophilic polymers insoluble in water, but capable to absorb large amounts of water through a swelling process. Swollen hydrogels swell to a volume much larger than their original size with a weight 10–1000 times higher than their initial one. The swelling capacity of hydrogels has been studied by different authors, as already reported for gelatin. It is well known that the presence of fixed charges, typical of polyelectrolyte gels, determines a significant swelling of the polymer in water. This behavior is due to a Donnan equilibrium established between gel and the external solution, whose ionic strength strongly affects the swelling degree [97]. In the previous works, [98,99] cellulose-based superabsorbent hydrogels, with sorption properties similar to those displayed by traditional acrylate-based products were synthesized and characterized by reacting in water mixtures of CMCNa and HEC crosslinked with divinylsulphone (DVS) or with a carbodiimide crosslinking agent. In this study citric acid (CA), a new crosslinking agent able to overcome toxicity and costs compared with the former reagents was selected.

Cellulose crosslinking reaction. CA, widely used in food and drug industry, is an excellent crosslinking agent. CA, extensively widespread in nature (lemon juice contains 5% of CA), is prepared commercially by fungal fermentation of glucose. CA and its salts, with a good affinity for metal ions, are used in a wide variety of applications: in soft drinks and effervescent salts, as an antioxidant in food, as a sequestering agent for metal ions, as a cleaning, and polishing agent for metals, as a mordant in dyeing. Moreover, CA and its salts have fundamental biological functions. For example, CA is involved as intermediate in the ''Krebs cycle'' in all living cells, also known as ''citric acid cycle'' for the production of usable energy [100]. Recently, CA was used as crosslinking agent in various cellulose derivative systems [100-102] and different mechanisms have been proposed in the literature to explain the crosslinking reaction of cellulose polymers with CA. Xie et *al*. [102] for example, studied the optimum conditions for corn starch and CA reaction to produce resistant starch and studied the thermal stability of citrate starch products. The authors reported that when CA is heated, it will dehydrate to yield the cyclic anhydride that reacts with starch; successively anther cyclic anhydride function can be achieved into CA structure through the other two non-reacted carboxylic groups allowing the attachment of another hydroxyl starch group (Fig. 30). Coma et *al*. [101] carried out the crosslinking of hydroxypropyl- methyl cellulose with CA simply heating the reagents and determining the rate of crosslinking. According to Zhou et *al*. [103] the two main stages of the reaction of polyfunctional carboxylic acids with cellulose are due to the attachment of the polyfunctional carboxylic acids via esterification with a cellulosic hydroxyl group and its further reaction- via esterification- with another cellulosic hydroxyl group producing a crosslink between cellulose chains. This mechanism is based on an anhydride intermediate formation. Attachment of the carboxylic acid moiety to celluloses hydroxyl group via esterification reaction of the first cyclic anhydride would expose a new carboxylic acid unit in CA, which has the proper chemical connectivity to form a new intra molecular anhydride moiety with the adjacent carboxylic acid unit. Further reaction with a cellulose hydroxyl of another chain can then lead to crosslinking [104].
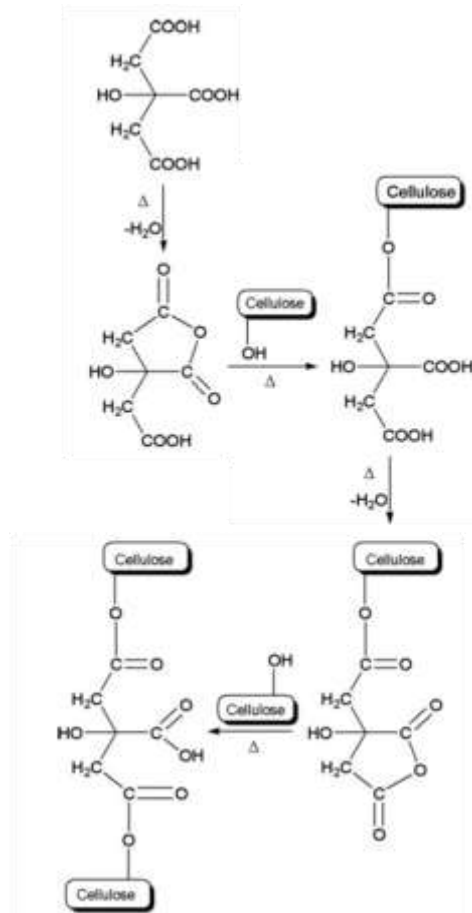
Fig. 30: Possible crosslinking reaction mechanism of citric acid with cellulose.

Inorganic phase: Hydroxyapatite

In the last 30 years, the synthesized calcium phosphate compounds have generated a great deal of interest because of the wide variety of their medical applications, especially in orthopedics and plastic and dental surgery. These bioceramics are biocompatible and bioactive because they display links with bone. Among these compounds hydroxiapatite, HA [$Ca_{10}(PO_4)_6(OH)_2$] has the chemical structure of the mineral component of bones. Infact, its synthetic formulation resembles with the crystalline bioapatite mineral which constitutes 45% by volume, 65% by weight of the mineral fraction of human bone [105]. Moreover, also the extracellular matrix of bone has been described as a composite material composed of collagen type I fibrils mineralized with nanocrystals of hydroxyapatite. Approximately 70% of bone by weight is composed of calcium salts, with hydroxyapatite $(Ca_{10}(PO_4)_6(OH)_2$ as the primary mineral constituent. Strictly speaking, bone mineral is not purely hydroxyapatite, and the presence of ion impurities has actually led to the consensus that a more accurate term for the inorganic component is carbonatehydroxyapatite with the formula $(Ca,Mg,Na)_{10}(PO_4HPO_4CO_3)_6(OH)_2$ [23]. Devoid of an organic component, calcium

48

salts such as hydroxyapatite are biocompatible, nonimmunogenic components of bone and are considered to be osteoconductive. Consequently, there has been much interest in designing synthetic osteoconductive grafting materials based on these naturally occurring calcium salts. HA is widely used to repair, fill, extend and reconstruct damaged bone tissue. It can also be used in soft tissue. Since 1920 its powder has been used with the aim of promoting bone consolidation [106]. This crystalline molecule was firstly used as a coating for metallic implants in order to improve the osteoconductive and osteointegrative properties of the prostheses [107]. This material can be obtained from mammal bones or coral. In the lab, it can be synthesized by reactions in solid state, co-precipitation, hydrothermal methods, or sol-gel process, among others. Precipitation in aqueous solutions is the experimental procedure most employed because HA is insoluble in water. The molar ratio of calcium to phosphorus Ca/P varies from 1.2 to almost 2 in HA. The stoichiometric molar ratio of HA is 1.67; however, this is not the value observed in the organism because small amounts of other materials such as carbon, nitrogen, iron and another elements are incorporated. Thus, the general chemical formula is $Ca_{10x}(HPO_4)_x(PO_4)_{6x}(OH)_{2x}$ where Young and Posner [108] determined the crystal structure of HA.

Numerous synthetic CaP biomaterials are commercially available [23] as hydroxyapatite, unsintered calcium deficient apatite, beta-tricalcium phosphate, or biphasic calcium phosphate. Hydroxyapatite can be produced with either a dense or macroporous morphology, and is typically sintered at temperatures above 1000 °C in granular or block forms. The high heat of sintering produces a material that cannot be reshaped to fit into a bone defect (i.e. if in block form) and is non-resorbable. Beta-tricalcium phosphate (β-TCP) has the formula $Ca_3(PO_4)_2$ and like hydroxyapatite is a brittle material with low fracture resistance. Both hydroxyapatite and β-TCP are biocompatible, osteoconductive, and bioactive (i.e. they develop a direct, adherent bond with bone) [23].

Under physiological conditions, hydroxyapatite is essentially a non-resorbable material, while on the other hand β-TCP has been shown to degrade within 6 weeks after implantation [109]. The dissolution of CaP biomaterials is dependent on composition (hydroxyapatite vs. β-TCP ratio), surface area of the implant (particulate vs. block form), porosity, and crystallinity (sintering creates larger, slower dissolving crystals) [23].

Biphasic CaP products which contain hydroxyapatite and β-TCP in various ratios (the higher the β-TCP content, the greater the resorbability [110] are aimed at the provision of a bone grafting material which is able to degrade within a physiologically optimized time frame, while providing some measure of mechanical stability until sufficient bone in-growth has occurred [109]. CaP cements are also available, and these combine a dry powder (CaP) and a liquid component (i.e. an

inorganic or organic acid, or sodium phosphate solutions) in a setting reaction that occurs under physiologic pH and temperatures [23]. A variety of CaP compounds have been used for the solid phase such as dicalcium phosphate, dicalcium phosphate dihydrate, calcium-deficient hydroxyapatite, and amorphous calcium phosphate. These cements are injectable and able to be molded for variable periods before hardening. They are also described as resorbable, though clinical experience has demonstrated retention of the material over extended periods. While CaP cements have been successfully used for clinical applications such as vertebroplasty [111] and bone defect repair, they are brittle and contraindicated for use in areas of mobility, active infection, or in situations where they directly contact the sinuses or dura.

At the beginning of the 70's, it was shown that HA displayed two crystalline systems, hexagonal and monoclinic. HA contained in teeth and bones and mineral HA present a hexagonal structure; instead of dental enamel HA has a monoclinical structure. HA obtained in the lab presents a structure which depends on the of method synthesis [112,113]

Graphene oxide

Graphene, a free-standing 2D crystal with one-atom thickness, has become one of the hottest topics in the fields of materials science, physics, chemistry, and nanotechnology [114]. This allotrope of carbon comprises layers of six-atom rings in a honeycombed network and can be conceptually viewed as a true planar aromatic macromolecule [115]. As a basic building block of other carbon allotropes, graphene can be wrapped to generate 1D fullerenes, rolled up to form 2D carbon nanotubes, and stacked to produce 3D graphite [116]. Although graphene is the fundamental basis of different carbon forms, it was first prepared unambiguously in 2004, 440 years after the invention of graphite, by peeling a single layer of graphene using sticky tape and a pencil [117]. During the past several years, various methods for producing graphene have been developed, such as micromechanical exfoliation, chemical vapour deposition, epitaxial growth, and chemically synthesis. Although it is considered as the basic block of carbon allotropes, graphene exhibits distinctly different properties, such as its unusual structural characteristics and electronic flexibility [118-120]. Other extraordinary properties include high planar surface (calculated value, $2630 m^2/g$) [121], superlative mechanical strength (Young's modulus,1100 GPa) [122], unparalleled thermal conductivity (5000 W/m/K) [123], and remarkable electronic properties.

As a result of the unique chemical and physical properties mentioned above, graphene and graphene-based nanomaterials have attracted strong interest in biological studies [124-127]. Various

graphene-based nanomaterials [128-133] have been used to fabricate functionalized biosystems integrated with nucleic acids (NAs), peptides, proteins and even cells. Moreover, the discovery of the adsorption of single-stranded DNA (ssDNA) onto graphene sheets, the ability of graphene to quench electron donors, the ability of graphene to protect biomolecules from enzymatic cleavage, as well as transportation capability in living cells and in vivo systems, have revealed the potential for graphene application in biological studies and biotechnology [134].

Synthesis of GO. Despite the relative novelty of graphene as a material of broad interest and potential [119,135]. GO has a history that extends back many decades to some of the earliest studies involving the chemistry of graphite. The first, well-known example came in 1859 when British chemist Brodie was exploring the structure of graphite by investigating the reactivity of flake graphite. One of the reactions he performed involved adding ''potash of chlorate'' (potassium chlorate; $KClO_3$) to a slurry of graphite in fuming nitric acid (HNO_3) [136]. Brodie *et al.* determined that the resulting material was composed of carbon, hydrogen, and oxygen, resulting in an increase in the overall mass of the flake graphite. He isolated crystals of the material, but the interfacial angles of the crystal lattice were unable to be measured via reflective goniometry. Successive oxidative treatments resulted in a further increase in the oxygen content, reaching a limit after four reactions. Nearly 40 years after Brodie's seminal discovery of the ability to oxidize graphite, Staudenmaier improved Brodie's $KClO_3$-fuming HNO_3 preparation by adding the chlorate in multiple aliquots over the course of the reaction (also, with the addition of concentrated sulfuric acid, to increase the acidity of the mixture), rather than in a single addition as Brodie had done. This slight change in the procedure resulted in an overall extent of oxidation similar to Brodie's multiple oxidation approach, but performed more practically in a single reaction vessel [137]. Nearly 60 years after Staudenmaier, Hummers and Offeman developed an alternate oxidation method by reacting graphite with a mixture of potassium permanganate ($KMnO_4$) and concentrated sulfuric acid (H_2SO_4), again, achieving similar levels of oxidation [138]. Though others have developed slightly modified versions, these three methods comprise the primary routes for forming GO, and little about them has changed. Importantly, it has since been demonstrated that the products of these reactions show strong variance, depending not only on the particular oxidants used, but also on the graphite source and reaction conditions.

Structural features. Aside from the operative oxidative mechanisms, the precise chemical structure of GO has been the subject of considerable debate over the years, and even to this day no

unambiguous model exists. There are many reasons for this, but the primary contributors are the complexity of the material (including sample-to-sample variability) due to its amorphous, berthollide character (i.e. non-stoichiometric atomic composition) and the lack of precise analytical techniques for characterizing such materials (or mixtures of materials). Despite these obstacles, considerable effort has been directed toward understanding the structure of GO, much of it with great success.

Many of the earliest structural models of GO proposed regular lattices composed of discrete repeat units. Hofmann and Holst's stucture (figure 30) consisted of epoxy groups spread across the basal planes of graphite, with a net molecular formula of C_2O [139]. Another remarkable model by Nakajima and Matsuo relied on the assumption of a lattice framework akin to poly(dicarbon monofluoride), $(C_2F)_n$, which forms a stage 2 graphite intercalation compound (GIC) [140]. These individuals also made a valuable contribution to understanding the chemical nature of GO by proposing a stepwise mechanism for its formation via 3 of the more common oxidation protocols [141]. The most recent models of GO have rejected the lattice based model and have focused on a nonstoichiometric, amorphous alternative. Certainly the most well-known model is the one by Lerf and Klinowski (figure 30). Lerf and Klinowski have published several papers on the structure and hydration behavior of GO, and these are the most widely cited in the contemporary literature. The initial studies done by Lerf and coworkers used solid state nuclear magnetic resonance (NMR) spectroscopy to characterize the material [142]. This was a first for the field as earlier models relied primarily on elemental composition, reactivity and X-ray diffraction studies. By preparing a series of GO derivatives, Lerf was also able to isolate structural features based on the material's reactivity [143].
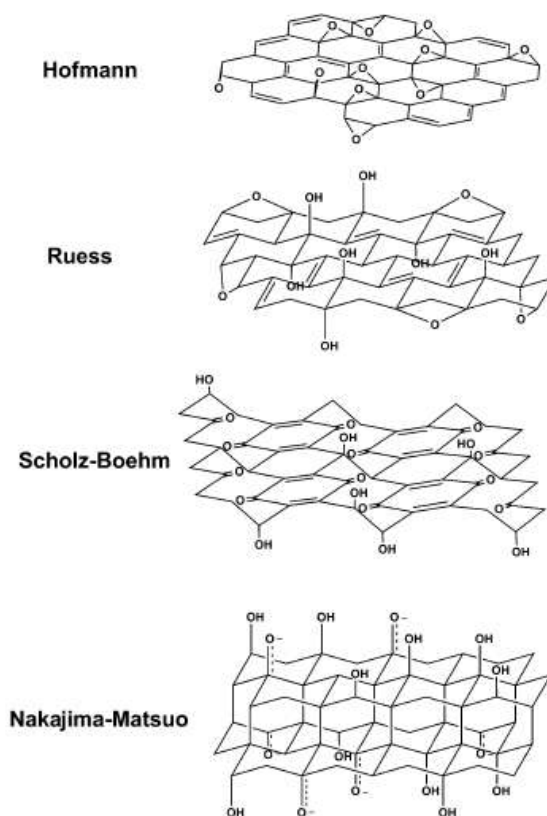
Fig. 31: Summary of several older structural models of GO
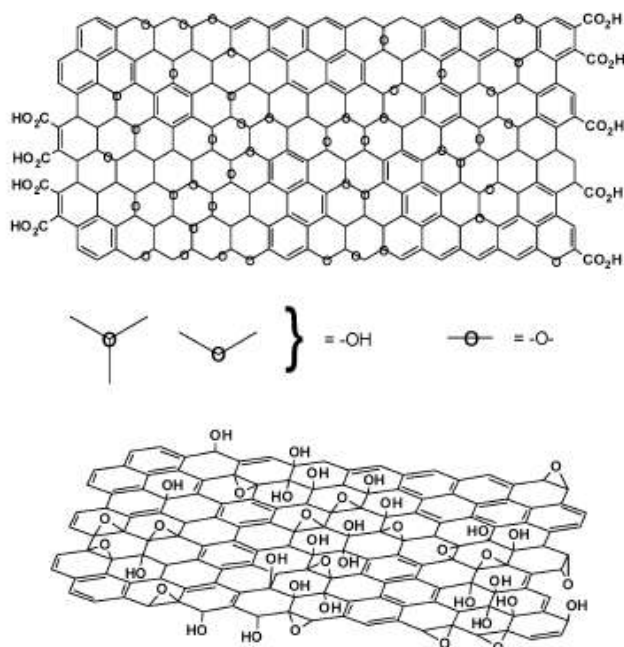
Fig. 32: Variations of the Lerf-Klinowski model indicating ambiguity regarding the presence (top [143]), or absence (bottom, [142]) of carboxylic acids on the periphery of the basal plane of the graphitic platelets of GO.

After several analyses about fundamental structural features of GO, it is clear the necessity of more complex picture to define the material. Lerf and coworkers determined that the double bonds were likely either aromatic or conjugated, the logic being that isolated double bonds would be unlikely to persist in the strong oxidizing conditions used (a modified Hummers method).

This revised Lerf–Klinowski model earlier indicates that carboxylic acid groups were present in very low quantities at the periphery of the graphitic platelets, in addition to other keto groups. As Brodie observed in 1859, along with many others since, Lerf and coworkers noted the thermal instability of GO. The decomposition process is known to involve the evolution of CO and CO_2, rather than O_2, due to the high surface reactivity of GO itself. Though the Lerf–Klinowski model remains largely unchanged since its initial report over 10 years ago, others have made slight modifications to the proposed structure including the presence of 5- and 6-membered lactols on the periphery of the graphitic platelets as well as the presence of esters of the tertiary alcohols on the surface, though all accounts maintain the dominance of epoxides and alcohols on the basal plane[146,145]. Cai *et al.* have also recently demonstrated the ability to isotopically label GO, greatly expanding the scope of potential spectroscopic techniques [148]. One notable exception to this adherence to the Lerf– Klinowski model has been proposed by Dekany and coworkers (figure 33)[146] The Dekany model work revived and updated the Ruess and Scholz–Boehm models, which suggested a regular, corrugated quinoidal structure interrupted by trans-linked cyclohexyl regions, functionalized by tertiary alcohols and 1,3-ethers.
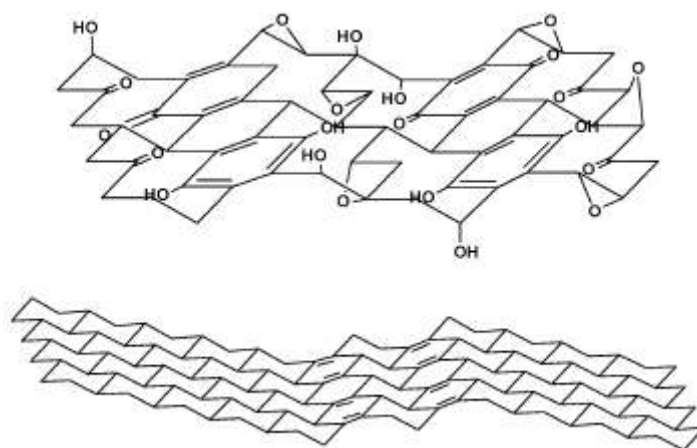
Fig. 33: Structure of GO proposed by Dekany and coworkers [148].

Dekany model is composed of two distinct domains: trans-linked cyclo-hexyl species interspersed with tertiary alcohols and and 1,3-ethers, and a corrugated network of keto/quinoidal species. No carboxylic acids are believed to be present in this description of GO.

As a final note, variations in the degree of oxidation caused by differences in starting materials (principally the graphite source) or oxidation protocol can cause substantial variation in the structure and properties of the material, rendering the term ''graphite oxide'' somewhat fluid, and subject to misinterpretation. This experimental observation has been compared with density functional calculations, which predict that partial oxidation is thermodynamically favored over complete oxidation [147]. However, the exact identity and distribution of oxide functional groups depends strongly on the extent of coverage. This is illustrated in the theoretical prediction that the ratio of epoxides to alcohols increases with increasing oxidation [147].

Chemical functionalization. An important GO aspect is the possibility to add other groups on graphene oxide platelets using various chemical reactions that provide for either covalent or non-covalent attachment to the resulting chemically modified graphenes (CMGs). Such approaches, which add functionality to groups already present on the graphene oxide, render graphene/graphite oxide a more versatile precursor for a wide range of applications. Graphene oxide platelets have chemically reactive oxygen functionality, such as carboxylic acid, groups at their edges (according to the widely accepted Lerf–Klinowski model), and epoxy and hydroxyl groups on the basal planes. An ideal approach to the chemical modification of graphene oxide would utilize orthogonal reactions of these groups to selectively functionalize one site over another. Demonstration of the selectivity of these chemical transformations remains challenging, however. In some instances, reaction with multiple functionalities is possible, and the wide range of chemical compositions present in the reactant known as ''graphene oxide'' makes isolation and rigorous characterization of the products practically impossible.

References

[1] Black J and Hastings G. Handbook of biomaterial properties: Chapman & Hall. 1998;24:590.

[2] Cowin SC. Bone Mechanics Handbook. Second edition. 2001: CRC Press, Boca Raton, USA.

[3] Ohman C, Baleani M, Perilli E, Dall'Ara E, Tassani S, Baruffaldi F, Viceconti M. Mechanical testing of cancellous bone from the femoral head: Experimental errors due to off-axis measurements. J Biomech 2007;40:2426-33.

[4] Turner CH, Cowin SC. Errors induced by off-axis measurement of the elastic properties of bone. J Biomech Eng 1988;110:213-5.

[5] Parfitt, A.M., et al., Bone histomorphometry: standardization of nomenclature, symbols, and units. Report of the ASBMR Histomorphometry Nomenclature Committee. J Bone Miner Res 1987;2:595-610.

[6] Malluche HH, Faugere MC. Atlas of mineralized bone histology. 1986:Karger AG, Basel, Switzerland.

[7] Weiss L. Cell and tissue biology. 1990: Urban & Schwarzenberg, Baltimore.

[8] Williams PL. Gray's anatomy. 38th edition. 1995: Churchill Livingstone, London, UK.

[9] Frost HM. Intermediary organization of skeleton. 1984: CRC Press, Boca Raton, USA.

[10] Hancox NM. The biology of bone. 1972: Campridge University Press,Cambridge.

[11] Currey JD. The many adaptations of bone. J Biomech 2003;36:1487-95.

[12] Currey JD. What should bones be designed to do? Calcif Tissue Int 1984;36: S7-10.

[13] Burr DB, Martin RB, Schaffler MB, Radin EL. Bone remodeling in response to in vivo fatigue microdamage. J Biomech 1985;18:189-200.

[14] Frost HM, Jee WS. Perspectives: a vital biomechanical model of the endochondral ossification mechanism. Anat Rec 1994;240:435-46.

[15] Wolff J. Über die innere Architektur der Knochen und ihre Bedeutung für die Frage vom Knochenwachstum. Virchows Arch Anat Physiol Klin Med 1870;50:389-453.

[16] Shanbhag AS, Jacobs JJ, Gilbert TT, Gilbert JL, J Black and Galante JO. Composition and morphology of wear debris in failed uncemented total hip replacement. J Bone Joint Surg Br 1994;76B:60-7.

[17] Ottani V, Martini D, Franchi M, Ruggeri A, Raspanti M. Hierarchical structures in fibrillar collagens. Micron 2002;33:587–96.

[18] Silver FH, Freeman JW, Seehra GP. Collagen self-assembly and the development of tendon mechanical properties. J Biomechanics 2003;36:1529–53.

[19] Kadler KE, Holmes DF, Trotter JA and Chapman JA. Collagen fibril formation. Biochem J 1996;316:1-11.

[20] Loret B and Simoes FMF. Articular cartilage with intra- and extrafibrillar waters: a chemo-mechanical model. Mech Mater 2004;36:515–41.

[21] Eisenberg SR, Grodzinsky AJ. Swelling of articular cartilage and other connective tissues: Electromechanochemical forces. J Orthop Res 1985;3:148–59.

[22] Bernhardt A, Lode A, Boxberger S, Pompe W, Gelinsky M. Mineralised collagen-an artificial, extracellular bone matrix—improves osteogenic differentiation of bone marrow stromal cells. J Mater Sci Mater Med 2008;19:269-75.

[23] LeGeros RZ. Calcium Phosphate-Based Osteoinductive Materials. Chem Rev 2008;108:4742–53.

[24] Downey PA, Siegel MI. Bone biology and the clinical implications for osteoporosis. Phys Ther 2006;86:77–91.

[25] Habibovic P, de Groot K. Osteoinductive biomaterials-properties and relevance in bone repair. J Tissue Eng Regen Med 2007;1:25-32.

[26] Holland TA, Mikos AG. Biodegradable polymeric scaffolds. Improvements in bone tissue engineering through controlled drug delivery. Adv Biochem Eng Biotechnol 2006;102:161-85.

[27] Khan Y, Yaszemski MJ, Mikos AG, Laurencin CT. Tissue Engineering of Bone: Material and Matrix Considerations. J Bone Joint Surg Am 2008;90:36-42

[28] Kretlow JD, Mikos AG. mineralization of synthetic polymer scaffolds for bone tissue engineering. Tissue Eng 2007;13:927-38.

[29] Salgado AJ, Oliveira JT, Pedro AJ, Reis RL. Adult Stem Cells in Bone and Cartilage Tissue Engineering. Curr Stem Cell Res Ther 2006;1:345-64.

[30] Kretlow JD, Young S, Klouda L, Wong M, and Mikos AG. Injectable Biomaterials for Regenerating Complex Craniofacial Tissues. Adv Mater 2009;21:3368-93.

[31] Barrère F, van der Valk CM, Dalmeijer RAJ, Meijer G, van Blitterswijk CA, de Groot K et al. Osteogenecity of octacalcium phosphate coatings applied on porous metal implants. J Biomed Mater Res Part A. 2003;66A:779–88.

[32] Burg KJL, Porter S, Kellam JF. Biomaterial developments for bone tissue engineering. Biomaterials 2000;21:2347–59.

[33] Mikos AG, Sarakinos G, Leite SM, Vacanti JP, Langer R. Laminated three-dimensional biodegradable foams for use in tissue engineering. Biomaterials 1993;14:323-30.

[34] Vazquez CG, Barba CP, and Munguıa N. Stoichiometric hydroxyapatite obtained by precipitation and sol gel processes. Revista mexicana de fisica. 2005;51:284–93.

[35] Peltola SM, Melchels FPW, Grijpma DK, Kellomäki M. A review of rapid prototyping techniques for tissue engineering purposes. Ann Med 2008;40:268-80.

[36] Wang F, Li MS, Lu YP, Qi YX. A simple sol–gel technique for preparing hydroxyapatite nanopowders. Mater Lett 2005;59:916–9.

[37] Lai JY. The role of bloom index of gelatin on the interaction with retinal pigment epithelial. Cells. Int J Mol Sci 2009;10:3442-56.

[38] Tabata Y, Ikada, Y. Protein release from gelatin matrices. Adv Drug Deliv Rev 1998;31:287-301.

[39] Lohre JM, Baclig L, Sagartz J, Guida S, Thyagarajan K, Tu R. Evaluation of two epoxy ether compounds for biocompatible potential. Artif Organs 1992;16:630–3.

[40] Rose PJ, Mark HF, Bikales NM Overberger CG Menges G Kroschwitz JI. Encyclopedia of polymer science and engineering, volume 7, 2nd edition, 1987.

[41] Fakirov S, Sarac Z, Anbar T, Boz B, Bahar I, Evstatiev M, et al. Mechanical properties and transition temperatures of cross-linked oriented gelatin. Coll Amp Polym Sci 1996;274:334–41.

[42] Yao CH, Sun JS, Lin FH, Liao CJ and Huang CW. Biological effects and cytotoxicity of tricalcium phosphate and formaldehyde crosslinked gelatin composite. Mater Chem Phys 1996;45:6–14.

[43] Lee CH, Singla A, Lee Y. Biomedical applications of collagen. IJP 2001;221:1-22.

[44] Prockop DJ. What hold us together? Why do some of us fall apart? What can we do about it? Matrix Biol 1998;16:519-28.

[45] Harkness RD. Biological functions of collagen. Biol Rev 1961;36:399-463.

[46] Veis A. In: The Macromolecular Chemistry of Gelatin. New York:Academic Press,1964.

[47] Johns P, Courts A. (1977) Relationship between collagen and gelatin. In: Ward, A. G., Courts, A. (eds) The Science and Technology of Gelatin, Academic Press, New York, pp 138 ± 178.

[48] Welz MM, Ofner CM III. Examination of self-crosslinked gelatin as a hydrogel for controlled release. J Pharm Sci 1992;81:85-90.

[49] Eastoe JE, Leach AA. Chemical constitution of gelatin. In: Ward AG, Courts A, editors. The Science and Technology of Gelatin. London: Academic Press, 1977 pp. 73-107.

[50] Nishi C, Nakajima N and Ikada Y. In vitro evaluation of cytotoxicity of diepoxy compounds used for biomaterial modification. J Biomed Mater Res 1995;29:829–34.

[51] Yao CH, Liu BS, Chang CJ, Hsu SH, Chen YS. Preparation of networks of gelatin and genipin as degradable biomaterials. Mater Chem Phys 2004;83:204–8.

[52] Sung HW, Huang DM, Chang WH, Huang RN, Hsu JCJ. Evaluation of gelatin hydrogel crosslinked with various crosslinking agents as bioadhesives. Biomed Mater Res Part A 1999;46:520–30.

[53] Lai JY and Li YT. Functional Assessment of Cross-Linked Porous Gelatin Hydrogels for Bioengineered Cell Sheet Carriers. Biomacromolecules 2010;11:1387–97.

[54] Kuijpers AJ, van Wachem PB, van Luyn MJA, Plantinga JA, Engbers GHM, Krijgsveld J, et al. In vivo compatibility and degradation of crosslinked gelatin gels incorporated in knitted Dacron. J Biomed Mater Res 2000;51:136–45.

[55] Zhang YZ, Venugopal J, Huang ZM, Lim CT, Ramakrishna S. Crosslinking of the electrospun gelatin nanofibers Polymer 2006;47:2911–7.

[56] Li ZY, Lam WM, Yang C, Xu B, N i GX, Abbah SA et al. Chemical composition, crystal size and lattice structural changes after incorporation of strontium into biomimetic apatite. Biomaterials 2007;28:1452-60.

[57] Hoare DG and Koshland DE Jr. A Method for the Quantitative Modification and Estimation of Carboxylic Acid Groups in Proteins. J Biol Chem 1967;242:2447-53.

[58] Grabarek Z and Gergely J. Zero-length crosslinking procedure with the use of active esters. Anal Biochem 1990;185:131-135.

[59] Nakajima N, Ikada Y. Mechanism of amide formation by carbodiimide for bioconjugation in aqueous media. Bioconjugate Chem 1995;6:123-30.

[60] Zeeman R, Dijkstra PJ, van Wachem PB, van Luyn MJA, Hendriks M, Cahalan PT et al. Successive epoxy and carbodiimide cross-linking of dermal sheep collagen. Biomaterials 1999;20:921–31.

[61] Huang-Chien Liang, Wen-Hisung Chang, Hsiang-Fa Liang, Meng-Horng Lee, Hsing-Wen Sung. Crosslinking Structures of Gelatin Hydrogels Crosslinked with Genipin or a Water-Soluble Carbodiimide. J Appl Polym Sci 2004;91:4017–26.

[62] Olde Damink LHH, Dijkstra PJ, van Luyn MJA, van Wachem PB, Nieuwenhuis P, Feijen J. Cross-linking of dermal sheep collagen using a water-soluble carbodiimide. Biomaterials 1996;17:765-73.

[63] Stainsby G. The gelatin gel and the sol-gel transformation. In: Ward AG, Courts A, editors. The Science and Technology of Gelatin. London: Academic Press, 1977 p. 179-207.

[64] Russo PS. A perspective on reversible gels and related systems. ACS SymposiumSeries 1987;350:1-21.

[65] Leucuta SE, Ponchel G, Duchêne D. Dynamic swelling behaviour of gelatin/poly (acrylic acid) bioadhesive microspheres loaded with oxprenolol. J Microencap 1997;14:501-10.

[66] Choi SSRJ. Physicochemical and sensory characteristics of fish gelatin. J Food Sci 2000;65:194–9.

[67] Lim YP, Mohammad AW. Physicochemical Properties of Mammalian Gelatin in Relation to Membrane Process Requirement. Food and Bioprocess Tech 2011;4:304-11.

[68] Zhu D, Jin L, Wang Y, Ren H. Swelling behavior of gelatin-based hydrogel cross-linked with microbial transglutaminase. J aqeic. 2012;63:11-20.

[69] Crescenzi V, Francescangeli A and Taglienti A. New gelatin-based hydrogels via enzymatic networking. Biomacromolecule. 2002;3:1384-91.

[70] Ross-Murphy SB. Structure and rheology of gelatin gels: recent progress. Polymer 1992;33:2622-7.

[71] Deiber JA, Ottonea ML, Piaggio MV, Marta B. Peirotti A. Characterization of cross-linked polyampholytic gelatin hydrogels through the rubber elasticity and thermodynamic swelling theories. Polymer 2009;50:6065-75.

[72] Pourjavadi A, Farhadpour B and Seidi F. Synthesis and investigation of swelling behavior of new agar based superabsorbent hydrogel as a candidate for agrochemical delivery. J Polym Res 2009;16:655-65.

[73] Pourjavadi A. Collagen-based highly porous hydrogel without any porogen: Synthesis and characteristics. Euro Polym J 2007;43:877–89.

[74] Gary M, Eichenbaum PFKA. Investigation of the Swelling Response and Loading of Ionic Microgels with Drugs and Proteins: The Dependence on Cross-Link Density. Macromolecules 1999;32:4867–78.

[75] English AE, Tanaka T, Edelman ER. Polyelectrolyte hydrogel instabilities in ionic solutions. J Chem Phys 1996;105:10606.

[76] Baker JP, Blanch HW, Prausnitz JM. Swelling properties of acrylamide-based ampholytic hydrogels: comparison of experiment with theory. Polymer 1995;36:1061-9.

[77] Bajpai AK, Shrivastava M. Dynamic swelling behavior of polyacrylamide based three component hydrogels. Journal of Macromolecular Science, Part A. 2000;37:1069–88.

[78] Narasimhan B. Mathematical models describing polymer dissolution: components for drug delivery. Adv Drug Del Rev 2001;48:195-210.

[79] Ofner III CM, Schott H. Swelling studies of gelatin I: gelatin without additives. J Pharm Sci 1986;75:790-6.

[80] Fan LT, Singh SK. Controlled Release-A Quantitative Treatment. Berlin: Springer-Verlag, 1989:105-6.

[81] Tomihata K, Burczak K, Shiraki K, Ikada Y. Crosslinking and biodegradation of native and denaturated collagen. Polym Prepr 1992;33:534-5.

[82] St. Pierre T, Chiellini E. Biodegradability of synthetic polymers used for medical and pharmaceutical applications: Part 1 -principles of hydrolysis mechanisms. J Bioact Compatible Polym 1986;1:467-97.

[83] Park K, Shalaby WSW, Park H. Biodegradable Hydrogels for Drug Delivery. Lancaster: Technomic Publ., 1993.

[84] Sykes P. A Guidebook to Mechanism in Organic Chemistry (4th edn). London: Longman Group Ltd, 1975:232-239.

[85] Shih C, Higuchi T, Himmelstein KJ. Drug delivery from catalysed erodible polymer matrices of poly(ortho-ester)s. Biomaterials 1984;5:237-40.

[86] Kirby AJ. Hydrolysis and formation of esters of organic acids. In: Bamford CH, Tipper CFH, eds. Comprehensive Chemical Kinetics Vol 10: Ester Formation and Hydrolysis and Related Reactions). Amsterdam: Elsevier, 1972;10:57-202.

[87] Vacanti CA, Vacanti JP. Langer R. Tissue engineering using synthetic biodegradable polymers. In: Shalaby SW, Ikada Y, Langer R, Williams J, eds. Polymers of Biological and Biomedical Significance (ACS Symposium Series 540). Washington, DC: ACS: 1994

[88] Langer R, Peppas N. Chemical and physical structure of polymers as carriers for controlled release of bioactive agents: a review. J Macromol Sci, Part C: Polym Rev1983;C23:61-26.

[89] Langer R. New methods of drug delivery. Science 1990;249:1527-32.

[90] Gijpferich A. Mechanisms of polymer degradation and erosion. Biomoterials 1996;17:103-114

[91] Cousins SK, Brown Jr RM. Cellulose I microfibril assembly: computational molecular mechanics energy analysis favours bonding by van der Waals forces as the initial step in crystallization. Polymer. 1995;36:3885–8.

[92] Atalla RH and VanderHart DL. Native cellulose: a composite of two distinct crystalline forms. Science 1984;223:283-5.

[93] O'Sullivan AC. Cellulose: the structure slowly unravels. Cellulose 1997;4:173-207.

[94] Klemm D, Heublein B, Fink H-P, Bohn A Cellulose: fascinating biopolymer and sustainable raw material. Angew Chem Int Ed 2005;44:2–37

[95] Lindman B, Karlström G, Stigsson L. On the mechanism of dissolution of cellulose. J Mol Liquids. 2010;156:76–81.

[96] Yamane C, Aoyagi T, Ago M, Sato K, Okajima K, Takahashi T. Two different surface properties of regenerated cellulose due to structural anisotropy. Polym J 2006;38:819–26.

[97] Esposito F, Del Nobile MA, Mensitieri G and Nicolais L. Water sorption in cellulose-based hydrogels. J Appl Polym Sci 1996;60:2403–7.

[98] Sannino A, Nicolais L. Concurrent effect of microporosity and chemical structure on the equilibrium sorption properties of cellulose-based hydrogels. Polymer 2005;46: 4676–85.

[99] Sannino A, Madaghiele M, Lionetto MG, Schettino T, Maffezzoli A. A cellulose-based hydrogel as a potential bulking agent for hypocaloric diets: An in vitro biocompatibility study on rat intestine. J Appl Polym Sci 2006;102:1524-30.

[100] Glusker JP. Citrate conformation and chelation: enzymic implications. Acc Chem Res 1980;13:345-52.

[101] Coma V, Sebti I, Pardon P, Pichavant FH, Deschamps A. Film properties from crosslinking of cellulosic derivatives with a polyfunctional carboxylic acid. Carbohydr Polym. 2003;51:265–71.

[102] Xie XS, Liu Q, Cui SW. Studies on the granular structure of resistant starches (type 4) from normal, high amylose and waxy corn starch citrates. Food Res Int. 2006;9:332-41.

[103] Zhou YJ, Luner P, Caluwe P. Mechanism of crosslinking of papers with polyfunctional carboxylic acids. J Appl Polym Sci 1995;58:1523-34.

[104] Demitri C, Del Sole R, Scalera F, Sannino A, Vasapollo G, Maffezzoli A, Ambrosio L, Nicolais L. Novel superabsorbent cellulose-based hydrogels crosslinked with citric acid. J Appl Polym Sci 2008;110:2453–60.

[105] Petit R. The use of hydroxyapatite in orthopaedic surgery: a ten-year review. Eur J Orthop Surg Traumatol. 1999;9:71-4.

[106] Jaffe WL, Scott DF. Current Concepts Review - Total Hip Arthroplasty with Hydroxyapatite-Coated Prostheses. J Bone Joint Surg Am 1996;78:1918-34.

[107] Faeda RS, Tavares HS, Sartori R, Guastaldi AC, Marcantonio Jr E. Biological Performance of Chemical Hydroxyapatite Coating Associated With Implant Surface Modification by Laser Beam: Biomechanical Study in Rabbit Tibias. J Oral Maxillofac Surg 2009;67:1706–15.

[108] Bigi A, Panzavolta S, Rubini K. Relationship between triple-helix content and mechanical properties of gelatin films. Biomaterials. 2004;25:5675–80.

[109] Spivak JM, Hasharoni A. Use of hydroxyapatite in spine surgery. Eur Spine J 2001;10:S197-S204.

[110] Daculsi G, Laboux O, Malard O, Weiss P. current state of the art of biphasic calcium phosphate ceramics. J Mater Sci Mater Med 2003;14:195-200.

[111] Oner FC, Dhert WJ, Verlaan JJ . Balloon vertebroplasty in combination with pedicle screw instrumentation: a novel technique to treat thoracic and lumbar burst fractures. Injury 2005;30: E73-E79.

[112] Kay MI, Young RA and Posner AS. Crystal structure of hydroxyapatite. Nature 1964;204:1050-2.

[113] Liu DM, Troczynski T, Tseng WJ. Water-based sol/gel synthesis of hydroxyapatite: process development. Biomaterials 2001;22:1721-30.

[114] Geim AK. Graphene: status and prospects. Science 2009;324:1530–4.

[115] Ruoff R. Calling all chemists. Nat Nanotechnol 2008;3:10–11.

[116] Rao CNR, Sood AK, Subrahmanyam KS, Govindaraj A. Graphene: the new two-dimensional nanomaterial. Angew Chem Int Ed 2009;48:7752–77.

[117] Novoselov KS. Electric field effect in atomically thin carbon films. Science 2004;306:666–9.

[118] Neto AHC, Guinea F, Peres NMR, Novoselov KS. The electronic properties of graphene. Rev Mod Phys 2009;81:109–62.

[119] Geim AK and Novoselov KS. The rise of graphene. Nat Mater 2007;6:183–91.

[120] Chen D, Tanga L, Li J. Graphene-based materials in electrochemistry. Chem Soc Rev 2010;39:3157–80.

[121] Stoller MD, Park S, Zhu Y, An J, Ruoff RS. Graphene-based ultracapacitors. Nano Lett 2008;8:3498–3502.

[122] Lee C, Wei X, Kysar JW, Hone J. Measurement of the elastic properties and intrinsic strength of monolayer graphene. Science 2008;321:385–8.

[123] Balandin AA, Ghosh S, Bao W, Calizo I, Teweldebrhan D, Miao F et al. Superior thermal conductivity of single-layer graphene. Nano Lett 2008;8:902–7.

[124] Wang Y, Lu J, Tang L, Chang H, Li J. Graphene oxide amplified electrogenerated chemiluminescence of quantum dots and its selective sensing for glutathione from thiol-containing compounds. Anal Chem 2009;81:9710–5.

[125] Wang Y, Li Y, Tang L, Lu J, Li J. Application of graphene-modified electrode for selective detection of dopamine. Electrochem Commun. 2009;11:889–92.

[126] Tang L, Wang Y, Li Y, Feng H, Lu J, Li J. Preparation, structure, and electrochemical properties of reduced graphene sheet films. Adv Funct Mater 2009;19:2782–9.

[127] Kanga X, Wanga J, Wua H, Aksayc IA, Liua J, Lin Y. Glucose oxidase–graphene–chitosan modified electrode for direct electrochemistry and glucose sensing. Biosens Bioelectron 2009;25:901–5.

[128] Stankovich S, Dikin DA, Dommett GHB, Kohlhaas KM, Zimney EJ, Stach EA, et al. Graphene-based composite materials. Nature 2006;442:282–6.

[129] Wang Y, Shao Y, Matson DW, Li J, Lin Y. Nitrogen-doped graphene and its application in electrochemical biosensing. ACS Nano 2010;4:1790–8.

[130] Li X, Wang X, Zhang L, Lee S, Dai H. Chemically derived, ultrasmooth graphene nanoribbon semiconductors. Science 2008;319:1229–32.

[131] Kong BS, Geng J, Jung HT. Layer-by-layer assembly of graphene and gold nanoparticles by vacuum filtration and spontaneous reduction of gold ions. Chem Commun 2009;16:2174–6.

[132] Zhang H, Lv X, Li Y, Wang Y, Li J. P25-graphene composite as a high performance photocatalyst. ACS Nano 2010;4:380–6.

[133] Ramanathan T, Abdala AA, Stankovich S, Dikin DA, Herrera- Alonso M, Piner RD, Adamson DH et al. Functionalized graphene sheets for polymer nanocomposites. Nat. Nanotechnol. 2008;3:327–31.

[134] Wang Y, Li Z, Wang J, Li J and Lin Y. Graphene and graphene oxide: biofunctionalization and applications in biotechnology. Trends Biotech 2011;29:205-12.

[135] Tung VC, Allen MJ, Yang Y, Kaner RB. Throughput Solution processing of large-scale graphene. Nat Nanotechnol 2009;4: 25–32.

[136] Brodie BC. On the atomic weight of graphite Philos. Trans. R. Soc. London, 1859, 149, 249– 259.

[137] Sinitskii A, Tour JM. Chemical Approaches to Produce Graphene Oxide and Related Materials. Graphene Nanoelectronics 2012, pp 205-234.

[138] Hummers WS, Offeman RE. Preparation of graphitic oxide. J Am Chem Soc 1958;80:1339.

[139] Hofmann U, Holst R. The acid nature and methylation of graphitic oxide. Ber Dtsch Chem Ges B 1939;72:754–71.

[140] Nakajima T, Mabuchi A, Hagiwara R. A new structure model of graphite oxide. Carbon 1988;26:357–61.

[141] Nakajima T, Matsuo Y. Formation process and structure of graphite oxide. Carbon 1994; 32:469–75.

[142] He H, Riedl T, Lerf A, Klinowski J. Solid-state NMR studies of *the* structure of graphite oxide. J Phys Chem 1996;100:19954–8.

[143] Lerf A, He H, Forster M, Klinowski J. Structure of graphite oxide revisited. J Phys Chem B1998;102:4477–82.

[144] Cai W, Piner RD, Stadermann FJ, Park S, Shaibat MA, Ishii Y, et al. Synthesis and Solid-State NMR Structural Characterization of ^{13}C-Labeled Graphite Oxide. Science 2008;321:1815–17.

[145] Gao W, Alemany LB, Ci L, Ajayan PM. Atomic layers of hybridized boron nitride and graphene domains. Nat Chem 2009;1:403–8.

[146] Szabo T, Berkesi O, Forgo P, Josepovits K, Sanakis Y, Petridis D, Dekany I. Evolution *of* surface functional groups in a series *of* progressively oxidized graphite oxides. Chem Mater 2006;18:2740–9.

[147] Boukhvalov DW, Katsnelson MI. Modeling of graphite oxide. J Am Chem Soc 2008;130: 10697–701.

CHAPTER 2

INJECTABLE MODIFIED HYDROXYAPATITE GEL FOR BONE DEFECT

*I*n the past decade osteoporosis has been widely recognized as a major health issue by medical profession. Public awareness has increased the demands on healthcare agencies. Many definitions of osteoporosis have been offered to describe variously the outcome events (fragility fractures), the process giving rise to porous bones, or the resultant diminution of bone mass. In particular, osteoporosis is a disease where bone resorption occurs faster than new bone production, causing the trabeculae to become thinner, which leads to a reduction in total bone density and strength. The disease eventually leads to bone fracture, especially in the hip, wrist, knee and spine. So, we propose an injectable systems (strontium-substituted hydroxyapatite cement) in order to stimulate osteoblast differentiation and inhibit osteoclast differentiation.

In general injectable materials (cements/natural polymer) hold great promise in tissue engineering applications due to the ability of these systems to conform to complex bone shapes, contours, and defects without invasive operations, thus reducing the negative aesthetic effects associated with these repeated procedures. In this chapter we describe different approaches to repair bone defects and to promote a potential osteoporosis-decrease-filler. The target is the osteogenic differentiation induced by polymeric (cellulose) or inorganic (hydroxyapatite) matrix of injectable systems, proposed as a filler materials. To increase matrix properties, we suggest different treatments or chemical modifications:

4. *Strontium-substituted hydroxyapatite cement (to contrast osteoporosis effects).*

5. *Bioactive hydroxyapatite - graphene oxide (to support high viability and osteogenic differentiation of hMSC cells).*

6. *Modified-cellulose hydrogels crosslinked by citric acid (to increase hydrophilicity and roughness surface in order to stimulate osteogenic differentiation of hMSC).*

2.1 STRONTIUM-SUBSTITUTED HYDROXYAPATITE CEMENT

Introduction

Osteoporosis is a systemic disease ''characterized by low bone mass and microarchitectural deterioration of bone tissue, leading to enhanced bone fragility and a consequent increase in fracture risk'' [1], which results from an impaired balance of bone resorption and formation by osteoclasts and osteoblasts, respectively. For the year 2000, the number of primary osteoporosis-related fractures was estimated to be 9 million worldwide, with 61% of fractures occurring in women [2]. Considering the worldwide demographic development, the burden of osteoporosis will further increase in the near future. Various therapies have been developed for the clinical treatment of osteoporosis based on either the inhibition of bone resorption (e.g. by bisphosphonates, strontium ranelate SrR, RANKL antibody denosumab) or the anabolic stimulation of bone formation (e.g. by parathyroid hormone peptides, SrR) [3,4]. The impact of strontium(II), acting both as an inhibitor of resorption as well as a stimulus of bone formation, has already been demonstrated *in vitro* and *in vivo* [4–6]. Strontium was shown to affect cellular processes via the membrane-bound calcium sensing receptor (CaSR), not only in osteoblasts but also in cells of the osteoclasts lineage, where CaSR interaction with strontium can inhibit pre-osteoclast maturation and induce apoptosis in mature osteoclasts [7,9,10]. Mesenchymal stem cell as well as pre-osteoblast proliferation and differentiation into bone-forming osteoblasts is enhanced by the presence of strontium as well as the rate of extracellular matrix formation and mineralization (new bone deposition) [4,5,7]. This effect is based on an influence of Sr^{2+} on the Wnt/b-catenin pathway resulting in enhanced extracellular matrix formation [4] and triggering of mitogenic signalling [8].

Furthermore, Bakker *et al.* recently found evidence that SrR affects the signalling between osteocytes and both osteoblasts and osteoclasts [11]. The mechanism is thought to lie in Sr^{2+} having the ability not only to increase osteoblast-related gene expression and the alkaline phosphatase (ALP) activity of mesenchymal stem cells (MSCs), but also to inhibit the differentiation of osteoclasts [12]. As a result, Sr^{2+} is thought to be effective in enhancing the bioactivity and biocompatibility of biomaterials and, in particular, to have potential in the treatment of osteoporosis [13,14]. A poly(methyl methacrylate) bone cement containing Sr-containing calcium phosphate has been reported to have enhanced bioactivity and biocompatibility, said to be due to the release of Sr^{2+}, which not only promoted osteoblast proliferation, but also facilitated precipitation of apatite, and thus increased the mechanical strength of the bone–implant interface [15,16]. An injectable, Sr-containing calcium phosphate bone cement (CPC) could meet the requirements of

vertebroplasty because its radio-opacity was three times that of cortical bone [17]. Recently, attention has been given to the modification of bioceramics with Sr, which has tended to enhance their biological performance, including 45S5 bioglass [18], hydroxyapatite (HA) [19] and α- and β-tricalcium phosphate [20,21].

In *vivo* tests with strontium-substituted hydroxyapatite (Sr/Ca = 0.10) cement were performed using a rabbit hip replacement model and an apatite layer was found six months later between the cement and the cancellous bone [22]. As reported, strontium-containing hydroxyapatite (Sr-HA) appears to be an interesting bone substitute material. Because of the difference in the atomic radius between strontium and calcium, the crystal lattice becomes distorted and therefore the Sr-HA stability decreases, facilitating its replacement by new bone [23]. Moreover, the ability of strontium to stabilize the apatitic structure against degradation by bacterial acids may be useful in preventing dental caries, considering the significant differences in strontium content in human enamel for high and low caries populations (104.1 and 184.0 μgg^{-1}, respectively) [24]. The inorganic phase constituting bone is a non-stoichiometric calcium-deficient apatite whose crystal structure is basically that of hydroxyapatite (HA); for this reason synthetic apatites are typically used as elective bone substitutes. Sr-substituted apatite powders have been prepared by ion exchange of Sr for Ca using a biomimetic approach [25] as well as by chemical synthesis [26,27]. Here, we propose Strontium - modified CaP gels obtained at room temperature by using sol-gel method. In fact, sol-gel synthesis approach appears to be among the most suitable route towards performing injectable calcium phosphate cements [28,29].

The sol-gel approach has recently attracted attention because of the well-known inherent advantages that include a homogeneous "molecular" mixing of the components, high purity of the final products, possibility to produce hybrid materials [30-32] and low temperature of synthesis allowing the incorporation of bioactive molecules.

Furthermore, the method allows the synthesis of calcium phosphate gels at different pHs where the gel formation is achieved without the need of any refluxing steps required for the synthesis by wet-chemical method [33]. In particular, calcium phosphate obtained by sol-gel synthesis combines hydroxyapatite (HA) with other calcium phosphate phases such as dicalcium phosphate (DCP), a precursor of natural HA in bone [34]. As sintered HA has a relatively slow rate of resorption *in vivo*, dicalcium phosphate (DCP) and dicalcium phosphate dehydrate (DCPD) have also been considered for their relatively more rapid resorption rate. The effect of these modified gel materials on the proliferation and differentiation of cell line osteoblast-like cells and stem cells have been studied in the light of the biomaterial compositional changes.

2.1.1 Materials and Methods

2.1.1.1 Synthesis of Sr modified Hydroxyapatite gels

Sr-HA gels containing 5 - 10 - 15 and 20 mol % Ca^{2+} replaced by Sr^{2+} were synthesized at room temperature by using calcium nitrate tetrahydrated $Ca(NO_3)_2 \cdot 4H_2O$ (Sigma-Aldrich, Italy) and di-ammonium hydrogen phosphate $(NH_4)_2HPO_4$ (Sigma-Aldrich, Italy) as precursors and using water as solvent. Strontium nitrate $Sr(NO_3)_2$ (Sigma-Aldrich, Italy) was dissolved in water and used to replace Ca^{2+} ions. In particular, the procedure (figure 1A) consists of adding di-ammonium hydrogen phosphate $(NH_4)_2HPO_4$ in water and, after 30min the medium alkalinity was adjusted by drop-wise addition of NH_4OH up to pH 9 (P solution). Calcium nitrate tetrahydrated was dissolved in water at room temperature (Ca solution); then $Sr(NO_3)_2$ was added forming Ca+Sr solution. After mixing for 20min, P solution was added drop wise to Ca+Sr solution in proper proportion in order to achieve a Ca+Sr/P ratio of about 1.67. CaP solutions were placed in a shaking incubator at 100 rpm, 37°C until gelling occurred. After gelling the gels were dialysed in 0.01M phosphate buffered saline pH 7.4 until equilibrated to the buffer pH.
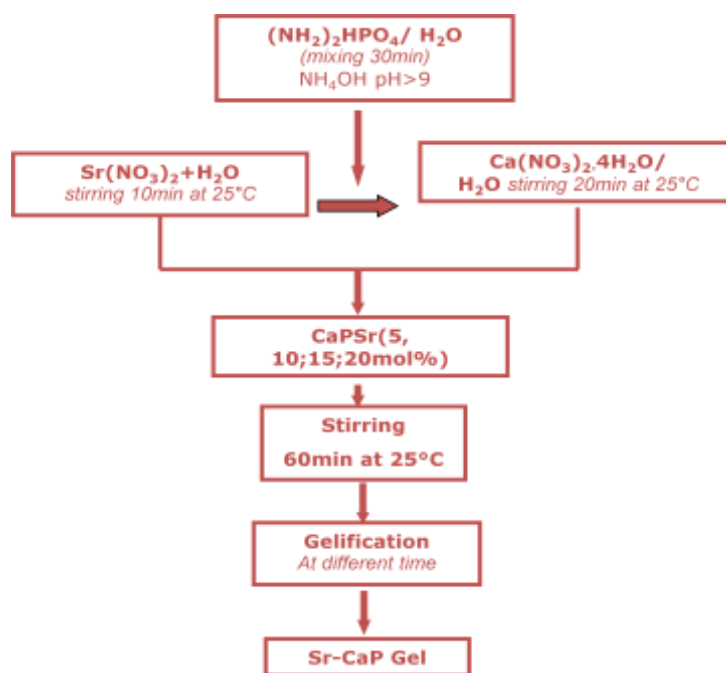
Fig. 1: Flowchart of Sr-HA synthesis by sol-gel method.

2.1.2 Characterization

2.1.2.1 Infrared Spectroscopy FTIR analysis

FTIR investigation was performed on non-modified hydroxyapatite and strontium-doped hydroxyapatite. In order to examine the chemical composition of Sr-HA, FTIR was performed to study the powder using a typical KBr pellet technique. The HA and Sr-HA powders were grounded with KBr in the proportion of 1/150 (by weight) and pressed into a 3mm pellet using a hand press. FTIR spectroscopy was performed on Nicolet Nexus spectrophotometer with KBr discs in the 500-4000 cm^{-1} region (4 cm^{-1} resolution, average 64 scans). FTIR investigation was performed on dry materials.

2.1.2.2 Morphological Investigations

The surfaces of gel materials were analysed by Scanning Electron Microscopy (SEM, JEOL 6310). For SEM analysis, the materials were mounted by a double adhesive tape to aluminum stubs. The stubs were sputter-coated with gold to a thickness of around 20nm. SEM analysis was performed at different magnification at 20 keV. The transmission electron microscopy (TEM) images were taken by a Hitachi H-9000NAR model instrument operated at an accelerating voltage of 100 kV. Samples for TEM imaging were prepared by placing a drop of the aged gel suspensions (the suspensions were diluted in deionized water and dispersed by ultrasonic waves before use) onto carbon coated copper grids, dried in air and loaded into the electron microscope chamber.

2.1.2.3 Biological studies

Cell proliferation

Cell proliferation assays were performed on human mesenchymal stem cells (hMSC) obtained from LONZA (Milano, Italy). hMSC were cultured in 75 cm^2 cell culture flask in Eagle's alpha minimum essential medium (α-MEM) supplemented with 10% fetal bovine serum, antibiotic solution (streptomycin 100 µg/ml and penicillin 100U/ml, Sigma Chem. Co) and 2 mM L-glutamine and hMSCs from passages 3 were used for all the experimental procedures and incubated at 37°C in a humidified atmosphere (5% CO_2, 95% air). For cell proliferation, hMSC were plated at concentration of $1.6x10^4$ in triplicate onto gel materials with and without Sr sterilized by autoclave at 121°C for 30 min. The cell proliferation was checked by the Alamar Blue assay for 3, 7, 14, 21

and 28 days of culture, the fluorescence was measured at 540 and 600 nm. The culture medium during experimental time was changed every two days.

Cell morphology

hMSC were seeded at 1×10^3/sample onto coupons of gel materials (HA, Sr-HA 5, 10, 15 and 20mol%) and then incubated with the tested gel materials for 24 h. At the end of the incubation time, the non-attached cells were removed by careful rinsing with PBS for three times and then incubated with cell tracker green CMFDA in phenol red-free medium at 37°C for 30 min. Subsequently cell culture was washed with PBS and incubated for 1 h in complete medium. The cell morphology and cell spreading pattern interaction of hMSC onto gel materials was evaluated by confocal laser scanning microscopy (LSM 510, CarlZeiss).

Colorimetric ALP activity assay

hMSC differentiation was tested by measuring their alkaline phosphatase (ALP) activity upon culture onto gel materials after 7, 14 and 21 days (SensoLyte pNPP ALP assay kit, ANASPEC, Milano, Italy). Briefly, at the end of each time point, cultures were washed gently with PBS followed by washing twice with cold 1X assay buffer (BD Biosciences, Milano, Italy). For extract cell layers the cultures were lysing with 1X lysis buffer with 0.2% of Triton X-100. The ALP activity was analyzed onto the cell lysates (50μl). Sample absorbance was measured in a 96-well plate at 405 nm. To correct the ALP values for the number of cells present on each gel material double stranded DNA (dsDNA), as a marker for cell number, was measured using a PicoGreen_dsDNA quantification kit (Invitrogen). First, 100μl of 200μl diluted Picogreen_dsDNA quantification reagent was added to 100 μl of cell lysates in a flat-bottomed, 96-well plate. Following 10 min incubation, the fluorescence of Picogreen was determined at a wavelength of 520 nm after excitation at 585 nm using a plate reader (multilabel counter 1420 Victor, Perkin-Elmer, Italy). dsDNA was quantified according to a calibration curve of l-dsDNA standard in 10 mM Tris, 1 mM EDTA, pH 7.5, buffer. Each experiment was performed three times in triplicate. The results of ALP activity were reported as nanograms (ng) of ALP normalized to the micrograms (μg) of total DNA content. ALP experiments were repeated twice and three gel scaffolds were used in each experiment.

Assay for gene expression

hMSC cultures onto HA and Sr-HA gel materials grown in medium for 21 days were characterized by reverse transcription-polymerase chain reaction (RT-PCR) for gene expression of bone-related markers. At the end of the culture period, total RNA was extracted from hMSC cultured onto gel materials using the Trizol reagent, according to the manufacturer's protocol (Invitrogen, Carlsbad, CA, USA). The RNA was precipitated with isopropyl alcohol and the final pellet resuspended in DEPC-water and DNAse I digested (Invitrogen Carlsbad, CA) to remove contaminating of genomic DNA. The absorbency at 260/280 nm was measured to determine the RNA concentration. One μg of total RNA was used to perform one-step RT-PCR reaction (Invitrogen Carlsbad, CA) according to the manufacturer's protocol. Briefly, cDNA synthesis program was 1 cycle at 60°C for 30 min followed of denaturation cycle of 94°C for 2 min. cDNA was amplified at 94°C for 15 s, 55°C for 30 s and 68°C for 1 min for 35 cycles in a thermal cycler (Applied, Biosystem). Primers used for amplification of bone-related molecules were upstream and downstream as follow for alkaline phosphatase (ALP): 5'-GGAGGGACCCTCGCCAGTGCT-3', 5'-AGAGGGCCACGAAGGGGAACT-3', osteocalcin (OCN): 5'-CAGCAGAGCGACACCCTAGACC-3', 5'-CATGAGAGCCCCTCACACTCC-3', osteopontin (OPN): 5'-TTCGGATGAGTCTGATGAGACC-3', 5'-GGAAGAACAGAAGCAAAGTGC-3'. Glyceraldheyde-3-phosphate dehydrogenase (GAPDH): 5'-CCACCCATGGCAAATTCCATGGCA-3', 5'-TCTAGACTGGCAGGTCAGGTCCACC-3' was utilized as housekeeping gene. Reaction products were separated using gel electrophoresis on 1.2% agarose gel stained with ethidium-bromide. Bands were visualized using ultraviolet illumination and captured with BioRad Imaging System (BIORAD).

2.1.3. Results

2.1.3.1 Synthesis of Gels Materials

A preliminary investigation showed a difference in the gelification time of the biomaterials prepared at different Sr concentration. In particular, gels prepared at 0, 10 and 15 mol% of Sr reached a final setting after 1hr of stirring at 40°C. The gels prepared at 5 and 20 mol% of Sr showed a slight delay, their gelation time was achieved after 2-3 hrs. However, all gels synthesised at room temperature could be successfully equilibrated at pH 7.4 without any significant dissolution thus ensuring their compatibility with biological systems.

2.1.3.2 Infrared Spectroscopy FTIR analysis

Figure 2 shows the FTIR spectrum of as-dried non-modified hydroxyapatite sample after 48 h aging time. The first indication of the formation of HA is in the form of broad FTIR band centered around 1000–1100 cm^{-1} [35]. Furthermore, the peaks around 3600 cm^{-1} and 601 cm^{-1} are the characteristic peaks of stoichiometric HA [36].
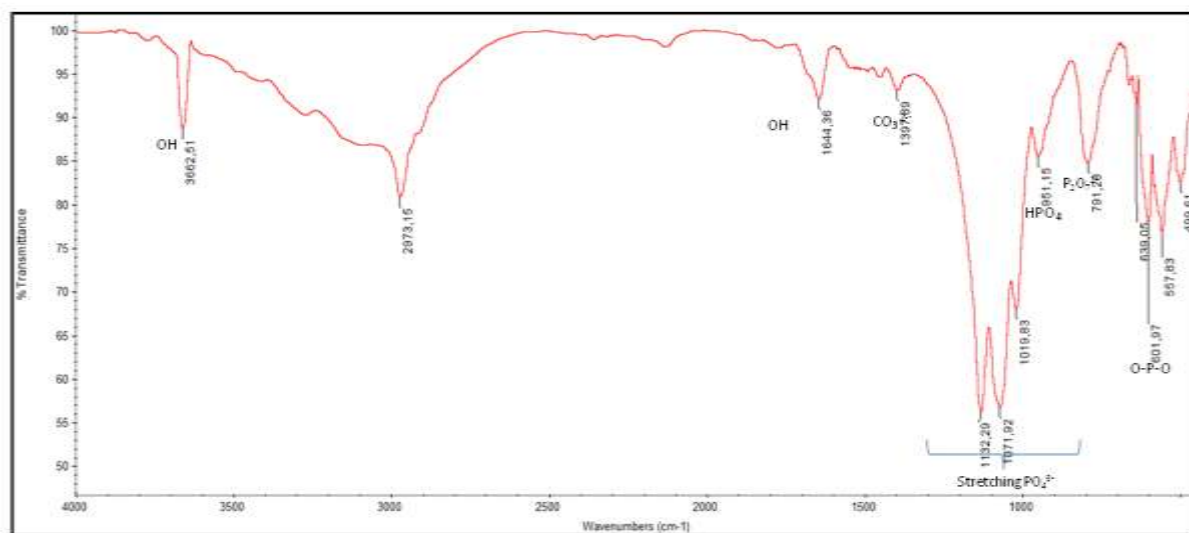
Fig.2: FTIR of non modified hydroxyapatite synthesized at room temperature.

The peak at 951 cm^{-1} [37–40] corresponds to a non-degenerate symmetric stretching mode, v_1, of the P-O bond in phosphate group. The weak peak at 499 cm^{-1} [41,42] is the doubly degenerate bending mode, v_2, of the phosphate group. As a major peak of phosphate group, triply degenerate asymmetric P-O stretching peak, v_3, which is the most intensified peak among the phosphate vibration modes, could be identified approximately around 1074 cm^{-1} [37–39,43]. The band between 564 cm^{-1} and 604 cm^{-1} [37,39] belongs to triply degenerate v_4, O-P-O bending mode in the phosphate group, which occupies two sites in the crystal lattice. Two distinguishable splitting of v_4 vibrations indicate the low site symmetry of molecules, as two peaks confirm the presence of more than one distinct site for the phosphate group in hydroxyapatite lattice [44]. The peaks at 633 and 3564 cm^{-1} [37–39] are assigned to the librational mode and intro molecular stretching vibration of the hydroxyl group in crystal structure of HA, respectively. The peak at 1644 cm^{-1} [45] is signature of the bending mode of hydroxyl group in the adsorbed water. The peak at 3664 cm^{-1} is assigned to free O-H stretching mode, which may be present on the surface of the crystallites. As the crystallization was carried out in alkaline range (pH=10.5), dissolving of atmospheric CO_2 yielding CO_3^{2-} based on the peaks at 1397 cm^{-1} [46]. The band at 875 cm^{-1} [44] indicates v_2 bending mode

of CO_3^{2-} group and suggests a B type carbonate substitution. The v_3 stretching mode of CO_3^{2-} groups was also observed at 1397 cm^{-1} [47] in the FTIR spectra. Carbonate ions can substitute for either OH$^-$ or PO_4^{3-} ions in the apatite structure. Since carbonates are constituents of bone structures [48], the presence of CO_3^{2-} may improve the bioactivity of HA rather than being a cause of concern.
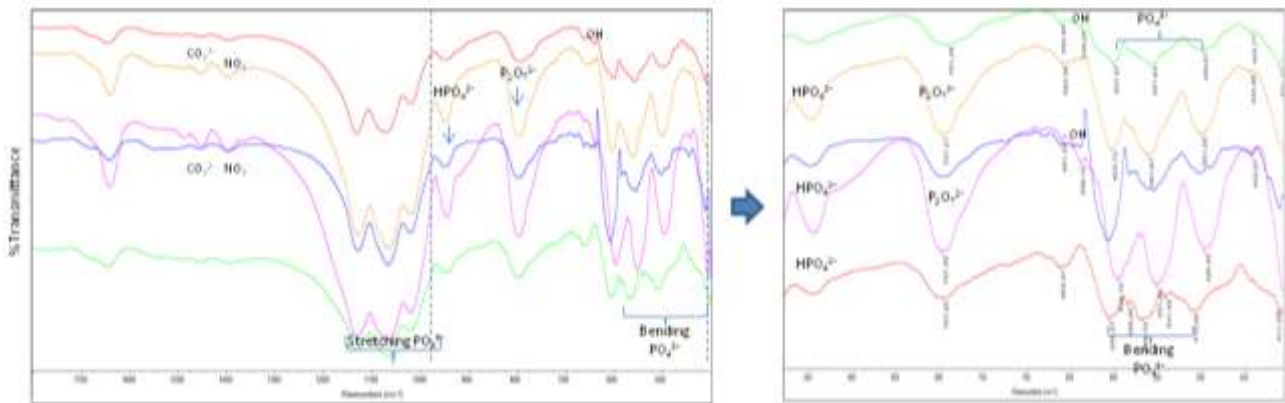
Fig. 3: FTIR of strontium-doped hydroxyapatite at 0 - 5 - 10 - 15 - 20mol%.

Figure 3 shows the FTIR spectra of the powders at different Sr concentrations. A typical HA structure containing sharp PO$_4$ bands at 1000 cm^{-1} – 950 cm^{-1} was observed. As the concentration of Sr increased, the OH bands at 550 cm^{-1} – 650 cm^{-1} disappeared gradually. This is because Sr has substituted OH and the reaction is represented by equation (1) below:

$$Ca_5(PO_4)_3OH \Rightarrow Ca_{5-x} Sr_x(PO_4)_3OH_{1-x}(SrO)_x \quad (1)$$

At about 1500 cm^{-1} – 1400 cm^{-1}, the HPO$_4$ band becomes more apparent while PO$_4$ band at about 1020 cm^{-1} shows reduction in its intensity as the concentration of Sr increases. The presence of HPO$_4^{2-}$ band at 875 cm^{-1} and P$_2$O$_7^{2-}$ band at 712 cm^{-1}, were detected in 5 - 10 and 15mol% Sr-doped HA; meanwhile, the two bands were reduced in 20 Sr-doped HA.

2.1.3.3 Morphological Investigations

SEM imaging performed on strontium-doped hydroxyapatite gel (figure 4A) and non-modified hydroxyapatite (Fig.4B) showed a change in crystal morphology when a Sr at 15mol% was introduced in substitution of Ca^{2+} ions. In that case, an agglomerate structure (figure 4A) with grains smaller than 1µm on average was observed. Moreover, a presence of microporosity due to solvent evaporation and ammonium nitrate removal was also observed. Meanwhile a crystal plates

with a length about 70 nm were observed in non-modified hydroxyapatite. EDS (figure. 4C) analysis performed on gel material with 15%mol Sr demonstrated a presence of the typical ions of modified-hydroxyapatite with an atomic ratio Ca+Sr/P about 1.65.

Elem	Weight%	Atomic%
O K	44.62	69.06
P K	14.33	11.46
CaK	25.43	15.71
AuL	4.11	0.52
SrK	11.50	3.25
Ca+Sr/P		1.65
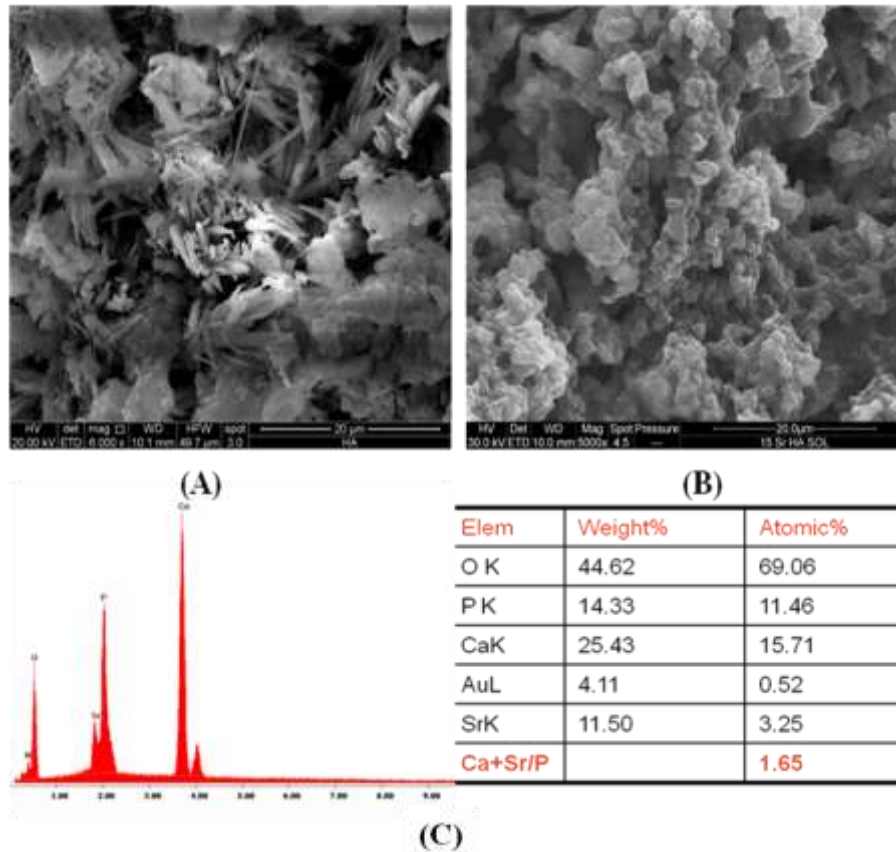
Fig. 4: SEM images of HA (A) and HA-15Sr (B). EDS analysis performed on Strontium-doped hydroxyapatite (C).

From the TEM evaluation in figure 5, it is shown that the HA particles show a length about 70-80nm and a diameter of 4-5nm. In 10 and 20mol% Sr-doped HA an agglomerate structure was observed; the particles were reduced in size, in fact a length of 40 nm and diameter of 10nm were observed. An increasing in the amount of Sr ions doped into HA made the agglomerated particles smaller. The substitution of large Sr^{2+} into small Ca^{2+} lead to denser atomic packing of the system causing retardation of crystals growth. When the crystal has less freedom to grow, the formation of TCP will be blocked and the particle size becomes smaller [49].
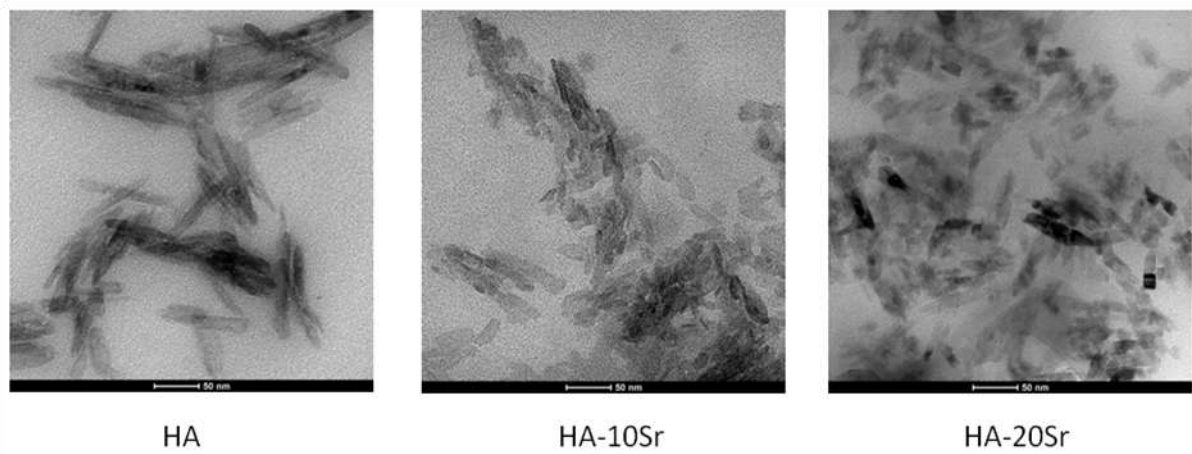
Fig. 5: TEM analysis on HA gel and strontium-doped hydroxyapatite at 10 and 20 mol%.

2.1.3.4 *Biological studies*

Figures 6 and 7 show the effect of the materials on the adhesion and metabolic activity of hMSC at different times. The cellular attachment is the first step in evaluating the biocompatibility of hMSC onto the HA material with and without Strontium. Figure 6 illustrates the hMSC cellular attachment onto each material after 1 day of cell culture. Moreover, in the presence of the doped HA with strontium cells attached to the surface and it can also observed that cells were beginning to flattened and elongated over the surface and this representative morphology is a positive sign that cells have a good biocompatibility and affinity for the HA scaffolds. Our results demonstrated that cell adhesion and spreading of cell were optimal in the cases where is present Sr and appeared not to be cytotoxic or show a negative response to cell adhesion when increased the strontium content (5, 10, 15 and 20 Sr mol%). In fact, the cell attachment and spreading was consistently higher on HA-15Sr and HA-20Sr when comparing to non-doped HA.

Cell proliferation is assessed by Alamar blue and as shown in figure 7 the cells on all scaffolds proliferate with time. hMSC cell proliferation on HA doped with different concentration of strontium induce similar levels of cell proliferation at all cell culture times. However HA-5Sr showed better cell proliferation as compared with control scaffold as HA and higher cell proliferation when compared with HA-10Sr, HA-15Sr and HA-20Sr. Meanwhile, gel materials with more Strontium (HA-10Sr, HA-15Sr and HA-20Sr) show a lower cell proliferation in the beginning of cell proliferation times then showed an increased cell proliferation after longer incubation times (14 to 21 days). Moreover, cell proliferation on the HA-10Sr, HA-15Sr and HA-20Sr showed similar cell metabolic respond and low cell proliferation is not originated by cytotoxicity of the material because Alamar blue showed metabolic activity in all incubation times;

so this behavior on the cell proliferation response might due to the differentiation tendency of hMSC on the scaffolds doped with more strontium.
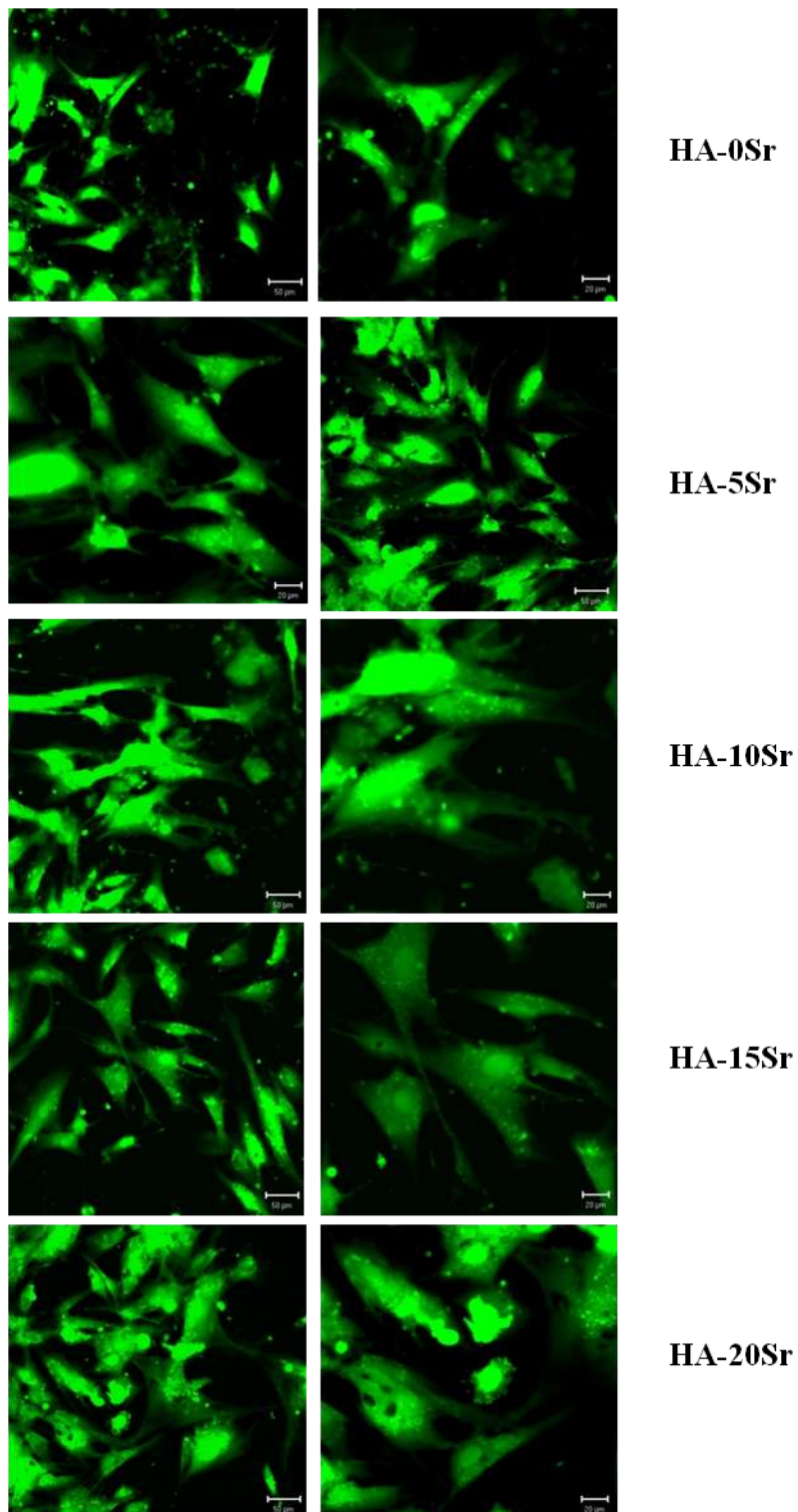
Fig. 6: Confocal images of hMSCs adhesion and cell material-interaction on HA-Sr (0 - 5-10-15-20mol%) base scaffolds after culturing for 24 h.
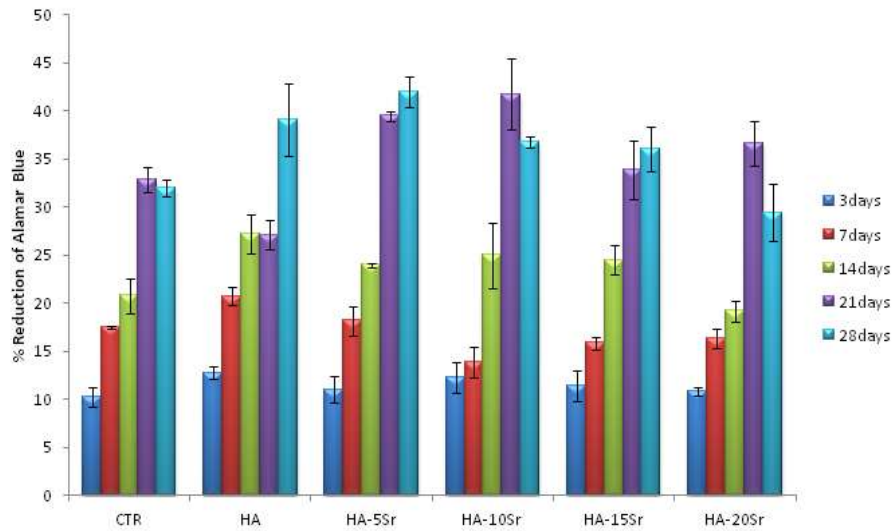
Fig. 7: Alamar blue of HA and HA-Sr (5-10-15-20 mol%) at 7, 14 and 21 days.

The ALP activity was determined on cell cultures and as early as 7 days (figure 8); cells already produce the early marker of osteogenic differentiation. ALP activity showed that at 7 and 14 days has an increased in amount of enzymatic activity on all HA scaffolds (HA-10Sr, HA-15Sr and HA-20Sr). However, at 21 days of culture there is a tendency to less activity on the ALP and could be part of the late phases of osteogenesis; although only the amount of ALP enzymatic activity continue on the HA-10Sr and HA-15Sr scaffolds.
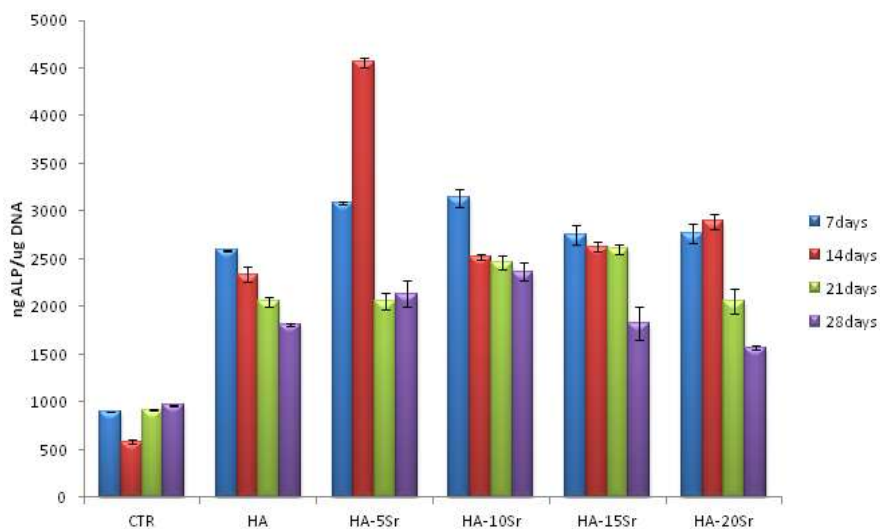
Fig. 8: ALP activity of HA and HA-Sr (5-10-15-20 mol%) at 7, 14 and 21 days in basal medium.

Gene expression analysis shows that HA doped with strontium significantly promote the expression of osteogenesis related genes including an early marker for osteogenic differentiation ALP; a non-collagen protein OPN and a late marker for osteogenic differentiation OCN. Figure 9 shows that HA-10Sr, HA-15Sr and HA-20Sr promote the expression of ALP; in contrast HA-10 and 20Sr promote the expression of OPN on lesser degree as compared with the expression of OPN promoted by HA-15Sr. Moreover, OCN expression was significantly enhanced on HA-15 and 20Sr meanwhile faint signal was detected on HA-10Sr.
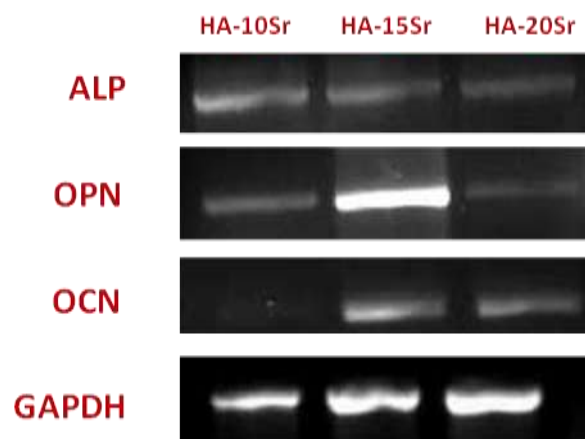
Fig. 9: Gene Expression of HA-strontium gel materials after 21 days of culture in a basal medium.

2.1.4 Discussions

The interest in Sr in the context of biomedical materials can be attributed to its apparently unique property of promoting ''uncoupled'' bone remodelling, i.e. not only stimulating osteoblast differentiation, but also inhibiting osteoclast differentiation [50]. The expectation or assumption is, therefore, that the continuous release of Sr can serve as a ''drug'' to stimulate bone regeneration.

In order to maintain the general physical, mechanical and chemical properties of the materials Sr is generally substituted for Mg or Ca, given their chemical similarity.

Strontium(II) ions have been demonstrated to both increase the bone formation by osteoblasts as well as to decrease the osteoclast-mediated resorption of the bone matrix [51,52]. Therefore, strontium has gained considerable attention in osteoporosis therapy because of its anti-resorptive and osteo-anabolic potential, which led to its clinical application in the form of strontium ranelate some years ago. Besides its systemic administration, a local release of Sr^{2+} ions from bone cements used in the treatment of osteoporotic bone fractures and defects is considered a promising approach since it could help to avoid implications of high dose treatment and compensate for the relatively

low bioavailability of the drug. In addition, the agent then is concentrated at the location of bone healing and can directly interact with all cell types present there.

In this study, the influence of strontium(II) modification of a hydroxyapatite-forming bone cement on proliferation and osteogenic differentiation of hMSC was investigated. Strontium was introduced into a calcium phosphate gel as substitute of Ca^{2+} ions by using a sol-gel technology. Moreover, we have evaluated the effect of Strontium on physico-chemical and morphological properties of hydroxyapatite gel. We have observed that for Sr–HA, while the crystal structure remained apatitic, even up to full substitution, the crystallinity decreased slightly, possibly due to the structural strain caused by the larger Sr ion [53], i.e. the slight disorder introduced by random substitution. In addition, CO_3^{2-} and HPO_4 were both detected with increasing Sr content, possibly due to the larger structural strain caused by partial substitution of Sr for Ca, which would suggest that Sr–HA can more easily accommodate more carbonate, resulting in the formation of a non-stoichiometric material. Moreover, Capuccini *et al.* [54] showed that the presence of strontium significantly improved osteoblast adhesion in early culture phases. Moreover, cell adhesion increased with increasing strontium content (1, 5, and 10 Sr at.%). The cytotoxicity of Sr-HA containing 1, 5, 10, and 100 mol. (%) was also evaluated by Yuan-Fei et al. [55] via methyltetrazolium (MTT) assay and showed that all of the bioceramics studied had good biocompatibility. Furthermore, osteoblast-like MG63 cells cultured on the Sr-HA nanocrystals containing 0, 1, 3, and 7 atom. (%) displayed good proliferation and increased values of the differentiation parameters [56]. Osteoprecursor cell behavior was examined through MTT reduction at 3, 7, and 14 days of incubation by culturing them onto 10 mol % Sr-HA surface. The authors concluded that Sr-HA induced better cell attachment and proliferation when compared to HA [57].

Here, we have demonstrated that strontium-doped hydroxyapatite gels up 20mol% show a good biocompatibility and are non toxic. Ours preliminary studies of the differentiation of hMSCs towards the osteoblastic-like phenotype was quantitatively determined by carrying out a destructive assay for ALP activity using the p-nitrophenyl phosphate method. ALP is an enzyme produced by differentiating osteoblasts and is present both on the extracellular membrane and in vesicles of the bone matrix, which is the initial site of the formation of calcium phosphate crystals. The enzymatic activity of ALP is crucial for the mineralization process; it acts on the organic phosphate to increase the local concentration of free phosphate and to induce the active transport of both phosphate and calcium across the cell membrane [58]. In our results a steady increase in ALP activity was observed, which may confirm the ability of the gel materials to support hMSC differentiation towards the osteoblast-like phenotype and future could support the ECM mineralization.

Osteogenic differentiation seems to be stimulated by the general presence of strontium, which was shown by the enhanced levels of ALP enzyme activity on all Sr-modified cements. This is strengthened by the higher expression of the late marker of osteogenic differentiation, osteocalcin (OCN). Gene expression shows that HA-10Sr, HA-15Sr and HA-20Sr promote the expression of ALP; in contrast HA-10 and 20Sr promote the expression of OPN on lesser degree as compared with the expression of OPN promoted by HA-15Sr. Moreover, OCN expression was significantly enhanced on HA-15 and 20Sr meanwhile faint signal was detected on HA-10Sr.

The results demonstrated that hydroxyapatite gel containing from 0 to 20 mol. (%) of Sr was successfully produced at room temperature and presented no cytotoxicity. The strontium incorporated in the HA crystal resulted in a solid gel shows good osteogenic properties. Further studies are required to evaluate the potential benefits of Sr-HA as a bone substitute biomaterial and its effects in osteoporosis treatment.

2.1.5 Conclusions

In this study, strontium-substituted hydroxyapatite with different Sr content (5%, 10%, 15% and 20% Sr-HA in mole ratio) has been synthesized at room temperature by using a sol-gel approach. The strontium incorporated in the hydroxyapatite structure decrease slightly the size of HA nanoparticles as demonsrated by morphological analyses. Moreover, the results demonstrated that strontium-doped hydroxyapatite gels up 20mol% show good biocompatibility without significative cytotoxic effect.

This work confirms the ability of the hydroxyapatite modified Sr materials to induce hMSC differentiation towards the osteoblast-like phenotype and future could support the ECM mineralization.

2.1.6 References

[1] Consensus development conference. Diagnosis, prophylaxis, and treatment of osteoporosis. Am J Med 1991;90:107–10.

[2] Johnell JA, Kanis O. An estimate of the worldwide prevalence and disability associated with osteoporotic fractures. Osteoporos Int 2006;17:1726–33.

[3] Rachner TD, Khosla S, Hofbauer LC. Osteoporosis: now and the future. Lancet 2011;377:1276–87.

[4] Yang F, Yang D, Tu J, Zheng Q, Cai L, Wang L. Strontium enhances osteogenic differentiation of mesenchymal stem cells and in vivo bone formation by activating WNT/Catenin signaling. Stem Cells 2001;29:981–91.

[5] Barbara A, Delannoy P, Denis BG, Marie PJ. Normal matrix mineralization induced by strontium ranelate in MC3T3-E1 osteogenic cells. Metabolism 2004;53:532–7.

[6] Marie PJ. Optimizing bone metabolism in osteoporosis: insight into the pharmacologic profile of strontium ranelate. Osteoporos Int 2003;14:S9–12.

[7] Bonnelye E, Chabadel A, Saltel F, Jurdic P. Dual effect of strontium ranelate: stimulation of osteoblast differentiation and inhibition of osteoclast formation and resorption in vitro. Bone 2008;42:129–38.

[8] Caverzasio J. Strontium ranelate promotes osteoblastic cell replication through at least two different mechanisms. Bone 2008;42:1131–6.

[9] Chattopadhyay N, Quinn SJ, Kifor O, Ye C, Brown EM. The calcium-sensing receptor (CaR) is involved in strontium ranelate-induced osteoblast proliferation. Biochem Pharmacol 2007;74:438–47.

[10] Hurtel-Lemaire AS et al. The calcium-sensing receptor is involved in strontium ranelate-induced osteoclast apoptosis. New insights into the associated signaling pathways. J Biol Chem 2009;284:575–84.

[11] Bakker AD, Zandieh-Doulabi B, Klein-Nulend J. Strontium Ranelate affects signaling from mechanically-stimulated osteocytes towards osteoclasts and osteoblasts. Bone 2013;53:112–9.

[12] Peng S, Zhou G, Luk KDK, Cheung KMC, Li ZY, Lam WM, et al. Strontium promotes osteogenic differentiation of mesenchymal stem cells through the Ras/MAPK signaling pathway. Cell Phys Biochem 2009;23:165–74.

[13] Meunier PJ, Roux C, Seeman E, Ortolani S, Badurski JE, Spector TD, et al. The effects of strontium ranelate on the risk of vertebral fracture in women with postmenopausal osteoporosis. New Eng J Med 2004;35:459–68.

[14] Blake GM, Fogelman I. Strontium ranelate: a novel treatment for postmenopausal osteoporosis: a review of safety and efficacy. Clin Interv Aging 2006;1:367–75.

[15] Cheung K, Lu W, Luk K, Wong C, Chan D, Shen J, et al. Vertebroplasty by use of a strontium-containing bioactive bone cement. Spine 2005;30:84–91.

[16] Ni GX, Lu WW, Chiu KY, Li ZY, Fong DYT, Luk KDK. Strontium-containing hydroxyapatite (Sr–HA) bioactive cement for primary hip replacement: an in vivo study. J Biomed Mater Res B 2005;77:409–15.

[17] Romieu G, Garric X, Munier S, Vert M, Boudeville P. Calcium–strontium mixed phosphate as novel injectable and radio-opaque hydraulic cement. Acta Biomater 2010;6:3208–15.

[18] Lao J, Jallot E, Nedlec JM. Strotnium-delivering glasses with enhanced bioactivity: a new biomaterial for antiosteoporotic applications? ChemMater 2008;20:4969–73.

[19] Li ZY, Lu WW, Lam WM, Yang C, Xu B, Ni GX, et al. Chemical composition, crystal size and lattice structural changes after incorporation of strontium into biomimetic apatite. Biomaterials 2007;28:1452–60.

[20] Pina S, Torres P, Goetz-Neunhoeffer F, Neubauer J, Ferreira J. Newly developedSr-substituted alpha-TCP bone cements. Acta Biomater 2010;6:928–35.

[21] Kannan S, Goetz-Neunhoeffer F, Neubauer J, Pina S, Torres P, Ferreira J. Synthesis and structural characterization of strontium- and magnesium-cosubstituted beta-tricalcium phosphate. Acta Biomater 2010;6:571–6.

[22] Ni GX, Lu WW, Xu B, Chiu KY, Yang C, Li ZY et al. Interfacial behaviour of strontium-containing hydroxyapatite cement with cancellous and cortical bone. Biomaterials 2006; 27:5127-33.

[23] Xue-Yang L and De-Min C. Effects of strontium substituted hydroxyapatite of different porosities on osteoblasts in vitro. J Oral Tissue Engineering 2005; 2:66-75

[24] Black J, Hastings G, editors Biomaterial properties. London: Chapman & Hall; 1998. p. 27.

[25] Cazalbou S, Combes C, Rey C. Biomimetic approach for strontium containing Ca–P bioceramics with enhanced biological activity. Key Eng Mat 2001;192–195:147–50.

[26] Verberckmoes SC, Behets GJ, Oste L, Bervoets AR, Lamberts LV, Drakopoulos M, et al. Effects of strontium on the physicochemical characteristics of hydroxyapatite. Calcif Tissue Int 2004;75:405–15.

[27] Li YW, Leong JCY, Lu WW, Luk KDK, Cheung KMC, Chiu KY,et al. A novel injectable bioactive bone cement for spinal surgery: a developmental and preclinical study. J Biomed Mater Res 2000;52:164–70.

[28] Kannan S, Goetz-Neunhoeffer F, Neubauer J, Pina S, Torres P, Ferreira J. Synthesis and structural characterization of strontium- and magnesium-co-substituted beta-tricalcium phosphate. Acta Biomater 2010;6:571–6.

[29] Kuriakose TA, Kalkura SNa, Palanichamyc M, Arivuolid D, Dierkse K, Bocellif G, et al. Synthesis of stoichiometric nanocristalline hydroxyapatite by ethanol-based sol-gel technique at low temperature. J Cryst Growth 2004;263:517-23.

[30] Dessì M, Raucci MG, Zeppetelli S, Ambrosio L. Design of injectable organic-inorganic hybrid for bone tissue repair. J Biomed Mater Res A. 2012;100:2063-70.

[31] Catauro M, Raucci MG, Ausanio G, and Ambrosio L. Sol-gel synthesis, characterization and bioactivity of poly(ether-imide)/TiO_2 hybrid materials. J Appl Biomater Biomech 2007;5:41-48.

[32] D'Antò V, Raucci MG, Guarino V, Martina S, Valletta R, Ambrosio L. Behaviour of human mesenchymal stem cells on chemically synthesized HA-PCL scaffolds for hard tissue regeneration. J Tissue Eng Regen Med. 2013 May 31.

[33] Raucci MG, Guarino V, Ambrosio L. Hybrid composite scaffolds prepared by sol-gel method for bone regeneration. Compos Sci Technol 2010;70:1861-68..

[34] Raucci MG, Alvarez-Perez MA, Meikle S, Ambrosio L, Santin M. Poly(Epsilon-lysine) dendrons tethered with phosphoserine increase mesenchymal stem cell differentiation potential of calcium phosphate gels. Tissue Eng Part A. 2014;20:474-85.

[35] Varma HK, Babu SS. Synthesis of calcium phosphate bioceramics by citrate gel pyrolysis method. Ceramics International 2005;31:109-114.

[36] Suchanek WL, Shuk P, Byrappa K, Riman RE, Ten Huisen KS, Janes VF. Mechanochemical–hydrothermal synthesis of carbonated apatite powders at room temperature. Biomaterials 2002;23: 699-710.

[37] Fowler BO. Infrared studies of apatites. I. Vibrational assignments for calcium, strontium, and barium hydroxyapatites utilizing isotopic substitution. Inorg Chem 1974;13:194-207.

[38] Gadaleta SJ, Paschalis EP, Camacho NP, Betts F,.Mendelhson R, Boskey AL. Fourier transform infrared spectroscopy of synthetic and biological apatites, in:Z. Amjad (Ed.), Mineral scale formation and inhibition, Plenum Press, New York,1995.

[39] Klee WE, Engel G. Infrared spectra of the phosphate ions in various apatites. J Inorganic and Nuclear Chemistry 1970;32:1837-43.

[40] Baddiel CB, Berry EE. Spectra-structure correlations in hydroxyapatite and fluorapatite. Spectrochimica Acta. Part A, Molecular and Biomolecular Spectroscopy 1966;22:1407-16.

[41] Liu Y, Wang W, Zhan Y, Zheng C, Wang G. A simple route to hydroxyapatite nanofibers. Materials Letters 2002;56:496-501.

[42] Han Y, Li S, Wang X, Chen X. Synthesis and sintering of nanocrystalline hydroxyapatite powders by citric acid sol–gel combustion method. Mater Res Bull 2004;39:25-32.

[43] Joris SJ, Amberg CH. Nature of deficiency in nonstoichiometric hydroxyapatites. II. Spectroscopic studies of calcium and strontium hydroxyapatites. J Physical Chemistry 1971;75:3172-78.

[44] Rehman I, Bonfield W. Characterization of hydroxyapatite and carbonated apatite by photo acoustic FTIR spectroscopy. J Materials Science. Mater Med 1997;8:1–4.

[45] Kuriakose T Anee, Narayana Kalkura S, Palanichamy M, Arivuoli D, Karsten Dierks, Bocelli G, Betzel C. Synthesis of stoichiometric nano crystalline hydroxyapatite by ethanol-based sol–gel technique at low temperature. J Crystal Growth 2004;263:517-23.

[46] Elliot JC. Structure and chemistry of the apatites and other calcium ortho phosphates, Elsevier, Amsterdam, 1994.

[47] Ślósarczy A. Paszkiewic Z. Paluszkiewicz C. FTIR and XRD evaluation of carbonatedhydroxyapatite powders synthesized by wet methods. J Molecular Structure 2005;744:657-61.

[48] Murugan R, Ramakrishna S. Development of nano composites for bone grafting. Compos Sci and Tech 2005;65:2385-2406.

[49] Mardziah CM, Sopyan Iand Ramesh S. Strontium-doped hydroxyapatite nanopowder via sol-gel method: effect of strontium concentration and calcination temperature on phase behavior. Trends Biomater. Artif Organs 2009;23:105-13.

[50] Marie PJ. Strontium ranelate: new insights into its dual mode of action. Bone 2007;40:5–8.

[51] Yang F, Yang D, Tu J, Zheng Q, Cai L, Wang L. Strontium enhances osteogenic differentiation of mesenchymal stem cells and in vivo bone formation by activating WNT/Catenin signaling. Stem Cells 2001;29:981–91.

[52] Reginster JY et al. Strontium ranelate reduces the risk of nonvertebral fractures in postmenopausal women with osteoporosis: treatment of peripheral osteoporosis (TROPOS) study. J Clin Endocrinol Metab 2005;90:2816–22.

[53] Li ZY, Lu WW, Lam WM, Yang C, Xu B, Ni GX, et al. Chemical composition, crystal size and lattice structural changes after incorporation of strontium into biomimetic apatite. Biomaterials 2007;28:1452–60.

[54] Capuccini C, Torricelli P, Sima F, Boanini E, Ristoscu C, Bracci B et al. Strontium-substituted hydroxyapatite coatings synthesized by pulsed-laser deposition: In vitro osteoblast and osteoclast response. Acta Biomaterialia 2008;4:1885-93.

[55] Yuan-Fei F and De-Min C. Influence of Sr^{2+} on strontium substituted hydroxyapatite's (Sr-HA) cytotoxicity. J Oral Tissue Engineering 2005;2:76-80.

[56]Capuccini C, Torricelli P, Boanini E, Gazzano M, Giardino R and Bigi A. Interaction of Sr-doped hydroxyapatite nanocrystals with osteoclast and osteoblast-like cells. J Biomed Mater Res Part A. 2009;89:594-600.

[57] Weichang X, Moore JL, Hosick HL, Bose S, Bandyopadhyay A, Lu WW et al. Osteoprecursor cell response to strontium-containing hydroxyapatite ceramics. J Biomed Mater Res Part A. 2006; 7:804-814.

[58] Ciapetti G, Ambrosio L, Savarino L, Granchi D, Cenni E, Baldini N, Pagani S, Guizzardi S, Causa F, Giunti A. Osteoblast growth and function in porous poly-ε-caprolactone matrices for bone repair: a preliminary study. Biomaterials 2003;24:3815–24.

2.2 BIOACTIVE HYDROXYAPATITE-GRAPHENE OXIDE INJECTABLE MATERIAL

Introduction

The synthesis of new biocompatible materials to be used in medicine has acquired a great deal of importance in material science [1]. Hydroxyapatite ($Ca_{10}(PO_4)_6(OH)_2$, HA) is the major component of natural bone tissues. It exhibits excellent biocompatibility and bioactivity with human tissues [2]; as a result, it is currently widely used in various forms and shapes in bone and tissue engineering. Nonetheless, the poor tensile strength and fracture toughness compared with natural bone limit its applications for replacing various parts of the bone systems.

However, the inferior wear resistance and fracture toughness of pure HA cannot match the mechanical behavior of natural bone and would hinder its clinical application in major load-bearing devices as coating materials. To solve this problem, materials such as polyethylene [3], Al_2O_3 [4], TiO_2 [5], zirconia (ZrO_2) [6,7] and carbon nanotubes (CNT) [8] are used as reinforcements in HA to improve its mechanical properties. Although increased mechanical properties have been obtained, these reinforcements, e.g. CNT, due to the presence of metallic catalyst therein, could usually impair the biological property of HA or have adverse effects on adjacent tissues [9]. Some reinforcing material (e.g., ZrO_2) could induce the decomposition of HA during the fabrication process, leading to a substantially reduction in the bioactivity of HA [10].

However, an ideal reinforcement material should impart mechanical integrity to the composite without diminishing its bioactivity. Carbonaceous materials with high chemical inertness are widely recognized to exhibit good biocompatibility [11]. A recently discovered carbon-based two-dimensional (2D) nanostructure, known as graphene, is particularly attractive.

Graphene is a flat monolayer of carbon atoms tightly packed into a two-dimensional (2D) honeycomb lattice and is a basic building block for graphitic materials of all other dimensionalities with unique physical, chemical, and mechanical properties [12]. Graphene and graphene oxide (GO) layers have become a hotspot so far and have been actively investigated to build new composite materials [13].

It has been shown that graphene induces no obvious toxic effects in vivo [14]. It possess the large aspect ratio, high mechanical strength, and superior electrical conductivity [15,16], as a result, has the potential to strengthen and toughen HA without offsetting its bioactivity.

The presence of abundant epoxide, hydroxyl and carboxylic groups on the GO basal plane could provide enormous reactive sites for chemical interactions. Furthermore, the good high mechanical properties, high hydrophilicity and good biocompatibility of GO sheets suggest that the GO could be ideal and promising nanoscale reinforcement fillers in biocomposites, enhance the interfacial bonding in the composites and increases its bioactivity.

The reactive oxygenic groups, present on the edges (carbonyl and carboxyl groups) and planes (hydroxyl and epoxide groups) of GO sheets, can stabilize the dispersion of GO in aqueous media, enhance the interfacial bonding within the components, and facilitate the stress transfer in the composites [17], which render GO as attractive and promising nanoscale reinforcement fillers in biocomposites (incorporated into either a polymer or an inorganic matrix) [18]. Improved mechanical properties have been observed in GO based chitosan [19], gelatin [20], starch [21], and poly(e-caprolactone) (PCL) [22] biopolymer composites. In addition, GO increased the bioactivity of gelatin [20] and PCL [22] during biomineralization, by promoting the nucleation of hydroxyapatite (HA) nanoparticles in simulated body fluid (SBF).

Recently, more and more research works have been devoted to the fabrication of graphene or its derivatives reinforced HA biocomposites [23-26]. The incorporation of graphene or its derivatives in HA composites has been reported in several literatures using biomimetic mineralization process [26,27], spark plasma sintering (SPS) technique [28], radio-frequency chemical vapor deposition [29], electrospinning method [30] and so on. The cytotoxicity of the graphene based fillers shown a dose-dependent [31]. And most of the resulting composites displayed a favorable biological performances toward the proliferation and growth of L929 fibroblast cells [32], MC3T3-E1 pre-osteoblast cells [33,34] and MG63 human osteosarcoma cells [32]. GO can be produced simply in large scale with significantly low cost and little impurities (metals) as opposed to CNT, a significant advantages for synthesizing high-performance biocomposites. In addition, GO is an emerging material with good biocompatibility [35] as well as antibacterial activity [36], which provide promising opportunities to improve orthopedic implant application [37].

For these reasons, our research activity concerns the possibility to use a dual approach to prepare biomineralized hydroxyapatite nanocrystals/graphene for bone tissue regeneration. The first approach is represented by sol-gel technology [38] that is a facile, economical and effective process to prepare hybrid material based on nano-HA embedded in GO sheet. The second approach concerns the use of biomimetic method in order to obtain a coating of calcium phosphate on GO sheet. In both cases, we evaluate their effect on human Mesenchymal Stem Cells (hMSC) in terms of proliferation and early osteogenic differentiation [39], in order to develop a new class of

multi-functional hybrid material with excellent biological and conductive properties, and make them highly promising materials for biomedicine.

2.2.1 Materials and methods

2.2.1.1 Synthesis of GO

Graphene oxide was synthesized from Graphene Nanoplatelets using a modified and simplified Hummers' method [40]. In particular this material was obtained by oxidation of 0,5g of GNP with 25mL of H_2SO_4 (sulfuric acid 99,999%, Aldrich), 1g of KNO_3 (potassium nitrate Aldrich) and 3g of $KMnO_4$ (potassium permanganate Aldrich). Typically a mixture of GNP and KNO_3 in H_2SO_4 was stirred for few min below 5°C in ice bath. After than $KMnO_4$ was added slowly with stirring in small portions to prevent temperature rise in excess of 20 °C. Then, the temperature of the reaction mixture was raised to 35 °C and the mixture was stirred for 60 min. After completion of the reaction, 100 mL of deionized water was gradually added into the solution. The suspension was reacted further by adding a mixture of H_2O_2 (7 mL, 30%) and water (55 mL). During oxidation, the color of the mixture changed from dark purplish-green to dark brown. To stop the oxidation process, H_2O_2 solution was added and the color of the mixture changed to bright yellow, indicating a high oxidation level of graphite. The GO was separated from the reaction mixture by filtration and successively was washed five times with deionized water until a pH of 4–5 was achieved. The washing process was carried out using a simple decantation of the supernatant with a centrifugation technique. During the washing process with deionized water, the graphite oxide underwent exfoliation, which resulted in thickening of the graphene oxide solution, forming graphene oxide gel which was used to obtain the graphene oxide solid.

2.2.1.2 In situ preparation of HA-GO

HA $[Ca_{10}(PO_4)_6(OH)_2]$ is synthesized by sol-gel process (figure 1). The molar ratio of calcium to phosphorus Ca/P varies from 1.2 to almost 2 in HA. The stoichiometric molar ratio of HA is 1.67; however, this is not the value observed in the organism because small amounts of other materials such as carbon, nitrogen, iron and another elements are incorporated.

$Ca(NO_3)_2x4H_2O$ and $(NH_2)_4H_2PO_4$ were used as the Ca and P sources, respectively. HA-GO with different GO content (1%, 1.5%, 2% w/w) were synthesized. $Ca(NO_3)_2x4H_2O$ and $(NH_2)_4H_2PO_4$

were dissolved in distilled water in appropriate ratio. Exfoliation of graphene was carried out in appropriated amount of water through sonication for several hours.

When $Ca(NO_3)_2 x4H_2O$ was completely dissolved in water, Ca^{2+} solution was added to GO sheet water solution to promote the interaction between ions Ca^{2+} and lateral and superficial groups of GO. A homogeneous system was obtained by ultrasonic dispersion for 30 min, after them a phosphorous solution was added drop wise and pH was adjusted at alkaline value (pH equal to 11) by NH_4OH solution. Gelation take place after 2hrs of magnetic stirring at room temperature.

2.2.1.3 Biomimetic approach to prepare biomineralized GO

To produce biomineralized products GO sheets were submitted to a bio-inspired procedure, namely biomimetic treatment, inspired by the method described by Kokubo and co-workers [41,42]. In particular, the treatment combines the preliminary use of a supersaturated SBF solution ($5xSBF_1$) to stimulate the nuclei formation, while a fresh chemically-modified solution ($5xSBF_2$) is further used, in order to promote the growing of apatite nuclei, once formed. Meanwhile, $5xSBF_1$ was prepared by sequentially dissolving $CaCl_2$, $MgCl_2 \cdot 6H_2O$, $NaHCO_3$ and $K_2HPO_4 \cdot 3H_2O$ in distilled water. Solution pH was lowered to 6 by adding hydrochloric acid HCl (1M) to increase the solubility. Na_2SO_4, KCl and NaCl were added until the previous solution become clear. The final pH was adjusted with 1M NaOH to reach a final pH equal to 6.5 ($5xSBF_1$).

Therefore, Mg^{2+} and HCO_3^- free 5xSBF was prepared by adding $CaCl_2$, $K_2HPO_4 \cdot 3H_2O$ and NaCl subsequently to distilled water up to obtain a fresh solution ($5xSBF_2$). In this case, the solution pH was lowered to 6.0 with hydrochloric acid to increase the solubility. Both solutions were buffered at pH 6.5 and 6 respectively, by using Trishydroxymethylaminomethane-chloric acid (Trizma-HCl). In table 1, the ionic concentration of blood plasma, SBF, $5xSBF_1$ and $5xSBF_2$ were reported. All solutions were prepared freshly before the use.

The biomimetic treatment consists in two steps in pH-controlled environment: during the first step, samples with pre-ordered size were soaked into $5xSBF_1$ at pH=6.5 where the 5xSBF solution volumes have been calculated respect to the total scaffold material surface by using an exposed surface to SBF volume ratio equal to 10 mm^2/ml, as reported in literature [43]. The solution temperature was fixed at 37°C during the treatment. After the sequential immersion in $5xSBF_1$ (3 days) and in $5xSBF_2$ (4 days), all scaffolds were gently rinsed in distilled water to remove excess ions and, then, dried overnight under laminar hood.

Ion Concentration (mM)	Na^+	K^+	Ca^{2+}	Mg^{2+}	HCO_3^-	Cl^-	HPO_4^-	SO_4^{2-}
Blood plasma	142	5	2.5	1.5	27	103	1	0.5
SBF	142	5	2.5	1.5	4.2	148	1	0.5
5xSBF$_1$	710	25	12.5	7.5	21	740	5	2.5
5xSBF$_2$	710	10	12.5	-	-	735	5	-

Table 1: The ionic concentration of human blood plasma, SBF, 5xSBF$_1$ and 5xSBF.

2.2.2 Characterization

2.2.2.1 X-Ray diffraction and Infrared Spectroscopy FTIR analyses

Phase analysis was conducted using X-ray diffraction (XRD) to detect phase composition and crystallinity of HA-GO materials. An X-ray diffractometer (XRD-PANalytical X'Pert Pro) was used; the specimens were scanned from $2\Theta = 0°$ to $70°$ using CuKα radiation. FTIR spectroscopy was performed on Nicolet Nexus spectrophotometer with KBr discs in the 500-4000 cm^{-1} region (4 cm^{-1} resolution, average 64 scans).

2.2.2.2 Morphological characterization

The morphology of the composite materials was characterized by using a Scanning Electron Microscope (SEM) and Transmission Electron Microscope (TEM). For SEM analysis, the materials were mounted by a double adhesive tape to aluminum stubs. The stubs were sputter-coated with gold to a thickness of around 20nm. SEM analysis was performed at different magnification at 20 keV. X-ray energy dispersive spectroscopy (EDAX, Genesis 2000i) analysis was used for a qualitative estimation of the Ca/P ratio.

The Transmission Electron Microscopy (TEM) images were taken by a Hitachi H-9000NAR model instrument operated at an accelerating voltage of 100 kV. Samples for TEM imaging were prepared by placing a drop of the aged HA-GO composite suspensions (the suspensions were diluted in deionized water and dispersed by ultrasonic waves before use) onto carbon coated copper grids, dried in air and loaded into the electron microscope chamber.

2.2.2.3 Bioactivity test

To evaluate the bioactivity properties of HA-GO hybrid material, only one formulation (HA-GO1,5wt%) was submitted to a bio-inspired procedure, inspired by the method described by Kokubo and co-workers [41,42] as discussed previously.

2.2.2.4 Biological properties

In vitro cell culture

Biological assays were performed using human mesenchymal stem cells line (hMSC) obtained from LONZA (Milano, Italy). hMSC were cultured in 75 cm^2 cell culture flask in Eagle's alpha Minimum Essential Medium (α-MEM) supplemented with 10% Fetal Bovine Serum (FBS), antibiotic solution (streptomycin 100 µg/ml and penicillin 100U/ml, Sigma Chem. Co) and 2 mM L-glutamine. hMSCs from passages 4 through 6 passage were used for all the experimental procedures and incubated at 37°C in a humidified atmosphere with 5% CO_2 and 95% air.

Viability test

To evaluate cell biocompatibility, hMSC were plated at concentration of 1.6×10^4 in triplicate onto HA, GO, GO_SBF and HA-GO materials at different concentrations (1 - 1.5 - 2 wt%). The medium in cell-load gel materials culture plates were removed after cultured for 7, 14 and 21 and the *in vitro* cell viability was checked by the Alamar blue assay (AbD Serotec, Milano, Italy). This assay quantified the redox indicator which changed to a fluorescent product in response to the chemical reduction by mitochondrial enzymes such as flavin mononucleotide dehydrogenase, flavin adenine dinucleotide dehydrogenase, and nicotinamide adenine dinucleotide dehydrogenase. In addition, a redox phenomenon gave a quantitative indication of metabolic activity of live cells. An aliquot of 1mL of Alamar Blue™ diluted 1:10 in phenol red-free medium was added to each well and incubated for a further 4 h at 37°C, 5% CO_2. Later, 200µL of this solution was transferred into a 96 well plate for colorimetric analysis. Wells without any cells were used to correct any background interference from the redox indicator. The optical density was immediately measured with a spectrophotometer (Sunrise, TECAN, Männedorf, Zurich, Switzerland) at wavelengths of 540 and 600 nm. The cell viability percentage was evaluated in according to the manufacturer's protocol. The culture medium during experimental time was changed every two days.

Alkaline Phosphatase assay

The alkaline phosphatase activity of the hMSC onto HA, GO, GO_SBF and HA-GO at different concentrations (1 - 1.5 - 2 wt%). was determined for 7, 14 and 21 days of culture by a spectrophotometric end-point assay that determined the conversion of colourless p-nitrophenyl phosphate as substrate to coloured p-nitrophenol following the manufacturer's protocol (Sensolyte pNPP ALP assay Kit, AnaSpec). Briefly, at the end of each time point, cultures were washed gently with PBS followed by washing twice with cold 1X assay buffer. For extract cell layers the cultures were lysing with 1X lysis buffer with 0.2% of Triton X-100. The phosphatase activity was analyzed onto the cell lysates (50μl) by measuring the ALP activity when ALP enzyme catalyzes the cleavage of a phosphate group and release p-nitrophenol from p-nitrophenyl phosphate in alkaline buffer solution after 30 min at 37°C. Sample absorbance was measured in a 96-well plate at 405 nm. To correct the ALP values for the number of cells present on each scaffold double stranded DNA (dsDNA), as a marker for cell number, was measured using a PicoGreen_dsDNA quantification kit (Invitrogen). First, 100μl of 200μl diluted Picogreen_dsDNA quantification reagent was added to 100 ml of cell lysates in a flat-bottomed, 96-well plate. Following 10 min incubation, the fluorescence of Picogreen was determined at a wavelength of 520 nm after excitation at 585 nm using a plate reader (multilabel counter 1420 Victor, Perkin-Elmer, Italy). dsDNA was quantified according to a calibration curve of l-dsDNA standard in 10 mM Tris, 1 mM EDTA, pH 7.5, buffer. Each experiment was performed three times in triplicate. The results of ALP activity were reported as nanograms of ALP normalized to the micrograms of total DNA content.

2.2.3. Results and discussions

2.2.3.1 In situ preparation of HA-GO

For HA-GO synthesis was supposed a simple mechanism (figure 1) where the oxygen-containing functional groups (such as hydroxyl and carboxyl identified by the FTIR analysis) present on the basal plane and edges of the GO sheets may play a pivotal part in anchoring calcium ions. When $Ca(NO_3)_2x4H_2O$ was added into the GO solution, the Ca^{2+} cations would be attracted and anchored on the oxygen atoms through electrostatic interactions [44] and functioned as the nuclei for the crystallization and growth of the HA particles. The Ca^{2+} could in situ react with the ambient drop wise phosphate ions via electrovalent bonds to form HA nanoparticles [45]. Furthermore the high pH values (pH > 10) and high reaction temperature could be beneficial for the in situ crystallization of HA on GO sheets with better crystallographic quality [46]. It is reported that high pH values

would promote the deprotonation of carboxyl groups (-COOH) on the GO sheets and make GO more charged and hydrophilic [47], which in turn might enhance the interaction between the GO substrates and HA nanoparticles.

2.2.3.2 Biomimetic approach to prepare biomineralized GO sheet

Biomimetic mineralization was induced by incubating GO sheet in a supersaturated $5\times$SBF solution. The presence of anionic functional groups in GO facilitates, in the first step of treatment (3days), the nucleation of biominerals by attracting more Ca^{2+} cations to deposit onto film surface and subsequently forming biominerals with PO_4^{3-}. The second step of treatment concerns the growth and crystallization of apatite in a Mg^{2+} and HCO_3^- free 5xSBF solution for 2 days (figure 2). In our experiments a deposition of amorphous calcium phosphate (ACP) was observed. ACP is often encountered as a transient phase during the formation of calcium phosphates in aqueous systems. Usually, ACP is the first phase that is precipitated from a supersaturated solution prepared by rapid mixing of solutions containing of calcium cations and phosphate anions [48]. ACP is also treated as a precursor of biological apatite during bone formation.
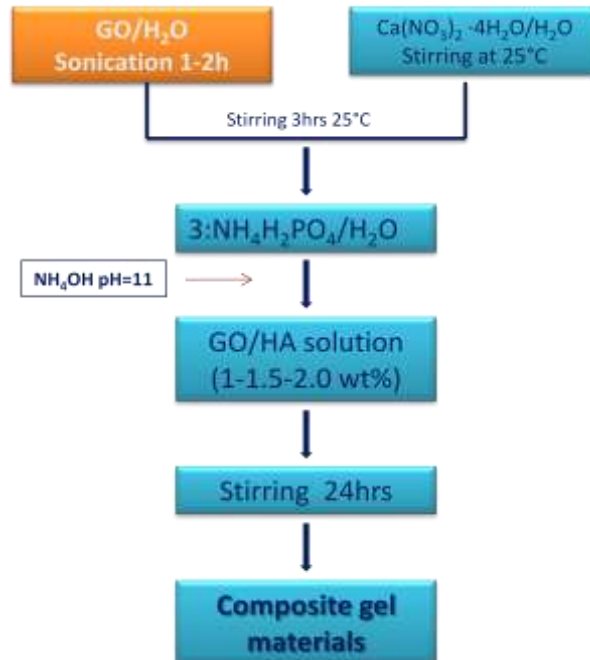
Fig. 1: Mechanism of in situ preparation of HA-GO hybrid materials by sol-gel method.
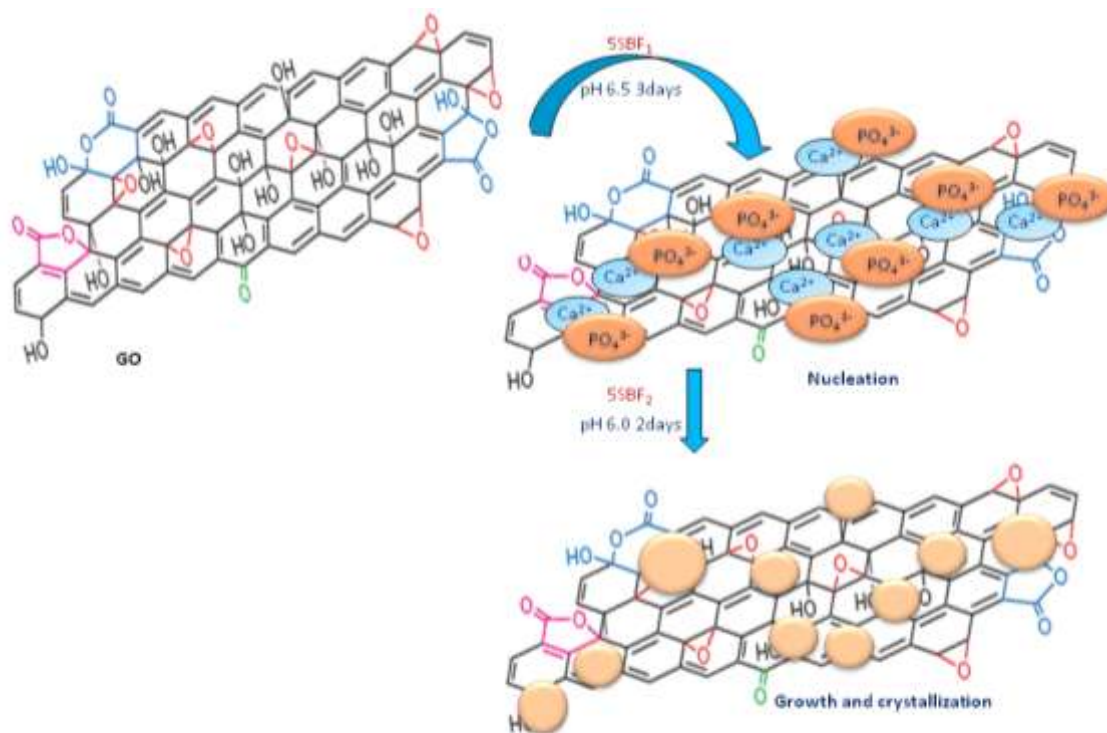
Fig. 2: Mechanism of biomimetic preparation of biomineralized GO.

2.2.3.3 X-Ray diffraction and Infrared Spectroscopy FTIR analyses

Sol-gel technology allows to synthesize HA-GO hybrid materials at room temperature. When $Ca(NO_3)_2$ was added into the GO solution, the Ca^{2+} cations would be attracted and anchored on the oxygen atoms through electrostatic interactions and functioned as the nuclei for the crystallization and growth of the HA nanoparticles as demonstrated by FTIR analysis.

The FTIR spectra of the GO, HA, GO and HA-GO at different concentrations are shown in figure 3A; meanwhile FTIR spectra of GO sheet before and after SBF treatment are shown in figure 3B. The transmittance bands at 3398 cm^{-1} were assigned to hydroxyl group (–OH) stretching, 1730 cm^{-1} to the stretching vibration of carboxyl groups (–COOH) on the edges of the basal planes or conjugated carbonyl groups (–C=O), 1623 cm^{-1} to the stretching vibration of C=C, 1266 cm^{-1} to the stretching vibration of C–OH, 1054 cm^{-1} to the stretching vibration of C–O, and the 833 cm^{-1} to the characteristic adsorption peak of epoxy groups. The stretching band of phosphate at 1039 cm^{-1} in pure HA shifted to 1037 cm^{-1} and 1033 cm^{-1} in HA-GO, respectively, indicating the formation of strong hydrogen bonding between the HA nanoparticles and the GO-based sheets.

The phases of the GO, HA, GO_SBF and HA-GO at different concentrations were investigated by XRD. The Bragg diffraction peaks of the two GO-based HA composites, shown in figure 4A,

agreed quite well with those of the pure synthesized HA (PDF# 09-0432) at 2θ values of 25.9°, 31.8°, 39.8°, 46.7°, 49.5° and 53.2°, which were indexed to be (002),(211), (310), (222), (213) and (004) planes, respectively. Meanwhile, the broad diffraction peaks suggested that the prepared HA particles were nanocrystallites [49], which were proposed to have superior osteointegrative properties toward micro HA [50,51], and were much easier to be embedded or incorporated into the GO matrix [52]. The strong and sharp (002) peak of the GO sheets at 2θ = 11.1°, as shown in the inset of figure, shifted and become more sharp in the composites, indicating the successful exfoliation of the graphene oxide sheets (due to the loss of their crystallographic order after being treated by ultrasonic dispersion) and the intercalation of the HA nanoparticles. Meanwhile an amorphous state appears in biomineralized composite obtained by biomimetic approach (figure 4B). This result could be obtained by a short treatment involving only 2 days of incubation (5xSBF$_2$) for growth and crystallization.
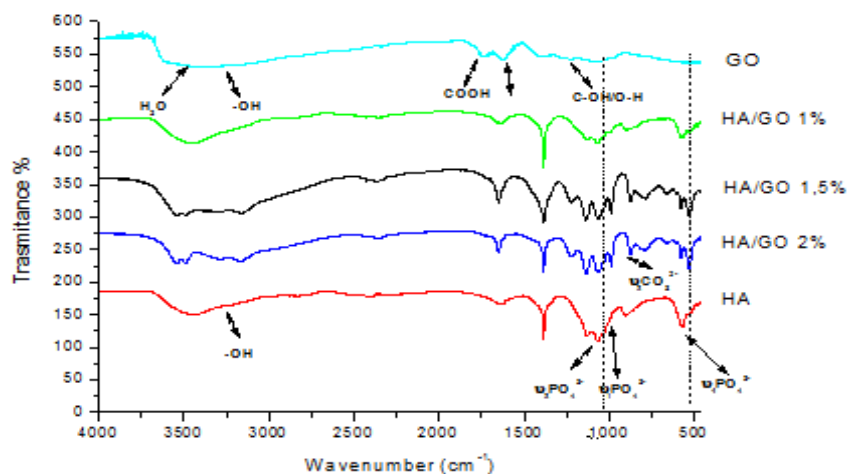
(A)
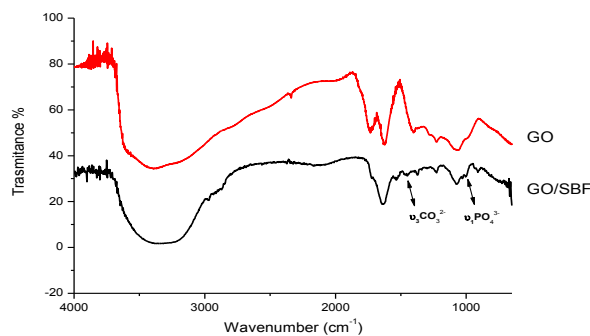
(B)

Fig. 3: FTIR analysis of GO, HA and HA-GO at different concentrations prepared by (A) sol-gel method and biomimetic approach (B).
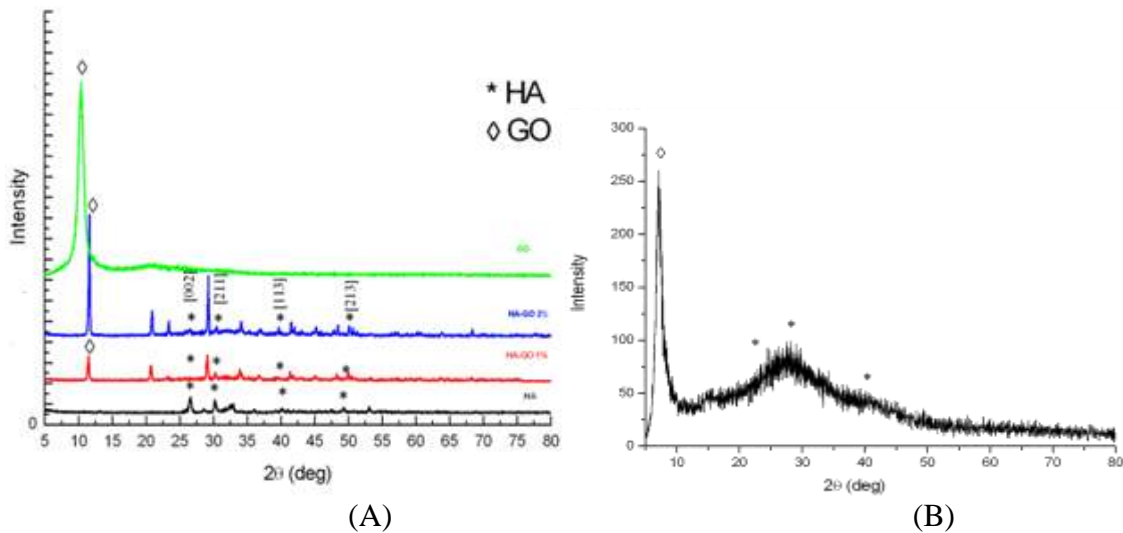
Fig. 4: XRD analysis of GO, HA and HA-GO at different concentrations prepared by (A) sol-gel method and biomimetic approach (B).

2.2.3.4 Morphological characterization

SEM and TEM analyses were performed on HA-GO hybrid materials obtained by in situ preparation and biomimetic approach. SEM images (figure 5) demonstrated that is not possible to evaluate a phase separation but there is a good intercalation of HA nanoparticles in GO sheet. Moreover for all materials with different amount of GO (1- 1.5 and 2wt%) is not observed the presence of any clusters (figures 5A-C). The Ca/P ratios of HA formed in graphene oxide determined by EDAX analysis (figre 5D) were about 1.65, slightly lower than the stoichiometric ratio of Ca/P in HA (1.67), but close to that of natural bone [53,54], which were thought to endow the biocomposites with higher bioactivity [55,56]. Meanwhile, different morphology was observed for composite material prepared by biomimetic approach. In fact, SEM/Energy Dispersive X-ray Spectroscopy (EDAX) image of GO sheet after treatment in supersaturated 5xSBF solutions is shown in figure 6. The image shows that after 3 days of soaking in $5xSBF_1$, followed by immersion for 4 days in 5xSBF, the GO sheet was covered by a calcium phosphate layer (figures 6A-B). The EDAX analysis shows that the layer is composed mainly of amorphous calcium phosphate, with a Ca/P molar ratio of 1.20 (figure 6C). More information are obtained by TEM analysis (figure 7). The TEM images of GO sheet (figure 7A) demonstrated a good exfoliation of material after ultrasonic treatment and by images is possible to evaluate that the presence of sheet modeling the distribution of ceramic nanoparticles. In fact, increasing GO amount a better dispersion id observed.
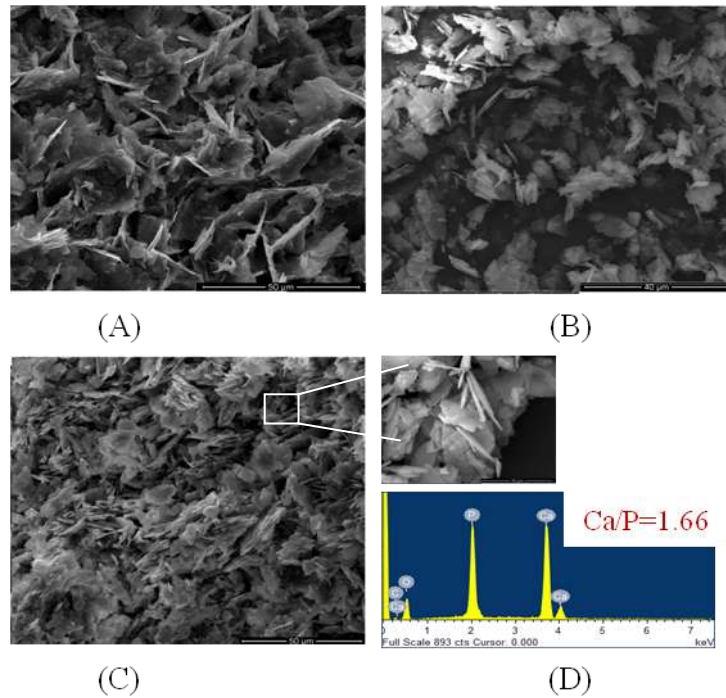
Fig. 5: SEM images of HA-GO 1 (A) - 1.5 (B) - 2 (C) wt%; EDS analysis performed on HA-GO 2wt% (D).

This behavior could be explained because the sol-gel reaction allows a good interaction between the oxygenated regions in hydrophilic zones, such as carboxyl and hydroxyl of GO and hydrophilic HA nanoparticles. Moreover, the uniformly dispersion is explained by nanometric size of hydroxyapatite synthesized by sol-gel method as demonstrated by TEM analysis (figure 7). The HA particles were in a typical spindle-like shape with a diameter of about 5 nm and a length of around 70 nm on the GO sheets.
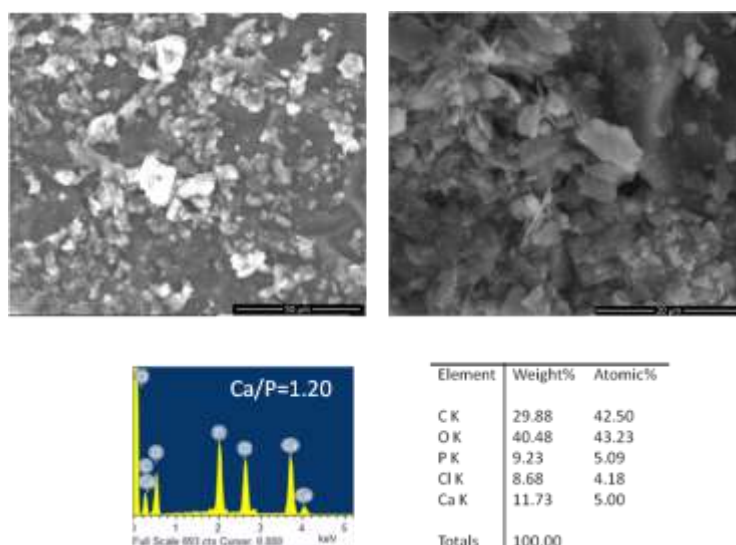
Fig. 6: SEM images at different magnifications and EDS analysis of GO sheet after 5 days SBF treatment.

In our study, the HA-GO samples were treated ultrasonically before TEM observation, it can be seen that almost no HA particles are scattered out of the matrix, indicating a strong interaction between the HA particles and the GO. The high specific surface area of GO is also beneficial for high loading levels of the HA particles and is helpful for forming an effective network inside the biocomposite. Different results were obtained by GO sheet after SBF treatment in both steps (figure 8). In fact, TEM analysis clearly shows that the particles of amorphous calcium-phosphate were nanosphere-like and not nanocrystalline HA with acicular shape as appear for nanocomposite HA-GO and in accordance with SEM results.
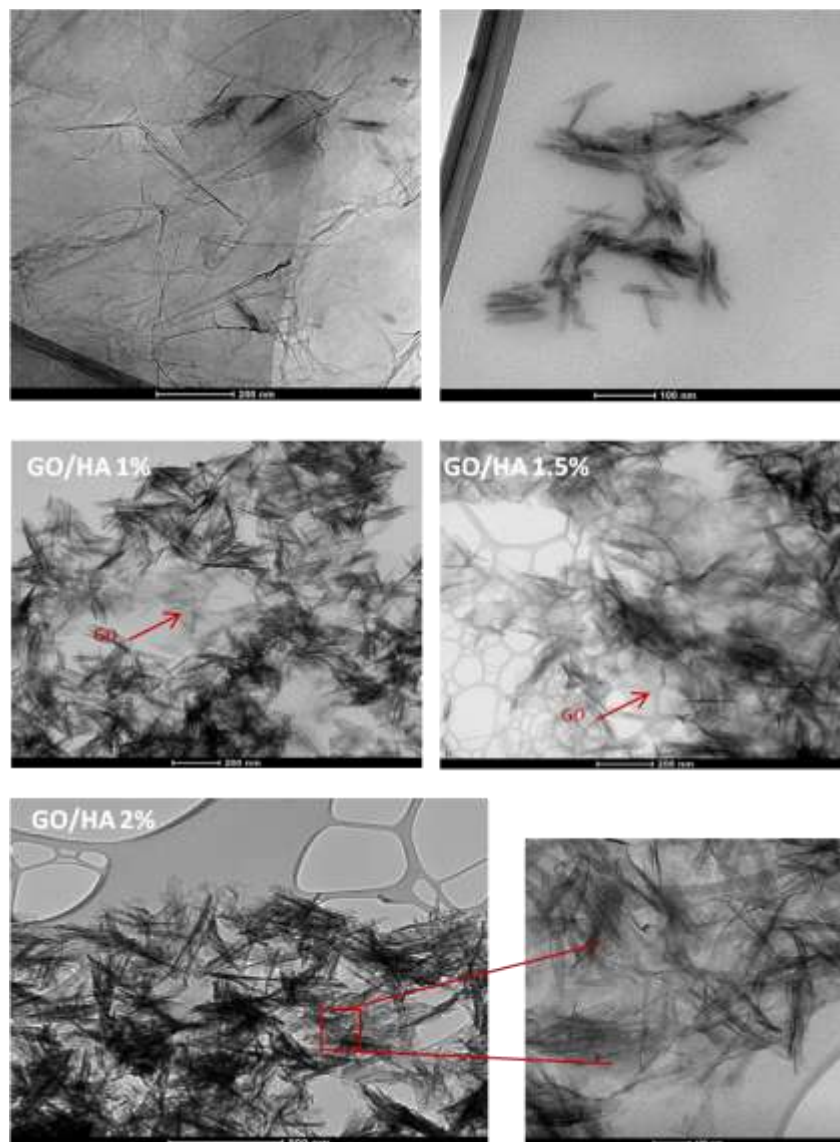
Fig. 7: TEM analysis of GO, HA and HA-GO at different concentrations.
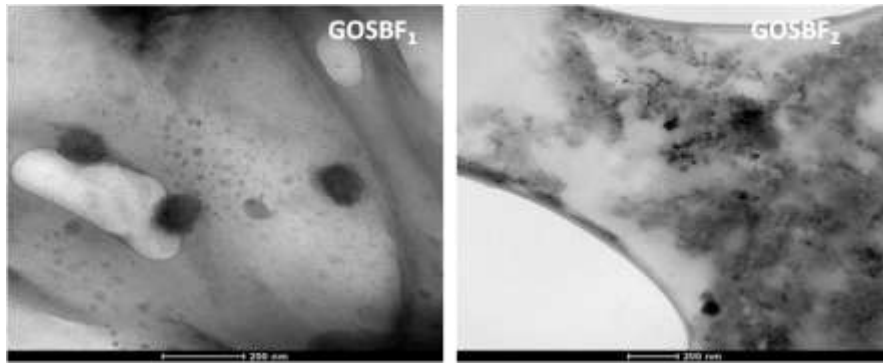
Fig. 8: TEM analysis of GO sheet after 5xSBF$_1$ and 5xSBF$_2$ treatments, respectively.

2.2.3.5 Bioactivity test

SEM observations performed on HA-GO1,5wt%, incubated for a shorter time (5days) in a supersatured 5xSBF solution further revealed that graphene–hydroxyapatite hybrid material highly accelerated the formation of HAp crystals (figure 9) on the surface than to GO sheet.
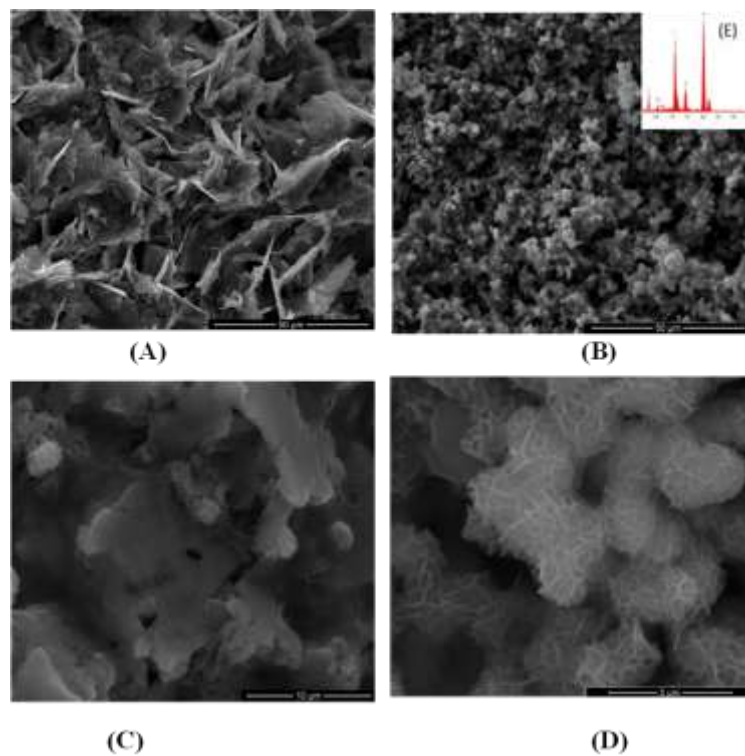
Fig. 9: SEM images of HA-GO1,5wt% in cross-section before (A) and after SBF treatment on surface at different magnification (B-D).

The images performed on the surface and in cross-section of HA-GO, demonstrated a hybridization of HA nanoparticles in GO sheet and an increasing of bioactive properties of materials after SBF treatment. In fact, in the figure is possible to evaluate the presence of coating on surface and some depositions of calcium phosphate intercalated among the GO sheet (Figures 9A-D).

The analyses show that the rose petal-like apatite crystallites are composed mainly of hydroxyapatite, with a Ca/P molar ratio of 1.67. The EDAX spectra clearly shows Ca and P peaks which are typical of hydroxyapatite (figure 9E), and smaller peaks of sodium, chlorine and magnesium due to the presence of impurities such as sodium, chlorine and magnesium commonly present in biomimetic apatite.

2.2.3.6 Biological results

It is no doubt that the material used for bone tissue engineering should be non-toxic and have good cell biocompatibility, which is a central criterion to ultimately decide the feasibility of implantation in body [57]. The information of proliferation on the materials provided by cell culture experiment *in vitro* is often used as an important initial evaluation of cell biocompatibility [58]. In this work human mesenchymal stem cells (hMSC), largely used to evaluate the regeneration of mineralized ECM in bone defects [59-62], were used as cell line model for *in vitro* testing of biocompatibility and osteogenic potential of the HA-GO materials.

The cell proliferation on the different materials (HA, GO, HA-GO, GO_SBF) were assessed using Alamar Blue test. Figure 10 shows the effect of the materials on the metabolic activity of hMSC after 7, 14 and 21 days of culture. According to the data, it can be found that MSCs dramatically increase with time during the *in vitro* culture period; suggesting that the materials are nontoxic, not affecting the cell proliferation and showed good biocompatibility. In particular, the results show that the cell proliferation is better for GO sheets than HA material, this is explained by the presence of active group and a charge surface. Moreover, GO_SBF materials after SBF treatment show a good proliferation in the time similar to GO sheet. This result could be explained by a large surface of GO in contact with cells and the presence of small clusters of amorphous calcium phosphate have a negligible effect on cell proliferation. Meanwhile, in the composite materials a slight decreasing of proliferation activity was observed even if it keep at higher value than the control.

Besides the amount of the proliferated cells, the differentiations of the cell should be another important parameter to estimate the biological effect of calcium phosphate particles. ALP activity

assay (figure 11) was used to evaluate the differentiation of hMSCs on the different composite materials (HA, GO, HA-GO, GO_SBF).
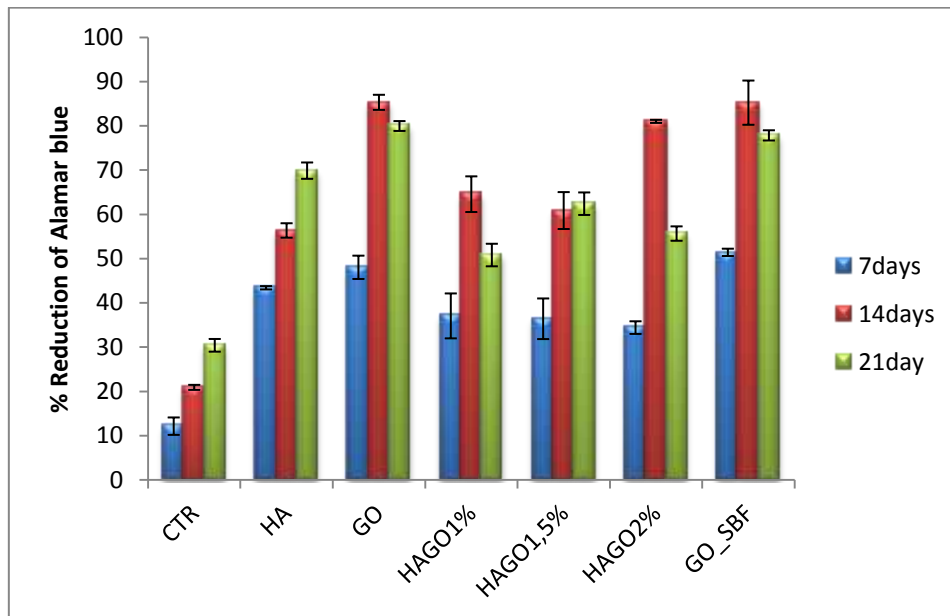
Fig. 10: Alamar blue of GO, HA, HA-GO (1 - 1,5 - 2wt%) and GO_SBF at 7, 14 and 21days.
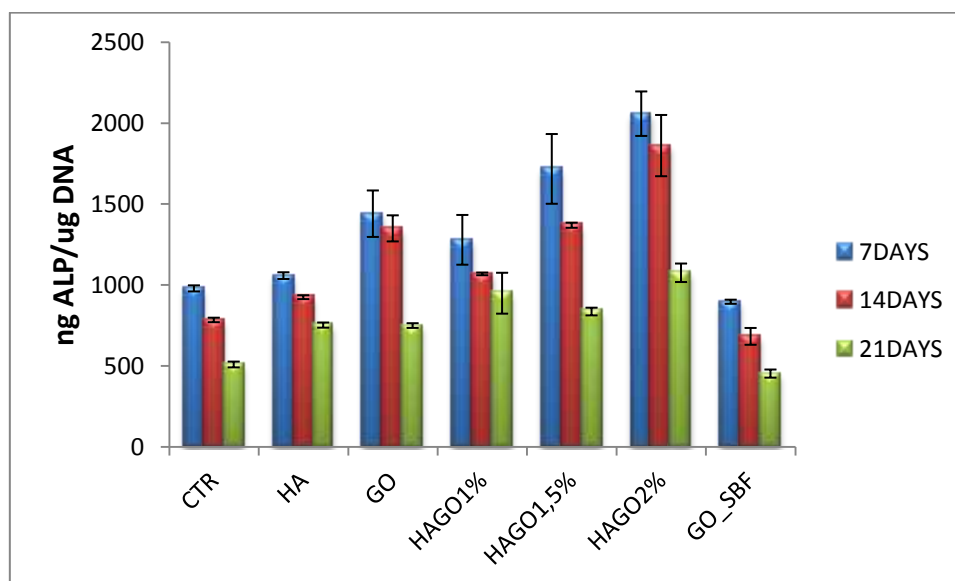
Fig. 11: ALP assay of GO, HA, HA-GO (1 - 1,5 - 2wt%) and GO_SBF at 7, 14 and 21days in basal medium.

Ours preliminary studies of the differentiation of hMSCs towards the osteoblastic-like phenotype was quantitatively determined by carrying out a destructive assay for ALP activity using the p-nitrophenyl phosphate method. ALP is an enzyme produced by differentiating osteoblasts and is present both on the extracellular membrane and in vesicles of the bone matrix, which is the initial

site of the formation of calcium phosphate crystals. The enzymatic activity of ALP is crucial for the mineralization process; it acts on the organic phosphate to increase the local concentration of free phosphate and to induce the active transport of both phosphate and calcium across the cell membrane [63]. ALP is an important feature of osteoblast cells expressed in their differentiation phase and a significant quantitative marker of osteogenesis.

The *in vitro* ALP activity of hMSC cells cultivating with HA-GO hybrids was evaluated. As shown in Fig. 11, the combination of HA and GO allows to obtain the ALP expression already in the first days of cell-materials interaction. The figure 11 shows that for GO and biocomposite obtained by sol-gel approach the ALP value are highest in the first 14 days; in particular it is possible to evaluate that ALP value increasing with the amount of GO in composite materials. Meanwhile the ALP values for GO sheet after SBF treatment are similar to control (CTR) and lowest than biocomposite materials. This result might be due to amorphous state of calcium phosphate clusters deposited on GO surface that delay the expression of ALP from hMSC in a basal medium without osteogenic factors like ascorbic acid, dexamethasone and β-glycerophosphate .

2.2.4 Conclusions

In this study, we have demonstrated a facile dual approach to prepare biomineralized hydroxyapatite nanocrystals/graphene oxide. In the first approach, we have demonstrated a facile solution-based *in situ* synthesis by sol-gel method of hydroxyapatite nanoparticles in graphene oxide sheets. The spindle-like HA nanoparticles with a diameter of about 5 nm and a length around 70 nm, were intercalated uniformly and strongly with the GO sheets. The interaction between HA nanoparticles and GO improves the bioactivity of materials demonstrated by the formation of a hydroxyapatite layer on material surface after biomimetic treatment. Moreover, the thus-formed HA-GO hybrids supported high viability of hMSC cells and induce an osteogenic differentiation evaluated by using a media without osteogenic factors. The second approach is represented by using a simple biomimetic method based on supersaturated 5xSBF solution. A layer of amorphous calcium phosphate (ACP) appears on GO sheet after 5 days of incubation. The composite sustains the cell viability and proliferation, however it delays the expression of ALP, early marker of osteogenic differentiation, in a basal medium. *In vitro* bioactivity and biocompatibility of biomineralized graphene materials present the new prospect of utilizing graphene-based materials in clinical and biomedical applications. The combination of HA with GO leads to the further development of a broad new class of multi-functional biomaterials.

2.2.5 References

[1] Hench LL. Bioceramics − From Concept to Clinic. J Am Ceram Soc 1991;74:1487−1510.

[2] Sautier JM, Nefussi JR, Forest N. Ultrastructural study of bone formation on synthetic hydroxyapatite in osteoblast cul- tures. Cells Mater.1991;1:209−17.

[3] Fang L, Leng Y and Gao P. Processing and mechanical properties of HA/UHMWPE nanocomposites. Biomaterials 2006;27:3701–07.

[4] Li J, Fartash B, Hermansson L. Hydroxyapatite-alumina composites and bone-bonding. Biomaterials 1995;16:417−22.

[5] Li H, Khor KA, Cheang P. Titanium dioxide reinforced hydroxyapatite coatings deposited by high velocity oxy-fuel (HVOF) spray. Biomaterials 2002; 23:85-91.

[6] Silva V, Lameiras FS, Dominguez RZ. Microstructural and mechanical study of zirconia-hydroxyapatite composite ceramics for biomedical applications. Compos Sci Technol 2001;1−2:133–36.

[7] Chiu CY, Hsu HC., Tuan WH. Effect of zirconia addition on the microstructure evolution of porous hydroxyapatite. Ceram Int 2007;33:715–18.

[8] Susmita M, Biswanath K, Swarnendu S, Abhijit C. Improved properties of hydroxyapatite−carbon nanotube biocomposite:Mechanical, in vitro bioactivity and biological studies. Ceram Int 2014;40:5635–43.

[9] Lahiri D, Ghosh S, Agarwal A. Carbon nanotube reinforced hydroxyapatite composite for orthopedic application: a review. Mat Sci Eng C-Mater 2012;32:1727–58.

[10] Choi JW, Kong YM, Kim HE, Lee IS. Reinforcement of hydroxyapatite bioceramic by addition of Ni_3Al and Al_2O_3. J Am Ceram Soc 1998;81:1743–8.

[11] Wang K, Ruan J, Song H, Zhang J, Wo Y, GuoS, Cui D. Biocompatibility of graphene oxide nanoscale. Res Lett 2011;6:8.

[12] Geim AK, Novoselov KS: The rise of graphene. Nat Mater 2007;6:183-91.

[13] Li X, Wang X, Zhang L, Lee S, Dai H. Chemically derived ultrasmooth graphene nanoribbon semiconductors. Science 2008;319:1229.

[14] Yang K, Zhang S, Zhang G, Sun X, Lee ST, Liu Z. Graphene in mice: ultrahigh in vivo tumor uptake and efficient photothermal therapy. Nano Lett 2010;10:3318−23.

[15] Wassei JK, Kaner RB. Mater. Graphene, a promising transparent conductor. Today 2010;13:52−59.

[16] Soldano C, Mahmood A, Dujardin E. Production, properties and potential of graphene. Carbon 2010;48:2127−50.

[17] Stankovich S, Dikin DA, Dommett GHB, Kohlhaas KM, Zimney EJ, Stach EA, et al. Graphene-based composite materials. Nature 2006;442:282–6.

[18] Mukhopadhyay P, Gupta RK. Trends and frontiers in graphene-based polymer nanocomposites. Plast Eng 2011;67:32–42.

[19] Yang X, Tu Y, Li L, Shang S, Tao X. Well-dispersed chitosan/graphene oxide nanocomposites. ACS Appl Mater Interfaces 2010;2:1707–13.

[20] Wan C, Frydrych M, Chen B. Strong and bioactive gelatin–graphene oxide nanocomposites. Soft Matter 2011;7:6159–66.

[21] Li R, Liu C, Ma J. Studies on the properties of graphene oxide reinforced starch biocomposites. Carbohydr Polym2011;84:631–7.

[22] Wan C, Chen B. Poly (e-caprolactone)/graphene oxide biocomposites: mechanical properties and bioactivity. Biomed Mater 2011;6:055010.

[23] Li M, Wang Y, Liu Q, Li Q, Cheng Y, Zheng Y, et al. In situ synthesis and biocompatibility of nano hydroxyapatite on pristine and chitosan functionalized graphene oxide. J Mater Chem B 2013;1:475–84.

[24] Neelgund GM, Oki A, Luo Z. In-situ deposition of hydroxyapatite on graphene nanosheets. Mater Res Bull 2013;48:175–9.

[25] Rodrìguez-Lorenzo LM, Benito-Garzo´n L, Barroso- Bujans F, Fernandez Mar. Synthesis and biocompatibility of hydroxyapatite in a graphite oxide matrix. Key Eng Mater 2008;396–398:477–80.

[26] Kim S, Ku SH, Lim SY, Kim JH, Park CB. Graphene–biomineral hybrid materials. Adv Mater 2011;23:2009–14.

[27] Liu H, Xi P, Xie G, Shi Y, Hou F, Huang L, et al. Simultaneous reduction and surface functionalization of graphene oxide for hydroxyapatite mineralization. J Phys Chem C 2012;116:3334–41.

[28] Zhu J, Wong HM, Yeung KWK, Tjong SC. Spark plasma sintered hydroxyapatite/graphite nanosheet and hydroxyapatite/multiwalled carbon nanotube composites: mechanical and in vitro cellular properties. Adv Eng Mater 2011;13:336–41.

[29] Biris AR, Mahmood M, Lazar M, Dervishi E, Watanabe F, Mustafa T, et al. Novel multicomponent and biocompatible nanocomposite materials based on few-layer graphenes synthesized on a gold/hydroxyapatite catalytic system with applications in bone regeneration. J Phys Chem C. 2011;115:18967–76.

[30] Ma HB, Su WX, Tai ZX, Sun DF, Yan XB, Liu B, et al. Preparation and cytocompatibility of polylactic acid/hydroxyapatite/graphene oxide nanocomposite fibrous membrane. Chinese Sci Bull 2012;57:3051–8.

[31] Lahiri D, Dua R, Zhang C, de Socarraz-Novoa I, Bhat A, Ramaswamy S, et al. Graphene nanoplatelet-induced strengthening of ultrahigh molecular weight polyethylene and biocompatibility in vitro. ACS Appl Mater Interfaces 2012;4:2234–41.

[32] Li M, Wang Y, Liu Q, Li Q, Cheng Y, Zheng Y, et al. In situ synthesis and biocompatibility of nano hydroxyapatite on pristine and chitosan functionalized graphene oxide. J Mater Chem B 2013;1:475–84.

[33] Parente P, Sa´nchez-Herencia AJ, Mesa MJ, Ferrari B. Functionalizing Ti-surfaces through the EPD of HA/NanoY$_2$O$_3$. J Phys Chem B 2013;117:1600–7.

[34] Lahiri D, Ghosh S, Agarwal A. Carbon nanotube reinforced hydroxyapatite composite for orthopedic application: a review. Mat Sci Eng C-Mater 2012;32:1727–58.

[35] FanH, Wang L, Zhao K, Li N, Shi Z, Ge Z, Jin Z. Fabrication, Mechanical Properties, and Biocompatibility of Graphene-Reinforced Chitosan Composites. Biomacromolecules 2010;11:2345–51.

[36] Akhavan O, Ghaderi E. Toxicity of graphene and graphene oxide nanowalls against bacteria. ACS Nano 2010;4:5731–36.

[37]Yang L, Zhang L, Webster TJ. Carbon nanostructures for orthopedic medical applications. Nanomedicine 2011;6:1231–44.

[38] Dessì M, Raucci MG, Zeppetelli S, Ambrosio L. Design of injectable organic-inorganic hybrid for bone tissue repair. J Biomed Mater Res A. 2012;100:2063-70.

[39] D'Antò V, Raucci MG, Guarino V, Martina S, Valletta R, Ambrosio L. Behaviour of human mesenchymal stem cells on chemically synthesized HA-PCL scaffolds for hard tissue regeneration. J Tissue Eng Regen Med. 2013 May 31.

[40] Park S, An J, Piner RD, Jung I, Yang D, Velamakanni A, et al. Aqueous suspension and characterization of chemically modified graphene sheets. Chem Mater 2008;20:6592–94.

[41] Abe Y, Kokubo T, Yamamuro T. Apatite coating on ceramics, metals and polymers utilizing a biological process. J Mater Sci Mater Med 1990;1:233–8.

[42] Tanashi M, Yao T, Kokubo T, Minoda M, Miyamoto T, Nakamura T, et al. Apatite coating on organic polymers by biomimetic process. J Am Ceram Soc 1994;7:2805–08.

[43] Tanahashi M, Hata K, Kokubo T, Minoda M, Nakamura T, Yamamuro T, in: Yamamuro T, Kokubo T, Nakamuro T. Eds. Bioceramics, vol.5, Kobunshi Kankokai, Kyoto, 1992, p.57.

[44] Cazorla C, Rovira C, Rojas V. Calcium-based functionalization of carbon nanostructures for peptide immobilization in aqueous media J Mater Chem 2012;22:19684–93.

[45] Zhao L and L. Gao. Novel in situ synthesis of MWNTs-hydroxyapatite composites. Carbon 2004;42:423–6.

[46] Wang P, Li C, Gong H, Jiang X, Wang H, Li K. Effect of synthesis conditions on the morphology of hydroxyapatite nanoparticles produced by wet chemical process. Powder Technol 2010;203:315–21.

[47] Kim J, Cote LJ, Kim F, Yuan W, Shull KR, J. Huang. Graphene Oxide Sheets at Interfaces. J Am Chem Soc 2010;132:8180–6.

[48] van Kemenade MJJM, de Bruyn PL. A kinetic study of precipitation from supersaturated calcium phosphate solutions. J Colloid and Interface Science 1987;118: 564–85.

[49] Aryal S, Bahadur KCR, Dharmaraj N, Kim KW, Kim HY. Synthesis and characterization of hydroxyapatite using carbone nanotube as a nanomatrix. Scr Mater 2006;54:131–5.

[50] Webster TJ, Ergun C, Doremus RH, Siegel RW, Bizios R. Biomaterials. Enhanced functions of osteoblasts on nanophase ceramics. 2000;21:1803–10.

[51] Shi Z, Huang X, Cai Y, Tang R, Yang D. Size effect of hydroxyapatite nanoparticles on proliferation and apoptosis of osteoblast-like cells. Acta Biomater 2009;5:338–45.

[52] Supova M. Problem of hydroxyapatite dispersion in polymer matrices. J Mater Sci: Mater Med 2009;20:1201–13.

[53] Liu H, Xi P, Xie G, Shi Y, Hou F, Huang L, Chen F, Zeng Z, Shao C, Wang J. Simultanous reduction and surface fictionalization of graphene oxide for hydroxyapatite mineralization. J Phys Chem C 2012;116:3334–41.

[54] Bourgeois B, Laboux O, Obadia L, Gauthier O, Betti E, Aguado Eet al. Calcium-deficient apatite: A first *in vivo* study concerning bone ingrowth. J Biomed Mater Res Part A. 2003;65A:402–8

[55] Zhao Y, Zhang Y, Hou S, Chu PK. Synthesis and cellular biocompatibility of two nanophase hydroxyapatite with different ca/p ratio. J Nanosci Nanotechnol 2011;11:11069–73.

[56] Raucci MG, Guarino V, Ambrosio L. Hybrid composite scaffolds prepared by sol–gel method for bone regeneration. Composites Science and Technology 2010;70:1861–8.

[57] Liuyun J, Yubao L, Chengdong X. Preparation and biological properties of a novel composite scaffold of nano-hydroxyapatite/chitosano/carboxymethyl cellulose for bone tissue engineering. J Biomed Sci 2009;16:65.

[58] Raucci MG, Alvarez-Perez MA, Demitri C, Sannino A, Ambrosio L. Proliferation and osteoblastic differentiation of hMSCs on cellulose-based hydrogels. J Appl Biomater Funct Mater 2012;10:302-7.

[59] Li WJ, Tuli R, Huang XX, Laquerriere P, Tuan RS. Multilineage differentiation of human mesenchymal stem cells in a three-dimensional nanofibrous scaffold. Biomaterials 2005;26:5158–66.

[60] Manferdini C, Guarino V, Zini N, Raucci MG, Ferrari A, Grassi F, Gabusi E, Squarzoni S, Facchini A, Ambrosio L, Lisignoli G. Mineralization behavior with mesenchymal stromal cells in a biomimetic hyaluronic acid-based scaffold. Biomaterials 2010;31:3986-96.

[61] Raucci MG, Alvarez-Perez MA, Meikle S, Ambrosio L, Santin M. Poly(Epsilon-lysine) dendrons tethered with phosphoserine increase mesenchymal stem cell differentiation potential of calcium phosphate gels. Tissue Eng Part A. 2014;20:474-85.

[62] Raucci MG, D'Antò V, Guarino V, Sardella E, Zeppetelli S, Favia P, Ambrosio L. Biomineralized porous composite scaffolds prepared by chemical synthesis for bone tissue regeneration. Acta Biomater 2010;6:4090-9.

[63] Ciapetti G, Ambrosio L, Savarino L, Granchi D, Cenni E, Baldini N et al. Osteoblast growth and function in porous poly-ε-caprolactone matrices for bone repair: a preliminary study. Biomaterials 2003;24:3815–24.

2.3 CELLULOSE-BASED HYDROGELS CROSSLINKED BY CITRIC ACID

Introduction

The classical tissue engineering paradigm relies on a scaffold that can be used as a space filling material for cell and therapeutic agent delivery. Injectable materials hold promise for tissue engineering applications as they offer some advantages over prefabricated scaffolds for certain indications. Injectable scaffolds eliminate the need for surgical interventions for delivery, and the minimally invasive procedure of injection reducing discomfort and complications for the patient [1]. Moreover, injectable scaffolds provide the ability to take the shape of the cavity in which they are placed and can thus fill irregular defects [2-4]. Aqueous polymer solutions that have the property to form a gel upon temperature change have been introduced for tissue engineering applications. These hydrogels do not require any additional chemical stimulus for their formation. Moreover, hydrogels due to their unique biocompatibility, flexible methods of synthesis, range of constituents, and desirable physical characteristics, have been the material of choice for many biomedical applications [5]. In particular, in the field of regenerative medicine they play a key role in supporting, promoting and stimulating the cell function, and for these reasons have been widely used [6-8]. Both natural-based and synthetic thermo-gelling polymer systems have been developed and tested in tissue engineering [9-11]. Among the natural polymer-based hydrogels that have been reported are cellulose derivatives, chitosan, and gelatin [12,13].

Cellulose is the world's most abundant natural, renewable and biodegradable polymer. Similarly to other polysaccharides, cellulose has a longstanding usage in medical applications due to its lack of toxicity (monomer residues are part of metabolites found in the human body), water solubility or high swelling ability, and stability to temperature and pH variations [14,15]. The biocompatibility of unmodified and derivative cellulose is well documented [16,17]. In this study, it was envisaged to take advantage of cellulose due to its good match with the mechanical properties of cortical bone and its hydroexpansivity, therefore allowing a satisfactory primary fixation to hard tissue [18]. Materials surface properties influence the composition of the adsorbed protein compounds, which in turn regulates how cells respond to the material [19-22]. Understanding the relationship between material surface properties, adsorbed molecules and cellular responses is essential to designing optimal material surfaces for implantation and tissue

engineering. In fact, it is recognized that the behaviour of the adhesion and proliferation of different cell lines on polymeric materials depend on the surface characteristic such as hydrophilicity/hydrophobicity, chemistry, charge, roughness etc. The presence of polar groups results in increased wettability of the material surface. It has been well-established that cells preferentially adhere to surfaces with moderate hydrophilicity [23,24]. For example, the highest cell adhesion of Chinese Hamster Ovary cells (CHO cells) was observed on surfaces with a water drop contact angles of about 50 degrees [23]. Good cell adhesion has been explained by the adsorption of protein molecules in an appropriate and flexible spatial conformation. This enables protein reorganization and accessibility of the specific ligands by cell adhesion receptors. On the other hand, on extremely hydrophilic surfaces, the cell adhesion-mediating proteins are bound too loosely, such that they do not ensure firm adhesion and spreading of cells on the material surface [25,26]. In contrast, hydrophobic surfaces are thought to cause strong adsorption and subsequent denaturation of proteins, which distorts the conformation of cell adhesion receptor-binding domains. In addition, a preferential and strong adsorption of albumin, which acts as non-adhesive for cells, has been reported on these surfaces [27].

Another important factor influencing the adhesion and subsequent behaviour of cells is the material surface roughness and topography [28]. Depending on the scale of irregularities of the material surface, we can distinguish macro-roughness (100 μm - millimetres), micro-roughness (100 nm - 100 μm), and nano-roughness (less than 100 nm), each with its specific influence. Macro-roughness seems to be favourable, because it enhances the anchorage of implant into the natural tissue and is not usually felt by the cells, e.g. it does not restrict their attachment and spreading [28]. The micro-scale roughness is more controversial, because the cells can be limited by the material surface topography in their adhesion area [29-31]. On the other hand, several authors have reported that osteoblasts, grown on micro-rough surfaces, were stimulated towards differentiation; as shown by their gene expression and higher level of mineralization in comparison with cells growing on smooth surfaces [32,33]. The nanoscale structure of the material surface have been found to have significant positive effects on osteoblast cell response, including initial cell adhesion and subsequent proliferation, and expression of differentiation markers. This finding is not so surprising when we keep in mind that the natural environment of cells, the extracellular matrix (ECM), is also organized into nano-dimensions. Interactions of cells and extracellular matrix (ECM) initiate signalling cascades involved in critical cell functions, such as regeneration [34-36]. An important goal of tissue engineering is to mimic critical aspects of the extracellular environment and to control cell function through cell–material

interactions [37]. The complexity of natural ECM and cell–matrix interactions makes design of materials for regenerative medicine applications challenging because a variety of factors will influence cell fate. The choice of the chemical environment used for a specific tissue engineering application is dependent on the desired outcome, and many studies have shown that chemical functionality and hydrophilicity have important roles in cell adhesion and function [38-40]. As a result, many of the newly-developed bio-inspired composite materials try to mimic this effect of ECM on cells by constructing nano-structured surfaces. The cells also require a certain level of substrate stiffness for their adhesion. During the process of adhesion and spreading, cells exert traction forces on the underlying substrate and they respond to comply. If the surface is too soft, as for example on polyacrylamide gels, it is not able to withstand these forces. The adhering cells are not able to spread: they are rounded, they show no assembly of cytoskeleton and focal adhesions, and consequently undergo apoptosis [41]. Moreover, a low, medium and high level of the substrate stiffness can direct the differentiation of mesenchymal stem cells towards neuronal, muscle or osteoblast phenotype, respectively [42].

In this work, cellulose-based hydrogels were prepared in order to evaluate the effect of material's surface modifications on biological response of hMSC. In particular, samples before and after citric acid (CA) treatment were investigated to address improved performances such as hydrophilicity, roughness and rheological properties. The goal of study is to identify a novelty injectable materials to use in minimal non-invasive surgery.

2.3.1 Material and Methods

2.3.1.1 Materials

Carboxymethyl cellulose (CMCNa) (MW 700 kDa, DS 0.9 viscosity 3400 cm/s), hydroxyl ethyl cellulose HEC (MW 250 kDa MS 2, viscosity 80–125 cm/s) and citric acid (CA) were purchased from Sigma-Aldrich (Milano, Italy) and used without any further purification.

2.3.1.2 Hydrogel Preparation

Different hydrogels were prepared in order to evaluate their suitability in the interactions with the selected cell line. Two different cellulose derivatives were used in the preparation: a sodium salt of carboxymethyl cellulose (CMCNa) and hydroxyl ethyl cellulose (HEC) (figure 1A). The CMCNa is a cellulose derivative with carboxymethyl groups ($-CH_2-COOH$) bound to some of

the hydroxyl groups of the glucopyranose monomers that make up the cellulose backbone. This functional group is responsible of the high sorption capacity due to the Donnan effect. HEC is a non-ionic polymer that is able to form stable networks with a lower sorption capacity. The samples were prepared via double esterification crosslinking using citric acid (CA) (figure 1B) as reported in a previous work [43].

Briefly, hydrogel samples were obtained by reacting, in distilled water, CMCNa and HEC with CA (20% w/w on polymer weight) as a crosslinking agent, respectively. First, a total polymer concentration of 2% by weight of water were used for the two cellulose derivatives, by stirring gently at room temperature until a clear solution was obtained. This final solution was used to mould 10-mm thick samples. All samples were first pre-dried at 30°C for 24 h to remove absorbed water and then kept at 80°C for 12h for the crosslinking reaction (figure 1C).

Crosslinked hydrogels, CMCNa-CA and HEC-CA, were compared with pure CMCNa and HEC as control. The samples were obtained by resuspending in PBS solution the samples after sterilization (autoclave, 121°C, for 20 min).

(A)

(B)

(C)
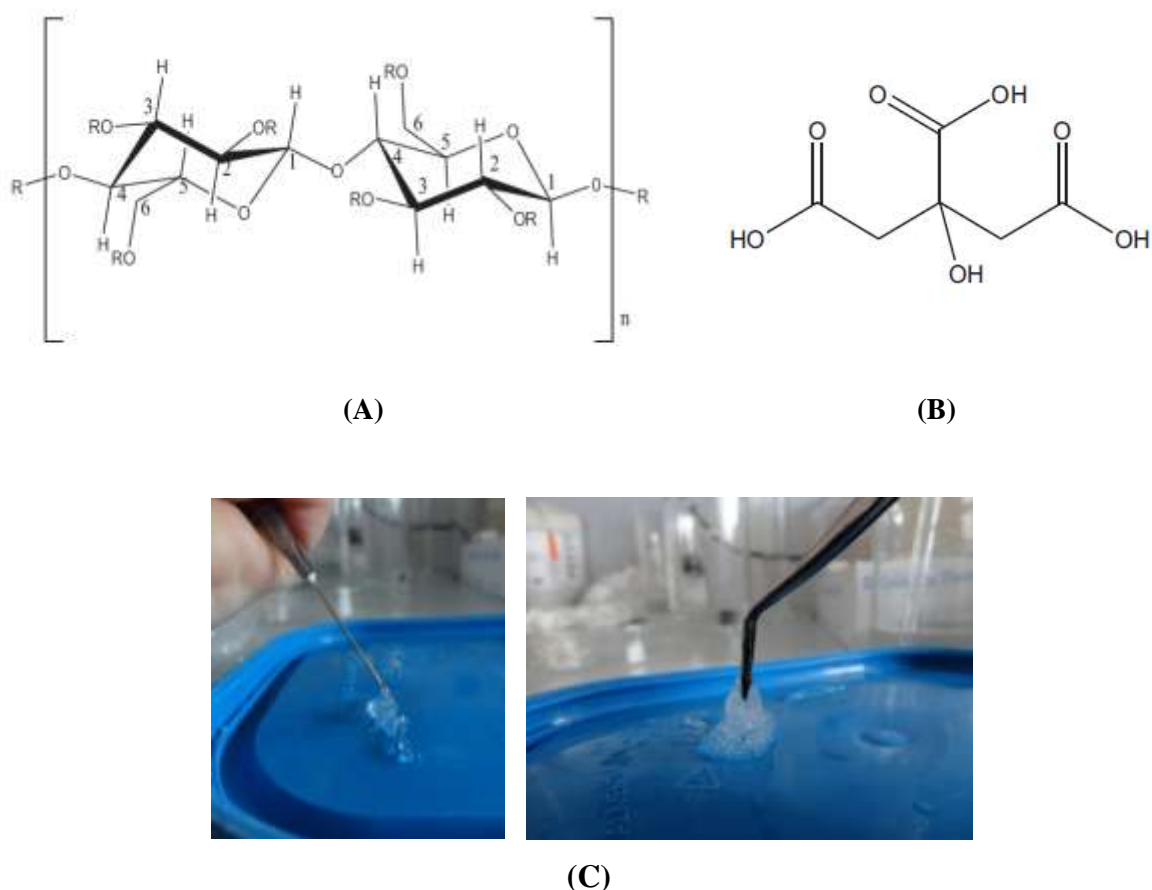
Fig. 1: Chemical Structure of cellulose derivatives **CMCNa**: R=H; $CH_2COO\text{-}Na^+$ **HEC**: R=H; $CH_2CH_2(OCH_2CH_2)_mOH$ (A) , citric acid cross-linker (B) and final product (C).

2.3.2 Characterization

2.3.2.1 Infrared Spectroscopy FTIR analysis

FTIR spectra were recorded on a Nexus FT-IR (Nicolet spectrometer) equipped with an attenuated total reflectance (ATR, Smart ARK, Nicolet) crystal sampler. Film samples were used directly on an ATR crystal sampler at a resolution of 4 cm^{-1}, average 64 scans, at absorbance range from 4000 cm^{-1} to 650 cm^{-1}.

2.3.2.2 Hydrophilicity

To determine surface hydrophilicity, contact angle measurements were carried out on different cellulose gels (CMCNa-CA, CMCNa, HEC and HEC-CA) by the sessile drop method [44], at room temperature, using an optical bench-type contact angle goniometer (Dataphysics OCA). Samples were previously dried at 25°C and 50% relative humidity, until constant weight was achieved. Four replicas of each sample were used and at least two drops of approximately 10 μL of deionized water was deposited on each film, and the static contact angle was measured for each drop.

2.3.2.3 Rheological Analysis

With the aim to prepare injectable hydrogels, the samples were milled using a Retsch rotor mill equipped with a screen with 1mm mesh. The resulting powder was sieved between 0.1 and 1 mm, and used without any further modification. The viscoelastic properties of the wet samples (5% and 10% w/w in 0.9% NaCl solution) were investigated by means of a rotational rheomether (Ares, Rheometric Scientific) equipped with parallel plates having a diameter of 25 mm. The plate surfaces were properly modified through a fabric-based adhesive tape to prevent hydrogel slipping [13]. The viscosity tests were performed in a "*steady state mode*" at room temperature (25 °C), setting a shear rate ranging from 0.1 to 100 s^{-1} with step increasement of 0.02 s^{-1}. The storage modulus (G') and loss modulus (G") were evaluated using the same experimental setup in a "*frequency sweep mode*" setting with a shear rate at 0.5 s^{-1}. All experiments were carried out in triplicate, and the average values were reported.

2.3.2.4 Atomic Force Microscopy

The morphology of the film surface was also studied by Atomic Force Microscopy (AFM Perception, Assing, Italy). Small pieces of films were glued onto metal disks and attached to a magnetic sample holder located on the top of the scanner tube. Phase images were recorded under ambient air conditions. All of the images were recorded in contact mode in air using silicon cantilevers. A standard statistical software package (SPSS version 20.0, SPSS IBM, New York, NY) was used for data analysis.

2.3.2.5 Biological studies
In vitro cell culture

Biological assays were performed using human mesenchymal stem cells line (hMSC) obtained from LONZA (Milano, Italy). hMSC were cultured in 75 cm^2 cell culture flask in Eagle's alpha Minimum Essential Medium (α-MEM) supplemented with 10% Fetal Bovine Serum (FBS), antibiotic solution (streptomycin 100 µg/ml and penicillin 100U/ml, Sigma Chem. Co) and 2 mM L-glutamine. hMSCs from passages 4 through 6 passage were used for all the experimental procedures and incubated at 37°C in a humidified atmosphere with 5% CO_2 and 95% air.

Cell morphology

The cell morphology and cell spreading pattern interaction of hMSC onto cellulose gels (CMCNa, CMCNa-CA, HEC and HEC-CA) were evaluated by confocal laser scanning microscopy (LSM 510, CarlZeiss). Briefly, hMSC at $2x10^3$ were seeded onto gel materials and incubated for 24h.   At the end of the incubation time, the non-attached cells were removed by rinsing carefully three times with PBS and then incubated with CellTracker™ Green CMFDA in phenol red-free medium at 37°C for 30 min. Subsequently cell culture were washed with PBS and incubated for 1h in complete medium. After period of time the cells were visualized on LSM.

Viability test

To evaluated cell biocompatibility, hMSC were plated at concentration of $1.6x10^4$ in triplicate onto different cellulose gels (CMCNa, CMCNa-CA, HEC and HEC-CA). The medium in cell-load gel materials culture plates were removed after cultured for 7, 14 and 21 and the *in vitro* cell viability was checked by the Alamar blue assay (AbD Serotec, Milano, Italy). This assay

quantified the redox indicator which changed to a fluorescent product in response to the chemical reduction by mitochondrial enzymes such as flavin mononucleotide dehydrogenase, flavin adenine dinucleotide dehydrogenase, and nicotinamide adenine dinucleotide dehydrogenase. In addition, a redox phenomenon gave a quantitative indication of metabolic activity of live cells. An aliquot of 1mL of Alamar Blue™ diluted 1:10 in phenol red-free medium was added to each well and incubated for a further 4 h at 37°C, 5% CO_2. Later, 200μL of this solution was transferred into a 96 well plate for colorimetric analysis. Wells without any cells were used to correct any background interference from the redox indicator. The optical density was immediately measured with a spectrophotometer (Sunrise, TECAN, Männedorf, Zurich, Switzerland) at wavelengths of 540 and 600 nm. The cell viability percentage was evaluated in according to the manufacturer's protocol. The culture medium during experimental time was changed every two days.

Alkaline Phosphatase assay

The alkaline phosphatase activity of the hMSC onto cellulose gel materials was determined for 7, 14 and 21 days of culture by a spectrophotometric end-point assay that determined the conversion of colourless p-nitrophenyl phosphate as substrate to coloured p-nitrophenol following the manufacturer's protocol (Sensolyte pNPP ALP assay Kit, AnaSpec). Briefly, at the end of each time point, cultures were washed gently with PBS followed by washing twice with cold 1X assay buffer. For extract cell layers the cultures were lysing with 1X lysis buffer with 0.2% of Triton X-100. The phosphatase activity was analyzed onto the cell lysates (50μl) by measuring the ALP activity when ALP enzyme catalyzes the cleavage of a phosphate group and release p-nitrophenol from pnitrophenyl phosphate in alkaline buffer solution after 30 min at 37°C. Sample absorbance was measured in a 96-well plate at 405 nm. To correct the ALP values for the number of cells present on each scaffold double stranded DNA (dsDNA), as a marker for cell number, was measured using a PicoGreen_dsDNA quantification kit (Invitrogen). First, 100μl of 200μl diluted Picogreen_dsDNA quantification reagent was added to 100 ml of cell lysates in a flat-bottomed, 96-well plate. Following 10 min incubation, the fluorescence of Picogreen was determined at a wavelength of 520 nm after excitation at 585 nm using a plate reader (multilabel counter 1420 Victor, Perkin-Elmer, Italy). dsDNA was quantified according to a calibration curve of l-dsDNA standard in   10 mM Tris, 1 mM EDTA, pH 7.5, buffer. Each experiment was performed three times in triplicate. The results of ALP activity were reported as

nanograms of ALP normalized to the micrograms of total DNA content. ALP experiments were repeated twice and three hydrogel scaffolds were used in each experiment.

RT-PCR assay

hMSC cultures onto carboxymethyl cellulose gel composite materials grown in medium for 21 days were characterized by reverse transcription-polymerase chain reaction (RT-PCR) for gene expression of bone-related markers. Total RNA was isolated from cell materials using TRI-reagent (SIGMA). The RNA was precipitated with isopropyl alcohol and the final pellet resuspended in DEPC-water and DNAse I digested (Life Technologies, Italy) to remove contaminating of genomic DNA. The absorbency at 260/280 nm was measured to determine the RNA concentration. One micrograms of total RNA was used to perform one-step RT-PCR reaction (Life Technologies, Italy) according to the manufacturer's protocol. Briefly, cDNA synthesis program was 1 cycle at 60°C for 30 min followed of denaturation cycle of 94°C for 2 min. cDNA was amplified at 94°C for 15 s, 58°C for 30 s and 68°C for 1 min for 40 cycles in a thermal cycler (Applied Biosystem). Primers used for amplification of bone-related molecules were upstream and downstream as follow: osteopontin: 5'-TTCGGATGAGTCTGATGAGACC-3',5'-GGAAGAACAGAAGCAAAGTGC-3'; osteocalcin: 5'-CAGCAGAGCGACACCCTAGACC-3',5'-CATGAGAGCCCCTCACACTCC-3 and Glyceraldheyde-3-phosphate dehydrogenase (GAPDH): 5´-CCACCCATGGCAAATTCCATGGCA-3', 5'-TCTAGACTGGCAGGTCAGGTCCACC-3' was utilized as housekeeping gene. Reaction products were separated using gel electrophoresis on 1.2% agarose gel stained with ethidium-bromide. Bands were visualized using ultraviolet illumination and captured with BioRad Imaging System (BIORAD).

2.3.2.6 Statistical Analysis

One-way analyses of variance (ANOVA) were performed to detect significant effects among treatment with post Bonferroni t-test. Results were considered to be significant at $p < 0.05$.

2.3.2 Results

2.3.2.1 Infrared Spectroscopy FTIR analysis

The structure of the salt form of CMC and HEC is presented in Figure 1, showing a carboxymethyl-substituted unit in the C(6) position and two unsubstituted cellulose units. In general, cellulose is made up of glucose rings connected by -C-O-C ether bonds known as β-1,4 glycosidic linkages with extensive intramolecular hydrogen bonding [45,46]. The cellulose monomer has a balance of hydrophilic (-OH, C-O-C) and hydrophobic (-CH, $-CH_2$-) sections. The substitution of carboxymethyl groups on the oxygen in the C(6) position imparts a pH-dependent anionic character to the molecule. Absorption band at $3318 cm^{-1}$ is due to the stretching frequency of the –OH group as well as intramolecular and intermolecular hydrogen bonds in a cellulose.
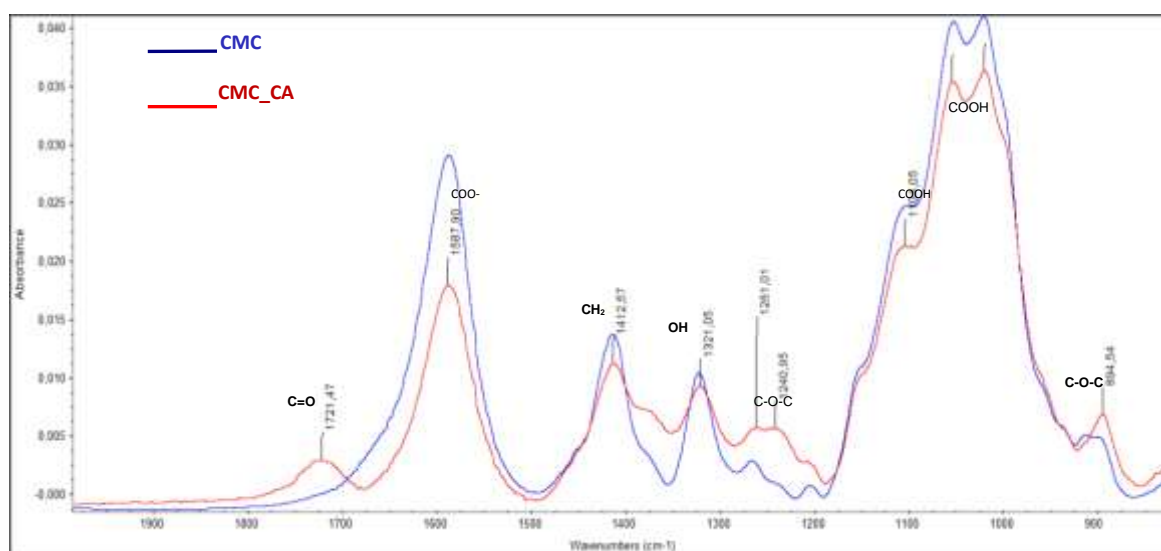
Fig. 2: FTIR analysis of CMCNa before (blue line) and after (red line) crosslinking reaction by citric acid.

Peaks at wavenumber of $1084.70 cm^{-1}$ is due to $>CH_2-O-CH_2$. Spectrum shows (figure 2) C-H stretching vibration at peak with wavenumber of $2925.20 cm^{-1}$. The peaks at 1450 and $1330 cm^{-1}$ were attributed to CH_2 and CH absorptions, respectively. The broad bands from 1200 to 1000 cm^{-1} were due to sugar ring absorption. The HEC spectrum (figure 3) shows the band at $1590 cm^{-1}$ whereas the absorbance of the carbonyl group at $1723 cm^{-1}$ appears only after chemical

treatment with citric acid. Crosslinked cellulose hydrogels showed a decreasing of OH intensity peak, probably due to the chemical interaction with citric acid.
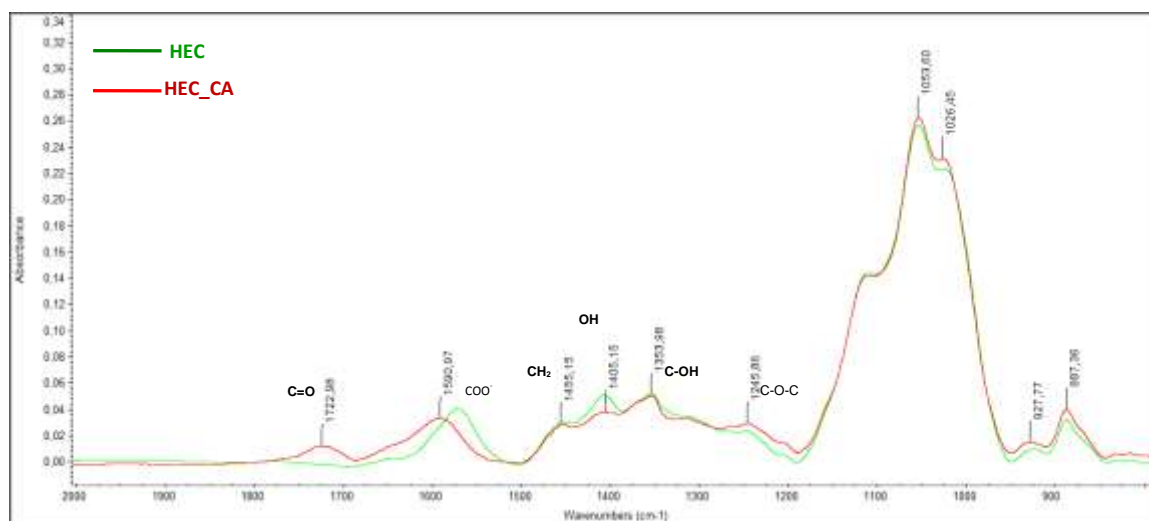
Fig. 3: FTIR analysis of HEC before (green line) and after (red line) crosslinking reaction by citric acid.

2.3.2.2 Hydrophilicity

The hydrophilicity of materials was determined by contact angle analysis. The figures show that the crosslinking by citric acid increases the hydrophilicity of materials by adding some -COOH groups on material surface.
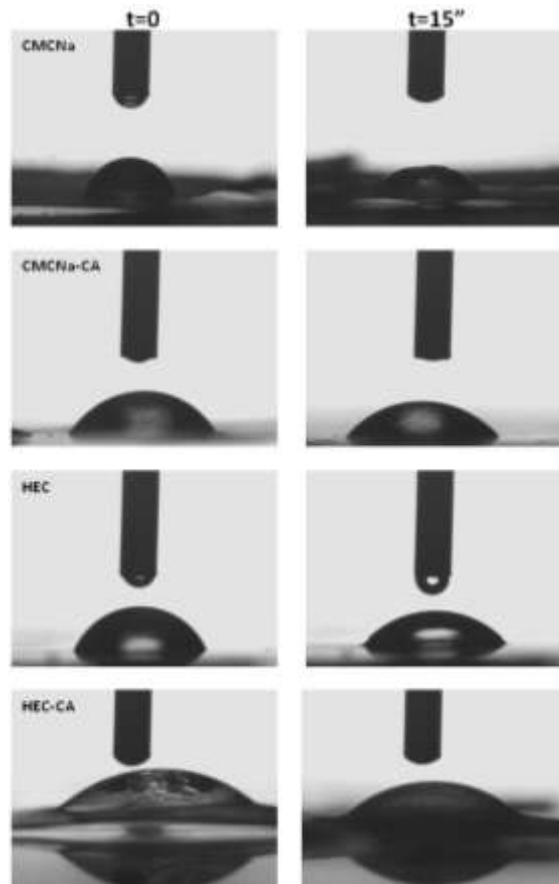
(A)
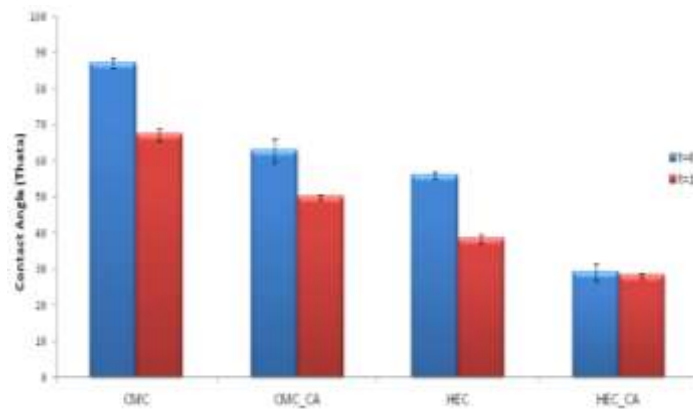
(B)

Fig. 4: Contact angle images of water drop at contact with hydrogel films at t=0 and after few seconds t=15sec. Contact angle values of different hydrogels (CMCNa, CMCNa-CA, HEC and HEC-CA) at t=0 and t=15" of contact with water drop.

In fact, in the images (figure 4A) it is possible to evaluate the different shape of water drop at contact with the hydrogel materials before (CMCNa, HEC) and after (CMCNa-CA, HEC-CA)

119

chemical reaction. Moreover , it possible to observe a straight geometry of drop after few seconds (15seconds) of contact with hydrogel surfaces. This behavior is typical of hydrophilic materials and it is confirmed by a decreasing contact angle values (figure 4B) after 15 seconds [44]. Furthermore, the results show that there is a decreasing contact angle values of about 50% and 67% after the crosslinking reaction between hydrogels HEC/HEC-CA and CMCNa/CMCNa-CA respectively.

2.3.2.3 Rheological Analyses

In this study, the shear rate-dependent viscosity of hydrated cellulose samples in a powder form as a function of concentration was evaluated. Figure 5A shows the viscosity values (recorded at a shear rate of 10 s^{-1}) for different samples and two different concentrations (5% and 10% w/w in 0.9% NaCl solution). The samples without CA (both for HEC and CMCNa) after hydration resulted in a viscous solution, while the corresponding ones with CA will led to hydrated rigid particles due to the effect of crosslink. For this reason, it is evident that the samples without CA tested at the higher concentration (10%) show an increased viscosity values if compared with those prepared at 5% w/w concentration. The effect of molecular weight of the starting material is evident with the superior viscosity of the CMCNa sample when compared to the HEC. In the case of the samples with CA, this is an effect due to the number of hydrated particles per unit volume and can be explained with a different surface to volume ratio. The sample with a concentration of 10% presents a number of hydrated particles per unit volume that is double that the sample with 5%, resulting with an increased surface to volume ratio. This led to an increased contact area between particles with a higher viscosity. In addition, the samples made entirely with CMCNa (with the presence of CA) presented a reduced viscosity values due to a coupled effect of the molecular weight and the polyelectrolyte nature of the polymer backbone. These factors play an important role in the crosslinking rate of the polymer and sorption capability respectively. In particular, the Donnan effect, typical of polyelectrolyte systems, dramatically reduces the absorption capacity in presence of a solution with NaCl, leading to a less viscous system due to a reduced volume of the hydrated material [47].
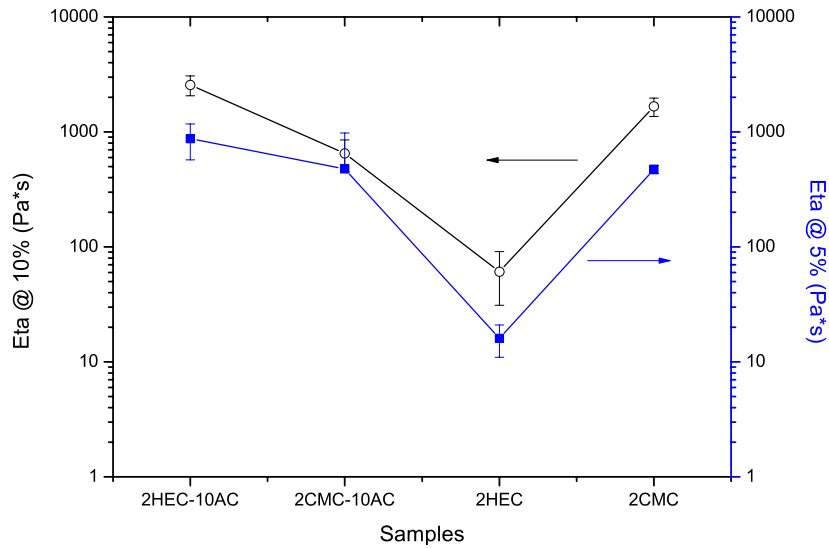
(A)
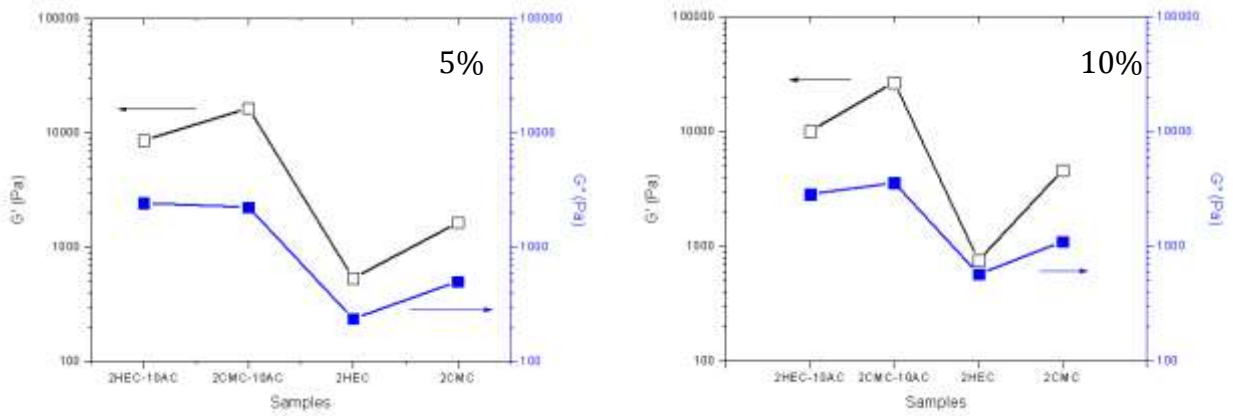
(B)

Fig. 5: (A) Viscosity of cellulose hydrogels CMCNa-CA, CMC, HEC and HEC-CA. (B) Rheological properties of cellulose hydrogels CMCNa-CA, CMC, HEC and HEC-CA.

The viscoelastic results performed on the same samples are shown in figure 5B. These results confirm the greater elastic response of the CMCNa based samples. These differences are addressed to the molecular weight of the starting cellulose and the effect of the crosslinker. The effect of concentration and the crosslinker is more evident for the G' values than the G". This confirmed the crosslinked hydrogel structure for the sample obtained in presence of CA.

2.3.2.4 Atomic Force Microscopy

An important factor influencing the adhesion and subsequent behaviour of cells is the material surface roughness. AFM images were taken to investigate surface morphology of hydrogels and determine the effect of crosslinker concentration on hydrogel surface roughness.

AFM images of hydrogels before and after citric acid crosslinking have been shown in figure 6.
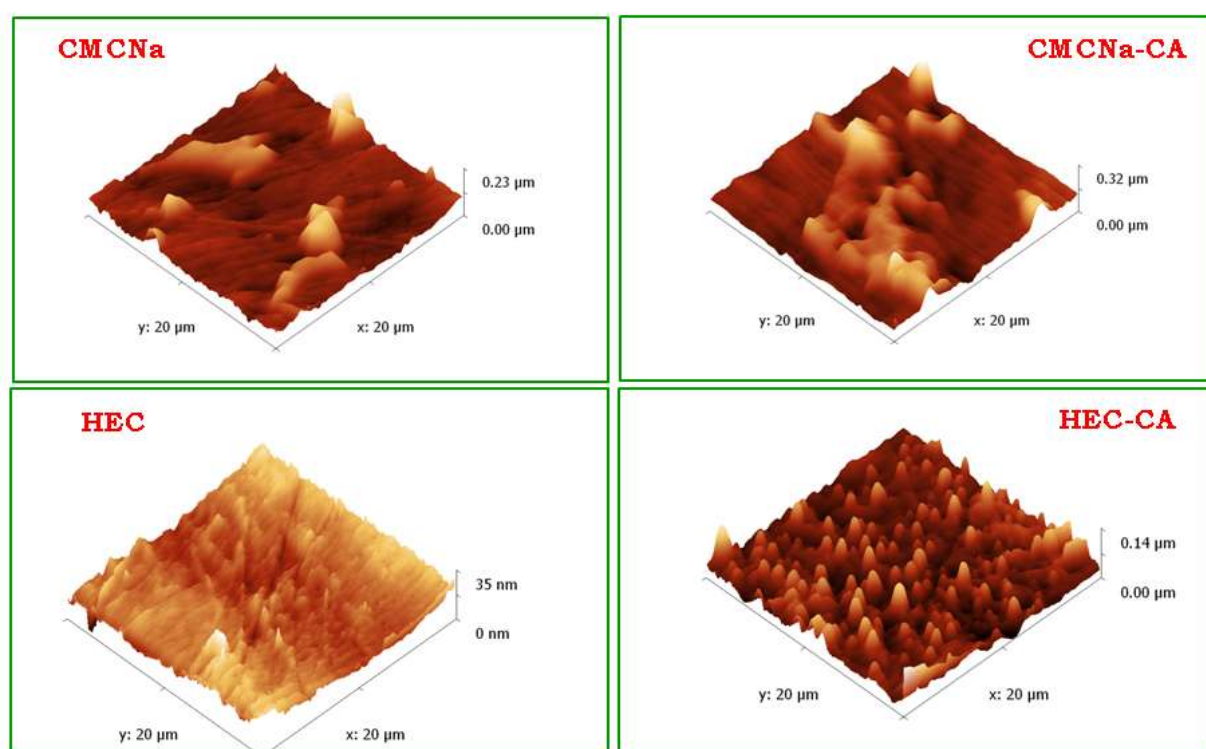
Fig. 6: AFM images of cellulose hydrogels CMCNa-CA, CMC, HEC and HEC-CA.

The change of morphology was evaluated for two types of hydrogel materials and a surface with the highest roughness was reported for HEC-CA hydrogel. However a citric acid treatment induces an increasing of roughness in terms of Ra and RMS as reported in Table 1. The Ra value is the most commonly used roughness parameter in both dentistry and engineering. Nevertheless, the Ra value is limited by the two-dimensional aspect, providing only information on the average roughness height, and also giving no information at all on the surface profile. Meanwhile, RMS (root mean square) is more sensitive to the occurrence of occasional high and low points. On average, the RMS values of CMCNa, CMCNa-CA, HEC and HEC-CA are 31.82, 39.72, 9.98, and 16.56 nm, respectively. AFM measurements show that RMS (nm) is related with citric acid concentration used for the crosslinking reaction. The nanoscale structure of the material surface

has been found to have significant positive effects on osteoblast cell response, including initial cell and expression of differentiation markers.

	Ra[nm]	RMS[nm]
CMC_Na	21.78±3.14	31.82±3.83
CMC_CA	30.10±1.08	39.72±0.91
HEC	6.46±2.45	9.98±3.63
HEC_CA	16.68±2.07	16.56±2.60

Table 1: Roughness in terms of Ra and RMS.

2.3.2.5 Biological studies

To determine whether the different cellulose gels materials (CMCNa, CMCNa-CA, HEC and HEC-CA) are suitable as cell scaffolds, we evaluated the morphology of adhering cells. After one day in culture, we found that cells were viable and showed good attachment and spreading on the different scaffold materials (figure 7).
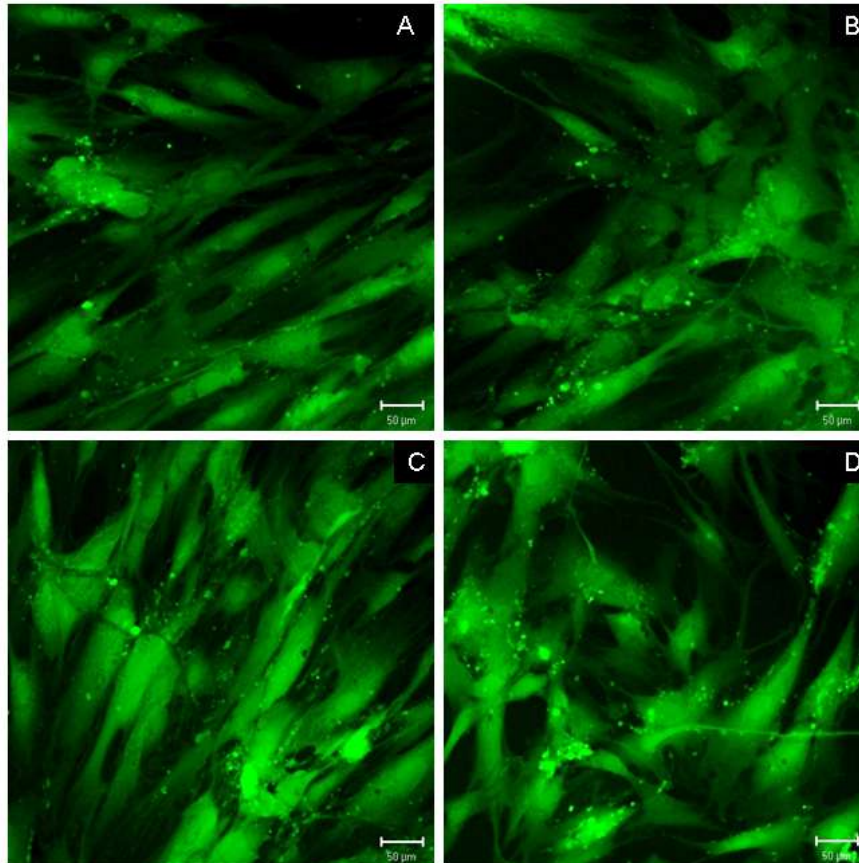
Fig. 7: Morphology of hMSCs adhesion and cell material-interaction on (A) CMCNa-CA; (B) HEC-CA; (C) CMC and (D) HEC hydrogel base scaffolds after culturing for 24 h.

The representative morphology of adhering cells on cellulose gels showed an elongated morphology or tends to adopt a polygonal morphology typical of fibroblast-like cells. On all cellulose hydrogels materials, the cell adhesion and spreading showing the cells firmly anchored and elongated to the gel surface scaffolds.

The cell proliferation on the different cellulose hydrogel materials (CMCNa, CMCNa-CA, HEC and HEC-CA) were assessed using Alamar Blue test. Figure 8 shows the effect of the hydrogel on the metabolic activity of hMSC after 7, 14 and 21 days of culture.
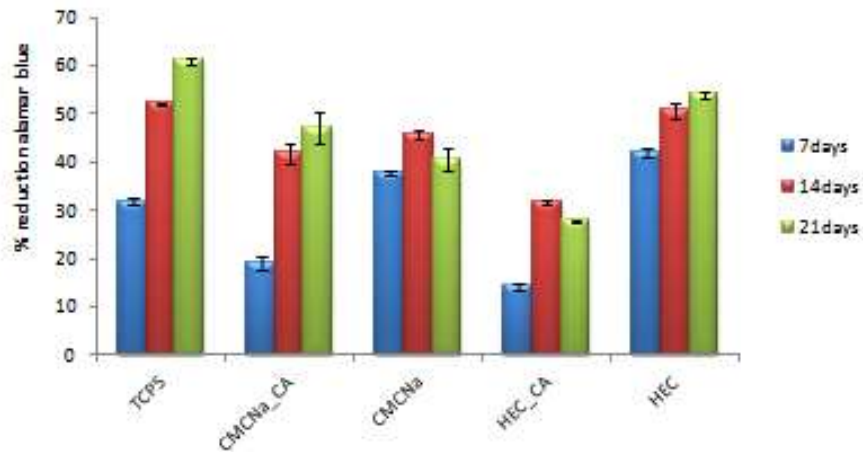
Fig.8: Alamar Blue assay of proliferation of hMSC material-interaction after 7, 14 and 21 days of cell culture.

According to the data, it can be found that MSCs dramatically increase with time during the *in vitro* culture period; suggesting that the cellulose gels are nontoxic, not affecting the cell proliferation and showed good biocompatibility. Meanwhile, a reduced proliferation was observed for hydrogels CMCNa-CA and HEC-CA; this behaviour could be explained by the promoting of differentiation of hMSC cells by the characteristic hydrogel surfaces properties (Figure 9).

To assess the development of the osteoblastic-like phenotype of MSCs grown on the different cellulose gels materials (CMCNa, CMCNa-CA, HEC and HEC-CA), ALP activity was performed after 7, 14 and 21 days of culture. As shown in figure 9, the ALP activity closely reflected the cell morphological features as they showed that the cells adhering on treated hydrogel had the highest differentiation level, where the ALP enzyme activity was significantly high, reaching its peak after 14 days of culture. In particular, CMC and HEC hydrogels after crosslinking by citric acid show a better differentiation with significantly increased ALP activity at different time when compared with non-modified hydrogels ($p < 0.005$). This behaviour can be explained by the nano-roughness induced by crosslinking surface that improves the expression of differentiation markers.
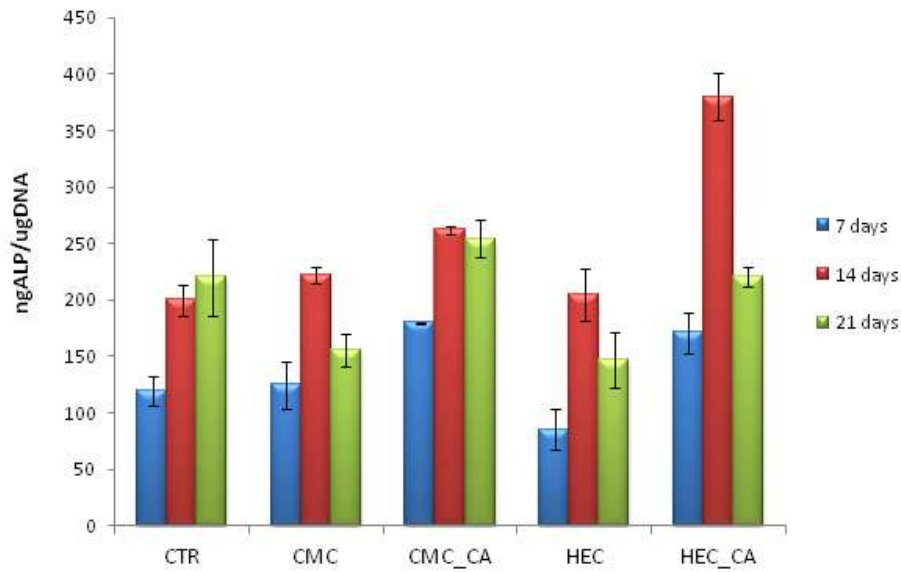
Fig. 9: ALP activity per µg DNA (DNA picogreen) of hMSCs cultured on gel materials at 7, 14 and 21 days**.**

The effects of the different cellulose gels materials on osteoblastic differentiation in MSCs were determined by gene expression analysis of bone-related markers as osteopontin (OPN) and osteocalcin (OCN) by RT-PCR. Figure 10 showed the up-regulation of these genes of MSCs culture on gels materials, suggesting the differentiation to osteoblastic-like phenotype throughout the assay period. This behaviour could be explained by the nano-roughness induced by crosslinking surface that could promote and improve the expression of differentiation markers. Based on the above results, the different cellulose hydrogel materials (CMCNa, CMCNa-CA, HEC and HEC-CA) had good cell biocompatibility *in vitro* and crosslinked hydrogels perform as a better support to induce an osteogenic differentiation through the expression of specific markers.
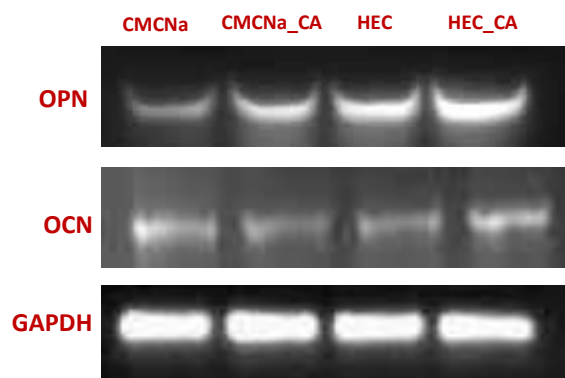
Fig. 10: RT-PCR analysis for the transcription of the bone-related markers as osteopontin (OPN) and osteocalcin (OCN) by hMSC cultured onto different cellulose gels materials CMCNa-CA, CMC, HEC and HEC-CA after 21 days of cell culture.

2.3.4 Discussion

Cellulose is a promising scaffold material for bone tissue engineering applications [48,49] due to its bone compatible mechanical properties [50,51] in combination with its good machinability. Nevertheless, the clinical use of cellulose as bone replacement material is limited due to its insufficient osteointegration [52].

Numerous efforts made to stimulate the bioactivity of cellulose. The substitution of functional groups (e.g., –COOH, –NH$_2$) was found to improve the bone-bonding ability of the cellulose derivates at the implant/tissue interface [53,54]. The good hMSC attachment and proliferation found can be attributed to the peculiar properties of modified cellulose hydrogels for biomedical applications, namely their high purity and high water uptake or swelling, causing less physical damage to cells [55], associated with their moderate hydrophilicity. In the literature, the role of hydrophilicity in cell adhesion has been widely discussed and, despite the difficulty in isolating this property from the other influencing ones, the general conclusion seems to be that moderate hydrophilicity favours cell adhesion, and extreme values inhibit this phenomenon [56,57].

Surfaces with –COOH also have shown an increase in cell growth. A more recent study showed that this phenomenon is dependent upon the concentration of –COOH on the surface, as an increase in functional group density results in a higher negative charge on the surface, which was shown to inhibit cell growth [58]. Surface wettability of artificial materials is one of the most important factors determining cell adhesion behaviours. Tamada *et al.* Claimed [59] that a surface with a water contact angle of 70 gave the most suitable surface for cell adhesion;

however, the surfaces used in these studies were prepared using commercially available polymers and were not well controlled for factors of roughness, ionic charges, surface rigidity, etc. It is no doubt that the scaffold used for bone tissue engineering should be non-toxic and have good cell biocompatibility, which is a central criterion to ultimately decide the feasibility of implantation in body [60]. The information of the cell attachment and proliferation on the scaffold provided by cell culture experiment *in vitro* is often use as an important initial evaluation of cell biocompatibility. In this work human mesenchymal stem cells (hMSC), largely used to evaluate the regeneration of mineralized ECM in bone defects [61], were used as cell line model for *in vitro* testing of cell–material interaction, biocompatibility and osteogenic potential of the cellulose hydrogel materials. The paper reported the possibility to introduce new hydrophilic components such as -COOH groups by a simple crosslinking of cellulose hydrogels using citric acid. The citric acid is a natural cross-linker component of lemon juice that allows a crosslinking of CMC and HEC at high temperature with an anhydride intermediate. The results show that the crosslinking reaction gives the final products (CMCNa-CA and HEC-CA) with lower contact angle and higher roughness. Furthermore, our results of the hMSC cells-material interaction by confocal microscopy observation and proliferation test by Alamar Blue assay showed that CMCNa, CMCNa-CA, HEC and HEC-CA gels scaffolds had no negative effects on biological respond of hMSC, are nontoxic and are cell biocompatible. Ours preliminary studies of the differentiation of hMSCs towards the osteoblastic-like phenotype was quantitatively determined by carrying out a destructive assay for ALP activity using the p-nitrophenyl phosphate method. ALP is an enzyme produced by differentiating osteoblasts and is present both on the extracellular membrane and in vesicles of the bone matrix, which is the initial site of the formation of calcium phosphate crystals. The enzymatic activity of ALP is crucial for the mineralization process; it acts on the organic phosphate to increase the local concentration of free phosphate and to induce the active transport of both phosphate and calcium across the cell membrane [62]. In our results a steady increase in ALP activity was observed, which may confirm the ability of the gel materials to support hMSC differentiation towards the osteoblast-like phenotype and future could support the ECM mineralization. Previous *in vitro* works clearly demonstrate that osteogenic cells from hMSC remain vital and differentiate in the presence of CMCNa [63]. We performed the evaluation of expression of bone-related proteins involved in the mineralization process as osteopontin and osteocalcin onto CMCNa, CMCNa-CA, HEC and HEC-CA gels scaffolds. In our hands, the potential of differentiation of hMSC was not affected by the gels scaffolds and the finding of gene expression do not rule out the possibility that the

128

chemical modification of CMCNa, CMCNa-CA, HEC and HEC-CA gels scaffolds change the response of hMSC required for reproducing the bone ECM.

Based on numerous previous studies and techniques, it is known that ALP expression rise as extracellular mineralization marker for osteoblasts phenotype and then declines as osteoid becomes heavily mineralized, while OCN expression is acquired latest and essentially is diagnostic of post-proliferative osteoblasts [64]. Some research groups [65] reported that the carboxylic acid group-grafted surfaces, even though they were negatively charged, show better cell attachment and proliferation than untreated hydrophobic surfaces. The results suggest that hydrophilic groups and their charge character as well as wettability play important roles for cell adhesion, spreading, and growth, even though cell-surface interaction is a very complicated phenomenon and thus it is still not clear which property could be really dominant for cell adhesion and growth on surfaces.

2.3.5 Conclusions

Citric acid could be successfully used as functionalizing agent for CMCNa and HEC hydrogel materials. Moreover, crosslinking by citric acid increases the hydrophilicity and roughness surface of modified-cellulose hydrogels. Injectable cellulose hydrogels have good effect on the cell attachment, cell proliferation and osteoblastic differentiation. Furthermore, the use of citric acid as crosslinker allows the attainment of a good hydrogel substrate that can stimulate osteogenic differentiation of hMSC by the expression of bone markers. For these reasons, cellulose hydrogels could have a great potential application as filler in bone repair and regeneration.

2.3.6 References

[1] Kretlow JD, Klouda L, Mikos AG. Injectable matrices and scaffolds for drug delivery in tissue engineering. Adv Drug Deliv Rev 2007;59:263–73.

[2] Raucci MG, Alvarez-Perez MA, Meikle S, Ambrosio L, Santin M. Poly(epsilon-lysine) dendrons tethered with phosphoserine increase mesenchymal stem cell differentiation potential of calcium phosphate gels. Tissue Eng Part A 2014;20:474-85.

[3] Dessì M, Raucci M.G, Zeppetell S, Ambrosio L. Design of injectable organic-inorganic hybrid for bone tissue repair. J Biomed Mater Res A. 2012;100:2063-70.

[4] D'Antò V, Raucci M.G, Guarino V, Martina S, Valletta R, Ambrosio L. Behaviour of human mesenchymal stem cells on chemically synthesized HA-PCL scaffolds for hard tissue regeneration. J Tissue Eng Regen Med. 2013 May 31. doi: 10.1002/term.1768.

[5] Gong JP, Katsuyama Y, Kurokawa T, Osada Y. Double network hydrogels with extremely high mechanical strength. Adv Mater 2003;15:1155–8.

[6] Demitri C, Giuri A, Raucci MG. Giugliano D, MadaghielM, Sannino A, Ambrosio L. Preparation and characterization of cellulose-based foams via microwave curing. Interface Focus 2014;4, 2013005; http://dx.doi.org/10.1098/rsfs.2013.0053.

[7] Raucci MG, Alvarez-Perez MA, Demitri C, Sannino A, Ambrosio L. Preparation of cellulose-based hydrogel for bone tissue engineering. Proliferation and osteoblastic differentiation of hMSCs on cellulose-based hydrogels. J Appl Biomater and Funct Materials 2012:10:302-7.

[8] Sannino A, Madaghiele M, Demitri C, Scalera F, Esposito A, Esposito V, Maffezzoli A. Development and characterization of cellulose-based hydrogels for use as dietary bulking agents. J Appl Polym Sci 2010;115:1438-44.

[9] Casciaro S, Conversano F, Musio S, Casciaro E, Demitri C, Sannino A. Full experimental modelling of a liver tissue mimicking phantom for medical ultrasound studies employing different hydrogels. J Mater Sci: Mater Med 2009;20:983-9.

[10] Demitri C, Sannino A, Conversano F, Casciaro E, Distante A, Maffezzoli A. Hydrogel based tissue mimicking phantom for in-vitro ultrasound contrast agents studies. J Biomed Mater Res - Part B Appl Biomater 2008;87:338-45.

[11] Casciaro S, Demitri C, Conversano F, Casciaro E, Distante A. Experimental investigation and theoretical modelling of the nonlinear acoustical behaviour of o liver tissue and comparison with a tissue mimicking hydrogel. J Mater Sci: Mater Med 2008;19:899-906.

[12] Brown EE, Laborie M.G.. Bioengineering Bacterial Cellulose/Poly(ethylene oxide) Nanocomposites. Biomacromolecules 2007;8:3074–81.

[13] Slaughter B. V, Khurshid SS, Fisher OZ, Khademhosseini A, Peppas NA. Hydrogels in Regenerative Medicine. Adv Mater 2009;21:3307–29.

[14] Sannino A, Maffezzoli A, Nicolais L. Introduction of molecular spacers between the crosslinks of a cellulose-based superabsorbent hydrogel: Effects on the equilibrium sorption properties. J Appl Polym Sci 2003;9:168-74.

[15] Sannino A, Nicolais L. Concurrent effect of microporosity and chemical structure on the equilibrium sorption properties of cellulose-based hydrogels. Polymer 2005;46:4676-85.

[16] Hon DN-S. Cellulose and its derivatives: Structures, reactions, and medical uses. In: Polysaccharides in Medicinal Applications. Dumitriu D (ed.). Marcel Dekker, New York, 1996, 87-105.

[17] Martson M, ViljantoJ, Hurme T, Laippala P, Saukko P. Is cellulose sponge degradable or stable as implantation materials? An in vivo subcutaneous study in the rat. Biomaterials 1999;20:1899-1995.

[18] Granja PL, De Jéso B, Bareille R, Rouais F, Baquey C, Barbosa MA. Mineralization of regenerated cellulose hydrogels induced by human bone marrow stromal cells. Euro Cells Mater 2005;10:31-9.

[19] Lamba NMK, Baumgartner JA, Cooper SL. Cell-synthetic surface interactions. In: Frontiers in Tissue Engineering. Patrick Jr CW, Mikos AG, McIntire LV (eds). Elsevier Science, Oxford, 1998, 121-137.

[20] Arola S, Tammelin T, Setala H, Tullila A, Linder MB. Immobilization–stabilization of proteins on nanofibrillated cellulose derivatives and their bioactive film formation. Biomacromolecules 2012;13:594–603

[21] Pohl M, Michaelis N, Meister F, Heinze T. biofunctional surfaces based on dendronized cellulose. Biomacromolecules 2009;10:382–9.

[22] Lord MS, Foss M, Besenbacher F. Influence of nanoscale surface topography on protein adsorption and cellular response. Nano Today 2010;5:66-78.

[23] Lee JH, Lee JW, Khang G, Lee HB. Interaction of cells on chargeable functional group gradient surfaces. Biomaterials 1997;18:351-8.

[24] Webb K, Hlady V, Tresco PA. Relative importance of surface wettability and charged functional groups on NIH 2T3 fibroblast attachment, spreading and cytoskeletal organization. J Biomed MaterRes 1998;41:422-30.

[25] Bačáková L, Filová E, Rypáček F, Švorčík V, Starý V. Cell adhesion on artificial materials for tissue engineering. Physiol Res 2004a;53:S35-S45.

[26] Bačáková L, Filová E, Kubies D, Machová L, Proks V, Malinová V, et al. Adhesion and growth of vascular smooth muscle cells in cultures on bioactive RGD peptide-carrying polylactides. J Mater Sci: Mater Med 2007a;18:1317-23.

[27] Arima Y, Iwata H. Effect of wettability and surface functional groups on protein adsorption and cell adhesion using well-defined mixed self-assembled monolayers. Biomaterials 2007;28:3074-82.

[28] Dulgar-Tulloch AJ, Bizios R, Siegel RW. Human mesenchymal stem cell adhesion and proliferation in response to ceramic chemistry and nanoscale topography. J Biomed Mater Res A. 2009;90:586-94.

[29] Bačáková L, Starý V, Kofroňová O, Lisá, V. Polishing and coating carbon fibre-reinforced carbon composites with a carbon-titanium layer enhances adhesion and growth of osteoblast-like MG63 cells and vascular smooth muscle cells in vitro. J Biomed Mater Res 2001;54:567-78.

[30] Lossdorfer S, Schwartz Z, Wang L, Lohman CH, Turner J D, Wieland M, Cochran DL, Boyan BD. Microrough implant surface topographies increase osteogenesis by reducing osteoclast formation and activity. J Biomed Mater Res A 2004;70:361-69.

[31] Tan J, Saltzman WM. Biomaterials with hierarchically defined micro- and nanoscale structure. Biomaterials 2004;25:3593-601.

[32] Intranuovo F, Favia P, Sardella E, Ingrosso C, Nardulli M, d'Agostino R, Gristina R. Osteoblast-like cell behavior on plasma deposited micro/nanopatterned coatings. Biomacromolecules 2011;12:380–7

[33] Lossdorfer S, Schwartz Z, Wang L, Lohman C, Turner J, Wieland M, Cochran D, Boyan BD. Microrough implant surface topographies increase osteogenesis by reducing osteoclast formation and activity. J Biomed Mater Res A 2004;70:361-9.

[34] Amis EJ. Combinatorial materials science: Reaching beyond discovery. Nature Mater 2004;3:83–85.

[35] Bianco P, Riminucci M, Gronthos S, Robey PG. Bone marrow stromal stem cells: Nature, biology, and potential applications. Stem Cells 2001;19:180–92.

[36] Meredith JC, Sormana JL, Keselowsky BG, Carcìa AJ, Tona A, Karim A, Amis EJ. Combinatorial characterization of cell interactions with polymer surfaces. J Biomed Mater Res A 2003;66:483–90.

[37] Saha K, Pollock JF, Schaffer DV, Healy KE. Designing synthetic materials to control stem cell phenotype. Curr Op Cheml Biol 2007;11:381–87.

[38] Anderson DG, Levenberg S, Langer R. Nanoliter-scale synthesis of arrayed biomaterials and its application to human embryonic stem cells. Nature Biotech 2004;22:863–6.

[39] Keselowsky BG, Collard DM, Garcia AJ. Surface chemistry modulates fibronectin conformation and directs integrin binding and specificity to control cell adhesion. J Biomed Mater Res A 2003;66:247–59.

[40] Nuttelman CR, Benoit DSW, Tripodi MC, Anseth KS. The effect of ethylene glycol methacrylate phosphate in PEG hydrogels on mineralization and viability of encapsulated hMSCs. Biomaterials 2006;27:1377–86.

[41] Engler A, Bačáková L, Newman C, Hategan, A, Griffin M, Discher DE. Substrate compliance versus ligand density in cell on gel responses. Biophysical J 2004;86:617-28.

[42] Engler AJ, Sen S, Sweeney HL, Discher DE. Matrix elasticity directs stem cell lineage specification. Cell 2006;126:677-89.

[43] Demitri C, Del Sole R, Scalera F, Sannino A, Vasapollo G, Maffezzoli A, et al. Novel Superabsorbent Cellulose-Based Hydrogels Crosslinked With Citric Acid. J Appl Polym Sci 2008;110:2453-60.

[44] Granja PL, Pouységu L, Deffieux D, Daudé G, De Jéso B, Labrugére C, Baqueyè C, Barbosa M.A. Cellulose Phosphates as Biomaterials. II. Surface Chemical Modification of Regenerated Cellulose Hydrogels. J Appl Polym Sci 2001;82:3354–65.

[45] Yalpani M. Polysaccharides: Syntheses, Modifications, and Structure/Property Relations; Elsevier: Amsterdam, 1988.

[46] Coultate TP. Food: The Chemistry of Its Components, 3rd ed.; Royal Society of Chemistry: Cambridge, U.K., 1996.

[47] Demitri C, Marotta F, Sannino A, Ron ES, Zohar Y Ambrosio L. Rheological and mechanical comparison between natural dietary fibers and a novel superabsorbent biodegradable hydrogel (SAEF®). Presented at the 24th European Conference on Biomaterials, Dublin, Ireland,4-8 September 2011.

[48] Entcheva E, Bien H, Yin L, Chung CY, Farrell M, Kostov Y. Functional cardiac cell constructs on cellulose based scaffolding. Biomaterials 2004;25:5753–62.

[49] Miyamoto T, Takahashi S, Ito H, Inagaki H, Noishiki Y. Tissue biocompatibility of cellulose and its derivatives. J Biomed Mater Res 1989;23:125–33.

[50] Eichhorn S J, Young RJ. The Young's modulus of a microcrystalline cellulose. Cellulose 2001;8:197–207.

[51] Poustis J, Baquey C, Chauveaux D. Mechanical properties of cellulose in orthopaedic devices and related environments. Clinical Mater 1994;16:119–24.

[52] Granja PL, Barbosa MA, Pouységu L, De Jéso B, Rouais F, Baquey C. Cellulose phosphates as biomaterials: mineralization of chemically modified regenerated cellulose hydrogels. J Mater Sci 2001;36:2163–72.

[53] Rhee SH, Tanaka J. Hydroxyapatite formation on cellulose cloth induced by citric acid. J Mater Sci: Mater Med 2000;11:449–52.

[54] Fricain JC, Granja PL, Barbosac MA, de Jésoe B, Barthea N, Baqueya C. Cellulose phosphates as biomaterials In vivo biocompatibility studies. Biomaterials 2002;23:971–80.

[55] Dumitriu S, Dumitriu M. Hydrogels as support for drug delivery systems. In: Polysaccharides in Medicinal Applications. Dumitriu S (ed.). Marcel Dekker, New York, 1996, 705-764.

[56] Lee JH, Lee JW, Khang G, Lee HB. Interaction of cells on chargeable functional group gradient surfaces. Biomaterials 1997;18:351-8.

[57] Choee JH, Lee SJ, Lee YM, Rhee JM, Lee HB, Khang G. Proliferation rate of fibroblast cells on polyethylene surfaces with wettability gradient. J Appl Polym Sci 2004;92:599-606.

[58] Webb K, Hlady V, Tresco PA. Relative importance of surface wettability and charged functional groups on NIH2T3 fibroblast attachment, spreading and cytoskeletal organization. J Biomed Mater Res 1998;41:422-30.

[59] Tamada Y, Ikada Y. Effect of preadsorbed proteins on cell adhesion to polymer surfaces. J Colloid Inter Sc 1993;155:334–9.

[60] Liuyun J, Yubao L, Chengdong X. Preparation and biological properties of a novel composite scaffold of nano-hydroxyapatite/chitosan/carboxymethyl cellulose for bone tissue engineering J Biomed Sci 2009;16:65.

[61] Li WJ, Tuli R, Huang XX, Laquerriere P, Tuan RS. Multilineage differentiation of human mesenchymal stem cells in a three-dimensional nanofibrous scaffold. Biomaterials 2005;26:5158–66.

[62] Ciapetti G, Ambrosio L, Savarino L, Granchi D, Cenni E, Baldini N, Pagani S, Guizzardi S, Causa F, Giunti A. Osteoblast growth and function in porous poly-ε-caprolactone matrices for bone repair: a preliminary study. Biomaterials 2003;24:3815–24.

[63] Trojani C, Weiss P, Michiels JF, Vinatier C, Guicheux J, Daculsi G, Gaudray P, Carle GF, Rochet N. Three-dimensional culture and differentiation of human osteogenic cells in an injectable hydroxypropylmethylcellulose hydrogel. Biomaterials 2005;26:5509–17.

[64] Malaval L, Liu F, Roche P, Aubin JE. Kinetics of osteoprogenitor proliferation and osteoblast differentiation in vitro. J Cell Biochem 1999;74:616-627.

[65] Jin Ho L, Jin Whan L, Gilson K, Hai Bang L. Interaction of cells on charge able functional group gradient surfaces. Biomaterials 1997;18:351-58.

Conclusions of chapter 2

In this chapter were proposed three injectable systems as a bone-filler:

1. Strontium-substituted hydroxyapatite cement (to contrast osteoporosis effects);
2. Bioactive hydroxyapatite - graphene oxide (to support high viability of hMSC cells);
3. Modified-cellulose hydrogels crosslinked by citric acid (to increase hydrophilicity and roughness surface in order to stimulate osteogenic differentiation of hMSC).

All these gel materials could have a different medical application, such as osteoporosis therapy, filler for different (in terms of dimension and shape) bone cavity caused by tumor removal, fractures or congenital defects, carrier to growth factors or pharmacy, detection systems, antitumor therapy, or as a multifunction systems.

Our researches have demonstrated that the injectable HA-modified systems (1 and 2) preserve the typical gel structure of traditional hydroxyapatite, in a macroscale. However in a nanoscale is possible to observe the real differences of the two systems: (1) HA structure results modified due to substitution of Ca with Sr atoms, during sol-gel synthesis. In particular, the nHA crystals have a different shape and crystalline decrease; (2) nHA, with a typical spindle-like shape and a typical dimensions of about (5x70 nm), is uniformly distributed on GO sheets. In this case, there is no one modification of traditional bond or atomic disposition during synthesis, that could be modified the nHA growth, but there is an electrostatic attraction between carboxyl group presents on GO sheets surface and Ca^{2+} ions.

Indeed, in the two different cellulose systems (CMCNa and HEC) (3) we have demonstrated that crosslinking treatment by citric acid (CA) increases the hydrophilicity, by adding some -COOH groups on material surface, and the roughness of materials.

The specific nanoscale structures of the materials surface have a significant positive effects on osteoblast cell response, including initial cell and expression of differentiation markers.

Infact, gel systems (1, 2 and 3) supported high viability of hMSC cells and have a good effect on cell attachment, proliferation and osteoblastic differentiation. In particular gene expression analysis shows that HA doped with strontium (1) and CMCNa-CA, HEC-CA hydrogels (3) significantly promote the expression of osteogenesis related genes including an early marker for osteogenic differentiation ALP; a non-collagen protein OPN and a late marker for osteogenic differentiation OCN.

Moreover, HA-GO hybrid system (2) induces an osteogenic differentiation evaluated by using a media without osteogenic factors.

The proposed materials for osseous defects associated with orthopaedic reconstructive surgery may be good candidates as delivery vehicles for cells or drugs such as antibiotics, since they would conform to the defect. Moreover, one of the major properties is that they could be used in minimally invasive procedures.

CHAPTER 3
POROUS SCAFFOLD FOR OSTEOCHONDRAL DEFECT

*A*rticular cartilage has limited reparative abilities. Purely chondral defects do not heal, and usually progress towards degeneration of the surrounding cartilage. Osteochondral defect - that is defect that penetrate the subchondral bone - can undergo spontaneous repair. Through an appropriate system it is possible to observe proliferation and differentiation of human mesenchymal stem cells (hMSCs), which invade the defect from the underlying bone marrow. The goal is hMSCs differentiation into fibroblasts, chondrocytes and osteoblasts, in order to synthesize new bone tissue in the base of the defect by both endochondral and direct intramembranous ossification, and synthesize cartilage tissue in the chondral region of the defect, with a layer of fibrous tissue forming at the articular surface.

Experimental studies have shown that several physical factors such as size and location of the defect, or load acting, can influence the quality, type and durability of the repair tissue.

Here, a new strategy of composite manufacturing has been proposed by two different techniques: bulk sol–gel transition and surface biomimetic treatment. Proposed approaches enable to efficiently exploit the peculiar features of composite material bulk, in the first case, and surfaces by modulating the spatial distribution of bioactive signals, in the second, moving toward a more efficient replacement of bone tissue.

Moreover bone/cartilage defect fillers promote a dual effect: 1) natural polymer matrix's effect; 2) presence of bioactive signals on the surface, inside the scaffold's structure or in a specific region of the same. The use of a 3D scaffold depends on the necessity to have a shape control, while the biological signals are induced by HA presence on the surface, as a coating, or within the structure as a gradient. As hydrogel, the structure can adapt perfectly to the shape defect.

In this chapter we propose two systems based on gelatin/hydroxyapatite, potentially able to support the osteochondral defect reparation.

3.1 BIOMINERALIZED GELATIN SCAFFOLD

Introduction

The development of materials by mimicking the structure and composition of human tissues, namely the biomimetic approach, has long been a major goal in the field of biomaterials and tissue engineering. In bone-tissue regeneration, gaining an insight into the hierarchical structure of the bone matrix, i.e., the nanocomposite consisting of mineralized hydroxyapatite (HA) nanocrystals and collageneous fibres, has caused a considerable amount of research to be direct toward the synthesis of bio-inspired and biomimetic systems [1-4].

Several synthetic scaffolds, such as biodegradable polymers and bioactive ceramics, which have been developed to sustain the wound site and subsequently replace and regenerate new tissues, have proven to be applicable clinically. Human hard tissues, such as bones and teeth, consist of cells and surrounding extra cellular matrix (ECM). The ECM composition of hard tissues is mainly organic collagen type I fibrils embedded with nanosized hydroxyapatite (HA) crystals. The ECM plays an important role in cell function and further tissue regeneration by providing specific signals to cells [5].

Significant effort has been exerted to develop artificial ECM to promote cell function and differentiation as a temporary scaffold. One approach used in the design of materials has focused on the degradation and ultimate replacement of the material with new tissue. Whether or not a material is biodegradable, its surface properties will influence the initial cellular events at the cell-material interface. Among the biomaterials proposed, the composites of HA and natural polymers, such as collagen and gelatin, have great deal of attention in a sense that the composite system can provide the compositional benefits and preserve the structural and biological functions of the damaged hard tissues in a more efficient and similar way to the natural system [6-8]. One of the major disadvantages of gelatin as a biomaterial is their high degree of biodegradation due to enzymatic digestion. An inadequate mechanical stability of protein-derived scaffolds will lead to a mismatch between the new bone formation and the scaffold degradation rates. An appropriate ratio between bone formation and scaffold degradation is essential to provide a suitable environment for bone growth in defective areas. To overcome this problem, gelatin was crosslinked by a chemical agents such as various aldehydes (e.g. glutaraldehyde, formaldehyde), acyl acid, carbodiimides, hexamethylene-diisocyanate. Among all, carbodiimide is a condensation agent used between carboxylic acid and amino groups to form amide-type bonds [9]. Crosslinking a gelatin hydrogel

with carbodiimide involves the activation of its carboxylic acid groups of glutamic or aspartic acid residues to give *O*-acylisourea groups, which form crosslinks after a reaction with its free amino groups of lysine or hydroxyline residues [9,10]. The cross-linked structure results in a lower degradation rate, increasing the longevity of materials in the living environment. Porous gelatin scaffold can be fabricated by using the freeze-drying method [11].

To engineer functional tissues and organs successfully, the scaffolds have to be designed to facilitate cell distribution and guide tissue regeneration in three dimensions. On the other hand, natural bone ECM is a composite mainly composed of nanofibrous type I collagen and partially carbonated hydroxyapatite (HA). HA is orderly deposited within nanofibrous collagen matrix. Hence synthetic HA has been developed in a variety of forms and is known to directly bond to bones and teeth in vivo [12]. Its excellent bioactivity and osteoconductivity led to potential use in hard-tissue substitutes and regeneratives [13-15].

However, it is highly brittle and stiff; therefore its shape and size availability is limited, and it is difficult to handle in clinical situations. In this manner, the composite design of gelatin and HA is expected to offer improved biocompatibility from biological and mechanical viewpoints. The gelatin-HA composite also is expected to be a good alternative for hard tissue regenerative, in view of combining the bioactivity and osteoconductivity of HA with the flexibility and hydrogel characteristics of gelatin.

A composite approach of the two components, gelatin and HA, has the potential to be an engineered biomaterial. Same authors suggest to disperse HA powders directly in the polymer solution. However, the HA powders in this case were not dispersed well or were easily agglomerated, and even settled, which made it difficult to form a controlled structure [16-18]. For this reason, we propose a biomimetic approach, that consist in the precipitation of nanoapatite crystals on the polymer surface [6-8,19], due to modified material surface properties and influence the composition of the adsorbed protein compounds, which in turn regulates how cells respond to the material [20,21].

The crosslinked gelatin-HA composites were fabricated as a porous scaffold, through a combination of two process as freeze-drying and biomimetic method, to offer a porous system with a high specific surface area for vascularization and cell ingrowth, and appropriate biological repeals, such as hydroxyapatite [22].

We hypothesized that such gelatin/nanoapatite composite scaffold would provide not only excellent biocompatibility but also advantageous scaffolding properties, such as enhanced cell adhesion, proliferation, and osteoblastic differentiation.

In the context of a program aimed at investigating the biological behavior of biomineralized gelatin, the *in vitro* biocompatibility was evaluated with cultured MG-63, in terms of cell adhesion, proliferation and differentiation. It was demonstrated that these materials are cytocompatible, non-cytotoxicity and support osteogenic differentiation.

3.1.1 Materials and methods

3.1.1.1 Materials

Gelatin type B (bovine skin, 225 Bloom), and type A (porcine skin, 90-110 Bloom), 1-ethyl-(3-3-dimethylaminopropyl carbodiimide hydrochloride) (EDC) and all reagents used to prepare SBF solution were purchased from Sigma-Aldrich (Milano, Italy).

3.1.1.2 Preparation of crosslinked Gelatin scaffolds

Gelatin (A and B) was dissolved in deionised water (5-10 w/w%,) at 40°C, rpm 100. After 30 min of stirring the solution was sonicated to remove air bubbles. The solution was poured into a multiwall plate and processed throw freeze-drying process for 48 h, due to obtain a cylindrical gelatin samples non crosslinked.

The main limitation of gelatin for the preparation of tissue substitutes is its rapid dissolution in aqueous environments, leading to fast degradation of grafts at body temperature. To overcame this gelatin drawback, it was proposed a crosslinking treatment.

The crosslinking reaction was obtained soaking porous lyophilized scaffold in a solution of acetone–water-based solvent (4:1 in volume) containing a water-soluble 1-ethyl-(3-3-dimethylaminopropyl carbodiimide hydrochloride) (EDC), firstly at room temperature for different times (1h, 3h and 6h) and then at 4°C for 24 h. The ratio of scaffold to solvent was fixed at 1% (w/v) from preliminary tests to maintain pore structures. The amount of crosslinking agent was 0.7% (w/v) respect to volume solution of acetone-water [23].

The crosslinked gelatin scaffolds were washed in bi-distilled water for several time to remove non-crosslinked components, EDC residual and eventual sub-products; then there were deswelling by dehydrated in ethanol.

3.1.1.3 Preparation of biomineralized scaffolds: Biomimetic surface treatment

To produce the apatite coating, scaffold substrates were submitted to a bio-inspired procedure, namely biomimetic treatment, inspired by the method described by Kokubo and co-workers [24] [25].

In particular, we used an accelerate treatment that combines the preliminary use of a supersaturated SBF solution ($5xSBF_1$) to stimulate the nuclei formation, while a fresh chemically-modified solution ($5xSBF_2$) is further used, in order to promote the growing of apatite nuclei, once formed. Meanwhile, $5xSBF_1$ was prepared by sequentially dissolving $CaCl_2$, $MgCl_2 \cdot 6H_2O$, $NaHCO_3$ and $K_2HPO_4 \cdot 3H_2O$ in distilled water. Solution pH was lowered to 6 by adding hydrochloric acid HCl (1M) to increase the solubility. Na_2SO_4, KCl were added until the previous solution become clear. The final pH was adjusted with 1M NaOH to reach a final pH equal to 6.5 ($5xSBF_1$).

Therefore, Mg^{2+} and HCO_3^- free 5xSBF was prepared by adding $CaCl_2$, $K_2HPO_4 \cdot 3H_2O$ subsequently to distilled water up to obtain a fresh solution ($5xSBF_2$). In this case, the solution pH was lowered to 6.0 with hydrochloric acid to increase the solubility. Both solutions were buffered at pH 6.5 and 6 respectively, by using Trishydroxymethylaminomethane-chloric acid (Trizma-HCl). In Table 1, the ionic concentration of blood plasma, SBF, $5xSBF_1$ and $5xSBF_2$ were reported. All solutions were prepared freshly before the use.

The biomimetic treatment consists in two steps in pH-controlled environment: during the first step, samples with pre-ordered size were soaked into $5xSBF_1$ at pH=6.5 where the 5xSBF solution volumes have been calculated respect to the total scaffold material surface by using an exposed surface to SBF volume ratio equal to 10 mm^2/ml, as reported in literature [26].

The solution temperature was fixed at 37°C during the treatment. After the sequential immersion in $5xSBF_1$ (4 days) and in $5xSBF_2$ (3 days), all scaffolds were gently rinsed in distilled water to remove excess ions and, then, dried overnight under laminar hood.

Ion Concentration (mM)	Na^+	K^+	Ca^{2+}	Mg^{2+}	HCO_3^-	Cl^-	HPO_4^-	SO_4^{2-}
Blood plasma	142	5	2.5	1.5	27	103	1	0.5
SBF	142	5	2.5	1.5	4.2	148	1	0.5
$5xSBF_1$	710	25	12.5	7.5	21	740	5	2.5
$5xSBF_2$	710	10	12.5	-	-	735	5	-

Table1: The ionic concentration of human blood plasma, SBF, $5xSBF_1$ and 5xSBF.

To increase the nucleation phase, the scaffold materials were tested by using two different pre-treatment:

- Preliminary treatment in $CaCl_2$ solution (0.1M) at 37°C for 2 days and then by accelerated biomimetic treatment;

- Preliminary treatment in $Ca(OH)_2$ solution (0.01 M) a 37°C for 30 min and then by a standard biomimetic ones: $1.5xSBF_1$ (4 days) and in SBF (3 days).

3.1.2 Characterization

3.1.2.1 Morphological analysis

The morphological analysis was performed on different scaffolds by using a Quanta FEG200 (FEI, the Netherland) Scanning electron microscope. The materials for SEM analysis were prepared by deposition of composite scaffold on one side of a double adhesive tape, and then stuck to an aluminium stub. The stub was then gold coated in an automatic sputter coater (EMSCOPE SC500, 20KV) to a thickness of around 30 nm. X-ray energy dispersive spectroscopy (EDAX, Genesis 2000i) was used for a qualitative estimation of elements in the material.

All the samples were, firstly dehydrated using a freeze-dryer, and then broken in section by using a liquid nitrogen in order to investigate the cross-section surface.

3.1.2.2 Swelling test

The swelling measurements of crosslinked gelatin scaffolds were carried out by using pieces of lyophilized samples (9x6 mm) immersed into 4 ml distilled water at 37°C for different times. The samples of swollen hydrogel were weighed after removal of surface water using filter paper at designed time intervals, and then weighed (Wt). Data presented in this experiment were the mean values of triplicate measurements.

The swelling ratio was calculated according to:

$$\text{swelling ratio (\%)} = (W_t - W_0)/ W_0 \times 100$$

where W_0 is the weight of the dried sample.

             W_t is the weight of the wetted sample after relative soaking period

3.1.2.3 Degradation tests

To evaluate the sample degradation, the gelatin scaffolds were soaked in 4 ml dH$_2$O, at 37°C. After the designated soaking time had elapsed, the scaffolds were freezed and lyophilized due to evaluate the real weight after defined degradation time. Data presented in this experiment were the mean values of triplicate measurements.

The degradation was calculated according to:

$$\text{Weight (\%)} = 100 - [(W_0 - W_f)/ W_f \text{ x } 100]$$

where W_0 is the weight of the dried no-depredated sample;

                W_f is the weight of the dried sample after relative soaking period.

3.1.2.4 Thermal analysis: DSC and TGA

Thermal gravimetric analysis (TGA) was performed by TA Instrument Q 5000 under nitrogen atmosphere and room temperature up to 800 °C, with a heating rate of 5 °C/ min.

Differential scanning calorimetry (DSC) was performed by TA Instrument Q 1000 under nitrogen atmosphere and setting a temperature stage: room temperature up to -5°C, and -5°C up to 250 °C, with a heating rate of 5 °C min-1.

3.1.2.5 XRD analysis

X-ray diffraction measurements (XRD) were performed with a Brucker diffractometer (equipped with a continuous scan attachment and a proportional counter) with Ni-filtered Cu Kα radiation (λ=1.54050 Å).

3.1.2.6 Mechanical test

The mechanical properties of the scaffolds were evaluated by compression tests. Tests were performed using a standard testing machine (Lloyd LR5K instrument, Fareham Hants, U.K.) equipped with a 10 N load cell. The gelatin, with and w/o biomineralized coating, cylinders were soaked in water until equilibrium swelling, and then tested in an aqueous environment. The

deformation range and the speed (mm/min) were calculated respectively as 75% and 10% of swelled sample height.

3.1.2.7 Biological test

Cell viability

The human osteoblastic cell strain MG-63 was cultured in α-Modified Eagle's medium (α -MEM) (Bio Wittaker, Belgium) containing 10% (v/v) FBS, 100 U/mL penicillin and 0.1 mg/mL streptomycin (HyClone, UK), in a humidified atmosphere at 37 °C and 5% CO_2.

Materials for cell-culture experiments, were prepared to cell seeding by soaking first in 70% ethanol (1 h) and then in 1% antibiotic/antimycotic in PBS (2 h), and prewetting in medium (2 h). 7 x 10^4 cells, resuspended in 50 ml of medium, were statically seeded onto the scaffold. Following seeding, the scaffolds were placed in 24 well culture plates and after the initial 2 h of cell attachment on prewetted scaffolds, it was added 1.0 ml of cell-culture medium. The samples were exposed to basal medium, comprising α -MEM supplemented with supplemented with 10% Fetal Bovine Serum (FBS), antibiotic solution (streptomycin 100 µg/ml and penicillin 100U/ml, Sigma Chem. Co) and 2 mM L-glutamine. The scaffolds were maintained in culture for 21 days and the cell-culture medium was changed every 2-3 days.

Cell proliferation was evaluated by using the Alamar Blue assay. This is based on a redox reaction that occurs in the mitochondria of the cells; the coloured product is transported out of the cell and can be measured spectrophotometrically. The cell–material constructs were removed from the culture plates at days 1, 7, 14 and 21, 28 washed with PBS (Sigma–Aldrich, Italy), and placed into 24 well culture plates. For each construct, 1 ml of DMEM medium without Phenol Red (HyClone, UK) containing 10% (v/v) Alamar Blue (AbD Serotec Ltd, Milano, Italy) were added, followed by incubation for 4 h at 37 °C and 5% CO_2. 200 µl of the solution were subsequently removed from the wells, transferred in a 96-well plate and the optical density was immediately measured using a spectrophotometer (Sunrise, TECAN, Männedorf, Zurich, Switzerland) at wavelengths of 540 and 600 nm. The number of viable cells correlates with the magnitude of dye reduction and is expressed as percentage of AB reduction [42].

Alkaline Phosphatase assay

The alkaline phosphatase activity of the cells onto gelatin materials was determined for 7, 14 and 21 days of culture. To measure ALP levels, the cells were lysed in cell lysis buffer (BD Pharmingen™)

and the ALP activity was measured using the SensoLyteTM pNPP Alkaline Phosphatase Assay kit (AnaSpec, DBA, Milano, Italy) according to the manufacturer's instructions. Briefly, at the end of each time point, cultures were washed gently with PBS followed by washing twice with cold 1X assay buffer. For extract cell layers the cultures were lysing with 1X lysis buffer with 0.2% of Triton X-100. The phosphatase activity was analyzed onto the cell lysates (50μl) by measuring the ALP activity when ALP enzyme catalyzes the cleavage of a phosphate group and release p-nitrophenol from p-nitrophenyl phosphate in alkaline buffer solution after 30 min at 37°C. Sample absorbance was measured in a 96-well plate at 405 nm. The ALP activity was calculated from standard curve after normalization to the total protein concentration, which was determined using a kit Pierce MicroBCA Protein Assay Kit (Thermo Fisher). To correct ALP for the amount of cells present in each scaffold, data are presented as nanograms of ALP normalized to the milligrams of total protein content (ng ALP)/mg proteins. Each experiment was performed three times in triplicate.

3.1.2 Results

3.1.3.1 Morphological analysis

Morphological investigations were performed to evaluate four different phenomena:

1)   Internal/external structure of gelatin scaffold realized by liophylization technology;

2)   Structural changes caused by degradation;

3)   Evaluation of different biomimetic treatments successful by EDS analysis:

- $5xSBF_1$ (4 days) + $5xSBF_2$ (3 days)
- $CaCl_2$ (0.1 M for 2 days) + $5xSBF_1$ (4 days) + $5xSBF_2$ (3 days)
- $Ca(OH)_2$ (0.01M for 30 min) + $1.5xSBF_1$ (4 days) + SBF (3 days)

4)   Mechanical test effect on scaffolds internal and external structure.

Effect of Lyophilization

Gelatin scaffolds were realized by lyophilization technology. Lyophilization or freeze drying is a process in which water is removed from a product after it is frozen and placed under a vacuum, allowing the ice to change directly from solid to vapor without passing through a liquid phase. The process consists of three separate, unique, and interdependent processes; freezing, primary drying (sublimation), and secondary drying (desorption). In particular the gelatin solutions were freeze at

-80°C to allow the internal desiderated structure, and then processed for 48 hrs to guarantee sublimation and desorption steps.
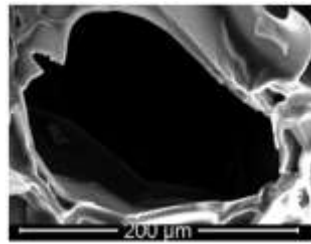
Fig. 1: SEM image: qualitative analysis of pore size.
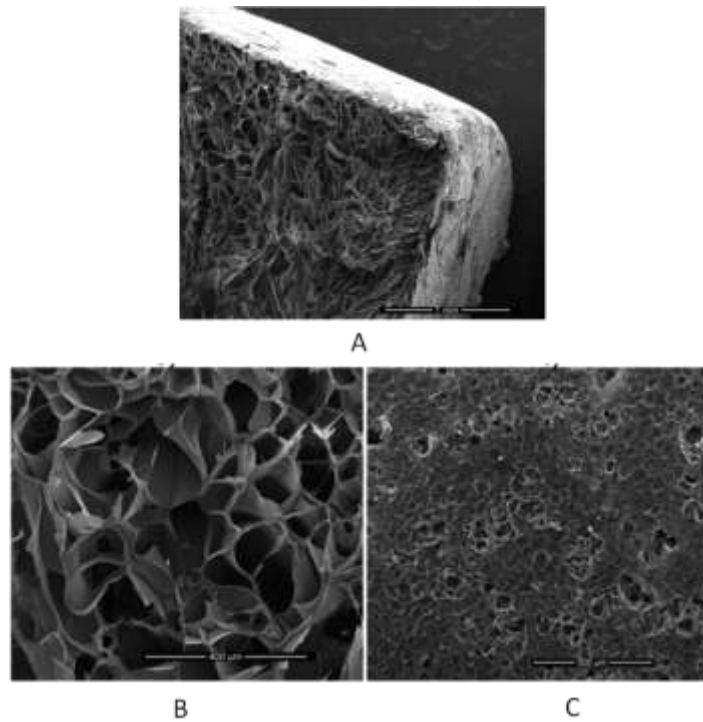
Fig. 2: SEM images of A5_1h scaffold (A). Magnification of internal (B) and external part of scaffold (C).

As shown in the images (figure 2), the internal scaffold has a interconnected porous structure, that should improve cells infiltration and growth, moreover for its hydrogel nature allows a nutrient and biology fluid transport.

The external section shows a compact structure may be depending on interaction between gelatin charges and mold walls; this effect is independent to mold material, infact the test were performed either Teflon or polystyrene (figure 3).

(A)   (B)
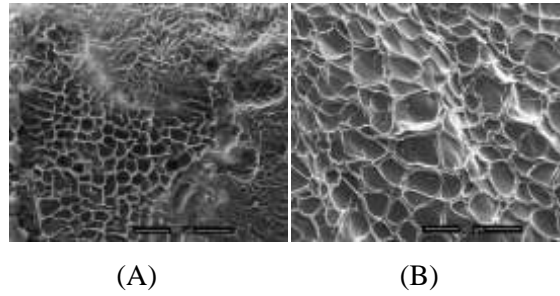
Fig. 3: SEM images of external surface of B10_3h scaffold realized in a Teflon mold (A) in a polystyrene mold (B).

Effect of Degradation

The degradation is an hydrolysis process where swelling, porosity and morphological changes are critical to its study [27]. Infact, firstly there is a water penetration through pores regions, and consequently, occurs the interaction between water solution sites and the hydrophilic groups of the hydrogel chains.

A characteristic morphology of the freeze-dried samples of the water-swollen hydrogel was observed. SEM analyses were performed on the samples taken at specific swelling times: 1, 4, 8, 12, 21, 28 days.

As shown in the figures 4 and 5, a simultaneously change of both internal and external parts during degradation process was observed. In particular the phenomenon is a bulk erosion and due to the particular sample structure, water erosion power consumes faster the internal part than the external ones. As consequence of this phenomenon an increasing of surface roughness, and a successive pores opening were observed.

A) B10_3h

| 1day | 4days | 8days | 12days | 21 days | 28days |

B) B5_3h

| 1day | 4days | 8days | 12days | 21 days | 28days |

C) A10_3h

| 1day | 4days | 8days | 12days | 21 days | 28days |

D) A5_3h

| 1day | 4days | 8days | 12days | 21 days | 28days |
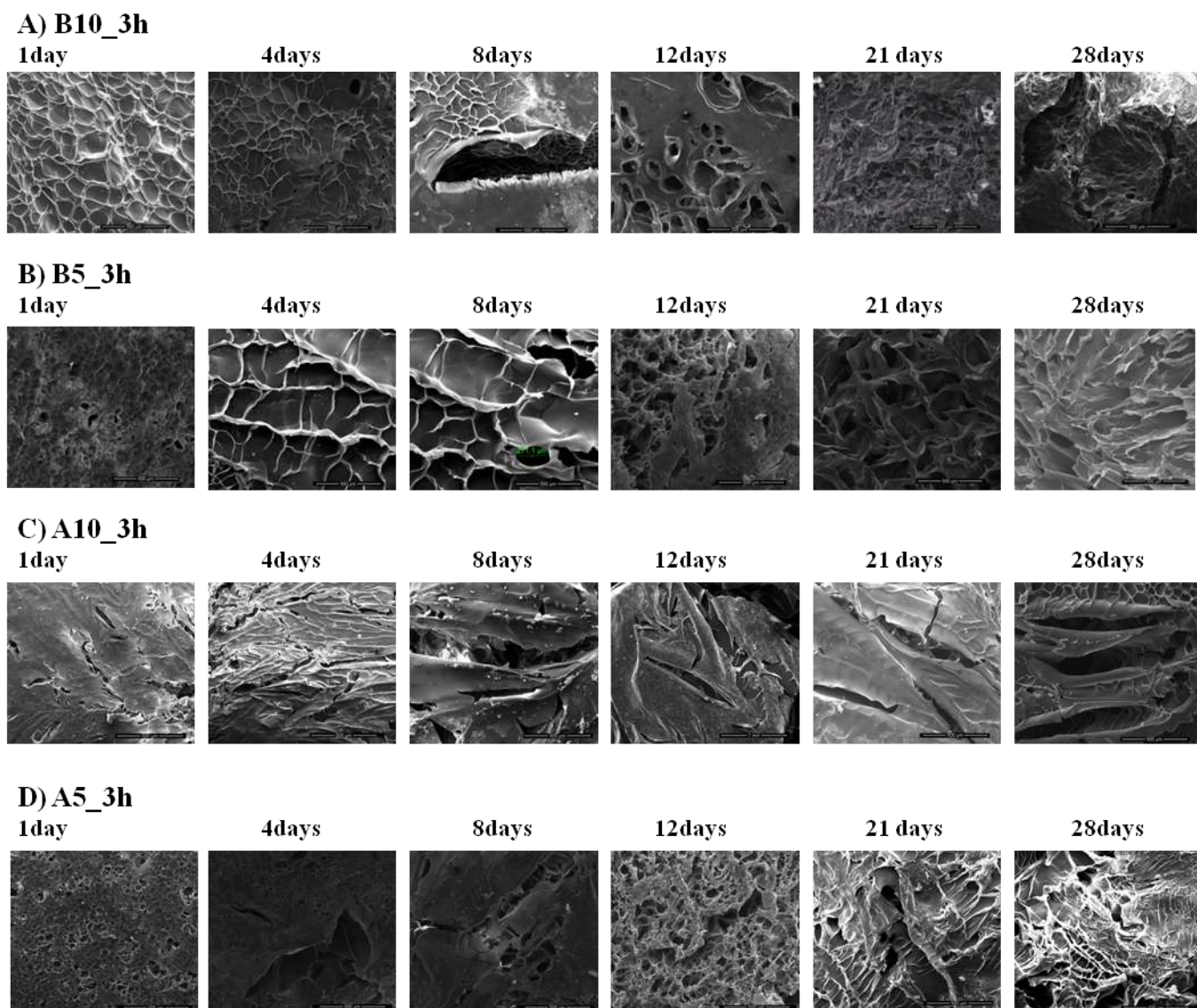
Fig. 4: SEM images of different gelatin scaffolds surface at different degradation time.

A) B10_3h

1day	4days	8days	12days	21 days	28days

B) B5_3h

1day	4days	8days	12days	21 days	28days

C) A10_3h

1day	4days	8days	12days	21 days	28days

D) A5_3h

1day	4days	8days	12days	21 days	28days
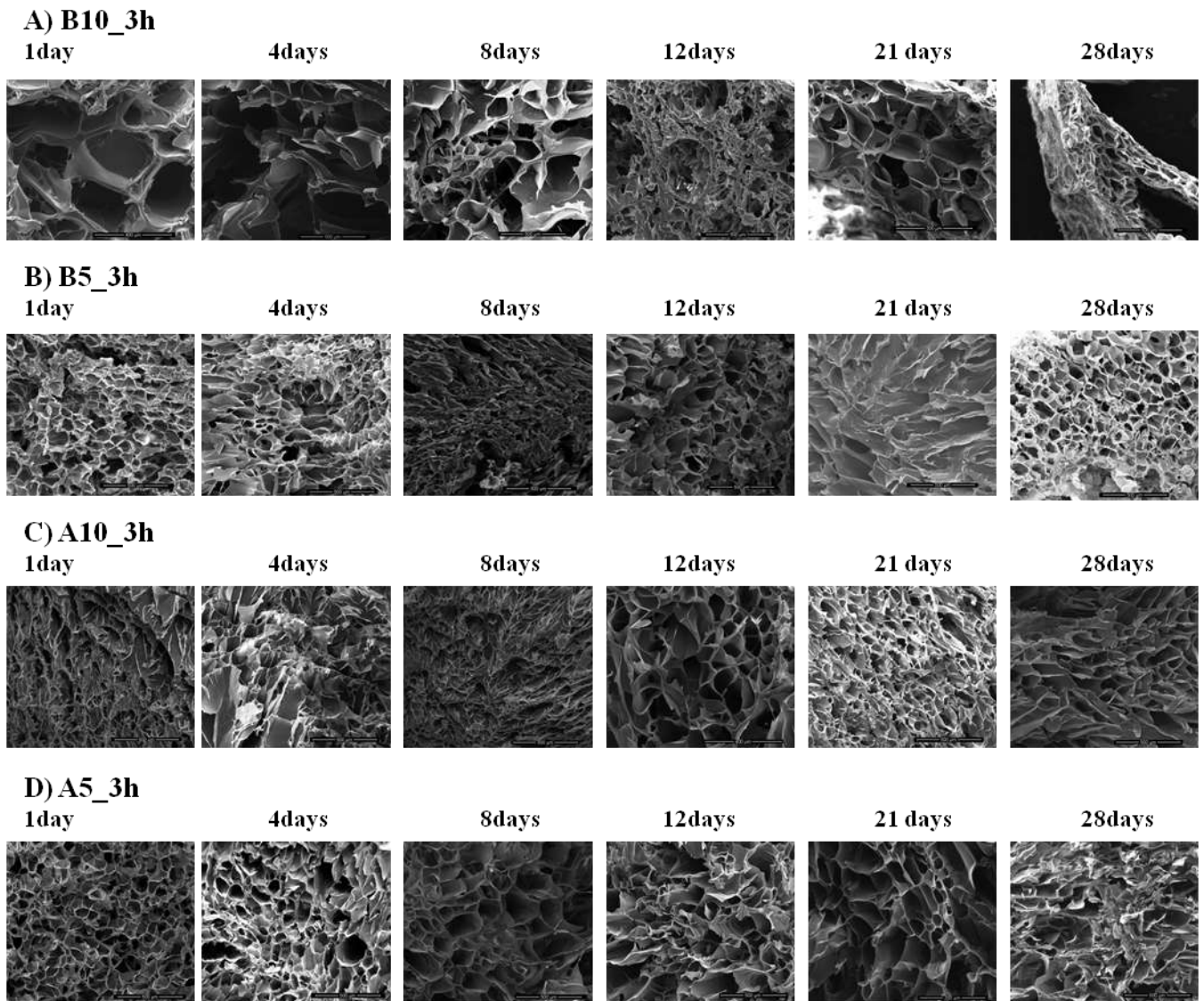
Fig. 5: SEM images of different gelatin scaffolds in cross-section at different degradation time.

On the whole, the images show a gradually degradation both the internal and external part of the scaffold. The materials preserve the internal structure since 28 days in water solution, to indicate the crosslinking effect by EDC.

Biomimetic treatment

The first treatment has been investigated is a accelerate Kokubo method, that involves samples incubation at 37°C, 4 day in $5xSBF_1$ and 3 days in $5xSBF_2$. The EDS (figure 6) analysis of the deposited apatite crystals shows the presence of Ca and P peaks typical of hydroxyapatite, meanwhile appear others peaks which are characteristic of the presence of impurities such as sodium and magnesium, which are common for biomimetic apatite. The Ca/P ratio (1.7), close to

the hydroxyapatite one, is the result of a right balance of the Ca/P phases solubility which has been assured by the leveling of the pH value down to 6.5 and 6 respectively, during each treatment steps. Moreover, it was possible to evaluate a presence of HA deposition on the internal pore walls, confirming that the high concentration of SBF solutions induces a fast and uniform deposition of hydroxyapatite on the gelatin scaffold.
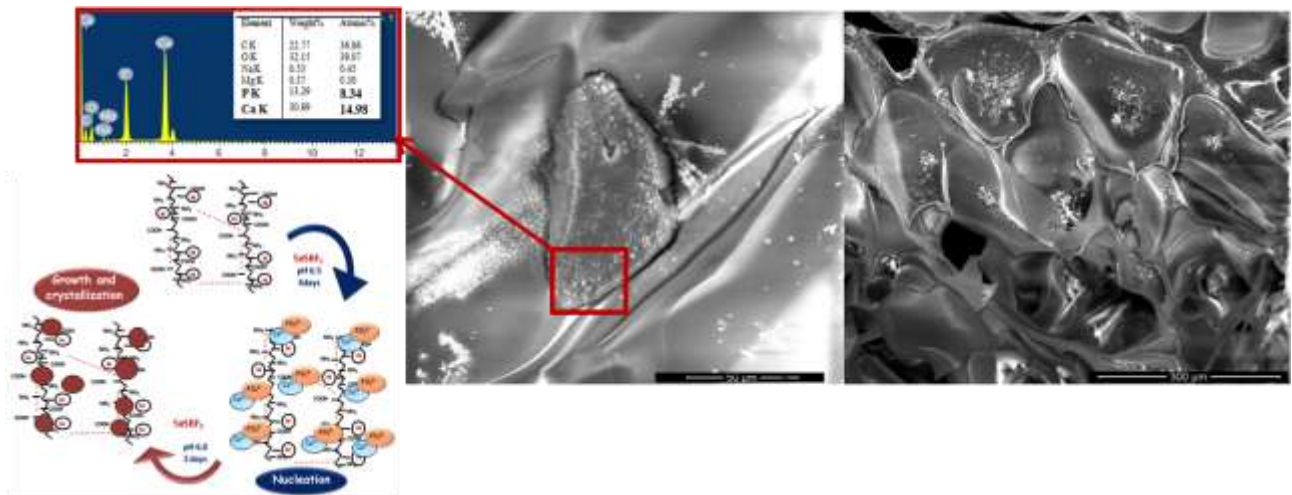
Fig. 6 : SEM/EDS images of gelatin scaffold after accelerate Kokubo treatment.

Furthermore, we performed two different pre-treatments on crosslinked gelatin scaffolds to induce higher crystal nucleation of the scaffold surface:

- $CaCl_2$ solution 0.1M +5xSBF$_1$ + 5xSBF$_2$;
- $Ca(OH)_2$ solution 0.01M +1.5xSBF$_1$ + SBF.

A preliminary step should catalyzes the apatite nucleation and the homogeneous distribution of nuclei on the scaffold surface whereas, a subsequent employment of Mg^{2+} and HCO_3^- free solution (5xSBF$_2$) should promote the growth of apatite crystals (Table 1). In particular, a saline solution may promote the Ca^{2+} deposition, in order to accelerate the next step of nucleation.

As shown in figures 7 and 8, on scaffold surface is evident an encouraging crystal deposition, but EDS analysis demonstrated an high presence of impurities, such as different salts common in SBF, SBF$_1$ and SBF$_2$ solution used to induce a coating.

According to EDS analysis, the accelerated Kokubo treatment shows the best results; infact by this method is possible to obtain an hydroxyapatite deposition with a minus amount of impurities. For this reason, all the samples were treated by $5xSBF_1$ for 4 days and $5xSBF_2$ for 3 days.
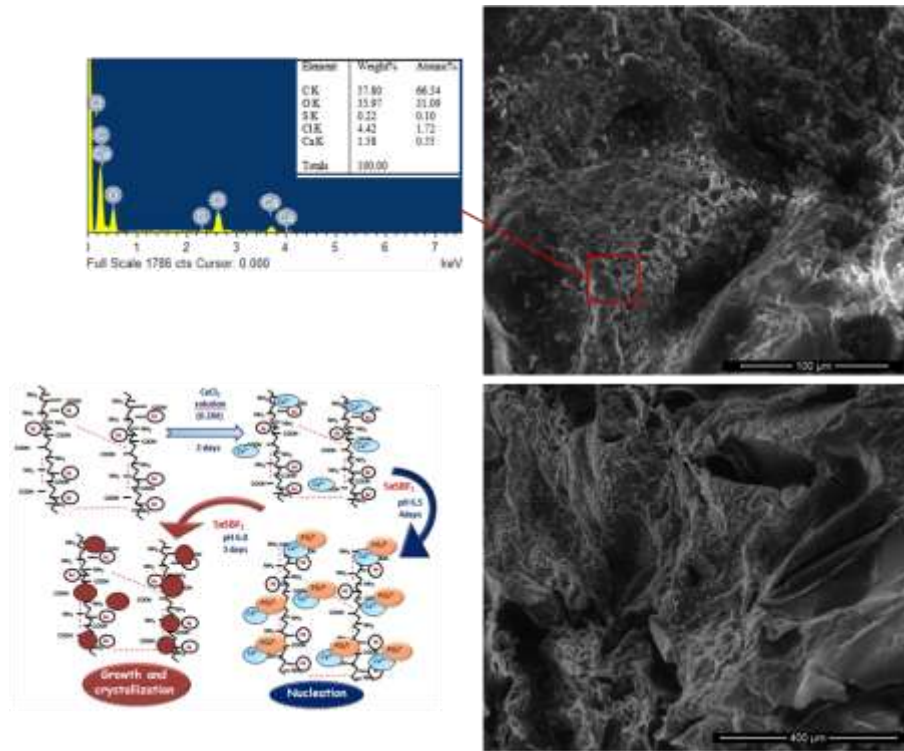
Fig. 7: SEM and EDS investigations on scaffold after pre-treatment in $CaCl_2$.
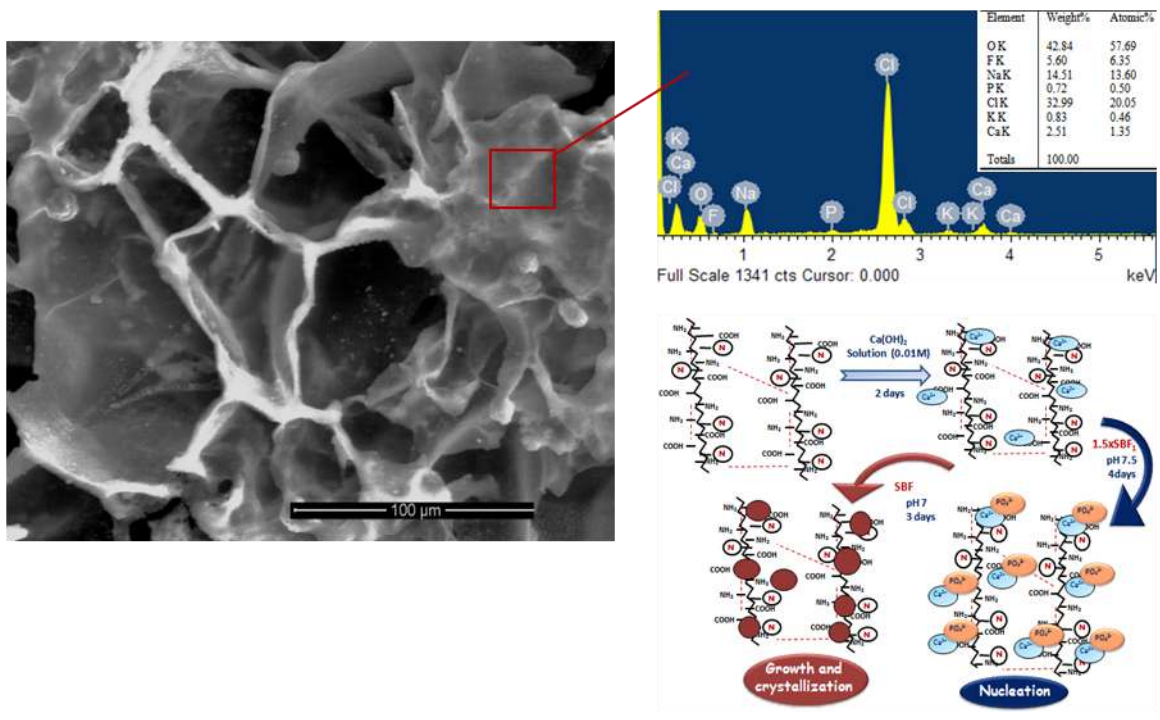
Fig. 8: SEM and EDS investigations after pre-treatment in Ca(OH)$_2$ solution 0.01M and then soaked in 1.5xSBF$_1$ and SBF solutions.
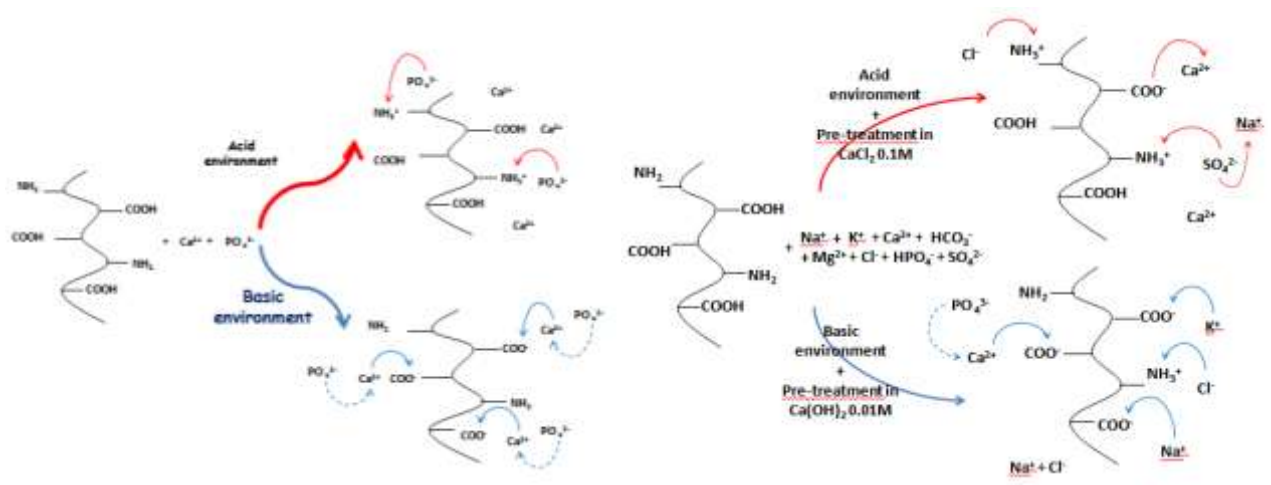
Fig. 9: Scheme of theoretical behavior (on left) andsperimental behavior (on right) during SBF treatment.

Mechanical test effect

To evaluate the structural modification of scaffolds after compression test and understood the different samples behavior, we propose an image analysis. The SEM images (figure 10) show an internal (a) and external (b) surface after mechanical test of B10_6h (a-b left) and

A5_1h (a-b right). It was reported the load direction in order to observe same structural modification. In the scaffold realized whit gelatin type A, there is not an internal/external orientation after compression; indeed in the other scaffolds, it is possible to observe an orientation in load direction. Moreover external surface of B10_6h shows two cricks in perpendicular direction to the load one: carry on the test, the external surface. Spite of cricks, the external structure has continued to support the applied load avoiding the cricks propagation; the final rupture of the sample took place in the direction of loading (figure 10Bleft)

B10 3h   A5 3h   **(A)**   B10_3h   **(B)**   A5_3h
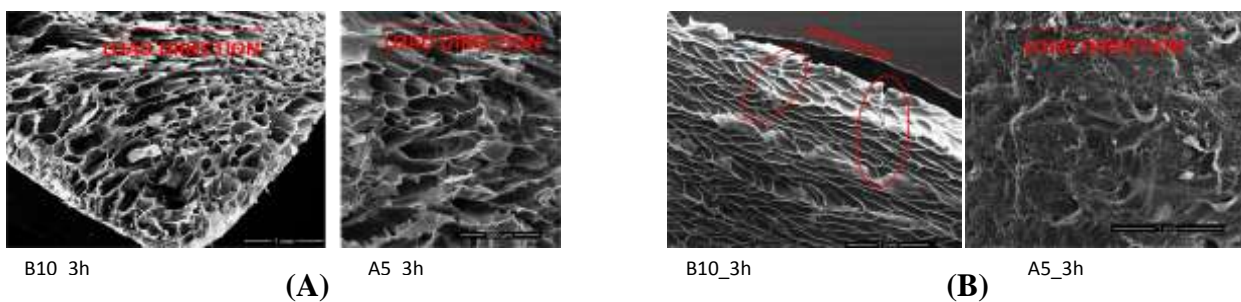
Fig.10: SEM images of B10_3h and A5_1h scaffolds after compression test of internal section (A); external section (B).

3.1.3.2 Swelling test

The swelling process could be divided into two stages: first one is represented by the fast swelling step occurring before t_{eq}, followed by an equilibrium swelling as second step. t_{eq} is a time at which the swelling became equilibrated and it is important to evaluate the swelling equilibrium. To evaluate the gelatin behavior before t_{eq}, it was considered a short range time between 1-24 hrs and the analysis were done at defined time.

The swelling equilibrium time for all samples were reported in the table below.

To study of the gelatin's swelling behavior for long time (after t_{eq}) and to obtain its complete screening, it was considered a large time range between 1- 28 days. Independently to crosslinking time, A5 and B5 scaffolds show (figure12) a higher water absorption than A10 and B10; this effect is correlated to the number of physical and chemical bonds in the structures.

Comparing the results of both type gelatin scaffolds, crosslinked and not, is evident their different behavior in aqueous environment. Following, it is shown non-crosslinked gelatin diagram. It was considerate a testing set, formed by porcine and bovine gelatin at two concentration, 5-10% w/v (A5, A10, B5, B10).
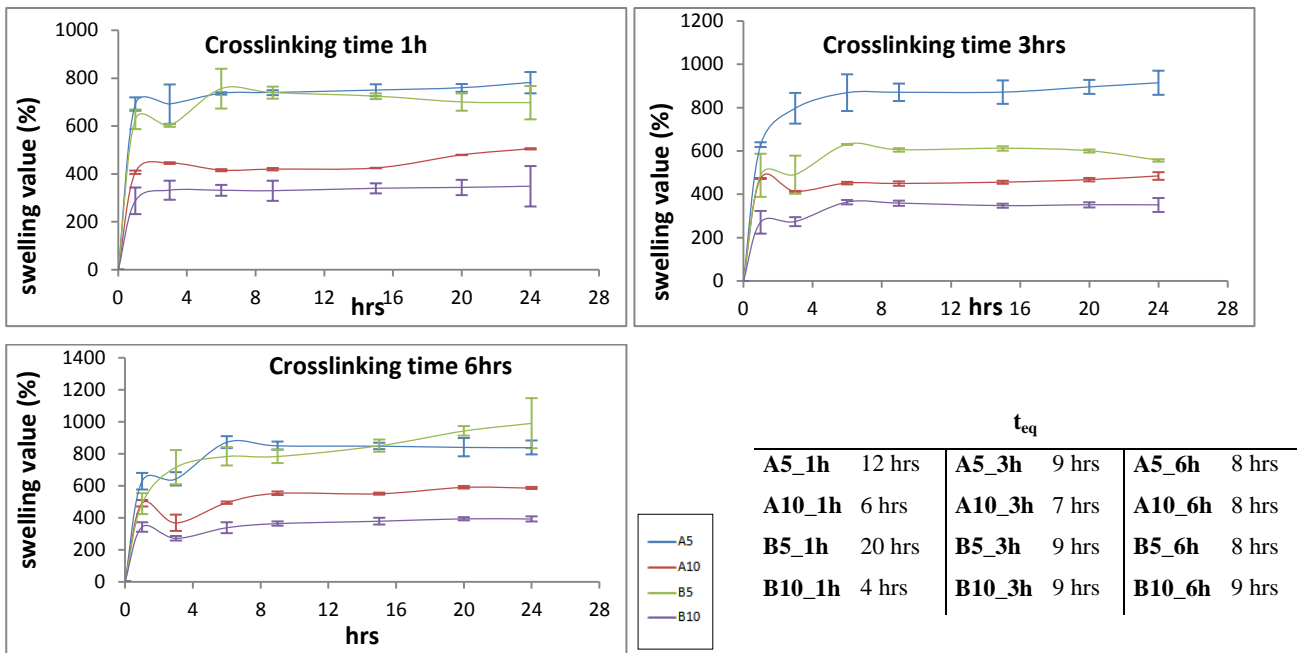
Fig. 11: Diagrams concerning the evaluation of swelling equilibrium value for different gelatin crosslinked samples at different times.
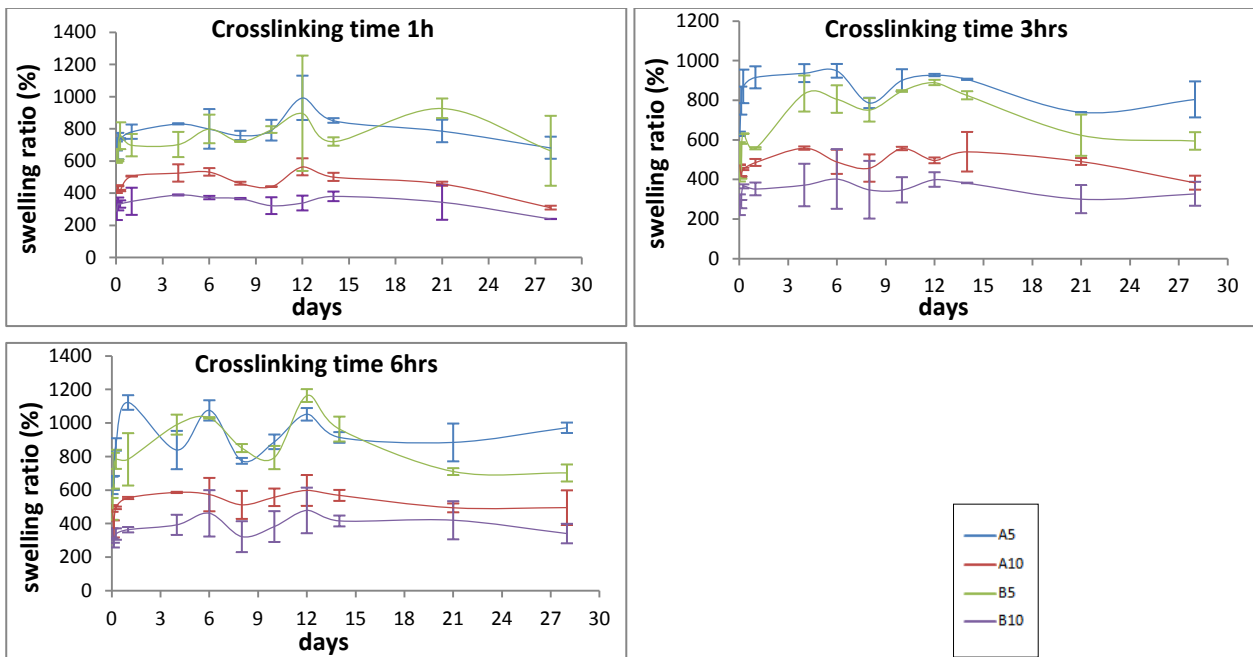
Fig. 12: Diagrams concerning the swelling values evaluation of gelatin scaffolds crosslinked by EDC (0.7w/w) in the range of 0-28 days.

As showed in the diagram 13, it is very difficult separated the two traditional part related to the hydrogel swelling behavior: infact, there is not an initial plateau that is an indicator of swelling equilibrium value. The curves slope increases up to reach a maximum (higher swelling value), then suddenly decrease.

Moreover non-crosslinked scaffolds show a higher swelling value than crosslinked one, and the maximum swelling value was reached faster.
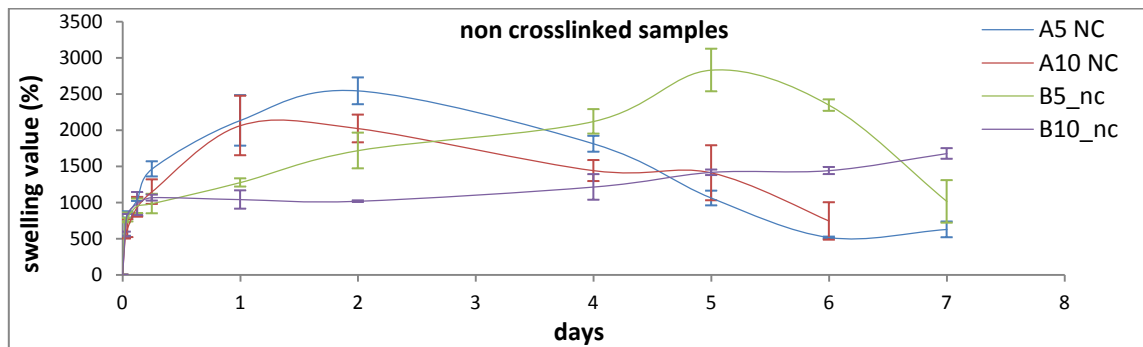
Fig. 13: Swelling test up to one week on non-crosslinked gelatin A and B (5 and 10wt%).

3.1.3.3 Degradation test

The lost weight(%) *vs* time, related to the four different crosslinked gelatin scaffolds is reported below.

The degradation diagram shows that the scaffolds with the lowest gelatin amount (A5 and B5) have a slower degradation than the other one (figure 14), probably because their internal structure helped the EDC penetration due to minus physical bands; as a consequence there is a magnitude EDC effect. Moreover the major degradation rate is registered in the first two weeks, then the degradation values reach a plateau zone.
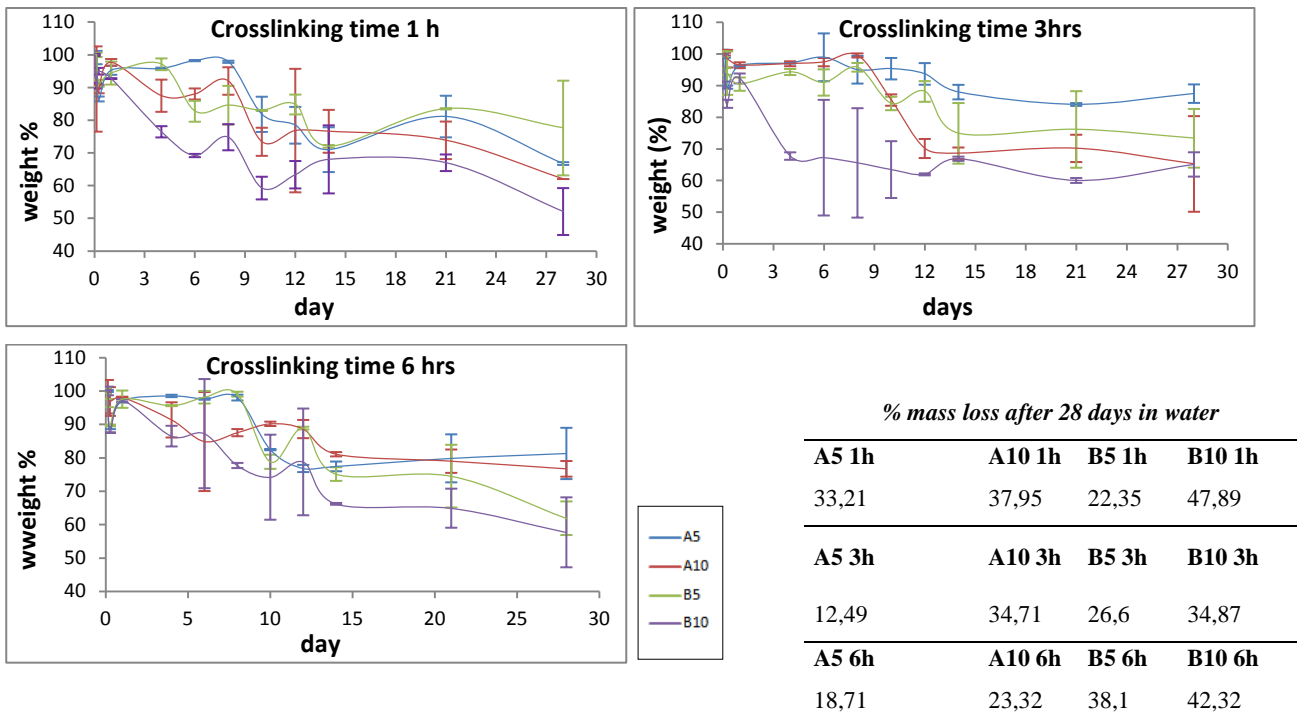
Fig. 14: Diagrams of degradation test and table with %mass loss after 28 days in aqueous environment.

As underline for the swelling behavior, also in this case the result is completely different respect non-crosslinked ones.

Following, it is shown the diagram related to the non-crosslinked gelatin. In this case it was considerate a testing set, formed by porcine and bovine gelatin at two concentration, 5-10% w/v. As reported in the diagram 15, the gelatin dissolves completely in the first week; even after few days the samples show a higher degradation value.
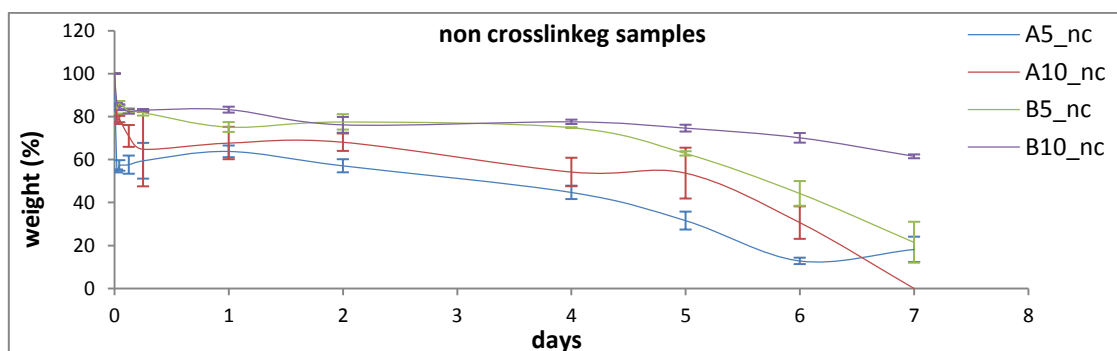
Fig. 15: Diagram of non-crosslinked scaffolds degradation behavior.

3.1.3.4 Thermal analysis: DSC and TGA

To evaluate the crosslinking time effect on gelatin structure is possible to analyze DSC and TGA curves. Following are reported thermal analyses on gelatin powder, and one type of gelatin scaffold crosslinked at different times (B5_1h, B5_3h, B5_6h).

(A)   **(B)**
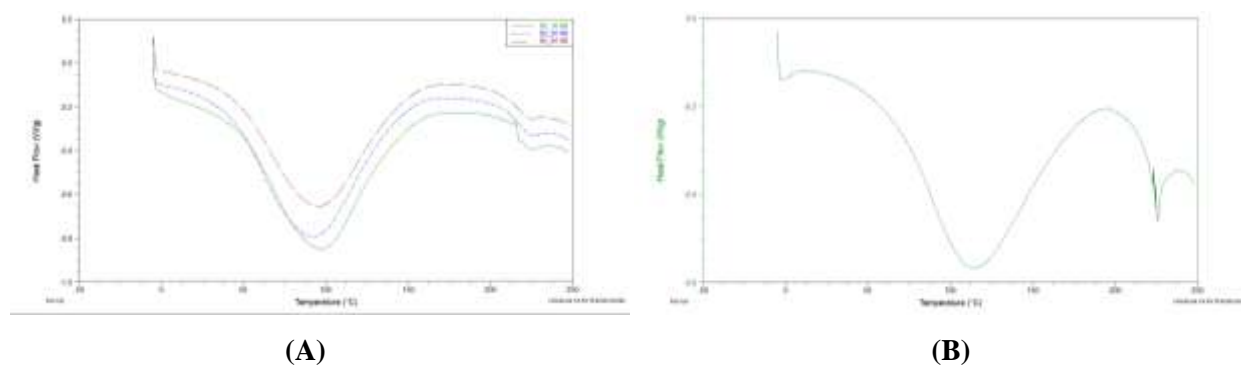
Fig. 16: DSC analysis: A) gelatin type B scaffold 5%w/v after crosslinked treatment at 1, 3, 6 hrs; B) gelatin powder type B.

	Ti	ΔH	T			Ti	ΔH_D	T_D
Gel powder	223,52°C	13 J/g	225,58°C		**Gel powder**	60,32°C	352,6 J/g	112,32°C
B5_1h	216,17°C	8,095J/g	222,68°C		**B5_1h**	42,08°C	539,7J/g	96,52°C
B5_3h	211,07°C	10,23J/g	223,99°C		**B5_3h**	38,82°C	522,2J/g	91,84°C
B5_6h	211,04°C	9,253J/g	222,81°C		**B5_6h**	41,01°C	469,9J/g	94,68°C

Table 2: Initial temperature (Ti), enthalpy (ΔH and ΔH_D) and maximum temperature (T and T_D) associated to gelatin structure degradation (on left), gelatin structure decomposition (on right).

The images (figure 16) show the presence of two important peaks: the first associated to trapped water in the structure and gelatin degradation phenomena, and the second to structural decomposition. The values of decomposition temperature, T, and decomposition enthalpy, ΔH, obtained for gelatin scaffold crosslinked with EDC solutions at different time are reported in Table 2 (on left). The values of degradation temperature, T_D, and degradation enthalpy, ΔH_D, obtained for gelatin scaffold crosslinked with EDC solutions at different time are reported in Table 2 (on right). T_i is the temperature at which start the phenomena.

The TGA analysis confirms the presence of two phenomena (figure 17). In particular, the first step is related to water evaporation and second to chemical bond C=C breaking. The table 3 shows the temperature range and the weight loss associated at themselves, and the residua at 800°C.
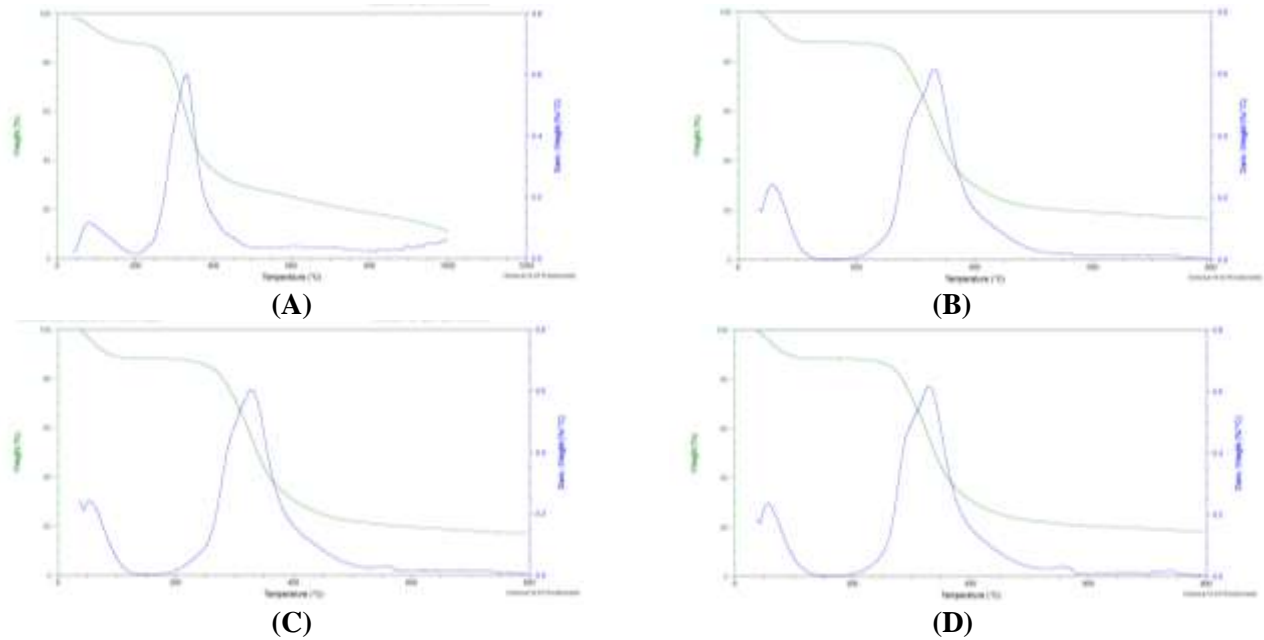
Fig. 17: TGA analysis: A) gelatin powder; gelatin B (5% w/v) crosslinked at 1h (B) 3h (C) and at 6h (D) in EDC solution.

MATERIAL	T range [°C]	Weight loss (%)	Residual (%)
Gelatin B	0-200	10,31	18,69
	200-800	71	
B5_1h	0-142	12,25	16,85
	142-800	70,9	
B5_3h	0-137	11,54	17,25
	137-800	71,21	
B5_6h	0-146	11,46	18,55
	146-800	69,99	

Table 3: Values related to TGA analysis.

3.1.3.5 XRD analysis

XRD reflection peaks can be used to monitored gelatin crystallinity before and after crosslinking treatment.
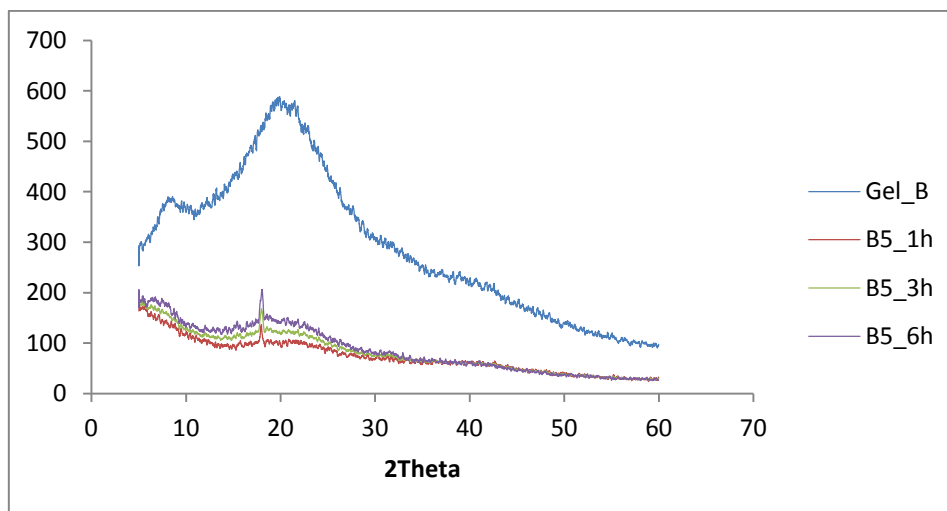
Fig. 18: XRD pattern of gelatin B powder, gelatin scaffold (B5%) crosslinked by EDC at 1, 3, 6 hrs.

As reported in the diagram, the pure gelatin showed a broad peak at $2\theta \approx 20°$ that is the characteristic peak of gelatin phase. The sharp peak reduction may be related to realization processes of gelatin crosslinked scaffold (gelatin dissolved in aqueous environment at 40°C, cooling at -80°C, lyophilized and then crosslinked). However, XRD results show a change of crystallinity phase of gelatin confirming TGA and DSC analyses.

3.1.3.6 Mechanical test

Young's modulus (E) was determined from static, unconfined compression tests carried out at 25°C in aqueous media. Higher temperatures were not used because the majority of the gels were not adequately stable above 25°C for such test methods. In controlled-deformation mode, samples were continuously compressed at a rate of 10% of swelled sample height (mm/min) from an initial pre-load force (0.01 N), up to 75% of swelled sample height.

Preventive mechanical properties were performed in a two different samples sets, in which the last part of production protocol is changed. After the crosslinking treatment in EDC solution the samples were:

1) submitted to second step of freeze-drying;
2) dehydrated in ethanol, to induce a de-swelling phenomena.

The results were shown in the following diagrams:
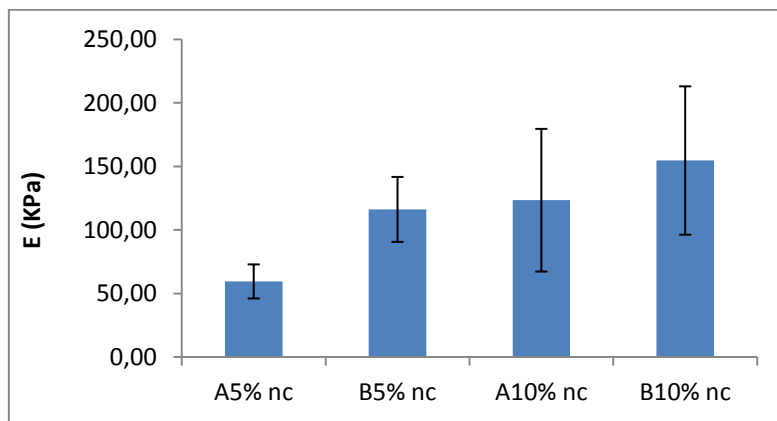
Fig. 19: Mechanical test results for samples with a double freeze-drying steps. For all the samples tested it was made a crosslinking treatment for 3 h.
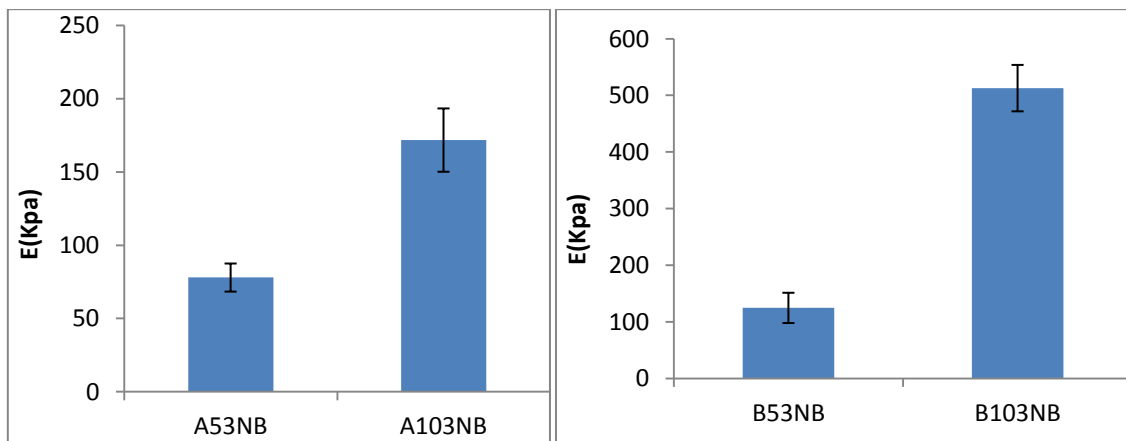
Fig. 20: Mechanical test results for samples with a one freeze-drying step. For all the samples tested it was made a crosslinking treatment for 3 h.

By this preliminary tests (figures 19 and 20), is evident that double liophylization has a negative effect on the gelatin scaffold structure. The table 4 shows an increase of the compression modulus:

last column in the table reports this percentage variation. According this results, the mechanical characterization is performed on scaffolds with one liophylization treatment.

Material	Double freeze-drying steps E (KPa) ± Std.Dev.	Single freeze-drying step E (KPa) ± Std.Dev.	E variation (%)
A5_3h nc	59,6 ± 13,4	77,98 ± 9,6	30,9 %
B5_3h nc	116,2 ± 25,6	124,7 ± 26,7	7,3 %
A10_3h nc	123,4 ± 56,1	171,8 ± 21,6	39,1 %
B10_3h nc	154,7 ± 58,4	512,8 ± 40,9	231,5 %

Table 4: Evaluation of compression modulus (E) after double and single freeze-drying steps.

We reported a typical curve stress-strain:
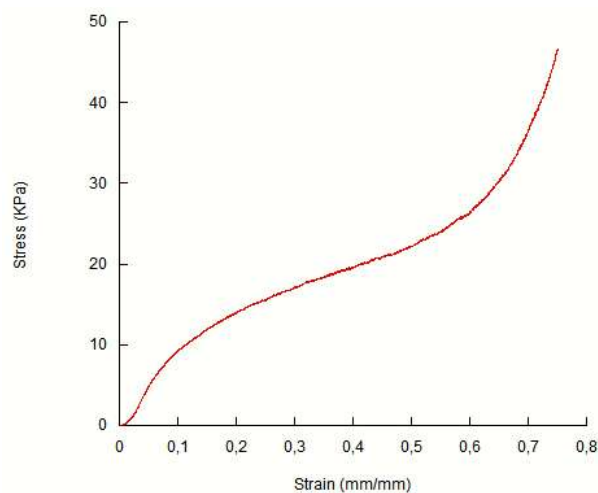
Fig. 21: Mechanical test performed on gelatin scaffold B5 crosslinked at 1h non biomineralized (B5_1h_NB)

It is possible to separate three different contributes:

- elastic part (important to determinate the modulus E), it depends on coating-like stiffness;
- viscous region, associated to internal chains reorganization during compression;
- last region associated to compact structure, when the porous structure is completely close.

Mechanical properties are important not only to understand the scaffold behavior, but also to obtain information on the crosslinking reaction. This information is derived by Young's modulus values.

The data reported in the table 6, represent the mean values (standard error of the mean) of *E*, obtained for gelatin A and B (10% w/v and 5% w/v) crosslinked with EDC at different times (1, 3, 6 hrs) and the same samples after biomimetic treatment; last column in the table reports the percentage variation of compression modulus.

As confirmed also by Pandit *et al.*[28] studies (table 5), the modulus E for non crosslinked gelatin is same magnitude order lower than crosslinked ones (biomimetic and not). Moreover the tables 6 show same differences between the samples with and w/o biomimetic treatment.

non crosslinked gelatin

Sample	Modulus (KPa)
A_10	0,179 (0,025)

Table 5: Modulus E value obtained in a compression test for gelatin scaffold non crosslinked (type A, 10% w/v) [28]

GELATIN SCAFFOLD CROSSLINKED IN EDC SOLUTION AT 1, 3, 6 hrs

No biomimetic treatment			Biomimetic treatment (5xSBF1 + 5xSBF2)			E variation
Sample	Modulus (KPa)	Std. Dev.	Sample	Modulus (KPa)	Std. Dev.	(%)
A5_1h_NB	79,5	4,5	A5_1h_B	59,1	15,4	34,6 %
A5_3h_NB	78,0	9,6	A5_3h_B	62,3	11,5	25,2 %
A5_6h_NB	103,6	9,2	A5_6h_B	43,4	8,4	138,7 %
A10_1h_NB	183,1	7,6	A10_1h_B	145,3	55,7	26,1 %
A10_3h_NB	171,8	21,6	A10_3h_B	216,0	43,9	20,5 %
A10_6h_NB	188,8	32,1	A10_6h_B	111,4	22,5	69,5 %
B5_1h_NB	195,2	52,2	B5_1h_B	139,0	39,7	40,6 %
B5_3h_NB	124,7	26,7	B5_3h_B	90,6	8,6	37,5 %
B5_6h_NB	123,8	5,8	B5_6h_B	110,5	7,3	12,0 %
B10_1h_NB	581,1	148,1	B10_1h_B	178,9	56,9	224,7 %
B10_3h_NB	512,8	40,9	B10_3h_B	285,8	91,6	79,5 %
B10_6h_NB	539,8	94,4	B10_6h_B	243,6	33,7	121,6 %

Table 6 : Modulus and std. dev. of gelatin A and B (10 and 5 % w/v) crosslinked at 1, 3, 6, hrs (on left), after biomimetic treatment (in the middle), and E variation (%).

In all tests the samples were equilibrated in deionized water up to equilibrium swelling. Obviously t_{eq} is different for the gelatin typologies as reported in the swelling tests results (fig. 11).
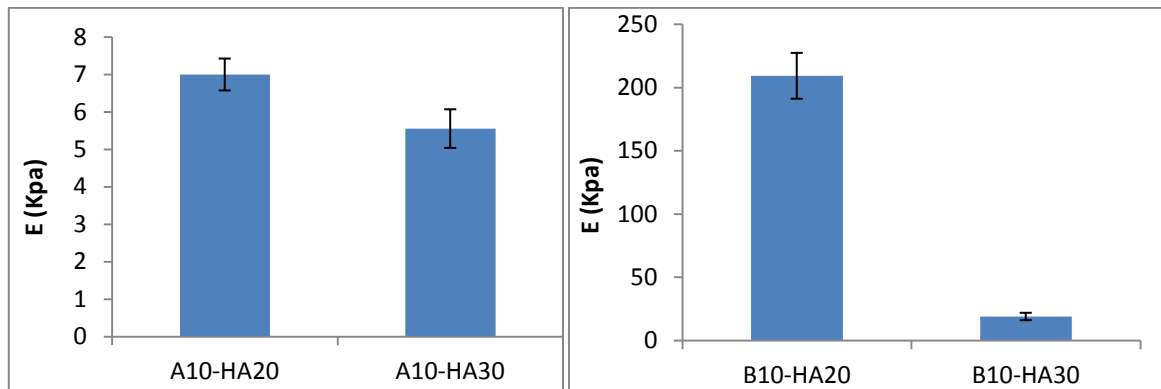
Fig. 22: Histogram of modulus related to all samples, before and after biomimetic treatment.

Fig.23: Photographs of mechanical test sequence for A5_1h (on left). Image of broken scaffold B10_6h after compression load (on right).

3.1.3.7 Biological test

To evaluate the influence of material surface on the cellular behavior, it is compared biological study on crosslinked gelatin, before and after biomimetic treatment. For this purpose the adhesion, proliferation and differentiation studies using pre-osteoblast (MG-63 cell line) were done. A biological analysis on crosslinked gelatin scaffolds, before and after SBF incubation, were reported in the diagram 24.
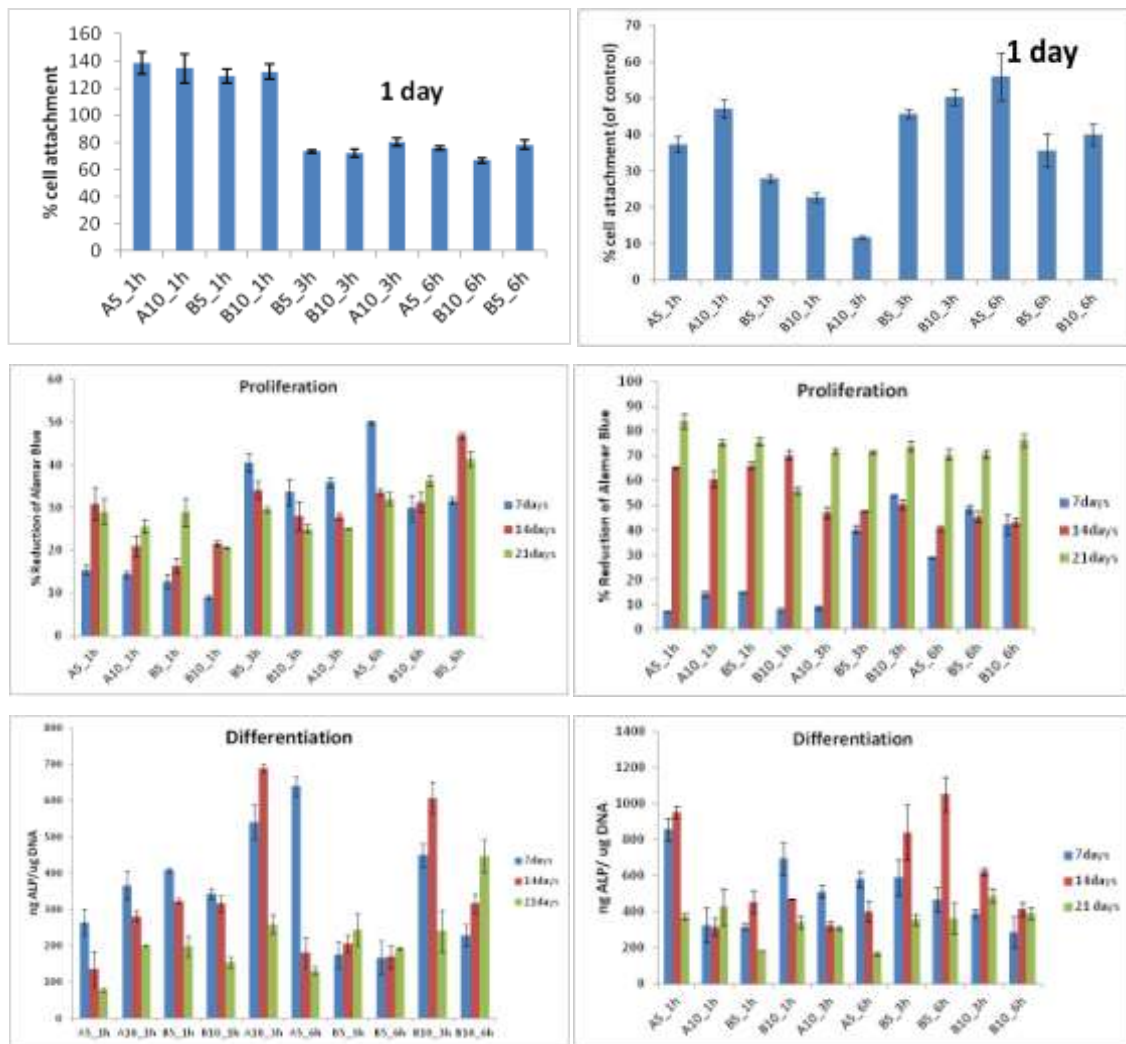
Fig. 24: MG63 cell-line adhesion, proliferation and differentiation of: (A) gelatin scaffold, (B) gelatin scaffold after biomimetic treatment.

MG-63 cells adhesion results in all samples free treatment were better than the other one. This because cells adhesion, after 1 day, strictly depend on the superface material morphology. The biomineralized gelatin scaffolds, as reported previously, have undergone a surface modification due to incubation for several time in different supersaturated SBF solutions, necessary to obtain hydroxyapatite coating. The proliferation and osteogenic differentiation, instead, depend on the combination of internal/external scaffold morphology and the presence of active biology signals (hydroxyapatite) on the pores surface.

The proliferation test performed on the both type of scaffolds, at long time 7, 14 and 21 days, shows higher values at 7 and 14 days reaching a plateau between 14 and 21 days for scaffold materials crosslinked for 3 and 6hrs. Moreover, better ALP activity results were observed for biomineralized

scaffolds confirming that the presence of solid bioactive signals on surface are important for the expression of early marker of osteogenic differentiation as ALP.

3.1.4 Discussion

Tissue engineering has emerged as a promising strategy to repair bone and cartilage defects. Many ways for guiding tissue regeneration involve the incorporation of varying degrees of biological context into implantable scaffolds to create biomimetic environments. One way to mimic this context is to create scaffolds from natural biopolymers such as gelatin, which incorporate many of the cues needed by cells (i.e. hydroxyapatite). The understanding of the interaction between bone cells and polymer surfaces is of paramount importance in the development of bone/cartilage filler biomaterials.

In this study we evaluated the chemo-physical, mechanical and biological difference between biomimetic and not gelatin-based scaffold.

Scaffolds were prepared starting to a gelatin solution, realized at T_a and then freezed at -80°C for several hours. The water, uniformly distributed into the gel, was sublimated by freeze-drying, to produce a three-dimensional structure with interconnected pores, as shown in the SEM image (figure 2). The temperature to freeze the samples, was chosen to guarantee porous dimension of 200 μm (fig. 1). Indeed, freeze-drying technique allows the formation of external coating-like compact structure (figure 2) probably derived to contact between mold walls and gelatin solution, during freezing; this effect is independent on mold typology (Teflon or polystyrene) (figure 3).

Gelatin is a natural polymer obtained by collagen denatured; to overcame its fast degradation in water environment, it proposes a crosslinking treatments that have the power to stabilized the gelatin chain limiting the number of free functional group and consequently the water effects. In particular, EDC solution is used to bond functional groups of amino acids in order to have an intramolecular and short-range intermolecular bond (amine bond), with some pendant side branches (N-acylurea groups). So crosslinked treatment creates a new stable chemical bonds in the hydrogel structure that limiting the internal chains mobility. The concept of chains mobility, for a crosslinked and not crosslinked hydrogel, is related to its capability of absorb and hold off water molecules, and swollen; it is depend on physical (entanglements) and chemical (hydrogen and/or amine) bonds. Obviously, the bonds number strongly depend on gelatin amount: for this reason, in non-crosslinked gelatin A and B scaffold realized whit 10%w/v of polymer, the chains have a lower mobility than 5%w/v ones. In spite of crosslinking treatment takes account of this difference, the samples realized

with less gelatin amount have slower degradation and higher swelling values than the other ones. In general, the gelatin's hydration mechanism is a capillary phenomenon consisting of water molecules penetrating the tiny interstices of triple-helical fibrils in the gelatin matrix, and is one of the most important parameter to evaluate hydrogels. In crosslinked structure, this phenomena is related also to crosslinking extension. Comparing figures 12 and 13 is evident the crosslinking success, and in particular the lower swelling values for B10 and A10, independently to crosslinking time.

The degradation phenomena (hydrolysis) is a bimolecular reaction in which water and the functional group possessing the labile bond, are involved [27]. The most important parameter for monitoring degradation is molecular weight of both gelatin type. As shown in the diagram 14, samples with the lowest gelatin amount (A5 and B5) have a slower degradation than the other ones, probably because their internal structure helped the EDC penetration due to minus physical bonds; as a consequence there is a magnitude EDC effect. Moreover the major degradation rate is registered in the first two weeks, then the degradation values reach a plateau zone. This effect should depend on degradation of uncrosslinked gelatin into the scaffold: infact it has been reported that after one week in aqueous environment the non-crosslinked gelatin undergoes a completely dissolution (fig. 15).

Besides loss of molecular weight and swelling values, other parameters have been proposed as a measure for crosslinking success, like mechanical strength and thermal analyses. In fact, by thermal analysis like DSC/TGA is possible to evaluate the thermal stability of gelatin before and after crosslinked treatment. For these analyses, raw gelatin powders (as a non-crosslinked sample) and gelatin B 5%w/v crosslinked at 1, 3, 6 hrs were considered.

As confirmed in literature, the endothermic peak of raw gelatin powder, appeared at 223°C in the figure 16, is a chemical decomposition temperature of gelatin [29,30]. This endothermic peak is evident also in the gelatin porous scaffold obtained from gel-solution.

Compared the temperatures related to this phenomena (table 2-left), we observed that gelatin powder shows higher **T** and **ΔH** respect all crosslinked gelatin scaffolds tested. It may depend on the amorphous structure of random coil conformations and lower contents of helical conformations in the gelatin crosslinked, meanwhile gelatin powder have a crystallinity structures [30] as demonstrated by XRD analysis. Indeed, there is not difference between gelatin scaffolds crosslinked at different times because this enthalpy and temperature are associated at phenomena depending to the C=C bond on the polymeric chain. B5_1h, B5_3h, B5_6h scaffolds and gelatin powder show

also a first large peak (figure 16) that depends on two different contributes: trapped water in the structure, and helix-coil transition of gelatin.

In general, there are three main types of waters in this structures typology: non-freezable bound water, freezable bound water, and free water [31]. A study from Lai *et al.* [41] demonstrated that freezable bound water did not exist in porous gelatin scaffolds, or the amount of this type of water was very small. One possible explanation for the water presence, is that the water molecules may be interacted with free carboxylic acid and amino groups of gelatin by hydrogen bonding [41].
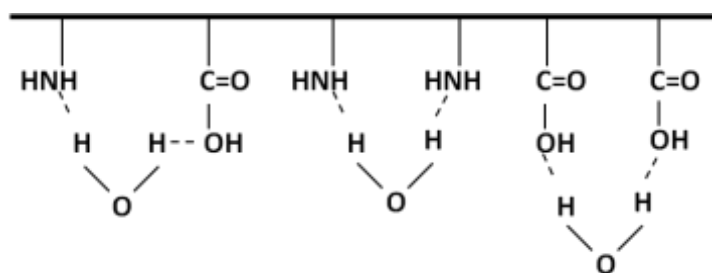
Fig. 25: Schematic interaction between gelatin structure and non-freezable water molecules by hydrogen bonding.

When the two hydrogen atoms of water molecules are firmly fixed to the amino acid residues of gelatin, such water is referred to as non-freezable bound water (figure 25); so we could have residual water in the structure. Moreover also the humidity could contribute to this phenomena. The large peak, indeed, is associated to the helix-coil transition of gelatin. Crosslinking increases the thermal stability of gelatin, as shown by the shift of the denaturation temperature to higher values. The values of denaturation temperature, T_D, and denaturation enthalpy, ΔH_D, obtained for gelatin scaffold crosslinked with EDC solutions at different time are reported in Table 2 (on right). T_i is the temperature at which start the phenomena.

The T_D increasing is in agreement with the simultaneous increase of crosslinking extent. It is generally accepted that the endothermic process present in the DSC thermogram of collagenous material involves rupture of hydrogen bonds and a rearrangement of the triple helix into a random configuration [32-34]. As reported (figure 16), the more stable is B5_1h scaffold, because shows the higher denaturation temperature (96.52°C) and enthalpy (539,7J/g); moreover this phenomena starts at 42.08°C. For this analysis the influence of external condition, like temperature and humidity (e.i. non-freezable bone water derivate by external environment), is equal for all the samples. So the contributes that emerge, is only the effect of crosslinking time.

To confirm these theories, in the figure 17 it is reported the TGA analysis realized for all samples (B5_1h, B5_3h, B5_6h and gelatin powder). The images show the presence of two distinct phenomena. The first step has a typical behavior of water loss that confirms the water presence in the samples. The second relevant step is associated at thermal degradation of the polymeric chain; the heat supplied breaks the carbon-carbon bonds present in the gelatin chain. The relevant residual % value, present in all TGA diagrams, is correlated to the carbon residual after pyrolysis. In this case the carbon residual remains as ashes because test were made in nitrogen and this prevents the formation of CO_2 gaseous.

In order to examine the effect of EDC and of crosslinking time, on crystal structure and crystallinity of gelatin scaffolds, XRD pattern are investigated. As show in figure 18, gelatin powder gives a typical XRD pattern of gelatin crystalline structure originated from α-helix and triple-helical structure. However, the scaffolds prepared from gelatin solution (B 5%w/v) and crosslinked by EDC (at 1, 3, 6 hrs) show less developed crystal structure and lower crystallinity. Moreover, amorphous structure were observed decreasing crosslinking time and recrystallization of gelatin does not occur.

As said before, also mechanical properties can be used to express the crosslinking effect on the structure. The tests were performed in aqueous environment and after swelling equilibration: the t_{eq} were reported in the figure 13. Our gelatin scaffolds have a particular external surface, that confers very relevant mechanical properties at the samples, as suggest comparing with literature results [28,43,44]. During the first times of compression test, the load is supported by the external structure until its collapse. Then the internal part provides to rearrangement chains and progressively were pressed up to fully collapse the structure. The critical point during the test is the external collapse: A5 and B5 scaffolds, that present a more soft and swelled structure were intact after the test; usually A10 and B10 scaffolds cricked on surface or even broken (figures 10 a-b left, and figures 23-on right). Seeing tables 5 and 6, is evident the enormous EDC contribute to improve the gelatin mechanical properties. Date in table 6 report Young's modulus value expressed in KPa; all B10 non biomineralized scaffolds have the major E values (581,1 ± 148,0 (KPa), 512,8 ± 41,0 (KPa) and 539,8 ± 94,4 (KPa) for 1, 3 and 6 hrs of crosslinked, respectively), but the higher E variation (%) after biomimetic treatment (224,7 %, 79,5% and 121,6% respectively). The samples that undergo a minor variation (%) of E values are A10_1h, A10_3h and A5_3h (E reduction about 26%, 20% and 25%) and B5_6h (E reduction about 12%).

After compression test, the scaffolds recovery initial shape as presented in the image 23; in the case of same B10 and A10 scaffolds, were recorded several broken.

Moreover, by mechanical test was demonstrated that double lyophilization weakens the structure (figures 19 and 20) and in particular scaffolds realize by single treatment show a modulus's increases of 30,9%, 7,2%, 39,1% and 231,5% (A5_3h, B5_3h, A10_3h and B10_3h) (table 4).

SEM and EDS analyses were used to evaluate the biomimetic treatment. As illustrated, three different approaches were made to obtain hydroxyapatite coating. The accelerated biomimetic approach consists of soaking the substrates in simulated body fluids at controlled temperature and pH to improve their bioactivity [35,36]. Generally, a thin layer of apatite may be obtained by using long immersion times (i.e, 7–14 days) with several refreshment of solution [36,37]. In our case the incubation time is 7 days, and EDS (figure 6) confirmed the CaP deposition.

In this system, the charged density is fixed, that is to say the number of nucleation sites is invariable, therefore the size of HA crystalline depended on the rate of crystalline growth: higher $[Ca^{2+}]$, $[PO_4^{3-}]$ made them more easy to access the surface of gelatin scaffolds and interactions among corresponding groups enhance, which lead to the rate of crystalline growth accelerated [43]. Then, we have tried to improve the calcium deposition adding a pre-treatment in $CaCl_2$ 0.1M for 2 days. However, the EDS results show (figure 7) the presence of numerous negative ions (presents in supersaturate SBF solution). Explanation should be the acid pH of $5xSBF_1$ (pH=6.5) and $5xSBF_2$ (pH=6). In acid environment (figure 9), infact, gelatin acts as base and takes up H^+ ions from the medium forming $-NH_3^+$ and -COOH and proteins become positively charged [38]. So, in this condition, all negative charge bond with gelatin, and the CaP deposition became very difficult. Indeed, in alkaline medium (figure 9), protein acts as an acid gives H+, forming $-COO^-$ and $-NH_2$ groups and proteins become negatively charged [38]. For this reason we have tried a pre-treatment in $Ca(OH)_2$ solution 0.01M (pH = 8-8.5) for several minutes. The reaction to produce $Ca(OH)_2$ is:

$$CaCl_2 + 2NaOH -> Ca(OH)_2 + 2NaCl$$
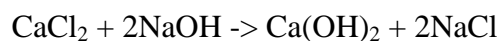
The treatment time was reduced at 30 min because, as demonstrated by Haixia et *al*. [38], hydrogel exhibits extensive swelling in environment with pH>8. Therefore, the osmotic pressure resulting from the mobile ion concentration difference between the gel and aqueous phase increased in a salt presence and consequently, the swelling ratio increased [39,40]. EDS (figure 8) shows impurities presence, and in particular the amount of sodium chloride is very significant.

In conclusion we are used the accelerated Kokubo method to obtain hydroxyapatite coating. However, during this treatment, crosslinked gelatin undergoes a morphological change due to the effect of water, temperature, pH and salts presence. The degradation of biomineralized gelatin scaffolds justifies lower E compression modulus (table 6) then non biomineralized ones, and also the worse MG-63 adhesion response after 1 day (figure 24). Known as, biological response in a

short time, strictly depend on the specific material topography, so also the presence of more free functional group, such as -COOH, may contribute to have a better adhesion. In a biomineralized scaffold, carboxyl groups are involved in a bond with CaP.

Proliferation and osteogenic differentiation, instead, depend on the combination of internal/external scaffold morphology and the presence of active biology signals (hydroxyapatite) on the pores surface. Indeed, biomineralized scaffold shows a better results, in particular in a short times (7-14 days). Moreover proliferation and differentiation tests show better results for materials at 5wt% of gelatin A; it may depend on the less compact structure.

3.1.5 Conclusions

Biomineralized gelatin scaffold was obtained by a combination of two simple methods as freeze-drying and biomimetic approach. The contributes of gelatin type/amount (Type A and B at 5 and 10 % w/v) and crosslinking time (1, 3, and 6 hrs) were evaluated, in order to study crosslinking treatment, biomimetic approach and MG-63 cells response.

This work shows that accelerated Kokubo treatment is able to create an hydroxyapatite coating on the surface and into the porous wall; but during this treatment, crosslinked scaffolds undergo a morphological change due to the effect of water, temperature, pH and salts presence. For this reason, mechanical properties and MG-63 adhesion response, after 1 day, decrease. Indeed, proliferation and osteogenic differentiation increase by the presence of active biology signals (hydroxyapatite).

Another important result is related to the crosslinking treatment by EDC. We propose three different time and analyze the treatment efficiency by physical (swelling and degradation behavior), thermal (DSC/TGA) an mechanical tests. Comparing non crosslinked samples and crosslinked one, is clear the efficiency of protocol proposed. The analyses confirm that crosslinked treatment by EDC at 1h is the best; instead there aren't relevant difference between 3 and 6 hrs. Its confirm that EDC reaction takes place in a short time.

3.1.6 References

[1] Kim HKM, Moran ME, Salter RB. The potential for regeneration of articular cartilage in defects created by chondral shaving and subchondral abrasion. J Bone Joint Surg1991;73A:1301–15.

[2] Kelly DJ, Prendergast PJ. Mechano-regulation of stem cell differentiation and tissue regeneration in osteochondral defects. J Biomech 2005;38:1413–22.

[3] Weineir S, Wagner HD. The material bone: structure-mechanical function relations Annu Rev Mater Sci1998;28:271-98.

[4] Neuman WF, Neuman MW. The chimical dynamics of bone mineral, University of Chicago Press, Chicago 1958.

[5] Boudreau N, Bissell MJ. Extracellular matrix signaling: integration of form and function in normal and malignant cells. Curr Opin Cell Biol 1998;10:640–46.

[6] Mann S, Ozin GA. Synthesis of inorganic materials with complex form. Nature 1996;365:499–505.

[7] Boskey AL. Will biomimetics provide new answers for old problems of calcified tissues. Calcif Tissue Int 1998;63:179–82.

[8] Zerwekh JE, Kourosh S, Schienbergt R. Fibrillar collagen–biphasic calcium phosphate composite as a bone graft substitute for spinal fusion. J Orthop Res 1992;10:562–72.

[9] Timkovich R. Detection of the stable addition of carbodiimide to proteins. Analytical Biochemistry 1977;79:135–43.

[10] Liang HC, Chang WH, Liang HF, Lee MH, Sung HW. Crosslinking Structures of Gelatin Hydrogels Crosslinked with Genipin or a Water-Soluble Carbodiimide. J Appl Polym Science 2004;91:4017–26.

[11] Kang HW, Tabata Y, Ikada Y. Fabrication of porous gelatin scaffolds for tissue engineering. Biomaterials 1999;20:1339–44.

[12] LeGeros RZ. Apatites in biological systems. Prog Crystal Growth 1981;4:1–45.

[13] Jarcho M. Calcium phosphate ceramics as hard tissue prosthetics. Clin Orthop 1981;157:259–78.

[14] Kim HW, Noh YJ, Koh YH, Kim HE, Kim HM. Effect of CaF_2 on densification and properties of hydroxyapatite–zirconia composites for biomedical applications. Biomater 2002;23:4113–21.

[15] Hench LL. Bioceramics: from concept to clinic. J Am Ceram Soc 1991;74:1485–1510.

[16] Yaylaoglu MB, Korkusuz P, Ors U, Korkusuz F, Hasirci V. Development of a calcium phosphate–gelatin composite as a bone substitute and its use in drug release. Biomaterials 1999;20:711–9.

[17] Fukunaka Y, Iwanaga K, Morimoto K, Kakemi M, Tabata Y. Controlled release of plasmid DNA from cationized gelatin hydrogels based on hydrogel degradation. J Control Rel 2002;80:333–43.

[18] Kim HW, Knowles JC, Kim HE. Hydroxyapatite and gelatin composite foams processed via novel freeze-drying and crosslinking for use as temporary hard tissue scaffolds. J Biomed Mater Res A 2004;72A:136–45.

[19] Chang MC, Ko C, Douglas WH. Preparation of hydroxyapatite–gelatin nanocomposite. Biomaterials 2003;24:2853–62.

[20] Lamba NMK, Baumgartner JA, Cooper SL (1998). Cell-synthetic surface interactions. In: Frontiers in Tissue Engineering. Patrick Jr CW, Mikos AG, McIntire LV (eds). Elsevier Science, Oxford, pp. 121-37.

[21] Granja PL, De Jéso B, Bareille R, Rouais F, Baquey C and Barbosa MA. Mineralization of regenerated cellulose hydrogels induced by human bone marrow stromal cells. European Cells and Materials 2005;10:31–9.

[22] Ramay HR, Zhang M. Preparation of porous hydroxyapatite scaffolds by combination of the gel-casting and polymer sponge methods. Biomaterials 2003;24:3293–3302.

[23] Kim HW, Knowles JC, Kim HE. Porous Scaffolds of Gelatin–Hydroxyapatite Nanocomposites Obtained by Biomimetic Approach: Characterization and Antibiotic Drug Release. J Biomed Mater Res Part B: Appl Biomat 2005;74B:686–698.

[24] Abe Y, Kokubo T, Yamamuro T. Apatite coating on ceramics, metals and polymers utilizing a biological process. J Mater Sci: Mater Med 1990;1:233–8.

[25] Tanashi M, Yao T, Kokubo T, Minoda M, Miyamoto T, Nakamura T, Yamamuro T. Apatite coating on organic polymers by biomimetic process. J Am Ceram Soc 1994;7:2805–8.

[26] Tanahashi M, Hata K, Kokubo T, Minoda M, Nakamura T, Yamamuro T, in: Yamamuro T, Kokubo T, Nakamuro T. Eds. Bioceramics, vol.5, Kobunshi Kankokai, Kyoto, 1992, p.57.

[27] Gijpferich A. Mechanisms of polymer degradation and erosion. Biomoterials 1996;17:103-14.

[28] Broderick EP, O'Halloran DM, Rochev YA, Griffin M, Collighan RJ, Pandit AS. Enzymatic Stabilization of Gelatin-Based Scaffolds. J Biomed Mater Res Part B: Appl Biomater 2005;72B:37–42.

[29] Cortesi R, Nastruzi C, Davis SS. Sugar cross-linked gelatin for controlled release: microspheres and disks. Biomaterials 1998;19:1641-9.

[30] Kia CS, Baeka DH, Ganga KD, Leea KH, Umb IC, Park YH. Characterization of gelatin nanofiber prepared from gelatin–formic acid solution. Polymer 2005;4:5094–5102.

[31] Li W, Xue F, Cheng, R. States of water in partially swollen poly(vinyl alcohol) hydrogels. Polymer 2005;46:12026–31.

[32] Achet D, He XW. Determination of the renaturation level in gelatin films. Polymer 1995;36:787-91.

[33] Tanioka A, Miyasaka K, Ishikawa K. Reconstitution of collagen fold structure with stretching gelatin film. Biopolymers 1976;15:1505-11.

[34] Bigi A, Cojazzi G, Panzavolta S, Rubini K, Roveri N. Mechanical and thermal properties of gelatin films at different degrees of glutaraldehyde crosslinking. Biomaterials 2001;22:763-8.

[35] Yamada S, Nakamura T, Kokubo T, Oka M, Yamamuro T. Osteoclastic resorption of apatite formed on apatite- and wollastonite-containing glass-ceramic by a simulated body fluid. J Biomed Mater Res 1994;28:1357–63.

[36] Manferdini C, Guarino V, Zini N, Raucci MG, Ferrari A, Grassi F et *al*. Mineralization behavior with mesenchymal stromal cells in a biomimetic hyaluronic acid-based scaffold. Biomaterials 2010;31:3986–96.

[37] Li P, Ducheyne P. Quasi-biological apatite film induced by titanium in a simulated body fluid. J Biomed Mater Res 1998;41:341–8.

[38] Zhu D, Jin L, Wang Y, Ren H. Swelling behavior of gelatin-based hydrogel cross-linked with microbial transglutaminase. Journal of aqeic. 2012;63:11-20.

[39] Baker JP, Blanch HW and Prausnitz JM. Swelling properties of acrylamide-based ampholytic hydrogels: comparison of experiment with theory. Polymer 1995;36:1061-9.

[40] Bajpai AK, Shrivastava M. Dynamic swelling behavior of polyacrylamide based three component hydrogels. J Macromol Sc Part A. 2000;37:1069–88.

[41] Lai JY and Li YT. Functional assessment of cross-linked porous gelatin hydrogels for bioengineered cell sheet carriers. Biomacromolecules 2010;11:1387–97.

[42] Tabata Y, Ikada Y. Protein release from gelatin matrices. Adv Drug Deliv Rev 1998;31:287-301.

[43] Kathuriaa N, Tripathi A, Kar KK, Kumar A. Synthesis and characterization of elastic and macroporous chitosan–gelatin cryogels for tissue engineering. Acta Biomater 2009;5:406–418.

[44] Bagley EB, Wolf WJ, Christianson DD. Effect of sample dimensions, lubrication and deformation rate on uniaxial compression of gelatin gels. Rheol Acta 1985;24:265-271.

3.2 GELATIN/HYDROXYAPATITE 3D MULTICOMPONENT SYSTEMS

Introduction

Tissue engineering offers a new promising approach to the creation of biological alternatives for bone and cartilage filler implants. Bone tissue is considered as minerals and proteins. The minerals are mostly apatites such as hydroxyapatite (HA, $Ca_{10}(PO_4)_6(OH)_2$), fluorapatite and carbonate-apatite [1]. In general, HA is a main component of bone mineral and in some cases carbonate-apatite is a main hard tissue component, as in dental enamel [2]. HA is widely accepted as a bioactive material for guided regeneration [3]. HA has excellent biocompatibility with hard tissues [4,5], and high osteoconductivity and bioactivity despite its low degradation rate, mechanical strength and osteoinductive potential [6,7]. Calcified tissue such as long bone and jaw bone is considered a biologically and chemically bonded composite between HA and type-I collagen [8]. Collagen is biocompatible, biodegradable and osteoinductive, acting as an excellent delivery system for bone morphogenetic proteins [9,10]. Gelatins (GEL) are compositionally virtually identical to the collagen from which they are derived. They have been shown to be biocompatible and resorbable. GEL is readily assimilated by the body [11]. A composite scaffold of HA and GEL is therefore expected to show increased osteoconductivity and biodegradation. The low mechanical properties exhibited by wet samples, suggesting their use as fillers and not replacers defect. One of the major problems in practice with type-I collagen is its cost and the poor definition of commercial sources of this material. Therefore in the present study, collagen type-I was replaced by GEL. Traditionally, the HA−polymer composites have been produced by dispersing HA powders in the polymer solution. However, the HA powders in this case were not dispersed well or were easily agglomerated, and even settled, which made it difficult to form a controlled structure [12,13].   Non-homogeneous distribution of ceramic particles within the polymeric matrix induces a dramatically reduction of the bioactive potential of the composite [18]. In this context, chemically inspired approaches based on the sol−gel transition and colloidal precipitation of calcium phosphates may efficiently improve the particles dispersion by a direct control of precipitated grain sizes though the interaction between calcium and phosphate precursors under controlled temperature and pH conditions [18,19]. Using this method, the gelatin−HA composites have been synthesized to maintain the nanoscale HA precipitates along the gelatin structure [14-17]. The major goal in fabricating scaffolds for tissue regeneration is to accurately control pore size and porosity. By using Freeze-Drying method, the liquid state structure of

composite is locked and the solvent is removed by rapidly cooling under vacuum [20-22]. 1-ethyl-(3-3-dimethylaminopropyl carbodiimide hydrochloride) (EDC) can be used as cross-linking agent in the making of GEL-hydroxyapatite composites.

In this chapter, we propose a gelatin–HA nanocomposites realized by in situ sol–gel transition. In this study we want show and compare biological responses and chemo-physical interaction between gelatin and hydroxyapatite components.

3.2.1 Materials and methods

3.2.1.1 Materials

Gelatin type B (bovine skin, 225 Bloom), and type A (porcine skin, 90-110 Bloom), 1-ethyl-(3-3-dimethylaminopropyl carbodiimide hydrochloride) (EDC), calcium nitrate, phosphate pentoxide, and all reagents used to prepare SBF solution were purchased from Sigma-Aldrich (Milano, Italy).

3.2.1.2 Gelatin-hydroxyapatite: Sol-gel synthesis

The gelatin–HA nanocomposite scaffolds were fabricated by sol-gel synthesis of HA within a gelatin sol and further freeze-drying, as reported in the flow chart (figure 1). Briefly, two types of viscous sols, gelatin, type B (pH= 5) and gelatin type A (pH=4.5) solutions were prepared in distilled water at 40°C with constant adjustments of the pH (10–10.5). Simultaneously calcium nitrate $Ca(NO_3)_2x4H_2O$ and ammonium hydrogen phosphate $(NH_2)_4H_2PO_4$ solutions were dissolved in distilled water and stirred for 2 hrs. The gelatin solutions were mixed progressively with calcium and phosphate solution, at constant stirring and at 40°C. Then a pH at alkaline values was adjusted to allow the sol-gel transition, and a stirring for 24hrs was performed to obtain the hydroxyapatite aging phenomena. The Ca/P ratio was fixed at 1.67 and the HA contents with respect to gelatin-HA were considered at 20 and 30 wt%. The gelatin amount respect the total water content is fixed at 10% w/v. After sonication (3 hrs), the gelatin-HA gel was poured into the Teflon moulds (5x10 mm) quenched to -80 °C and freeze-dried for 48 h.

The dried scaffolds were cross-linked within an acetone–water based solvent (4:1) containing a water-soluble 1-ethyl-(3-3-dimethylaminopropyl carbodiimide hydrochloride) (EDC), firstly at room temperature for 3h and then at 4°C for 24 h. The ratio of gelatin scaffold to solvent was fixed at 1% (w/v) from preliminary tests to maintain pore structures. The amount of crosslinking agent

was 0.7% (w/v) respect volume solution of acetone-water [23]. The samples were fully rinsed with distilled water, dehydrated with ethanol (10 minutes at 60:40 and 80:20 ethanol/water, 30 minutes 100% ethanol) to preserve the internal structure and then left under the hood overnight to allow the total solvent evaporation.

(A)   (B)
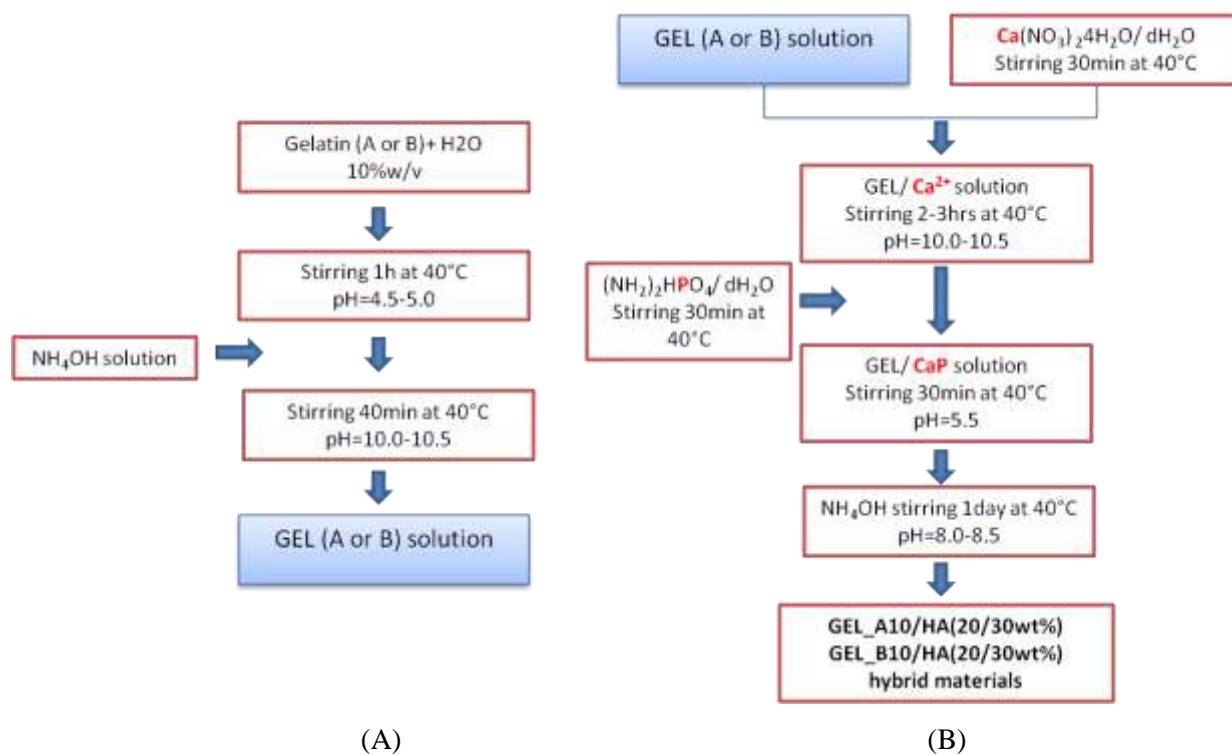
Fig. 1: Flow chart of preparation process. (A) preparation of gelatin solution. (B) preparation of GEL/HA hybrid material at different concentration.

3.2.2 Characterization

3.2.2.1 Morphological analysis

The morphology of composites was characterized by using a scanning electron microscope (SEM) and Transmission Electron Microscope (TEM). SEM images were taken by a Quanta FEG200 (FEI, the Netherland) Scanning electron microscope. The materials for SEM analysis were prepared by deposition of composite scaffold on one side of a double adhesive tape, and then stuck to an aluminium stub. The stub was then gold coated in an automatic sputter coater (EMSCOPE SC500, 20KV) to a thickness of around 30 nm. X-ray energy dispersive spectroscopy (EDAX, Genesis 2000i) was used for a qualitative estimation of Ca/P ratio on the material. All the samples were,

firstly dehydrated using a freeze-dryer, and then broken in section by using a liquid nitrogen in order to investigate the cross-section surface.

The transmission electron microscopy (TEM) images were taken by a Hitachi H-9000NAR model instrument operated at an accelerating voltage of 100 kV. Samples for TEM imaging were prepared by placing a drop of the aged GELATIN-HA composite suspensions (the suspensions were diluted in deionized water and dispersed by ultrasonic waves before use) onto carbon coated copper grids, dried in air and loaded into the electron microscope chamber.

3.2.2.2 Thermal gravimetric analyses

Thermal gravimetric analyses (TGA) were performed by TA Instrument Q 5000 under nitrogen atmosphere and room temperature up to 800 °C, with a heating rate of 5 °C/ min.

3.2.2.3 Infrared Spectroscopy FTIR analyses

Phase analysis was conducted using FTIR spectroscopy was performed on Nicolet Nexus spectrophotometer with KBr discs in the 500-4000 cm^{-1} region (4 cm^{-1} resolution, average 64 scans).

3.2.2.4 Mechanical test

The mechanical properties of the scaffolds were evaluated by compression tests. The tests were performed using a standard testing machine (Lloyd LR5K instrument, Fareham Hants, U.K.) equipped with a 10 N load cell. The gelatin, biomineralized and not, cylinders were soaked in water until equilibrium swelling, and then tested in an aqueous environment. The deformation range and the speed (mm/min) were calculated respectively as 75% and 10% of sample height.

3.2.2.5 Biological test

Viability test

As preliminary biological studies, cell biocompatibility was evaluated by using MG63 that were plated at concentration of $1x10^4$ in triplicate, into a basal medium. All the scaffolds were tested (A10_HA20 – A10_HA30 – B10_HA20 – B10_HA30). The medium in cell-load gel materials

culture plates were removed after cultured for 1, 3 and 7 and the *in vitro* cell viability was checked by the Alamar blue assay (AbD Serotec, Milano, Italy). This assay quantified the redox indicator which changed to a fluorescent product in response to the chemical reduction by mitochondrial enzymes such as flavin mononucleotide dehydrogenase, flavin adenine dinucleotide dehydrogenase, and nicotinamide adenine dinucleotide dehydrogenase. In addition, a redox phenomenon gave a quantitative indication of metabolic activity of live cells. An aliquot of 1mL of Alamar Blue™ diluted 1:10 in phenol red-free medium was added to each well and incubated for a further 4 h at 37°C, 5% CO_2. Later, 200μL of this solution was transferred into a 96 well plate for colorimetric analysis. Wells without any cells were used to correct any background interference from the redox indicator. The optical density was immediately measured with a spectrophotometer (Sunrise, TECAN, Männedorf, Zurich, Switzerland) at wavelengths of 540 and 600 nm. The cell viability percentage was evaluated in according to the manufacturer's protocol. The culture medium during experimental time was changed every two days.

3.2.3 Results

3.2.3.1 Morphological analysis

SEM analysis was used to observe the nanocomposite samples morphology, and the hydroxyapatite distribution into the scaffold.

Fig. 2: SEM image: longitudinal-section of B10_HA20 scaffold.
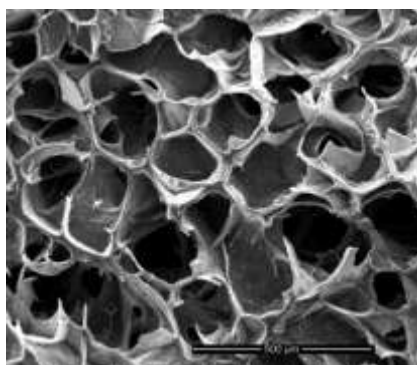
As reported in the figure 2, B10_HA20 longitudinal section have an homogeneous hydroxyapatite distribution. Different result was observed for B10_HA30. In fact, figure 3 shows the internal longitudinal section of scaffold. It is possible to evaluate a change of morphology due to inhomogeneous HA distribution in the polymeric matrix. In particular on a section (shown in

figures 3B and D) there is a uniform CaP coating, while on the other one (figures 3C and E) is present plate-like crystals, typical HA crystalline morphology. It is possible to explain this difference by the presence, into the scaffolds, of HA gradient.
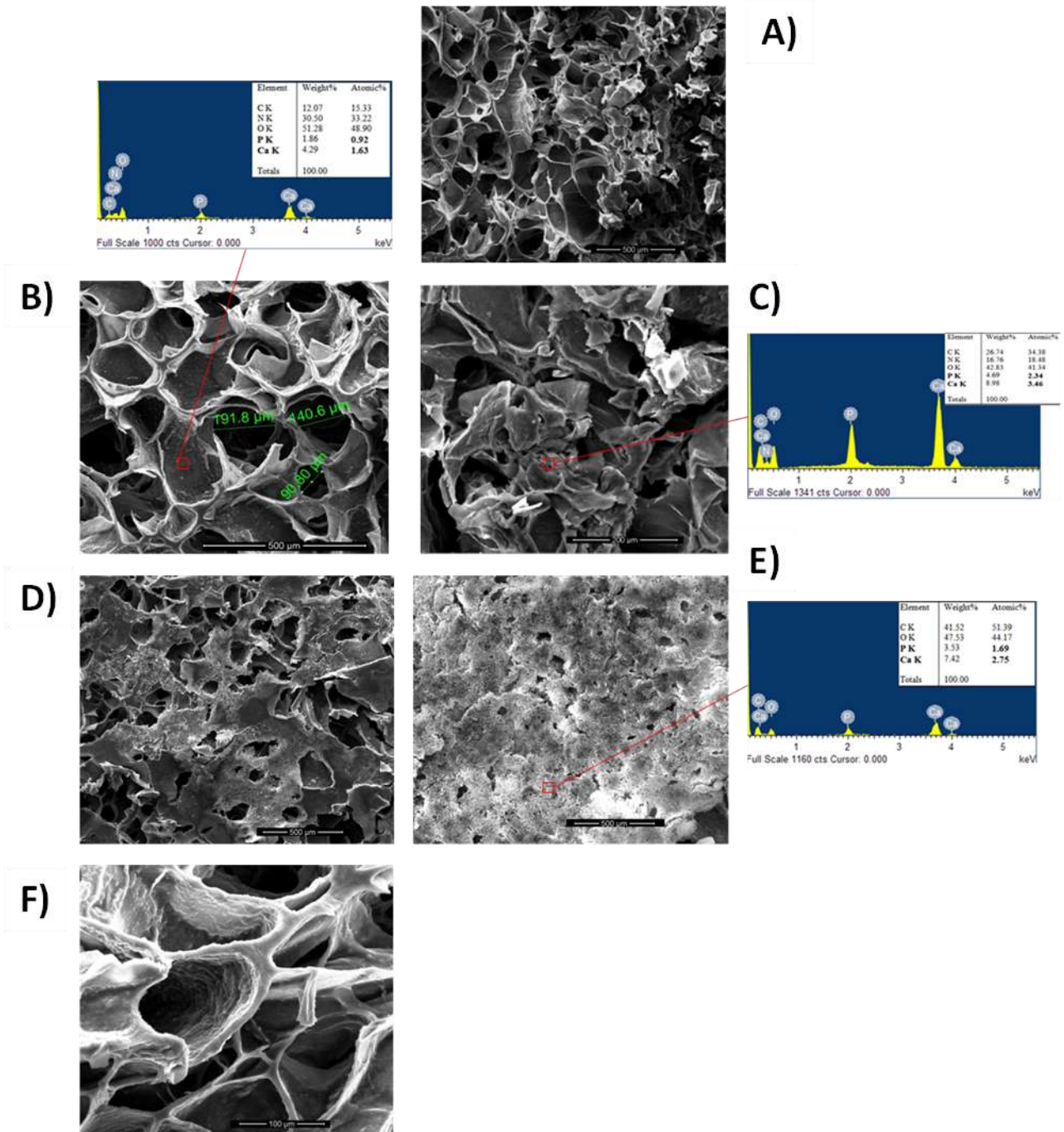

Fig. 3 : SEM/EDS analyses of B10_HA30 scaffold. A) morphology change in the scaffold section and HA gradient; B) and C) internal section of two scaffold extremities, top and bottom respectively; D) and E) external surface of two scaffold extremities, top and bottom respectively; F) porous magnification.

The gradient and the homogeneous distribution of the inorganic component inside the scaffold were shown in the figures 3(a) and (b) respectively.

To evaluate the correlation between nHA crystal shape and HA/GEL ratio, were reported TEM images (figure 4): the presence of gelatin in the scaffold reduces the crystallinity on HA nanoparticles.
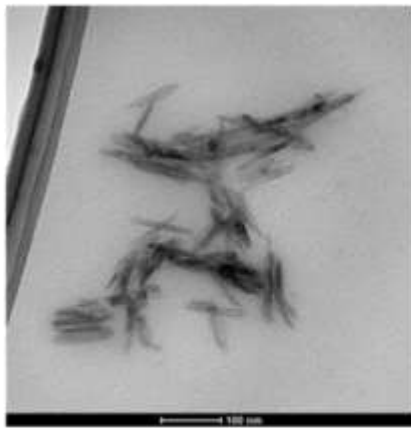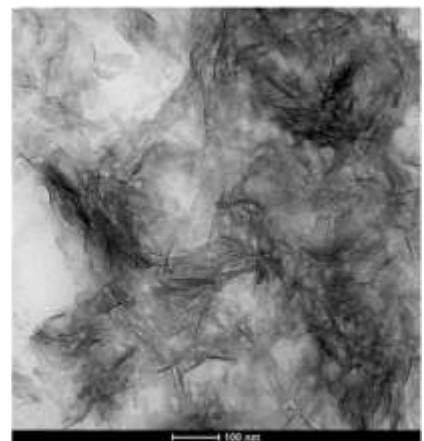
Fig . 4: TEM images of HA crystals obtained by sol-gel technique with different gelatin/hydroxyapatite ratio: (A) only HA and 70/30 - Gel/HA (B).

3.2.3.2 Thermal gravimetric analyses

The thermogravimetric plots of the composite scaffolds were used to determine the inorganic phase content, which was evaluated from the residual weight of the samples. To perform the analysis, the samples were cut in a three part (superior, inferior, central part), that were tested separately, in order to evaluate a different hydroxyapatite distribution into the vertical section. The experimental data,

reported in tables 1 and 2, were obtained comparing gelatin/hydroxyapatite residual% with gelatin scaffolds one.

In order to evaluate the thermal stability and the phase transformation, TGA of inferior section of B10_HA30 scaffold was reported in the figure 6. It was performed a study on different contributes to weight loss during analysis.
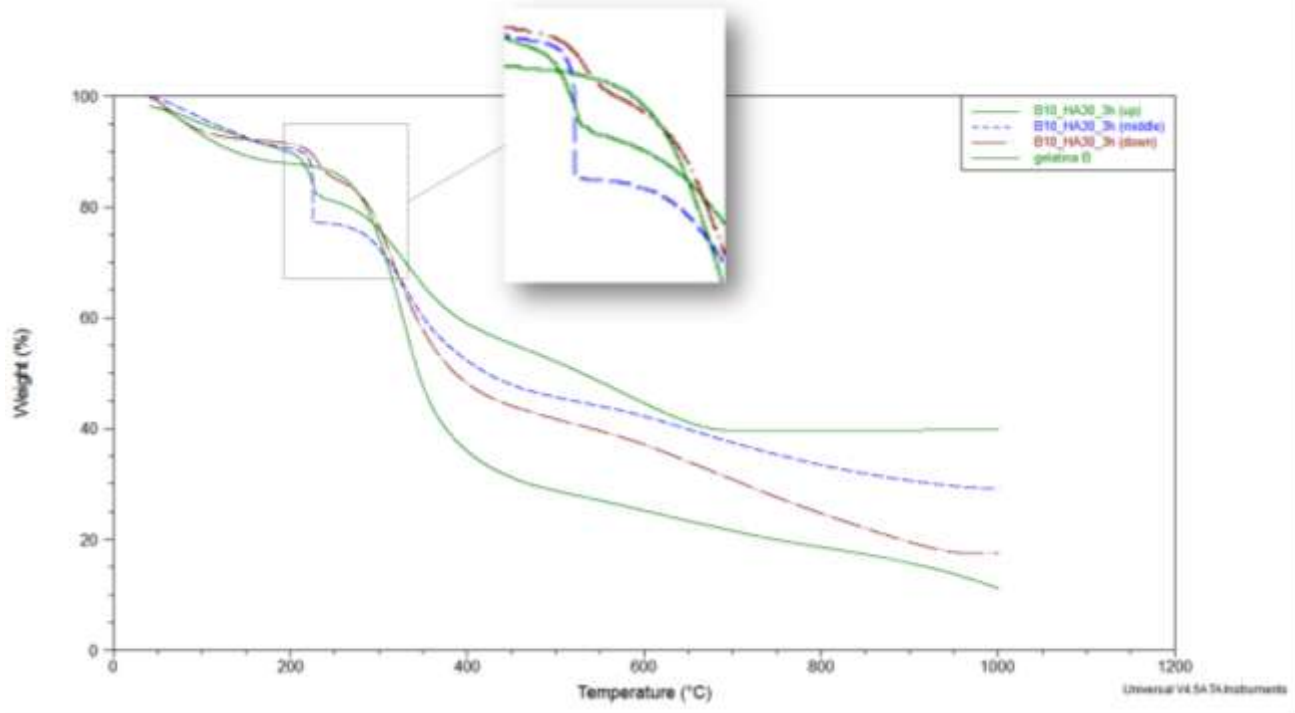
Fig. 5: TGA analyses of B10_HA30 up, middle and down part and table with residual value(%).

HA gradient		
Sample	residual (%)	HA residual (%)
B10_HA30 (up)	39,9	27,9
B10_HA30 (middle)	29,1	17,2
B10_HA30 (down)	17,4	5,5
B10_3h	14,9	

Table 1: residual value (%) of B10_HA30 up, middle and down part, and of gelatin scaffold.
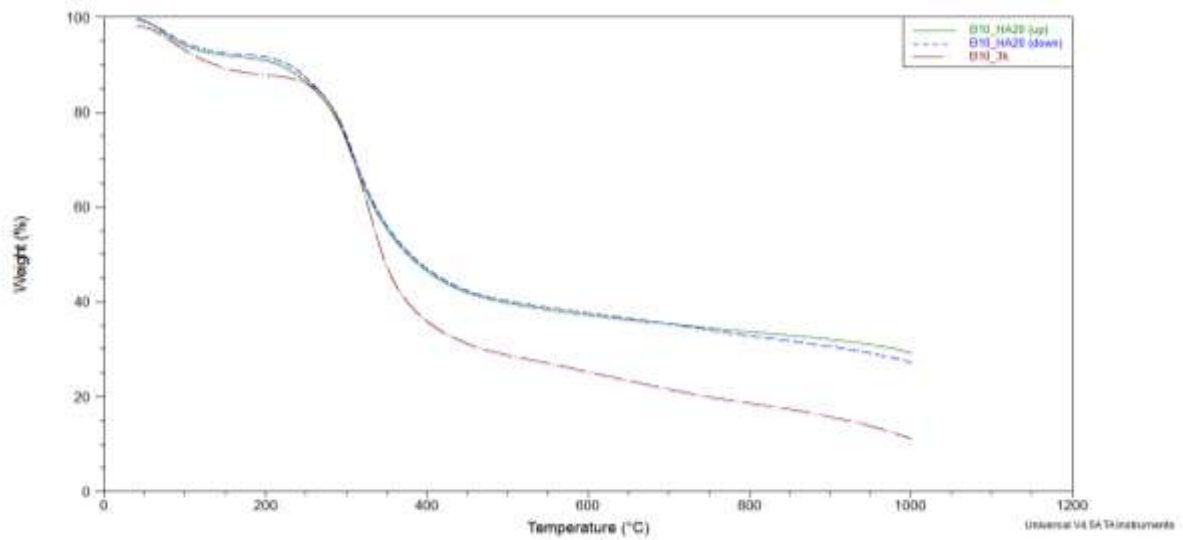
Fig. 6: TGA analyses of B10_HA20 up and down part and table with residual value(%).

Uniform HA distribution		
Sample	residual (%)	HA residual (%)
B10_HA20 (up)	28,3	16,3
B10_HA20 (down)	29,2	17,3
B10_3h	14.9	

Table 2: Residual value (%) of B10_HA20 up, middle and down part, and of gelatin scaffold.

Fig. 7: B10_HA30 (down) thermogram image and the study of different contributes on the weight loss.

3.2.3.3 Infrared Spectroscopy FTIR analysis

The FTIR spectrum of the gelatin /hydroxyapatite scaffold are shown in Figure below. In order to obtain information on chemical interaction between organic and inorganic phase, the analyses were made on two section of B10_HA30 scaffold: superior (up) and inferior (down) ones.

As reported in the figure 8, C = O stretching was distributed at 1630-1695 cm^{-1} for the amide I, N-H deformation at 1500-1550 cm$^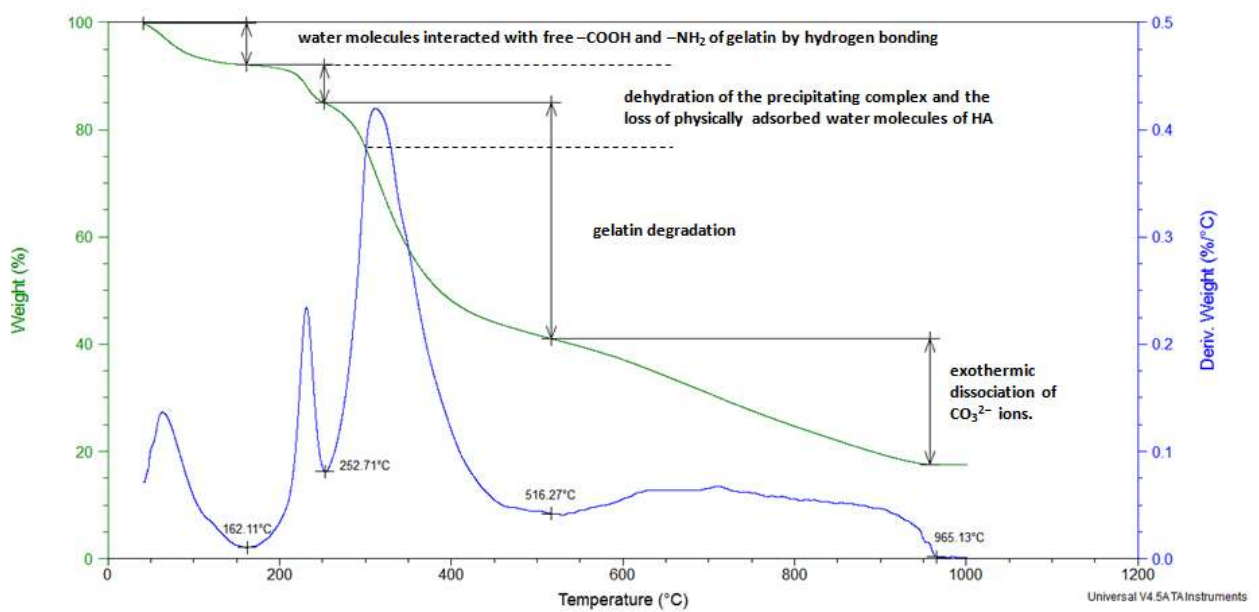{-1}$ for the amide II [24,25]. The phosphate band is between 900 and 1200 cm^{-1}, and typical peaks of phosphate vibration is at 1019 cm^{-1}; peaks for CO_3^{2-} vibration mode are appeared at the positions of 740, 840, 876 cm^{-1}.
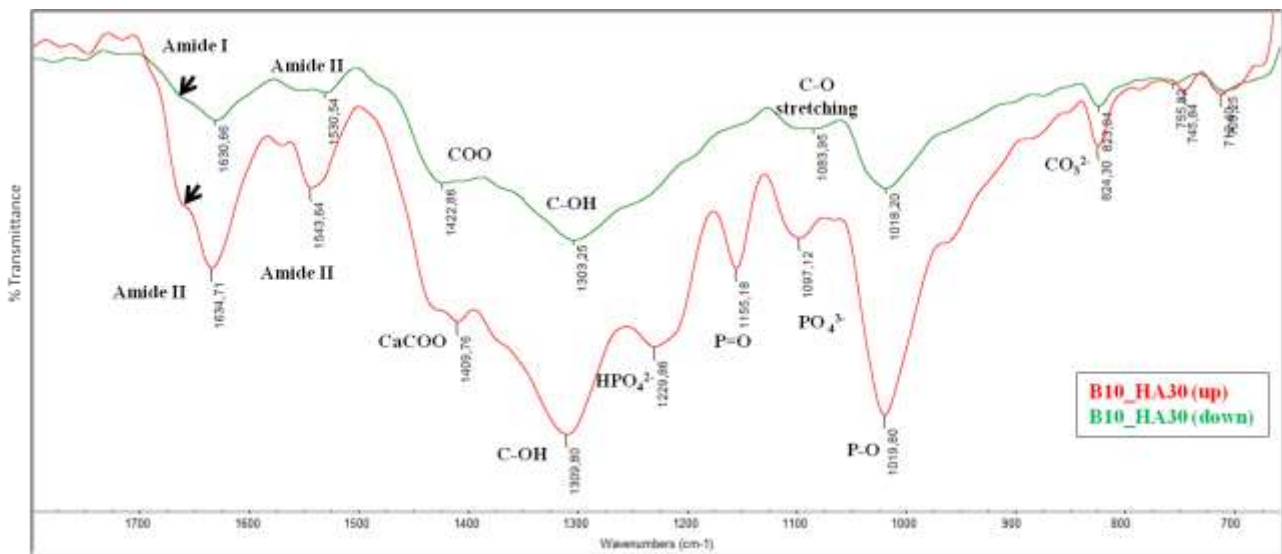
Fig. 8: FTIR analysis of superior (up) and inferior (down) sections of B10_HA30 scaffold.

3.2.3.4 Mechanical test

Young's modulus (E) was determined from static, unconfined compression tests carried out at 25°C in aqueous environment. Higher temperatures were not used because the majority of the gels were not adequately stable above 25°C for such test methods. In controlled-deformation mode, samples were continuously compressed at a rate of 10% of swelled sample height (mm/min) from an initial preload force (0.01 N), up to 75% of swelled sample height.

Mechanical properties are important not only to understand the scaffold behavior, but also to obtain information on the crosslinking reaction. This information is derived by Young's modulus values. The data in figure 9 and Table 3 represent the mean values (standard error of the mean) of E, where is clear the difference between samples obtained by gelatin type A, and type B; moreover

B10_HA20 scaffold compressive modulus (209,183±18.113 KPa) is several magnitude orders higher than the other.

Sample	Modulus (KPa)	Std. Dev.
A10-HA20	7,0	0,4
A10-HA30	5,5	0,5
B10-20	209,2	18,1
B10-30	19,0	2,9

Table 3: Modulus E (KPa) and standard deviation of gelatin/hydroxyapatite scaffold.
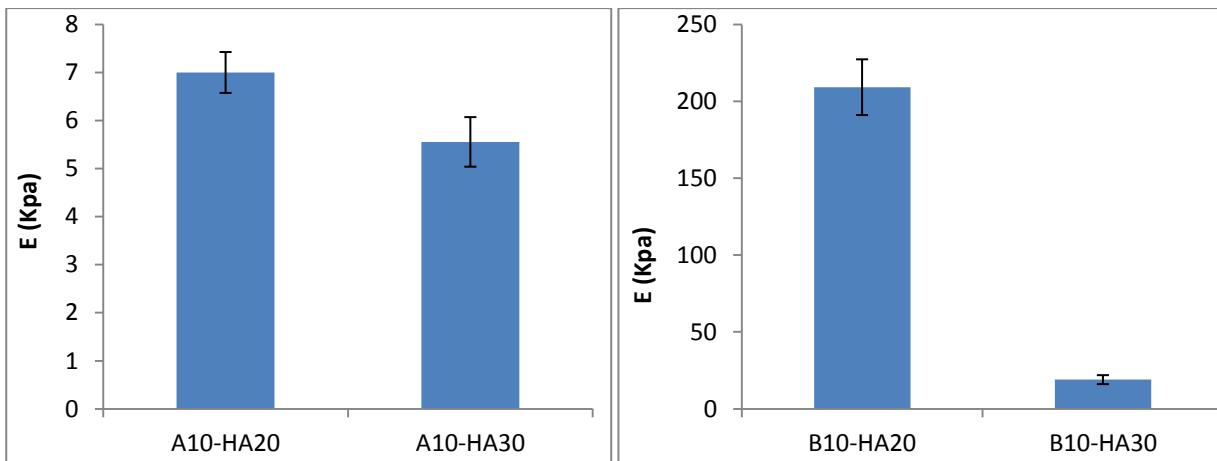
Fig. 9: Diagram of compression modulus E (KPa) relative to gelatin type A/HA (left) and gelatin type B/HA (right).

3.2.3.5 Biological test

Only preliminary biological studies were performed on HAGEL scaffolds. The cell proliferation at short time on the different materials (A10_HA20 – A10_HA30 – B10_HA20 – B10_HA30) were assessed using Alamar Blue test. Figure 10 shows the effect of the gel materials on the metabolic activity of MG63 after 1, 3 and 7 days of culture. According to the data, it can be found that a good proliferation was observed for scaffolds at low presence of hydroxyapatite nanoparticles. Meanwhile, a reduced proliferation was observed for materials at HA30%. This behavior was explained by a probably increased rate of differentiation of MG63 adhering on the surface of scaffold due to more presence of bioactive signals.
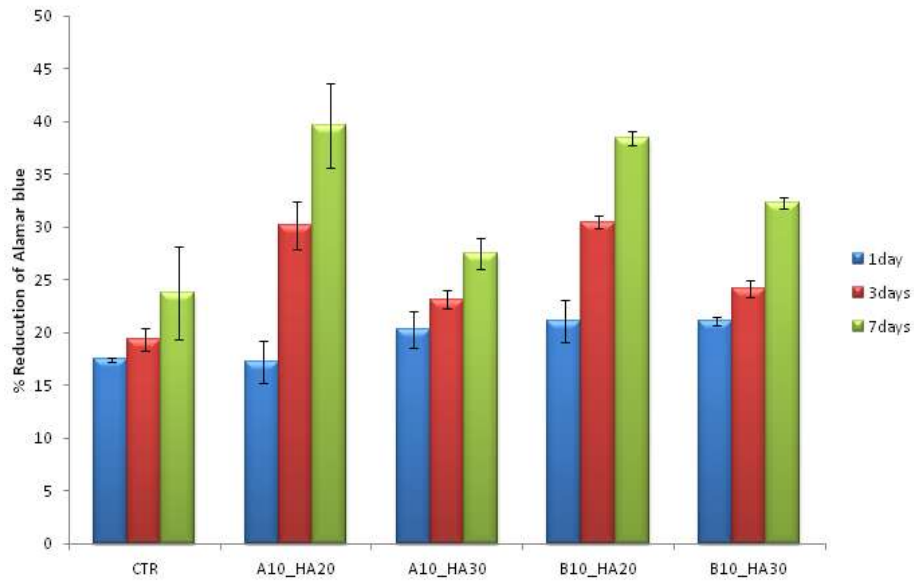
Fig. 10: Alamar Blue asay of all gelatin/hydroxyapatite scaffolds after 7, 14 and 21 days of cell culture.

3.2.4 Discussion

Porous gelatin/hydroxyapatite scaffolds with different gelatin type and inorganic contents, were prepared by in situ sol-gel approach and freeze–drying process. As reported in literature [26,27] hydroxyapatite should improve the osteogenic differentiation while gelatin should increase the chondrocyte proliferation. The aim is create an HA gradient into the scaffold section, in order to modulate biological signals. To evaluate homogeneity/ gradient of the inorganic component distribution, scaffolds were evaluated by morphological and thermogravimetric analysis.

SEM images show that inorganic phase into the sample, display a rough surface. Moreover is possible to distinguish a completely different morphology on the longitudinal direction: plate-like crystals is evident only in the figures 3 C and E. In all images, EDS analyses show that Ca/P ratio is very close to hydroxyapatite one (1.67). By sol-gel transition in gelatin solution combined with freeze-drying, it possible to obtain a tridimensional gelatin structure completely covered by hydroxyapatite crystals. As shown by SEM, and confirmed by TEM, the crystal shape depend on HA/GEL ratio. Based on the TEM results, the average of nHA crystalline decrease with gelatin presence (as show in figure 4). This may be caused by different intensities of interactions between ions; with adding Gel, the abundant supply of COO^- coordination sites available for complexation with Ca^{2+} ions leads to a very large number of nuclei for the growth of nHA crystalline so that these crystalline cannot grow very large [28].

The charged density is fixed in gelatin structure, that is to say the number of nucleation sites is uniformly distributed, therefore the size/shape of nHA crystalline depended on the rate of crystalline growth, or rather $[Ca^{2+}]$ $[PO_4^{3-}]$ concentration [29]. Higher $[Ca^{2+}]$ and $[PO_4^{3}]$ lead to the rate of crystalline growth accelerated [29].

In our case, the $[Ca^{2+}][PO_4^{3-}]$ distribution into the solution is inhomogeneous in longitudinal direction due to a CaP gradient in the structure: for this reason, in the part where HA presence is lower (figures 3B,D), crystals growth slowly and nHA crystalline decrease. Indeed in the part where HA presence is higher (figures 3C,D), typical hydroxyapatite plate-like crystals is evident. For this reasons, in the B10_HA20 samples, the higher gelatin (80% w/w) leads the interaction between COO^- and Ca^{2+} and reduces the crystalline growth. As confirmed by SEM image (figure 2) the gelatin structure is completely covered by hydroxyapatite, but the CaP deposition have not the plate-like crystal shape (as in the case illustrate in the figure 3B).

The thermogravimetric plots of the composite scaffolds were used to determine the inorganic phase content, which was evaluated from the residual weight of the samples. The experimental data, reported in tables 1 and 2, show that in B10_HA20 the inorganic phase content is uniformly distributed into the scaffold, and confirm HA gradient in the B10_HA30 sample. HA residual% calculate by residual value are very close to the original amounts of calcium phosphate used to prepare the scaffolds. Moreover in the B10_HA30 sample the HA gradient is verified by gradually HA% reduction (27,9 – 17,2 – 5,5%) into the longitudinal section (table 1).

In order to evaluate the thermal stability and the phase transformation, TGA of inferior section B10_HA30 scaffold was reported in the figure 7. The first endothermic region shows (in the deriv. weight curve) different peaks, which correspond to three phenomena: the first is the loss of water molecules that interacted with free carboxyl acid and amino acid presents in the gelatin, by hydrogen bonding (50-162.1°C); the last two, are the loss of dehydration of the precipitating complex and the loss of physically adsorbed water molecules of the hydroxyapatite powder (162.1-255.7°C). These phenomena occur since 300°C, and partially fall in the gelatin degradation range (250- 550°C). Moreover, it can be explained by the following reaction:

$$Ca_{10}(PO_4)_6(OH)_2 \rightarrow Ca_{10}(PO_4)_6(OH)_{2-2x}O_xH_x + {}_xH_2O \ \ [30, 31]$$
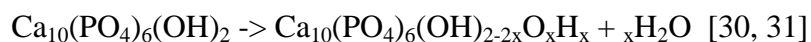
The exothermic dissociation of CO_3^{2-} is reported [32, 33] to occur at the temperature range between 500 to 900°C in nitrogen atmosphere.

The magnification in the diagram 5 (B10_HA30) shows a different behavior in a gelatin degradation zone. As reported in literature [34] at this gap, corresponds the degradation of non

crosslinked organic phase. So, as will be demonstrate below, it is related with crosslinking efficiency.

The FTIR spectrum of superior (up) and inferior (down) section of gelatin B10%w/v and 30 wt% HA composite, are shown in figure 8. The composite spectrum are similar to the spectra of real bone [2,35,24]. As reported in literature [22], the band at 1337 cm^{-1} in gelatin B is attributed predominantly to the so-called wagging vibration of proline side chains. Therefore, this band does not simply represent the carboxyl group, but it is one of a number of bands in the range of 1400-1260 cm^{-1} which are attributed to the presence of gelatin type-I [24,36]. The peak at   1337 cm^{-1} band in gelatin shifts at 1400 cm^{-1} in gelatin/hydroxyapatite composite; it has been effectively used to confirm the chemical bond formation between carboxyl ions in gelatin and HA phases [24,37-38]. During the process of HA-GEL composite, the Ca^{2+} ions will make a covalent bond with R-COO$^-$ ions of GEL molecules.

The appearance of an amide I mode indicated that HA-GEL composites adopt a predominantly α - helical configuration and this is confirmed by the appearance of amide II at ~1540 cm^{-1} [22,38,39]. The strong COO$^-$ peaks at 1638 cm^{-1} in gelatin move to higher wavenumber at 1651–1655 cm^{-1} in all nH/Gelatin samples due to the Ca^{2+} ions coupled with the COO$^-$ through electrostatic interaction [40] and the intensity increase with the enhancing of HA content. Infact, peaks at 1422 cm^{-1} in B10_HA30 (down) shift to lower wavenumber at 1409 cm^{-1} in B10_HA30 (up); this indicated that there are a kind of chemical interactions between the calcium ions and the COO$^-$ in gel [28,41,42].

The intensity of phosphate and CO_3^{2-} vibration, suggests the presence of different hydroxyapatite amount into the scaffold. In general the process to obtain crystalline hydroxyapatite is more complex. It is usually held that the initiation of the mineral crystalline during tissue calcification is caused by heterogeneous nucleation [44,45]. The above results demonstrated that the nucleation of nHA crystalline on the gelatin surfaces is critically dependent on the charged functions groups that existed in the gelatin, e.g. negatively charged COO$^-$ and/or C=O groups and positively charged amino groups. That is to say the COO$^-$, C=O and amino groups offer the nucleation sites for HA crystalline through binding or chelating oppositely charged ions, calcium and phosphate [46,47]. Therefore, there is a heterogenous nucleation and growth of nHA on the gelatin in-situ. At first, calcium ions enrich on the carboxyl groups and amino groups Gel in the solution, and then PO_4^{3-} enrich on the amino groups of Gel or at the calcium complexes, all these enrichments may be attributed to electrostatic interaction or/and polar interaction [28]. In our case are absent typical peaks of amino groups and PO_4^{3-} interaction, as reported by Yao et *al.* [28]. Secondly heterogenous

nucleation of nHA enrich with Ca^{2+} and PO_4^{3-} at pH 11. Finally nano-crystalline of HA growth, stirring at 85 rpm at 40°C for 24 hrs.

To evaluate mechanical properties and correlation between compression modulus and crosslinking efficiency, all the samples were tested in an aqueous environment, after soaking in distilled for 1h. As demonstrated by Goudarzi et *al.* [22] the compressive modulus of HA-GEL scaffolds should increase with HA content. In our case the behavior is inverted (figure 9 and table 3); this could be explain by a reduced of crosslinking treatment. Gelatin-hydroxyapatite scaffolds were realized in order to promote interaction between COO^- of gelatin, and Ca^{2+} of HA, as previously demonstrated. Moreover, crosslinked treatment by EDC, involves COOH of gelatin, and NH_2 of carbodiimide. In each steps, were taken in consideration gelatin carboxyl groups. SEM/TEM have demonstrated high HA presence into the structure. As already explained, the inorganic phase is very relevant in the system, so as to create a plate-like crystals, typical of crystalline hydroxyapatite in the zone of maximum HA gradient (B10_HA30 samples). Probably, gelatin carboxyl groups were saturated to have higher gelatin/hydroxyapatite interaction; so in the following step (crosslinked treatment) there were few free COOH groups to permit a good crosslinking. In this perspective, increasing HA content, crosslinking efficiency decrease, as also the mechanical properties. Indeed there is a clear difference between samples obtained by gelatin type A, and type B; moreover B10_HA20 scaffold compressive modulus (209,183±18.113 KPa) is several magnitude orders higher than the other. It could be depend on carboxyl group content of different gelatin types; as reported [37,43], gelatin A contains 77 COOH per 1000 amino acids while gelatin B contains 118 COOH per 1000 amino acids. So probably in the B10_HA20 the total calcium phosphate amount isn't necessary to saturate gelatin carboxyl group, and the crosslinking treatment success. Moreover, gelatin type A has low number of carboxyl groups, so as to saturated all of them whit both calcium phosphate concentration $(20 - 30\%)$. Another date to confirm this theory, is the image of samples after 1h in water.

Fig. 11: Photo of crosslinked GEL/HA scaffolds dry, and wet (after 1h in distilled water).

In gelatin/hydroxyapatite scaffold, increasing inorganic phase and decreasing carboxyl group (content in polymer typology), success of crosslinking by EDC drastically decreases and consequently compression modulus is very low and swelling behavior after 1h (short time) is very relevant. This result is demonstrated also by TGA analysis, and in particular in the magnification present in the figure 5. Infact, as said before, the gap corresponds to the non crosslinked organic phase, and this is relevant in a scaffold section whit high HA present.

In accordance with biological preliminary tests, the material are nontoxic, not affecting the cell proliferation and shows good biocompatibility.

3.2.5 Conclusions

Porous gelatin/hydroxyapatite scaffolds with different gelatin type (A and B 10%w/v) and inorganic contents (20 and 30 %w/w), were prepared by in situ sol-gel approach, and then freeze–drying the composites. In our work we have demonstrated that, by an opportune GEL/HA ratio (B10_HA30 and A10_HA30), is possible to create an HA gradient into the scaffold section, as confirmed by morphological (SEM), thermal (TGA) and chemo-physical (FTIR) analyses. Moreover during the process, the Ca^{2+} ions will make a covalent bond with R-COO$^-$ ions of GEL molecules, determining reduced nHA dimension. Due to the hydroxyapatite gradient, the $[Ca^{2+}][PO_4^{3-}]$ distribution into the solution is inhomogeneous in longitudinal direction: for this reason, in the part where HA presence

is lower, crystals growth slowly and nHA crystalline decrease. Indeed in the part where HA presence is higher, typical hydroxyapatite plate-like crystals is evident.

Moreover, also the crosslinking treatment by EDC solution, was investigated. Thermal (TGA), an mechanical analyses show that in gelatin/hydroxyapatite scaffold, success of crosslinking by EDC depend on number of carboxyl group (content in polymer typology) and inorganic phase amount. Biological test performed by MG-63, demonstrates nontoxicity and good biocompatibility of the materials.

3.2.6 References

[1] Gineste L, Gineste M, Ranz X, Ellefterion A, Guilhem A, Rouquet N and Frayssinet P. Degradation of ydroxyapatite, fluoroapatite, and fluorohydroxyapatite coatings of dental implants in dogs. J Biomed Mater Res 1999;48:224-34.

[2] Sonju Clasen AB and Ruyter IE. Quantitative determination of type A and type B carbonate in human deciduous and permanent enamel by means of Fourier transformation infrared spectroscopy. Adv Dent Res 1997;11:523-7.

[3] Cerroni L, Filocamo R, Fabbri M, Piconi C, Caropresso S and Condo SG. Growth of osteoblast like cells on porous hydroxyapatite ceramics: an in vitro study. Biomed Eng 2002;19:119-24.

[4] Wozney JM and Rosen V. Bone morphogenetic protein and bone morphogenetic protein gene family in bone formation and repair. Clin Orthop Rel Res 1998;346:26-37.

[5] Suchanek W and Yoshimura M. Processing and properties of hydroxyapatite-based biomaterials for use as hard tissue replacement implants. J Mater Res 1998;13:94-117.

[6] Asashina I, Watanabe M, Sakurai N, Mori M and Enomoto S. Repair of bone defect in primate mandibule using a bone morphogenetic protein (BMP) hydroxyapatite collagen composite. J Med Dent Sci 1997;44:63-70.

[7] Myung CC, Ching-Chang K, William HD. Preparation of hydroxyapatite-gelatin nanocomposite. Biomaterial. 2003;24:2853-62.

[8] Rose PI Gelatin. In: Encyclopedia of Polymer Science and Technology. (Kroschwitz, J.I., editor), Vol. 7, Wiley, New York, (1985) pp. 488-513.

[9] Reddi AH. Role of morphogenetic proteins in skeletal tissue engineering and regeneration. Natl Biotechnol 1998;16:247-52.

[10] Chevallay B and Herbage D. Collagenbased biomaterials as 3D scaffold for cell cultures: applications for tissue engineering and gene therapy. Med Biol Eng Comput 2000;38: 211-8.

[11] Cooper CW and Falb RD. Surgical adhesives. Ann NY Acad Sci 1971;146:218-24.

[12] Yaylaoglu MB, Korkusuz P, Ors U, Korkusuz F, Hasirci V. Development of a calcium phosphate–gelatin composite as a bone substitute and its use in drug release. Biomaterials 1999;20:711–9.

[13] Kim HW, Knowles JC, Kim HE. Hydroxyapatite and gelatin composite foams processed via novel freeze-drying and crosslinking for use as temporary hard tissue scaffolds. J Biomed Mater Res A 2004;72A:136–45.

[14] Mann S, Ozin GA. Synthesis of inorganic materials with complex form. Nature 1996; 365:499–505.

[15] Zerwekh JE, Kourosh S, Schienbergt R. Fibrillar collagen–biphasic calcium phosphate composite as a bone graft substitute for spinal fusion. J Orthop Res 1992;10:562–72.

[16] Chang MC, Ko C, Douglas WH. Preparation of hydroxyapatite–gelatin nanocomposite. Biomaterials 2003;24:2853–62.

[17] Kim HW, Kim HE, Salih V. Stimulation of osteoblast responses to biomimetic nanocomposites of gelatin–hydroxyapatite for tissue engineering scaffolds. Biomaterials 2005;26:5221–30.

[18] Raucci MG, Guarino V, Ambrosio L. Hybrid composite scaffolds prepared by sol–gel method for bone regeneration. Compos Sci Tech 2010;70:1861–68.

[19] Huang LY, Xu KW, Lu J. A study of the process and kinetics of electrochemical deposition and the hydrothermal synthesis of hydroxyapatite coatings. J Mater Sci Mater Med 2000;11:667–73.

[20] Whang K, Thomas CK, Nuber G, Healy KE. A novel method to fabricate bioabsorbable scaffolds. Polymer 1995;36: 837-42.

[21] Healy KE, Whang K and Thomas CH. Method of fabricating emulsion freeze-dried scaffold bodies and resulting products. U.S. Patent 1998; 5, 723,508.

[22] Narbat MK, Orang F, Hashtjin MS, Goudarzi A. Fabrication of Porous Hydroxyapatite-Gelatin Composite Scaffolds for Bone Tissue Engineering. Iran Biomed J 2006;10:215-23.

[23] Kim HW, Knowles JC, Kim HE. Porous Scaffolds of Gelatin–Hydroxyapatite Nanocomposites Obtained by Biomimetic Approach: Characterization and Antibiotic Drug Release. J BiomedMater Res Part B: Appl Biomat2005;74B:686–98.

[24] Myung CC, Junzo T. FT-IR study for hydroxyapatite-collagen nanocomposite cross-linked by glutaraldehyde. Biomaterials 2002;23:4811-8.

[25] George S. (2002) Infrared and Raman Characteristic Group Frequencies. 3th edition, ISBN: 0470093072, John Wiley & Sons, pp. 40-53

[26] Rosa AL, Belotia MM, van Noort R. Osteoblastic differentiation of cultured rat bone marrow cells on hydroxyapatite with different surface topography. Dent Mater 2003;19:768–72.

[27] Awad HA, Quinn Wickham M, Leddy HA, Gimble JM, Guilak F. Chondrogenic differentiation of adipose-derived adult stem cells in agarose, alginate, and gelatin scaffolds. Biomaterials. 2004;25:3211–22.

[28] Junjie Li, YiPing Chen, Yuji Yin, Fanglian Yao, Kangde Yao. Modulation of nano-hydroxyapatite size via formation on chitosan–gelatin network film in situ. Biomaterials 2007;28:781–90.

[29] Panzavolta S, Fini M, Nicoletti A, Bracci B, Rubini K, Giardino R, Bigi A. Porous composite scaffolds based on gelatin and partially hydrolyzed a-tricalcium phosphate. Acta Biomater 2009;5:636–43.

[30] Murray MGS, Wang J, Pontoon CB, Marquis PM. An improvement in processing of hydroxyapatite ceramics. J Mater Sci 1995;30:3061-74.

[31] Azami M, Moztarzadeh F, Tahriri M. Preparation, characterization and mechanical properties of controlled porous gelatin/hydroxyapatite nanocomposite through layer solvent casting combined with freeze-drying and lamination techniques. J Porous Mater. 2010;17:313–20.

[32] Murugan R, Ramkrishna S, Panduranga RK. Nanoporous hydroxy-carbonate apatite scaffold made of natural bone. Mater Lett 2006;60:2844–7.

[33] Bundela H, Bajpai AK. Designing of hydroxyapatite-gelatin based porous matrix as bone substitute: Correlation with biocompatibility aspects. eXPRESS Polymer Lett2008;2:201–13.

[34] Tadic D, Epple M. A thorough physicochemical characterisation of 14 calcium phosphate-based bone substitution materials in comparison to natural bone. Biomaterials 2004;25:987–94.

[35] Chang MC, Ikoma T, Kikuchi M and Tanaka J. Preparation of a porous hydroxyapatitecollagen nanocomposite using glutaraldehyde as a cross linking agent. J Mater Sci Lett 2002;20:1129-1201.

[36] George S. (2002) Infrared and Raman Characteristic Group Frequencies. 3th edition, ISBN: 0470093072, John Wiley & Sons, pp. 40-53.

[37] Kuijpers AJ, Engbers GHM, Feijen J. Characterization of the Network Structure of Carbodiimide Cross-Linked Gelatin Gels. Macromolecules 1999;32:3325-33.

[38] Doyle BB. Infrared spectroscopy of collagen and collagen like polypeptides. Biopolymers 1975;14:937-57.

[39] Epaschalis EP, Betts E, Di Carlo E, Mendelsohn R and Boskey AL. FTIR microspectroscopic analysis of normal human cortical and trabecular bone. Calcif Tissue Int 1997;61:480-6.

[40] Wang Y, Yang C, Chen X, Zhao N. Biomimetic formation of hydroxyapatite/collagen matrix composite. Adv Eng Mater 2006;8:97–100.

[41] Li Z, YuBao L, Aiping Y. Preparation and in vitro investigation of chitosan/nano-hydroxyapatite composite used as bone substitute materials. J Mater Sci-Mater Med 2005;16:213–9.

[42] Yamaguchi I, Tokuchi K, Fukuzaki H, Koyama Y, Takakuda K, et al. Preparation and microstructure analysis of chitosan/hydroxyapatite nanocomposites. J Biomed Mater Res 2001;55:20–7

[43] Rose PI. In Encyclopedia of Polymer Science and Engineering, 2nd ed.; Mark HF, Bikales NM, Overberger CG, Menges G, Kroschwitz JI, Eds.; Wiley-Interscience: New York, 1987; Vol. 7, p 488.

[44] Jakobsen RJ, Brown LL, Hutson TB, Fink DJ, Veis A. Intermolecular interactions in collagen self-assembly as revealed by Fourier transform infrared spectroscopy. Science 1983;220:1288–90.

[45] Linde A. Dentin mineralization and the role of odontoblasts in calcium transport. Conn Tissue Res 1995;33:163–70.

[46] Zhai Y, Cui FZ. Recombinant human-like collagen directed growth of hydroxyapatite nanocrystals. J Cryst Growth 2006;291:202–6.

[47] Tanaka S, Shiba N, Senna M. Change in the morphology of hydroxyapatite nanocrystals in the presence of bioaffinitive polymeric species under the application of electrical field. Sci Technol Adv Mater 2006;7:226–8

Conclusions of chapter 3

Tissue engineering strategies rely on the use of cells, bioactive factors, and scaffolds or combinations thereof. Complex tissues must be engineered with the structural and functional characteristics of native tissue in a process that is not only biocompatible but also interactive and integrative with neighboring tissues simultaneously. In our case, osteocondral region has a distinct tissue (bone and cartilage) with different physic, mechanic, morphology and biology characteristics. The extracellular matrix of bone has been described as a composite material composed of collagen type I fibrils mineralized with nanocrystals of hydroxyapatite. To mimic natural structure, we propose a gelatin (denatured collagen) scaffold biomineralized by nHA. The introduction of biological signals (hydroxyapatite) was realized by bulk sol-gel transition and surface biomimetic treatment.

In this chapter, we propose two systems:

3. Gelatin scaffold crosslinked by EDC solution, and biomineralized by accelerate Kokubo treatment;

4. Gelatin/hydroxyapatite scaffold realized by in situ sol-gel synthesis and crosslinked by EDC solution.

In the first structure (1) the matrix is constituted by natural polymer and biological signals (nHA) create a coating on the porous surface. In a Kokubo treatment, the HA crystalline depend on treatment time: in our systems, after 7 days, there is a sufficient HA crystalline phase to obtain an increasing of osteogenic proliferation and differentiation.

In the other system (2), indeed, the matrix is a combination of gelatin/hydroxyapatite, where the biological signals are present into the scaffold as a gradient. The chemical interaction between Ca^{2+} and COO^- involves a polymeric matrix completely covered by nHA crystalline. In this case the crystalline degree is modulated by gelatin/hydroxyapatite ratio (different into the scaffold due to the presence of inorganic phase gradient): where $[Ca^{2+}][PO_4^{3-}]$ concentration are higher, typical hydroxyapatite plate-like crystals is evident.

Moreover, our results show the crosslinking treatment (by EDC) successes (1), and its dependence on gelatin type and gelatin/hydroxyapatite ratio (2).

In summarize, the two gelatin/hydroxyapatite systems could have a great potential application as filler in osteocondral repair and regeneration.

Conclusions and future work

*I*n this work three injectable systems were proposed as bone-filler (Strontium-substituted hydroxyapatite cement, Bioactive hydroxyapatite - graphene oxide, Modified-cellulose hydrogels crosslinked by citric acid) and two different gelatin scaffolds biomineralized by nHA. All these systems could have different medical applications, such as: osteoporosis therapy; filler for different (in terms of dimension and shape) bone/osteochondral defects caused by tumor removal, fractures or congenital defects; carrier to growth factors or pharmacy; detection systems; antitumor therapy; or as multifunctional systems.

Our research demonstrated that specific nanoscale structure of the injectable material's surface has significant positive effects on osteoblast cell response, including initial cell growth and expression of differentiation markers (such as OPN, OCN). Moreover, gel systems support high viability of hMSC cells and have a good effect on cell attachment, proliferation and osteoblastic differentiation. A promising increase of osteogenic proliferation and differentiation has been observed in gelatin scaffold crosslinked by EDC solution and biomineralized by modified Kokubo treatment.

Another important result is the presence of biological signals (HA) gradient into the gelatin/hydroxyapatite scaffold realized by in situ sol-gel synthesis. This systems could have a great potential application as filler in osteocondral repair and regeneration, allowing a simultaneous regeneration of both cartilage and subchondral bone. In that case an osteogenic differentiation should increase with the gradient, meanwhile the chondrogenic differentiation should decrease inthe same direction. For this aim, as **future work** we propose a gene expression analysis of bone-related markers as osteopontin (OPN) and osteocalcin (OCN) and cartilage-related markers as callagen (COL II) aggregan or SOX9.

The distribution and size of the pores, as well as the nano/macro-surface structure, might play an important role for osteogenic and chondrogenic differentiation in vitro (as reported in this work) and in vivo. However, future studies will have to identify the relevant parameters of the scaffolds and injectable systems to optimize in vivo study.